DESIGN AND PERFORMANCE OF RESONANT CAVITIES

FOR COMMUNICATION SYSTEMS

The theory and performance of resonant cavities for application in mobile radio and base-stations in the VHF and UHF bands are investigated.

by

S. ADEKUNLE ADENIRAN

A Thesis submitted to the University of Bradford for the Degree of

Doctor of Philosophy

May 1984

Postgraduate School of Studies in Electrical
& Electronic Engineering
University of Bradford
BRADFORD BD7 1DP
England

The work described in this thesis has not been accepted for any degree, and is not being concurrently submitted in candidature for any degree.

..... Candidate

..... Supervisor

ACKNOWLEDGEMENTS

The author is grateful to Professor D P Howson, who supervised the work reported here, for his valuable contributions by way of several helpful discussions and suggestions. To Mr G Spence and some other technical staff, the author wishes to acknowledge his indebtedbess and to express his appreciation of their invaluable assistance in the technical aspects of the work. Thanks are also due to Mrs D F Connor who typed the manuscript. It is with pleasure that the author thanks his brother, Olasupo, 'Remi, Kikelomo, Olukemi, Folorunso and Akinwumi for their support and encouragement.

ABSTRACT

It is often necessary to operate a number of radio communication channels from a single control room without time-sharing between the various channels. Here it is necessary to operate a number of transmitters and receivers simultaneously from the same base station or mobile unit without interference. The best method to achieve this has been found in the use of filters inserted in the transmission line between the antenna and the transmitter(s) on one hand and the receiver(s) on the other hand.

The basic unit employed in the design of microwave filters is usually a cavity resonator of which the most important factors are the Q, insertion loss and resonant frequency. However, a problem which frequently arises with cavity resonators is the accurate determination of these resonant characteristics complicated by the presence of coupling port, materials and various design and geometrical deviations. Such cavities have been investigated in several cases and the results have been generalised, but this investigation has been conducted to examine thoroughly most of the problems being met in present practice. Design and development of some common resonant structures are considered. Emphasis is placed on solutions found to special problems especially regarding complicated boundary conditions. Furthermore, investigation includes methods for optimising resonant parameters such as insertion loss and Q, trading of insertion loss with coupled cavity selectivity, frequency tuning and compensation for frequency variations due to wide ranges of operating temperatures. By comparing Q values obtained in practice with theoretical values, it has been possible to establish an appropriate Q loss budget so as to facilitate accurate prediction of coupled cavity unloaded Q. A satisfactory agreement between theory and practice

has been obtained.

By application of the results of theoretical analysis and experiment, it is shown that microwave filters can be designed to have a desired insertion loss and off-band attenuation slope. Steps leading to designs of any number of cascaded cavities in a two-port network and, subsequently,multi-port networks are discussed in detail.

LIST OF CONTENTS

CHAPTER ONE

I N T R O D U C T I O N

1.1 The Scope of the Thesis

Resonant cavities are numerous and can be divided into two major categories: firstly, the dielectric resonators for which apart from being characterised by low Q-factors have very few analytic geometrical shapes in the family. This set of resonant cavities has not found many useful applications in the area of microwave communications. Secondly, the set of hollow resonators bounded by metallic conductor surfaces and usually characterised by high quality factors. This set of cavities are many and can be derived from virtually any coupled metallically enclosed or semi-enclosed volume. However, only those with analytic geometries have known wave solutions and have been explored fully for application in filter related networks. Others have been analysed using typical cut and run trial methods or the approximate techniques. Fortunately, because of the present advent of digital computers, extensive numerical solutions of the Maxwell's and general wave equations for less complicated boundary surfaces have been made possible.

Waveguide cavities and cavities with less complicated surfaces as found in re-entrant or multi-cylindrical coaxial cavity resonators are treated. In the process of analysis, the author has tried as much as possible to avoid very complicated mathematical expressions. Where these are involved, especially where it involves transcendental functions, detailed explanations of derivations have been included and various relationships are defined. For this purpose complicated integrals of basic Bessel's functions are included in the Appendices. Numerical techniques and computer solutions are well illustrated. Computer programs

and subroutines in FORTRAN for the numerical solutions are included for such analysis.

One of the problems which complicate the exact knowledge of a resonator is found in coupling to external circuits. Here, particular interest has been placed in resonant cavities coupled by means of loops. Consequently, simple geometrical surfaces have been chosen for the study and characterisation of the loop. Emphasis has been placed on such resonant characteristics as the cavity unloaded Q as affected by the loop and other sources of geometrical deviation from the ideal situation. Tuning procedures for the set of cavities which are not otherwise tunable and general techniques for temperature compensation have been analysed. A distinguishing feature of the investigation is that it runs through specialised cavity designs to generalised resonant cavity application in communication networks. Design details of complex networks are well analysed with emphasis placed on the design of filter units and the interconnection to a common junction of many units. Although the investigation has been carried out for cavities operating in the UHF band for dimension reasons, it is believed that the findings at UHF would hold for VHF cavities.

In all aspects of the thesis, useful references have been included at the end of each chapter and a general bibliography of other referred materials in the course of the research has been included at the end of the thesis.

1.2 The Scope of the Chapters

Chapter Two, the earliest analytical chapter, is involved with a brief study of waveguide resonators (resonators derived from waveguides), in particular rectangular cavities, and the study of loop coupling and its effect on resonant parameters. Because of the problem of tuning with waveguide cavities, Chapter Three has been devised for the treatment of high-Q hybrid mode cavities of re-entrant coaxial and multicylindrical types. However, analysis of frequency tuning in waveguide cavities is thought inevitable. Therefore, Chapter Four describes an intensive analytical procedure for tuning of waveguide cavities by means of thin screws or plungers inserted in electric field antinodes. Furthermore, it investigates a cheap and effective temperature compensation mechanism for tunable cavities exploring the advantages of linearity in tuning curves of most tunable cavities over narrow ranges of frequencies. In Chapter Five, a brief but qualitative analysis of the effects of gaps and holes in the metal faces of resonant cavities is touched. Chapter Six is involved with the general application of cavity resonators in communication networks. The aim has been to make the analysis generally applicable to all types of resonant cavities for which such parameters as resonant frequency, unloaded Q, and the insertion loss can be calculated or measured. It further describes how filter units comprising of two ports can be constructed from cavities and tested, and what the likely resonance expectations when many units are connected to the same junction as is usually the case with duplexers, multiplexers, etc.

CHAPTER TWO

CHARACTERISTICS OF LOOP COUPLED CAVITY RESONATORS

2.1 Introduction

Attempts to predict accurately the resonant parameters of a loop-coupled resonant cavity have led to various analytical methods as will be outlined. Particularly using a single mode solution it is possible with most structures to design a section of a waveguide which will resonate somewhere within a known narrow frequency band and for which, as first approximation, the length of the resonator must be a multiple of half guide wavelength. In general, for simplification and uniqueness, coupled resonant cavities have been represented by equivalent lumped-parameter networks[1,2,3,4]. However the presence of one or two coupling devices greatly complicates the accurate determination of the elements of the equivalent network and subsequently the exact resonant parameters. Because of this departure from an ideal case, it has been necessary to adjust theory empirically for conformity with practice, or vice versa. The first of the two methods considered here has been attempted by Howson et al[17]. This method consists of adjusting the equivalent network representation so that practice conforms closely with theory. This has been found satisfactory over the frequency range 80-500MHz. The other method involves direct adjustment of the coupling device itself to offset the source of discrepancies. It has also been found satisfactory for the frequency range 1GHz to 1.7GHz, as will be outlined here. Without loss of generality such adjustment is envisaged to cover both the VHF and UHF bands.

Whatever adjustment is done, practice has revealed that even at the best coupled cavity performance there is usually an additional loss which

manifests clearly in the unloaded coupled cavity Q. In other words, the observed cavity Q is often lower than the theoretical value. This chapter thus partly establishes what a designer should expect in practice.

All the investigations carried out here were made at the simplest and fundamental TE_{101} mode of rectangular cavity for which the ideal cavity field and equivalent lumped element parameters are known. The hope is that if the 'exact' theoretical result is compared with the practice, it becomes very easy to predict,in general, the resonant parameters of all types of coupled cavities. Finally, because of handling, small cavities operating around 1.5GHz frequency band were used in the investigation.

2.2 Coupled Cavity Design Procedures

It is a common practice to design a cavity by considering the fundamental resonant mode or a single mode which is widely separated from other modes. For instance, when a rectangular cavity is employed as a filter network, the fundamental TE_{101} mode is commonly employed most especially because it is the mode with the lowest frequency obtainable for the volume and one can easily design the cavity separating the mode from higher order modes by simple choice of dimensions. By separating the desired mode from other modes the influence of these modes on the desired mode is reduced. Figure 1 is a view of typical rectangular cavity, dimensions $x = a_1, y = b, z = a_2$. Because the fields depend on the x and z axes, the unperturbed cavity resonant frequency depends on the cavity dimensions along the two axes. A list of normalised eigenfunctions, eigenvalues and unloaded quality factors for TE and TM rectangular, cylindrical and coaxial cavities has been given by Kinzer and Wilson[10] . These resonant parameters are always different from the

practice because of mechanical and geometrical deviations and various perturbations resulting from coupling and finishing. Therefore, for reasons of uncertainty in the exactness of the expected resonant frequency, it is of importance to design the cavity to resonate at slightly higher frequency since it is easy to tune from a higher frequency to the required lower frequency. However, the tuning range should be less than 0.5% so that the effect of tuning on the other resonant parameters would not cause significant deviation from the expected values. Tuning procedures form the context of Chapter Four. For an unperturbed rectangular cavity, the resonant frequency of a TE_{101} mode is given as

$$f_o = 2.998E8/\sqrt{[(\frac{1}{a_1})^2 + (\frac{1}{a_2})^2]} \qquad (1)$$

where a_1, a_2 are cavity dimensions along x, z axes respectively.

The cavity Q is derived from the energy relationship in the cavity. For an ideal resonant cavity for which the boundary walls are made of metal, conductivity σ, the Q-factor for the TE_{101} mode is given as:

$$Q_o = \frac{\lambda_o \pi}{\sqrt{8R_s}} \sqrt{\frac{\mu}{\varepsilon}} \frac{b(a_1^2+a_2^2)^{3/2}}{a_2^3(a_1+2b) + a_1^3(a_2+2b)} \qquad (2)$$

From the definition the Q factor is strictly dependent on volume-to-surface area ratio of the cavity. By minimising the surface area internal to a cavity a high unloaded Q can be achieved for any volume at the resonant frequency. This requirement necessitates the use of square faces for which $a_1 = a_2 = a$. The Q, from equation (2), depends on the depth, b, of the cavity. In other words, by varying b Q can be changed. The rate at which the cavity can be tuned has been found dependent of the depth of the cavity for the mode (Chapter Four). So, in effect, b has dual first order roles to play in designing a rectangular cavity (and cylindrical cavity). Initially, a maximum allowance should

be made for the Q_o variation due to both coupling, imperfections and the incorporation of a tuning plunger. Moreover to separate the fundamental mode from higher order modes, b must be smaller than a. Usually b is between one-third and one-quarter the value of a.

The cavity is usually used with loop coupling. In this case we shall consider cavity coupled to external circuits by two identical coupling loops in which one excites the cavity in the normal mode and acts as the input while the other is the output. The loops are positioned such that their planes are normal to a component of the magnetic field. They are introduced at the broad surface as a means of reducing the influence of the side walls on the equivalent loop inductance terms (Collins[15]). The sizes and positions of the loops would depend on the resonant specifications - the selectivity requirement and the maximum allowable insertion loss. It has been shown that selectivity and insertion loss can be varied with little effect on the experimental Q_o.

2.3 Equivalent Circuit Representation and General Modelling

Microwave cavities are inherently very complex networks with an infinite number of natural resonant frequencies and may be modelled with either lumped equivalent circuits or as distributed transmission lines bounded by known discontinuities. The properties of cavities of simple geometry have been studied by Borgnis (1939), Hansen and Richtmeyer (1939), Condon (1942), Slater (1942, 1946), and a host of others using Maxwell's equations of the electromagnetic field. The problem of a cavity coupled by a single loop has been studied by Hansen[5], Condon[2], Slater[4], Crout[8] and Banos[3]; and the case of a double loop coupling has been given a wider analytical attention. Such work has included that of Beringer[3], Schelkunoff[1,14], and Ragan[6]. The general form, shown

in Fig. 2(a) as derived by Fano and Lawson[6], has taken into consideration all possible resonant modes in the cavity. The modified general form shown in the literature has for a real cavity open circuit impedances given as

$$Z_{11}(\omega) = R_1 + j\omega L_{10} - j\frac{1}{\omega C_{10}} + j\sum_{k=1}^{\infty}\frac{\omega^3 M_{1k}^2}{L_k\left(j\frac{\omega\omega_k}{Q_k} + (\omega^2-\omega_k^2)\right)}, \qquad (3a)$$

$$Z_{22}(\omega) = R_2 + j\omega L_{20} - j\frac{1}{\omega C_{20}} + j\sum_{k=1}^{\infty}\frac{\omega^3 M_{2k}^2}{L_k\left(j\frac{\omega\omega_k}{Q_k} + (\omega^2-\omega_k^2)\right)} \qquad (3b)$$

and

$$Z_{12}(\omega) = j\omega M_o - j\frac{1}{\omega C_{12}} + \sum_{k=1}^{\infty}\frac{j\omega^3 M_{1k}M_{2k}}{L_k\left(j\frac{\omega\omega_k}{Q_k} + (\omega^2-\omega_k^2)\right)}. \qquad (3c)$$

In deriving these equations it was assumed that the dimensions of both loops and the holes are so small compared to the size of the resonator and the wavelength that the normal mode fields inside the unperturbed cavity remain unaltered by the loop and coaxial line. Each resonant loop representing one of the natural resonant modes of the cavity and the capacitors and the ideal transformer together represent direct capacitive coupling between input and output terminals. Since most cavity designs usually employ the fundamental modes which are far removed from the higher order modes, a single mode version of the equations is usually employed. It is clear that, ideally, there is no mutual coupling between the different modes of the cavity in consequence of the orthogonality relations. The direct coupling between the loops is assumed to be negligible because the loops are not in close proximity. In other words C_{10}, C_{20}, M_o, C_{12}, $M_{1k}(k\neq1)$, $M_{2k}(k\neq2)$ all vanish. The

general form thus reduces to the single mode version as derived by Schelkunoff[1,13]:

$$Z_{11}(\omega) = R_1 + j\omega L_{10} + \frac{j\omega^3 M_{11}^2}{L_1\left(j\frac{\omega\omega_1}{Q_1} + (\omega^2-\omega_1^2)\right)} \quad , \tag{4}$$

$$Z_{22}(\omega) = R_2 + j\omega L_{20} + \frac{j\omega^3 M_{22}^2}{L_1\left(j\frac{\omega\omega_1}{Q_1} + (\omega^2-\omega_1^2)\right)} \tag{5}$$

and

$$Z_{12}(\omega) = \frac{\omega^3 M_{11} M_{22}}{L_1\left(j\frac{\omega\omega_1}{Q} + (\omega^2-\omega_1^2)\right)} \quad . \tag{6}$$

Equations (4), (5) and (6) represent the transfer impedance of a doubly coupled cavity for which one loop excites the cavity and the other loop forms the output from the cavity. The system thus behaves as a two-port network. The equations are appropriate for the series RLC equivalent circuit (and can be modified for the shunt GLC circuit). In these equations R_1, R_2 are the loop wire resistances and other forms of dissipation in the input and output circuits respectively with exclusion of input and output loads. Because of easy means of computation, this set of equations can be readily used in characterising the coupled cavity.

The parameters required of the cavity are the ideal cavity's equivalent lumped inductance L_1, the unperturbed cavity unloaded quality factor, Q, and the natural resonant frequency of the fundamental mode.

2.4 Analysis of the Network

Fig. 2(b) depicts the modified circuit diagram of the doubly coupled cavity. This is represented in Fig. 2(c) by a block diagram. Z_G, Z_L are the generator and load impedances respectively. For laboratory measurement,

$$Z_G = Z_L = 50\Omega$$

On normalisation to unity,

$$Z_G = Z_L = 1$$

The transfer impedance [Z] is represented by equations (4), (5) and (6). If the coupling line is uniform and of normalised characteristic impedance of 1Ω, one can write for the input and output impedances

$$Z_{IN} = Z_{11} - \frac{Z_{12}^2}{Z_{22} + Z_L} \tag{7}$$

and

$$Z_{OUT} = Z_{22} - \frac{Z_{12}^2}{Z_{11} + Z_G} \tag{8}$$

respectively. Since the input and output couplings are identical,

$$Z_{11} = Z_{22}$$

$$\therefore \quad Z_{IN} = Z_{OUT}$$

It is obvious that by virtue of the external reactive components, the resonant frequency of the coupled cavity would be different from the natural resonant frequency of the excited normal mode. Thus in this equation, an implicit function of frequency, the resonant frequency can be obtained numerically.

The usual definition of resonance is that the imaginary part of the impedance vanishes at the resonant frequency. It is therefore

possible that by minimising numerically the imaginary part of equation (7) (or equation (8)), the resonant frequency can be deduced. However the accuracy of the result varies considerably with changing loop position and diameter.

The loss function defined as

$$L_A = \left(\frac{Z_L}{Z_L + Z_G}\right)^2 \left|\frac{E_g}{E_L}\right|^2 = \left|\frac{E_g}{2E_L}\right|^2 \qquad (9)$$

is given as

$$L_A(\text{dB}) = 20 \log_{10}\left(\frac{(Z_{11}+Z_L)^2 - Z_{12}^2}{2Z_{12}Z_L}\right) \qquad (10)$$

the minimum of which can be obtained at the coupled cavity resonant frequency and gives the insertion loss of the network. Thus, by minimising this loss function, the resonant frequency and insertion loss are obtained directly. The accuracy is high and consistent. By taking the half-power bandwidth, the loaded Q factor can be obtained. Such resonant parameters as the input (or output) reflection coefficient are computed directly from the input (or output) impedances.

$$\Gamma = (Z_{OUT} - Z_L)/(Z_{OUT} + Z_L) \qquad (11)$$

is the complex reflection coefficient from which the return loss and the input (or output) VSWR can be computed:

$$\text{Return loss (dB)} = -20 \log_{10}|\Gamma| \qquad (12)$$

and

$$\text{VSWR} = \frac{1+|\Gamma|}{1-|\Gamma|} \qquad (13)$$

2.5 Computation of Equivalent Network Parameters

As an initial step to the characterisation and general design parameters specification of a typical rectangular resonant cavity, the unknown terms in equations (4),(5) and (6) are determined. These are obtained by assuming that the coupled cavity forms an ideal case without extra losses of stored energy or any form of perturbation.

2.5.1 Cavity unloaded Q and the equivalent inductance

The original cavity is defined for complete boundary walls; on coupling, this is violated. As a first approximation we assume the coupled cavity unloaded Q to be the same as the unperturbed cavity Q for the mode of interest. For a TE_{101} rectangular cavity mode, this factor, best defined from energy relationships is given , from equation 2, as

$$Q_o = \pi b \sqrt{(\frac{\mu}{2\varepsilon})} / (R_s(a+2b)) \qquad (14)$$

where R_s is the skin resistance defined as

$$R_s = \sqrt{(\pi f_o \mu/\sigma)}$$

and σ is the conductivity of the material from which the cavity wall is constructed. μ, ε are the permeability and permittivity of the medium filling the cavity respectively.

Most of the equivalent lumped inductance proposed are direct energy-voltage or energy-current relationship. Such direct translation does not conform with the general impedance concept of a waveguide as proposed by Schelkunoff[7]. By regarding a cavity as an equivalence of a transmission line stub, we can proceed to find an equivalent inductance as follows:

Assuming the cavity is cut by a perfectly conducting wall from a waveguide of an equivalent characteristic impedance $Z_o(\omega)$, the impedance

seen from the input can be written as[11]:

$$Z(\omega) = jZ_o(\omega)\tan \beta\ell \ , \tag{15}$$

where Z and Z_o are functions of the frequency, β is the line propagation constant given as

$$\beta = \frac{2\pi}{\lambda_g}$$

and λ_g is the guide wavelength.

For a waveguide supporting TE mode, $Z_o(\omega)$ is given as[12]

$$Z_o(\omega) = \sqrt{\frac{\mu}{\varepsilon}} \cdot \frac{b}{a} \cdot \frac{\lambda_g}{c} \cdot \frac{\omega}{2\pi} \ , \tag{16}$$

where $c = 2.998E8\ ms^{-1}$ is the velocity of light in free space; and a,b are the guide's dimensions along x- and y-axes respectively. Neglecting any loss in the guide walls, in terms of LC series circuit, $Z(\omega)$ can be written as

$$Z(\omega) = j(\omega L_o - \frac{1}{\omega C_o}) \ . \tag{17}$$

If we further assume L_o, C_o independent of frequency at close proximity of resonance, then

$$\left.\frac{dZ(\omega)}{d\omega}\right|_{\omega\to\omega_o} = \left. L_o + \frac{1}{\omega^2 C_o}\right|_{\omega\to\omega_o} = \left. L_o(1 + \frac{\omega_o^2}{\omega^2})\right|_{\omega\to\omega_o}$$

Therefore

$$\left.\frac{dZ(\omega)}{d\omega}\right|_{\omega\to\omega_o} = 2L_o \tag{18}$$

By differentiating equation (14) with respect to ω and noting that

$n\lambda_g = 2\ell$ at ω_o for TE_{101} mode,

$$L_o = \tfrac{1}{2}\mu\frac{b}{a}\ell\frac{\lambda_{go}^2}{\lambda^2} \quad .$$

For $\ell = a$,

$$L_o = \mu b\frac{2a^2}{\lambda_o^2} \quad . \tag{19}$$

2.5.2 The mutual inductance, M[9]

The mutual inductance M between a loop and cavity is given as

$$M = \frac{\int\vec{B}.\vec{ds}}{I}$$

where I is the total current flowing in the cavity walls and $\vec{ds}$ is an element of the cross-sectional area of the loop. This has been analytically given[3] as:

$$M = \mu k_o \int\vec{H}_a.\vec{ds} \tag{20}$$

where $\vec{H}_a$ is the normalised magnetic field induction in the cavity.

Fig. 3a represents a two-dimensional schematic diagram of the coupling loops and the cavity plate containing them. The centres of the coupling loops are denoted O, O' and are t cm from the edges at Z=0 and Z=a respectively as shown in Fig. 3b. The mutual inductance between the loop centred on O and the cavity is given as

$$M_{11} = \pi\mu k_o d J_1\left(\frac{\pi d}{a}\right)\cos\left(\frac{\pi t}{a}\right)/\left(\frac{\pi}{a}\right) \tag{21}$$

Because the coupling is a symmetrical one

$$M_{22} = -M_{11} \tag{22}$$

2.5.3 Loop Inductance

Collin[15] using image methods has obtained for a semi-circular loop of diameter 2d and wire diameter 2r in a waveguide an expression for its reactance given as

$$X = \frac{\omega\mu d}{2}\left(\ln\frac{8d}{r} - 2\right) - \frac{\omega\pi^2 d^4 \mu}{2}\left[\frac{k_o^2}{4\pi b}(2-\gamma) + \frac{13\pi}{24a^2 b} + \frac{0.6}{\pi b^3} + \right.$$

$$\left. + \frac{3k_o^4 b}{576\pi} + \frac{k_o^2}{4\pi b}\ln\frac{k_o^2 ab}{4\pi(1-\cos k_o b)} - \frac{1}{2ab}\sum_{n=2}^{\infty}\left(\frac{k_o^2}{\Gamma_{no}} + \Gamma_{no} - \frac{n\pi}{a} + \frac{k_o^2 a}{2n\pi}\right)\right] \quad (23)$$

where $k_o = \frac{2\pi}{\lambda_o}$,

and

$$\Gamma_{no} \cong \frac{n\pi}{a} - \frac{k_o^2 a}{(2n\pi)}$$

It is observed that for $\frac{d}{r} \geq 8$, the exact inductive reactance differs from the static formula for the self-inductive reactance of a semi-circular loop with a background earth-plane by less than 5%. Therefore, the loop inductance can be represented by the inductance of a half-loop in free space given as

$$L = \frac{\mu d}{2}\left(\ln\frac{8d}{r} - 1.75\right) . \quad (24)$$

The background plane of the loop is not a complete ground plane. Because the coupling is by induction, the radiation resistance associated with loops in free space is neglected. The wire resistance of the loop is neglected as this is very small for copper or silvered-copper wire in common use. This approximation is strictly reliable for cases when $2r \cong 0.2d$. Moreover the loop wire is expected to be thin otherwise its perturbing influence would distort the fields in such a way that equation (22) becomes invalid. An optimum range of the ratio of wire diameter to loop diameter can be defined as presented analytically in the following section.

2.6 Optimum ratio of wire to loop diameters

Computer solutions to equations (4), (5) and (6) and experiments using typical semi-circular wire loops designed from various gauge wires employing 1GHz, 1.5GHz and 1.7GHz resonant cavities were undertaken. The aim is to establish the optimum range of $\frac{d}{r}$ for best cavity overall performance. Actually, the first two cavities were used to establish the relationship between d and r while the 1.7GHz circular cavity was employed to check the relationship.

With a 1.5GHz resonant cavity coupled by a loop of 1.0cm diameter chosen from wire gauge ranging from 16 to 24, Table 1(a) shows the way the resonant parameters depend on the wire diameter. It is clear that the best unloaded Q values were obtained for wire diameters 0.7112mm and 0.9144mm but the best overall performance was achieved with 20 gauge wire representing 9.144% of loop diameter. Theory and practice could be observed to be in close agreement for this ratio.

The 1GHz cavity being bigger than the 1.5GHz cavity demands a bigger loop. For the cavity, the loop size was chosen as 1.5cm diameter. Table 1(b) contains data on the cavity and shows that bigger wire was necessary to achieve the best overall performance.

From the two tables, by comparing theory and practice, the best performance can be achieved when the wire size is between the narrow range 9.1%-12% the size of the loop irrespective of the operating wavelength. An inference one can draw here is that the increasing perturbing influence of the loop for bigger loop sizes is the cause of lower measured values of loaded Q and the general departure from theory of practice. One could have attributed the differences between theory and practice for thin loop wires on the larger wire resistance due to the skin effect but this cannot be adequately justified by theory. Table 1(c) obtained

Table 1(a)

Cavity type: Rectangular
Dimensions: 13.9945 x 13.9945 x 4.0 cm
Loop position: t = 2.5cm
Loop diameter: = 1.0cm
Uncoupled cavity, Q_o = 15000
Resonant frequency = 1.5GHz
Coupling cable type = RG58C/U 50Ω

Wire dia. (mm) (Gauge)	Wire dia. / Loop dia.	Insertion Loss dB		Loaded Q		Unloaded Q
		Theory	Practice	Theory	Practice	(Practice)
1.625 (16)	0.16256	0.45	0.44	758	662	13402
1.2192 (18)	0.12192	0.52	0.54	885	822	13640
0.9144 (20)	0.09144	0.62	0.64	1025	1019	14251
0.7112 (22)	0.07112	0.70	0.66	1158	1041	14225
0.5588 (24)	0.05588	0.78	0.80	1294	1221	13869

Table 1(b)

Cavity type: Rectangular
Dimensions: 21.101 x 21.101 x 6.03 cm
Loop position, t = 4.0cm; Loop size: 1.5cm diameter
Uncoupled cavity, Q_o; 18000
Resonant frequency, 1.0GHz
Coupling cable type: RG58C/U 5001

Wire dia. (mm) (Gauge)	Wire dia. / Loop dia.	Insertion Loss dB		Loaded Q		Unloaded Q
		Theory	Practice	Theory	Practice	(Practice)
1.6256 (16)	0.1084	0.49	0.46	1006	876	16980
1.4224 (18)	0.0948	0.52	0.54	1077	1037	17196
1.2192 (19)	0.08128	0.58	0.56	1166	1076	17035
0.9144 (20)	0.061	0.65	0.70	1332	1304	16842

Table 1(c)

Cavity type: Cylindrical cavity
Frequency range: 1.4-1.7GHz
Loop size: 1.0cm diameter
Loop position, t = 3.5cm
Uncoupled cavity, Q = 22500 at 1.72GHz
Resonant frequency 1720MHz (circular cavity)

Wire dia. (mm) (Gauge)	Wire dia. / Loop dia.	Insertion Loss(dB)	Loaded Q	Unloaded Q
1.2192 (18)	0.12192	0.46	930	18024
0.9144 (20)	0.09144	0.48	1112	20871
0.7112 (22)	0.07112	0.66	1571	21461
0.5588 (24)	0.05588	0.70	1514	19550

for a 1.7GHz cylindrical tunable cavity supporting TM_{010} mode constitutes a further evidence that these results may be general for all types of resonant cavities.

From Table 1(c) it is possible to conclude that the relative size of wire diameter to loop diameter is an important quality factor for a cavity operating in its fundamental resonant mode. (Noting that we are basically concerned with the cavity excited in its lowest resonant mode). Later experiments were undertaken to characterise the loop and find the optimum loop size for a cavity excited in its fundamental resonant mode. It will also be shown later that the choice of the loop size depends, additionally, on the expected resonant characteristics.

2.7 Characterisation of the loop

The solutions to equations (4), (5) and (6) were obtained by solving for the resonant frequency numerically. Such solutions have shown that there is disagreement in the resonant parameters obtained from theory and those obtained from practice even though the trend of variations remains the same. A study of coupled resonant cavities has revealed that the additional losses are due to any or both of:

(i) the perturbing influence of the loop wire and the discontinuity in the wall due to the coaxial line

(ii) the direct coupling from loop to the coaxial line.

Chapter Five is designed to examine the former case.

Literature has shown that the loop diameter must be a small fraction of the cavity dimensions. In addition, the excitation current must be constant over the length of the coupling loop for the self-inductance term, equation (24), to be applicable. Hence

$$\frac{\pi d}{\lambda} \ll \frac{1}{2}$$

i.e.

$$\frac{d}{\lambda} \ll \frac{1}{2\pi}$$

If the loop is too small, however, it results in undercoupling which manifests appreciably in the insertion loss. Too large a coupling loop results in over-coupling and therefore low selectivity. Table 2(a) compares theory and practice when semi-circular loops are used.

The insertion loss for loop sizes smaller than 1.0cm could be observed to depart appreciably from theory while bigger loop sizes left the cavity with lower selectivity than theory would suggest. At mid-range of loop size, theory and practice can be said to closely agree except for the loss in the unloaded Q. However, the loss in Q is more

Table 2(a)

Cavity type: rectangular
Frequency: 1.5GHz range
Wire diameter: 0.9144(mm) -(20 gauge wire)
Loop position, t = 2.5cm
Coupling cable: RG58 C/U 50Ω

Loop dia. (cm)	Insertion loss (dB) Theory	Practice	Q_L Theory	Practice	Q_o Theory = 15000
0.6	1.95	2.22	3020	2856	12663
0.8	0.98	1.12	1525	1450	13639
1.0	0.62	0.66	1025	1040	14216
1.2	0.44	0.42	741	666	14102
1.5	0.30	0.32	515	442	13021

pronounced with smaller and larger loops. For the size of the coupling cable and the resonant frequency therefore the best resonant parameter is achieved when the loop is centred closely to a diameter of $\frac{1}{20}\lambda_o$.

From the Table and later experiments it became clear that there is usually a general departure from theory when the ratio $\frac{\text{loop diameter}}{\text{coaxial line radius}}$ approaches unity. That is, as the diameter of the coupling loop approaches the radius of the coupling cable there is increased additional losses. This has been attributed to the increased direct coupling from loop to the line. Similar leakage has been represented by a capacitance in parallel with the loops self-inductance term (Howson). Such loss could however be represented by an LCR equivalent circuit. For the 1.5GHz cavity with loop diameter 1.0cm and coupling coaxial line equivalence of RG58 C/U 50 coaxial cable, practice agrees closely with theory considering selectivity and insertion loss. The resonance loss with big loops is due mostly to the perturbing influence of the loop

wire. A practical situation where the ratio would approach unity is not generally recommended. However, in some situations this cannot be helped. For example, when the need arises for increased power transmission the use of a bigger cable is inevitable. In addition, it might be necessary to design a cavity for high selectivity with minimum additional loss in Q. The demand for high selectivity requires small coupling loop,hence a tentative increased insertion loss and added loss in the Q. In the former case, it is possible to compensate for additional losses by increasing the loop diameter. The case with such loop adjustment is that more energy is coupled into the cavity than the line. There is thus decrease in insertion loss but more at the expense of selectivity which may not augur well for the design specification. The situation becomes more critical when high selectivity is required with high power transmission capability of the cable. It should be noted with reservation that the best way to offset the effect of the coaxial line size is not by increasing the loop diameter because, as is obvious from Table 2(b), such would on its own cause extra loss in the unloaded Q.

For a TE_{101} rectangular cavity, and most networks employing cavities excited in their fundamental resonant modes, the magnetic field is usually invariant in the direction along the plane of the loop normal to the plate containing it, y-axis in this case. This facilitates the adjustment of the loop such that the excited field 'falls totally' within the cavity and the amount of direct coupling thus reduces to the minimum level. A geometrical structure appropriate for this has been found in a dome-like loop for which the perfect semi-circular loop is carried on two short and parallel legs each of length d_1, as in Fig. 3(b).

Table 2(b) (See Table 2(a) for data on cavity)

Coupling cable UR72 50Ω (diameter 7.2mm)

Loop diam. (cm)	Insertion Loss		Q_L		Q_o
	Theory	Practice	Theory	Practice	
0.6	1.95	2.68	3020	2975	11205
1.0	0.62	0.70	1025	1055	13624
1.5	0.30	0.32	471	495	13017

Table 3(a)

Cavity: Rectangular
Dimensions: 13.843 x 13.843 x 4.0767 cm
Loop diameter: 0.70 cm
Loop position t = 2.5 cm

d_1 (mm)	Insertion loss (dB) Theory : 1.32	Q_L Theory: 2141	Q_o Theory ≅ 15000
0.0	2.02	2488	11992
1.0	1.90	2443	12436
2.0	1.64	2239	13011
3.0	1.38	2053	13982
4.0	1.30	1964	14132
5.0	1.02	1509	13622
6.0	0.84	1184	12842
7.0	0.62		

Table 3(b)

Design data as for Table 3(a)

Loop diameter: 1.0 cm

d_1 (mm)	Insertion loss (dB) Theory : 0.61	Q_L Theory : 1036	Q_o Theory : 15200
0.0	0.72	1078	13550
1.0	0.66	1011	13821
2.0	0.62	964	13993
3.0	0.56	866	13984
4.0	0.54	757	12562

As a means of characterising the loop, the size of the coupling cable was increased by replacing the RG58 C/U cable by UR 72 50Ω type coaxial line, diameter 7.2mm.

Tables 3(a) and (b) show theoretical and practical data obtained for loop diameters 7.0mm and 10.0mm respectively. As can be observed from Table 3(a) there was close agreement between theory and practice for the length d_1 between 3mm and 4mm. In terms of insertion loss there was close agreement when d_1 was 4mm (or close to 4mm). Values lower than this would generally cause additional insertion loss resulting from leakages while values higher up would decrease the selectivity more than it would improve the insertion loss as a result of increased perturbing influence of the loop. In other words, beyond a certain critical value of d_1 related to the loop and line diameters, theory and practice would not agree. With a 1.0cm loop, Table 3(b), the length d_1 of the 'dome loop' was found to decrease for an adequate compensation. From Tables 2(b), 3(a) and (b), one can observe that when the loop diameter is not less than about three times the cable diameter, theory and practice closely agreed, in that sense of it, with minimum possible additional loss with the use of 'ordinary' semi-circular loop. Below the limit, it is possible to recoup the loss through the dome structure for which the length d_1 is given as

$$d_1 \cong 2r_c - d - \delta \qquad (25)$$

and for $2r_c > d$, where δ denotes that d_1 is a bit smaller than $2r_c - d$. It should be emphasised that this adjustment of loops would only bring more closely the agreement between theory and practice and cannot offset totally the additional loss by virtue of discontinuities in the wall introduced by the coupling. Moreover the extra loss due to perturbing influence of loop wire itself can only be reduced or eliminated when

the loop is removed completely from the cavity ! It has proved possible in addition to shift empirically any of the insertion loss and selectivity at will using the dome-like loop structures. In other words, as will be shown later in the analysis, it is possible to trade off any of the insertion loss and selectivity for one another simply using dome-loop structures.

2.8 Test Experiments

Effects of Coupling Loop Position and Diameter

Earlier in the characterisation of coupled cavities, variation of the resonant parameters with the loop and wire sizes were investigated. From the investigation, it proved possible to obtain the optimum design parameters for which theory and practice are best related. Using these optimum design parameters, the effects of loop positions on the parameters could be investigated.

Figs. 4(a),(b),(c) and (d) show plots of frequency, loaded Q, insertion loss and unloaded Q against normalised coupling position, $\frac{2t}{a}$, respectively. As regards selectivity and insertion loss plots, there are close agreements between theory and practice; the slight variations are experimentally allowable. One striking fact is that it is possible to obtain as low or as high selectivity as possible and as permitted by the minimum allowable insertion loss simply by altering the loop positions in the cavity. However, observations have revealed, Fig. 4(d), that as much as 4% variation in Q_o is possible even with coupling positions within the range $0.15 \leq \frac{2t}{a} \leq 0.6$. The best coupled cavity performance seems achievable for $0.2 \leq \frac{2t}{a} \leq 0.4$, for which the loss in Q_o of less than 6% is achievable but with limited variability of selectivity and insertion loss. Even in view of experimental errors, more additional loss is incurred as t increases beyond $\frac{2t}{a} = 0.5$. Moreover,

the closer the positions of the loops are to the centre, the closer their proximity contrary to the assumptions in defining equations (4), (5) and (6).

The possibility of changing the selectivity and insertion loss by alteration of the loop position is discouraged because of either narrow range by which the parameters can be varied otherwise wide variations of Q_o or the likely invalidation of the design equations (4), (5) and (6). More so the physical alteration of a loop position is not an easy task if the best cavity performance is to be achieved. However, by varying the loop positions it is possible, as is obvious from Fig. 4(d), to get good coupling position for a reasonably high Q_o. It is also possible in this case to design the cavity and coupling for good Q_o and selectivity for as high or as low an insertion loss.

Figs. 5(a),(b),(c) and (d) show plots of resonant frequency, loaded Q, insertion loss and unloaded Q as functions of loop diameter (corrected loop sizes) respectively. The plots of Figs. 5(b) and (c) show that theory and practice agree closely and that it is as well possible to vary any of the insertion loss and selectivity at the expense of one another in the same manner as altering coupling positions. Better still, Q_o variations for a wide variation of insertion loss and selectivity is limited to about 2% as in Fig. 5(d). By coupling the cavity at the optimum coupling position range $0.2 \leq \frac{2a}{t} \leq 0.4$, it is possible, as in this case, to obtain less than 6% loss in Q_o even with wider variation of selectivity and insertion loss. (For all practical cases, a resonance loss of 7% should be allowed even though being aware that the coupled cavity may not exhibit a resonance loss in Q_o of more than 6%). In general, the selectivity would approach the unloaded Q_o as the insertion loss increases.

This study, so far, has revealed the possibility of empirically adjusting the theoretical unloaded Q_o to conform with practice while it has made known that measured insertion loss and selectivity can be approximated to the calculated values, if need be. On the other hand, even though the plots of Figs. 4(a) and 5(a) show good agreement between theory and practice and by projection, that theory and practice follow the same trend, the discrepancies cannot be tolerated where applications demand exact resonant frequencies. Such differences cannot however be helped in reality because of uncertainties in the geometry and dimensions of a physical phenomenon. The exact resonant frequency is always obtained by tuning.

2.9 Conclusions

The analysis above has shown that resonant cavities characteristics can be optimised to some extent by variation of coupling loop shape which compensates in part for the effects of coupling port hole and the perturbing influence of the loop wire. In addition, it has been shown that by proper choice of the shape and dimensions of the loop, theory and practice can be made to agree more closely. To the nearest approximation, a loop coupled cavity has been shown to have operating average Q factor centred on 94% of the unperturbed empty cavity Q_o. However, as has been demonstrated, the value would vary with both coupling loop size and position in the cavity. It has been found that the best coupling loop diameter is about one-twentieth the resonant wavelength while the best loop wire size is between 9.1% and 12% of the size of the loop. It is evident that insertion loss and loaded Q can be traded by varying the dimensions of the coupling loop and position, but the change in insertion loss is not usually commensurate

with the change in loaded Q as to keep the unloaded Q factor constant. While leakages from the cavity manifest more on the insertion loss and exerts less influence on the selectivity than expectations, various material perturbations influence the resonant frequency and selectivity more than the insertion loss.

Frequency shift caused by perturbing influences of the hole and loop wire and that partly due to geometrical and mechanical deviation of the cavity shape, unlike Q_o, insertion loss and Q_L, cannot be tolerated; usually this can only be corrected by means of a tuning screw (Chapter 4).

The analysis has demonstrated further that over quite a wide range of insertion loss and loaded Q variabilities, Q_o may not vary by more than 4%. However, loss in Q_o or Q_o variation would depend on the extent of perturbation of a cavity resonator and its departure from the ideal situation.

2.10 References

1. Schelkunoff, S A: 'Representation of impedance functions in terms of resonant frequencies', Proc. IRE, Vol. 32, pp. 88-89, Feb. 1944.

2. Condon, E U: 'Forced oscillations in cavity resonators', J. Appl. Physics, Voll 12, p.129, 1941.

3. Montgomery, C G; Dicke, R H & Purcell, E M: Principles of Microwave Circuits', Radiation Lab. Series Vol. 8, McGraw Hill Book Co. Inc, 1948.

4. Slater, J C: 'Forced oscillations and cavity resonators', RL Report No. 188, Dec. 1942.

5. Hansen, W W: 'A type of electrical resonator', J. Appl. Physics, Vol. 9, p.654-663, 1938.

6. Ragan, C L: 'Microwave transmission circuits', Radiation Lab. Series Vol. 9, McGraw Hill Book Co. Inc., NY, 1948.

7. Schelkunoff, S A: 'Impedance concept in waveguides', Quarterly of Appl. Maths., Vol. II, No. 1, pp. 1-15, (April 1944).

8. Crout, P D: 'An extension of Lagrange's equations.... ', J. Appl. Physics, Vol. 19, 1948, p.1007

9. Ishii, T K: 'Microwave Engineering, Ronald P., 1966.

10. Kinzer, J P & Wilson, J G: 'Some results on cylindrical cavity resonators', BSTJ, Vol. 26, pp. 410-442, (1947).

11. Pipes, L A: 'Computation of the impedances of non-uniform lines by a direct method', AIEE, Nov. 1956, pp. 551-4.

12. Wheeler, G J: Introduction to Microwaves', Prentice-Hall Inc., Englewood Cliffs, NJ, 1963, p.63.

13. Ghose, R N: Microwave circuit theory and analysis', McGraw Hill Book.Co. Inc., NY, 1963.

14. Schelkunoff, S A: Electromagnetic waves', Bell Telephone Labs Series D. van Nostrand Com. Inc., NY, 1943.

15. Collin, R E: Field theory of guided waves , McGraw Hill Book Co. Inc., 1960, p.282.

16. Casimir, H B G: 'On the theory of electromagnetic waves in resonant cavities', Philips Res. Rpt., Vol. 6, pp. 162-82, June 1951.

17. Howson, P R & Howson, D P: 'The design of VHF and UHF transmitter combiners using loop-coupled cavity resonators', University of Bradford, PGEEE Rep. No. 296/1.

18. Owens, R P: 'Equivalent circuit parameters of a cavity resonator', Electronics Letters, Vol. 3, No. 7, July 1967, pp. 327-8.

19. Toman, M P & Ishii, T K: 'Equivalent circuit parameters of a cylindrical cavity resonator', Electronics Letters, Vol. 3, 1967, pp. 36-38.

20. Collin, R E: 'Foundation for microwave engineering', McGraw Hill, 1966, Ch. 5.

21. Ramo, S & Whinnery, J R: 'Fields and waves in modern radio', John Wiley & Sons Inc., NY, 1964.

22. Matthaei, G L; Young, L & Jones, E M T: 'Microwave filters, impedance matching networks and coupling structures', McGraw Hill Book Co., 1964, pp. 35-39.

23. Altman, J L: 'Microwave circuits', D Van Nostrand Co. Inc., NY, 1964.

24. Seidel, D B: 'Excitation of a wire in a rectangular cavity', Vol. 1, Theory, Report No. AD-A059 812, May 1978.

25. Slater, J C: 'Microwave electronics', Rev. of Mod. Phys., Vol. 18, p.467, 1946.

26. Goubau, G: 'Electromagnetic waveguides and cavities', Pergamon Press, 1961.

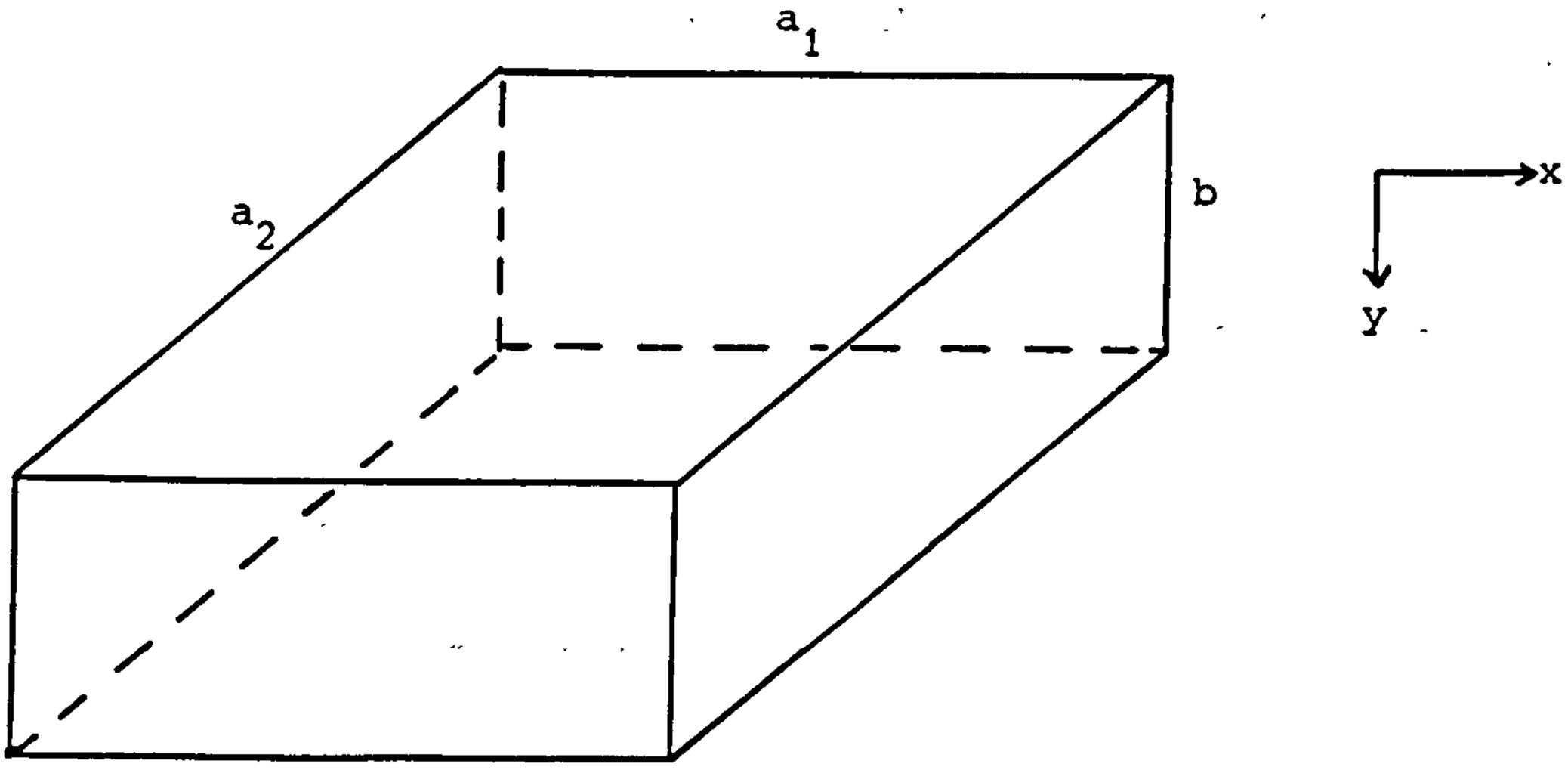

Figure 1 A rectangular cavity

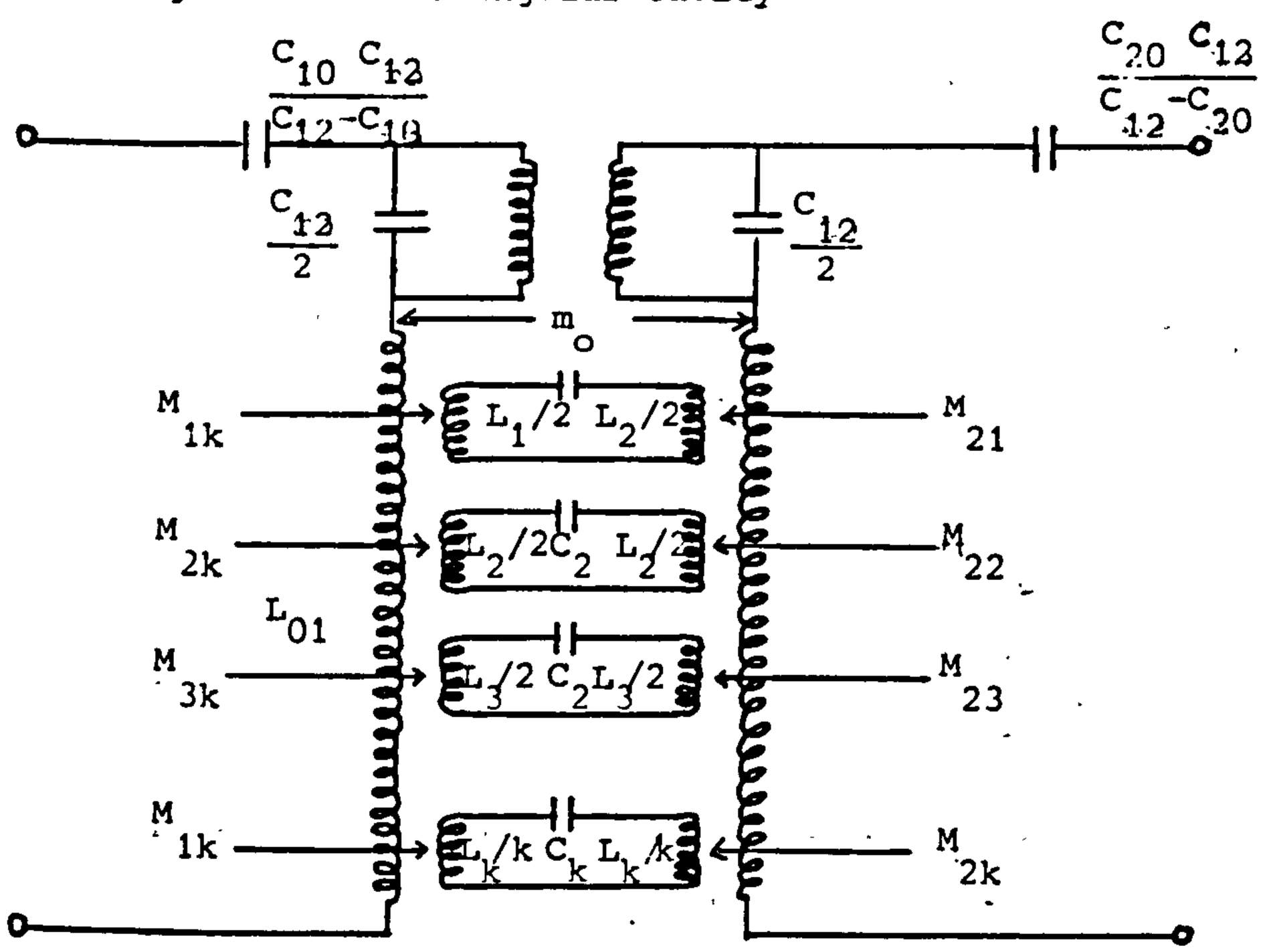

Figure 2(a) Equivalent circuit of lossless two-port resonant cavity

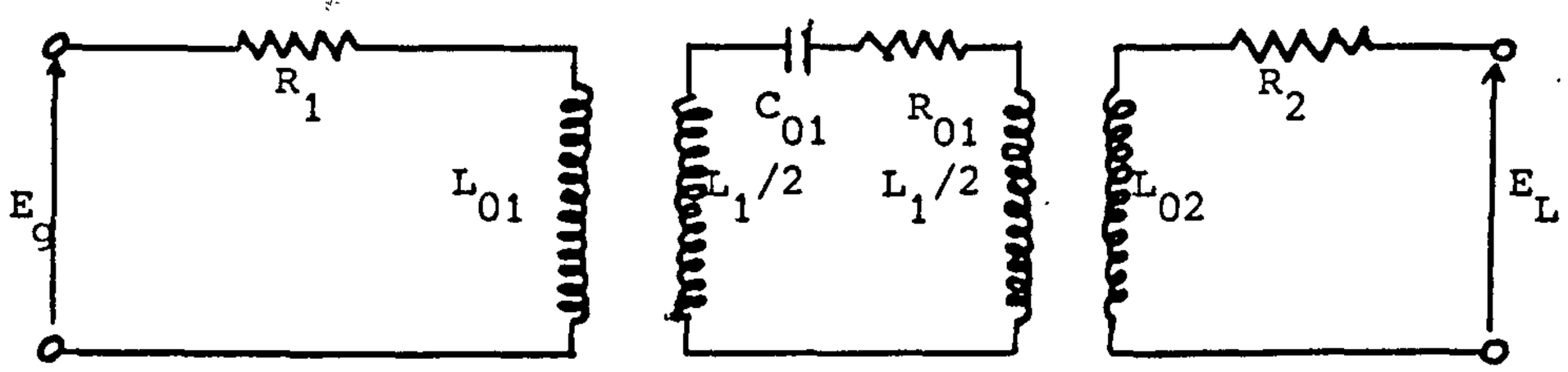

Figure 2(b) Modified single mode version of Figure 2(a)

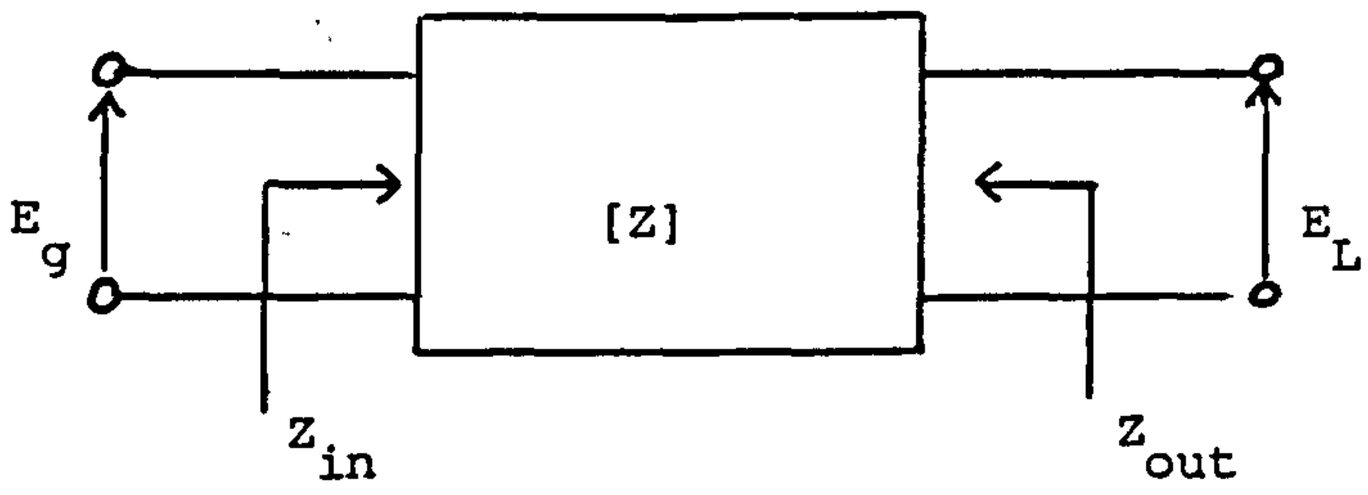

Figure 2(c) Block diagram of Figure 2(b)

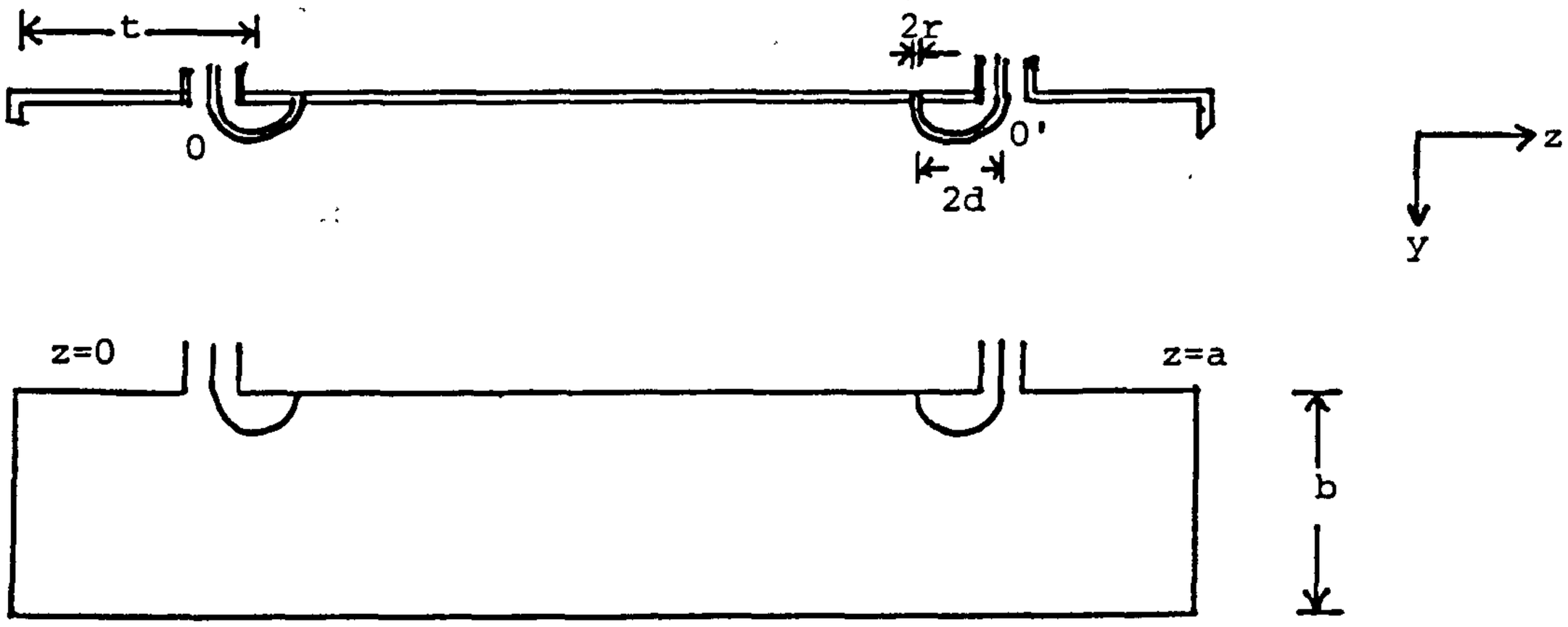

(a) Cross-section of the plane of the loops showing loops' dimensions and positions and the cavity internal dimensions

Figure 3

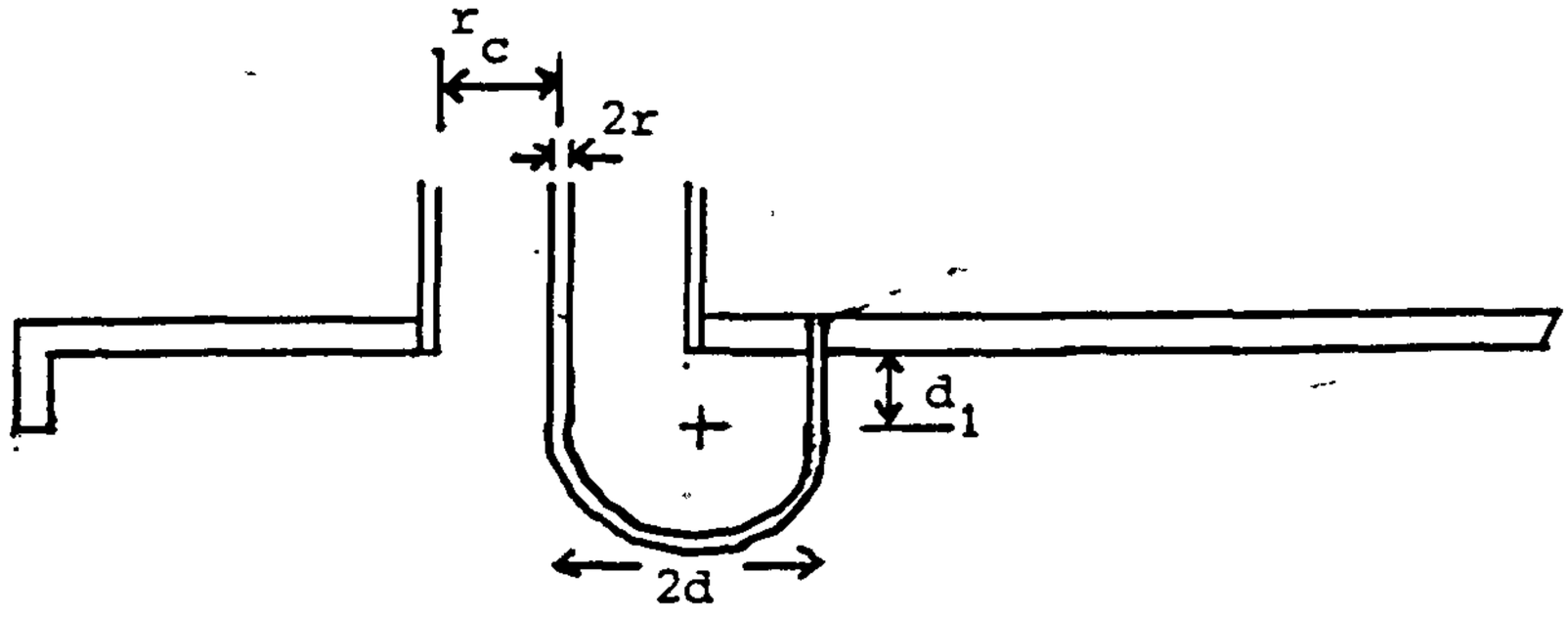

(b) A dome-shaped loop

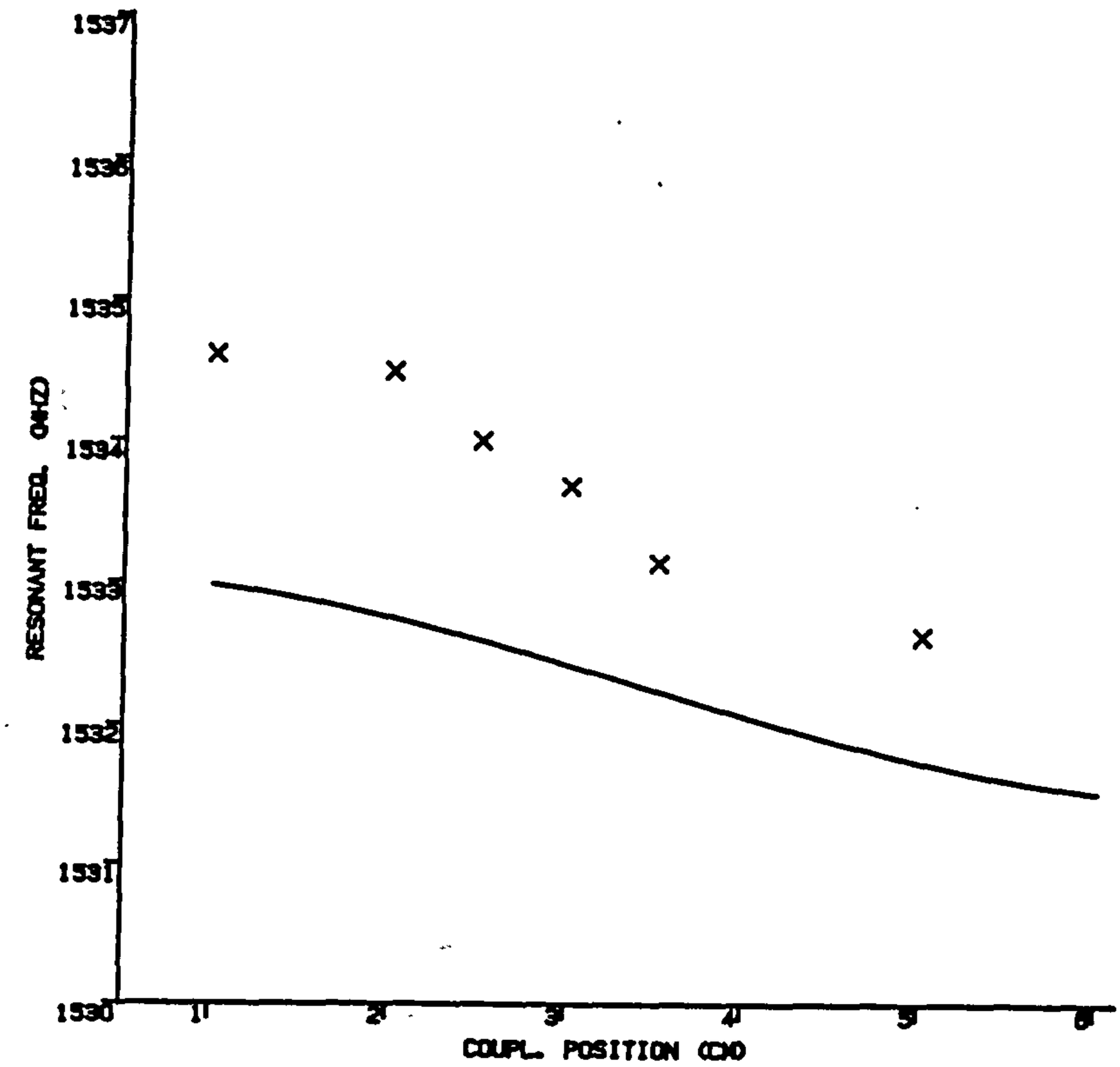

(a) Resonant frequency

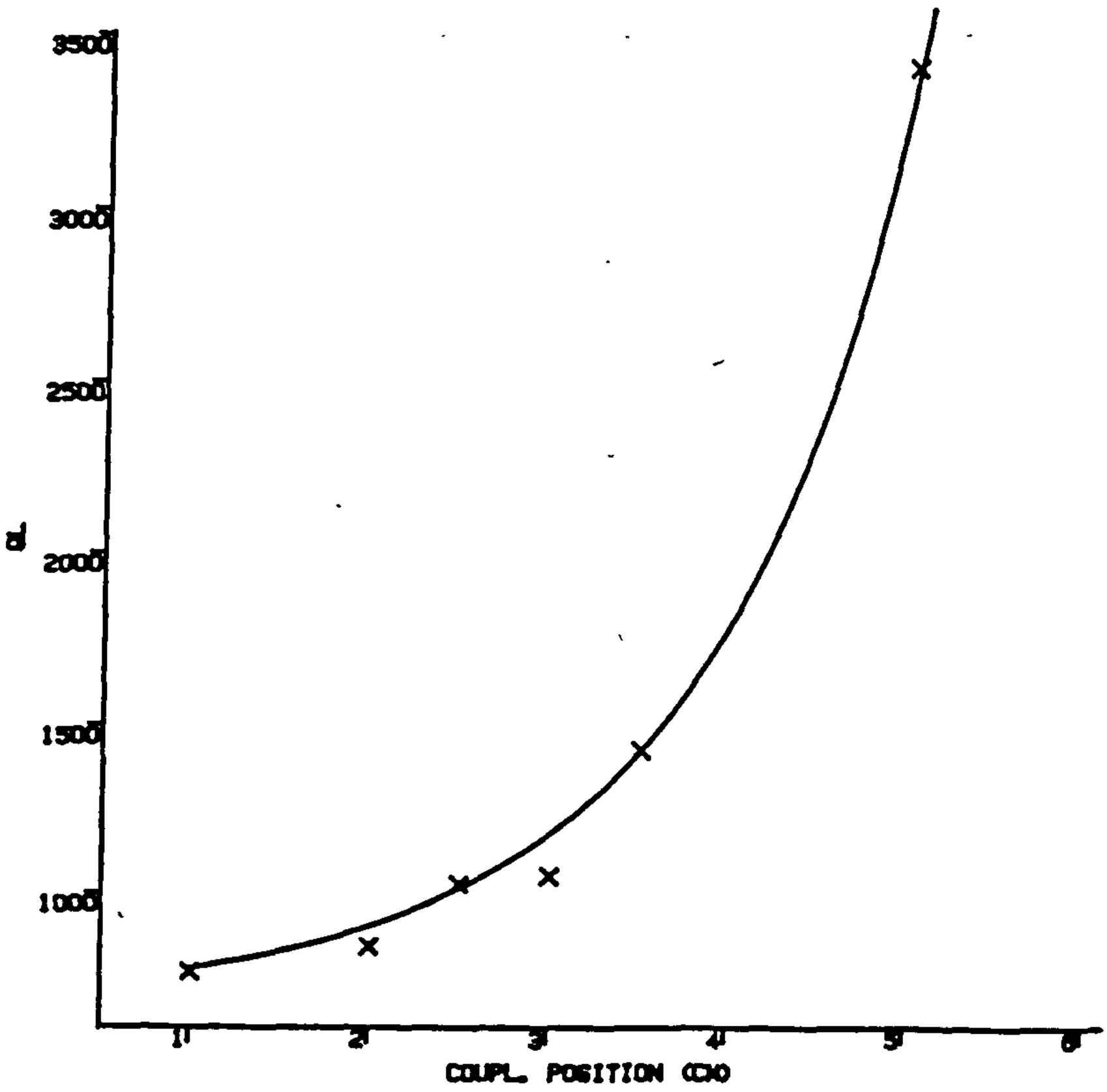

(b) Loaded Q

Figure 4 Resonant characteristics vs. coupling position

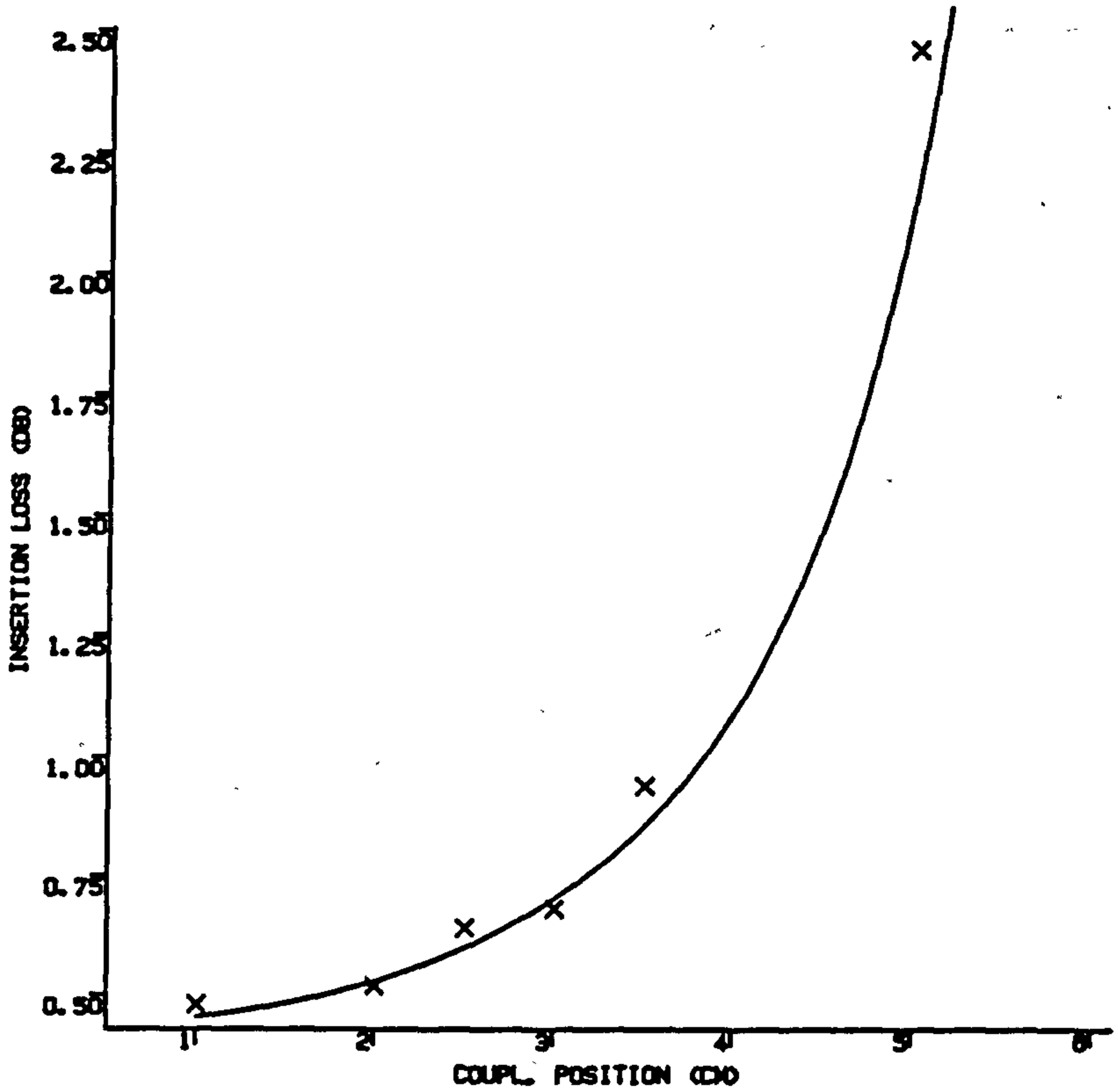

(c) Insertion loss

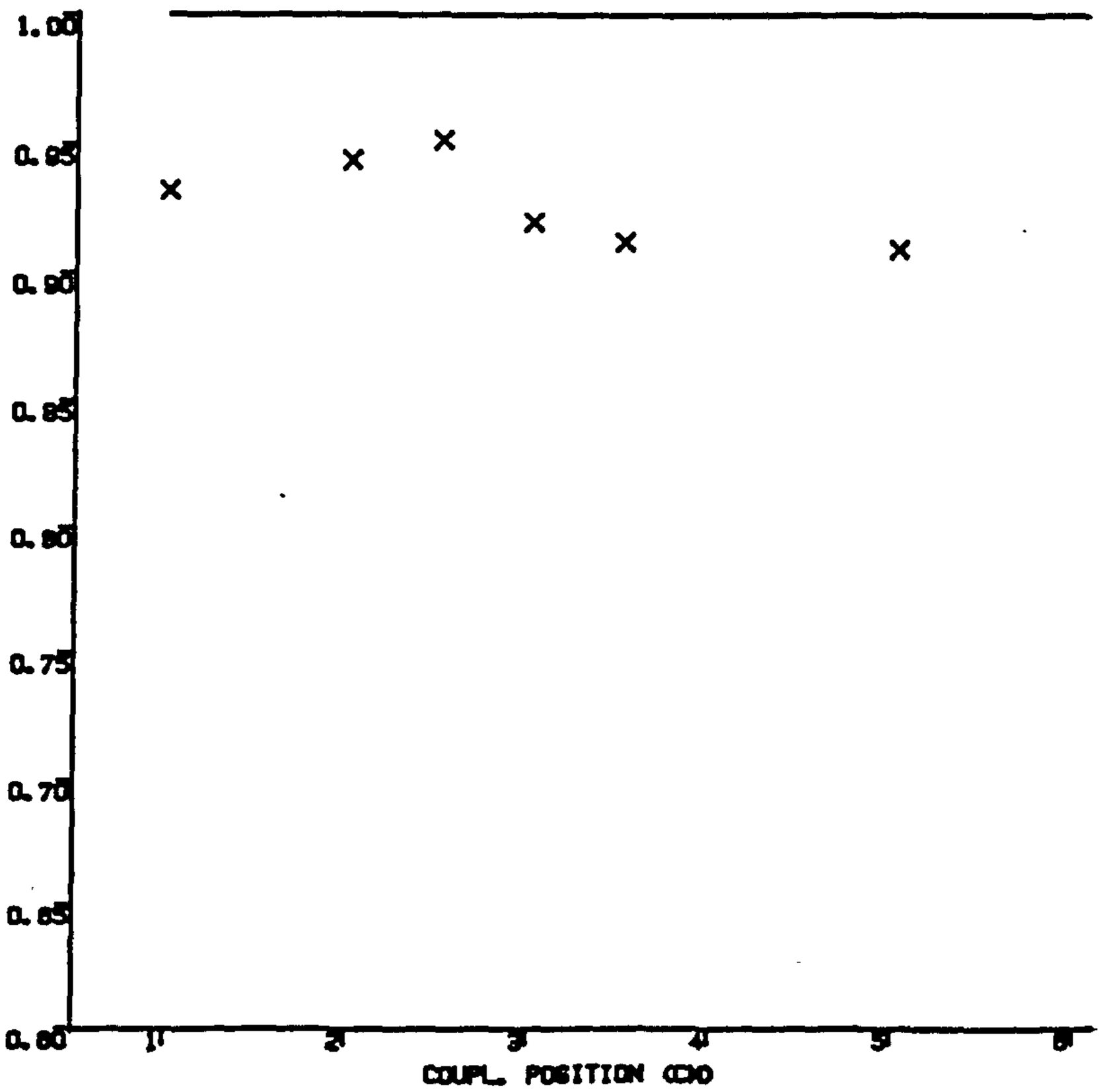

(d) Normalised Q

(Q_o = 15200)

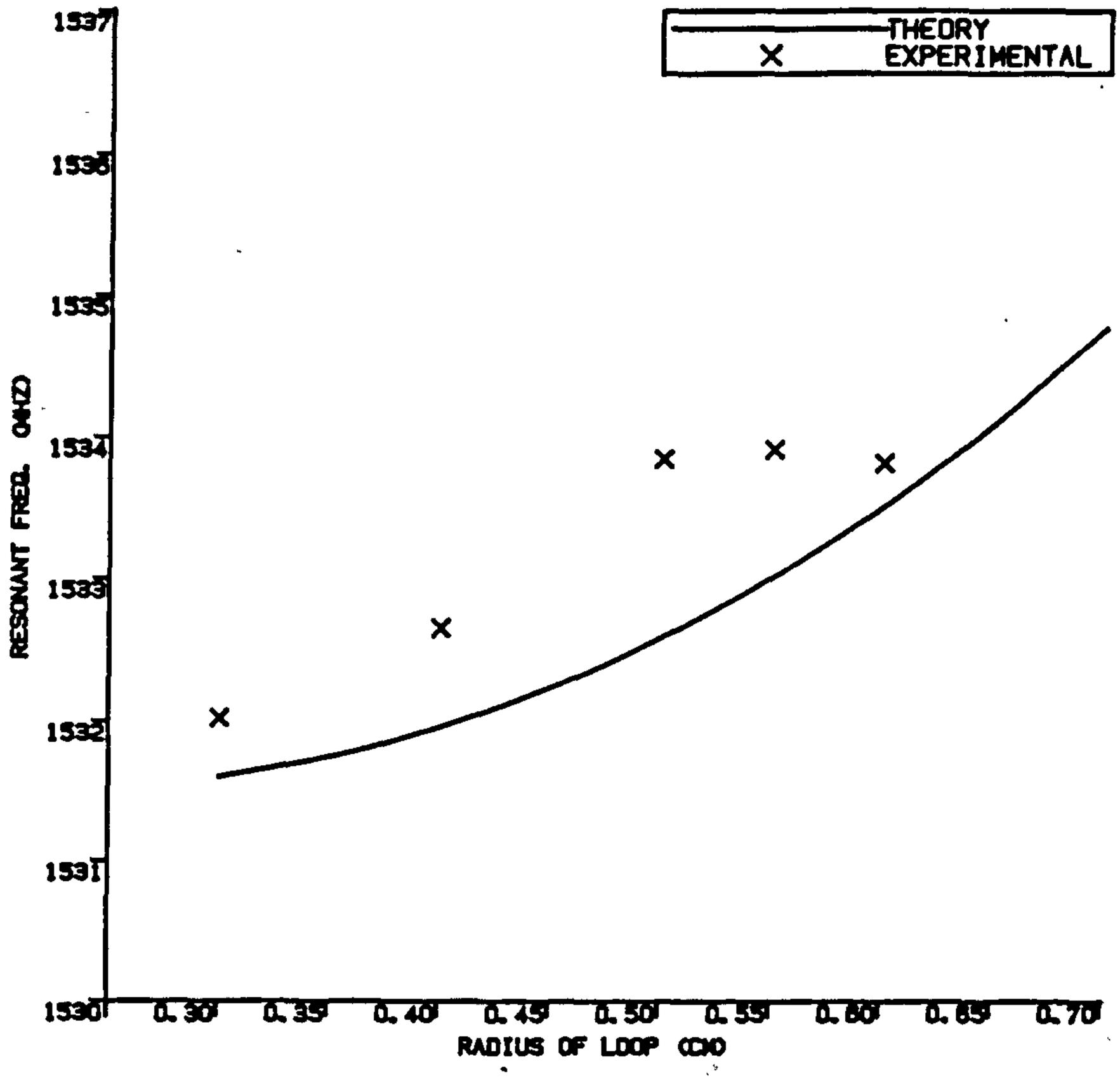

(a) Resonant frequency

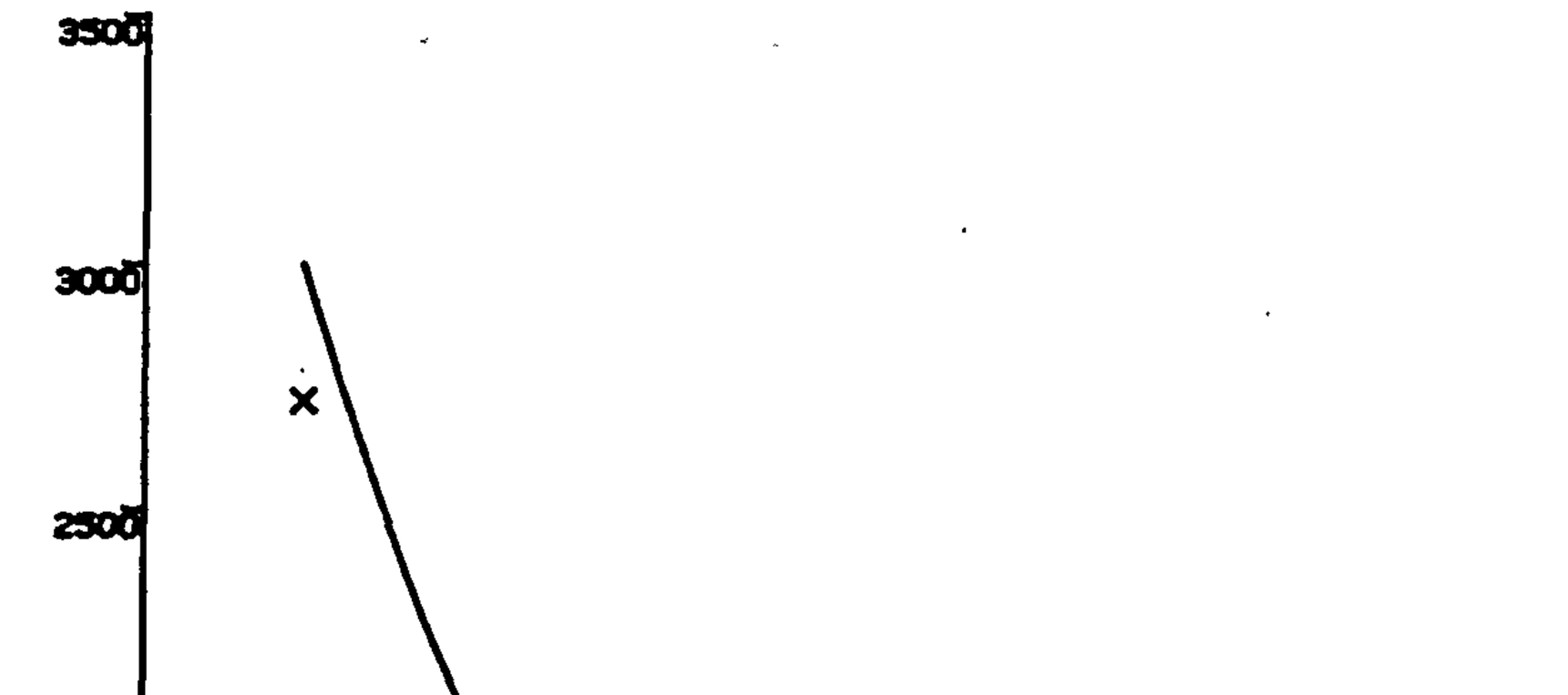

(b) Loaded Q

Figure 5 Resonant characteristics vs. coupling loop radius

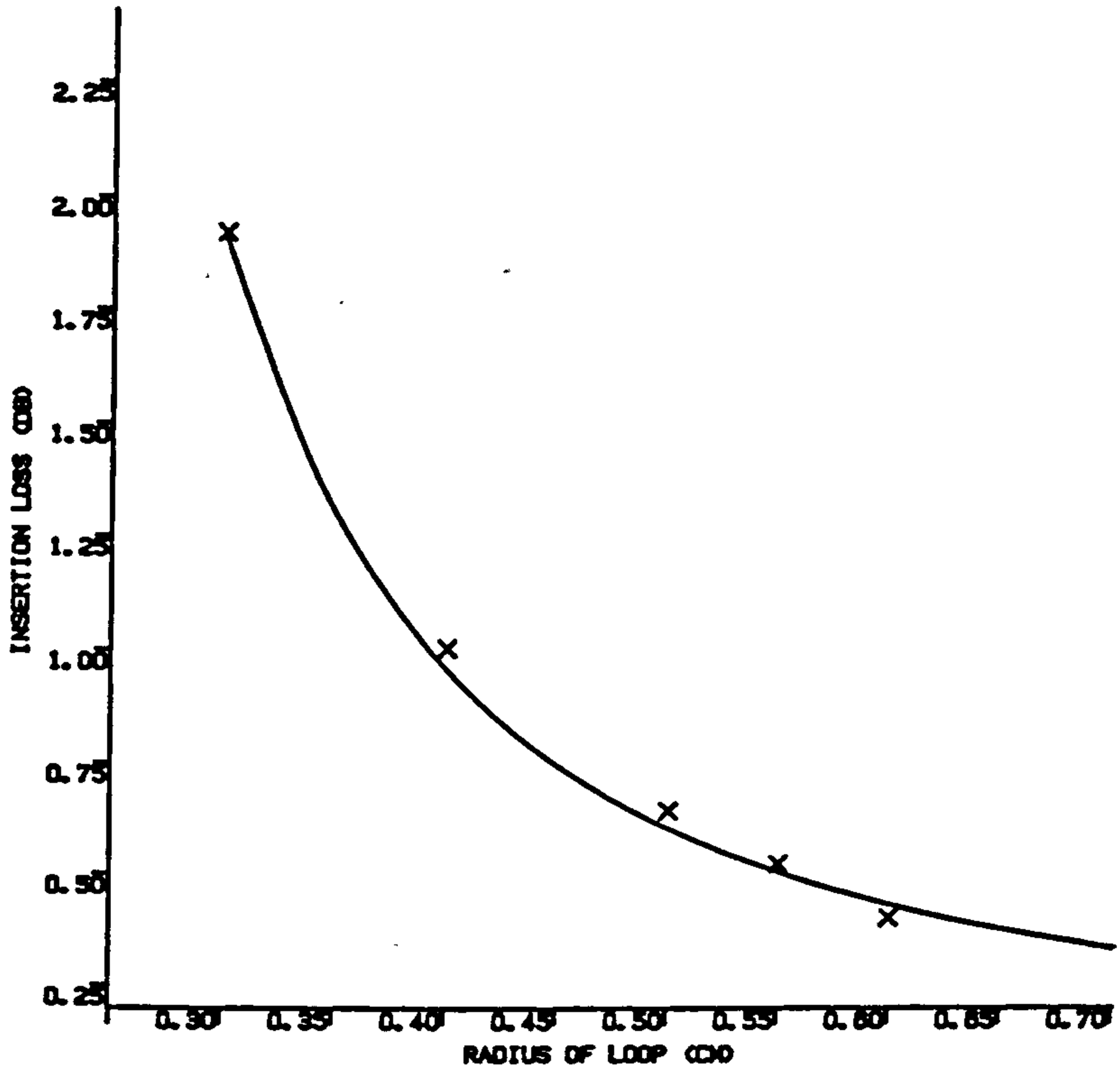

(c) Insertion loss

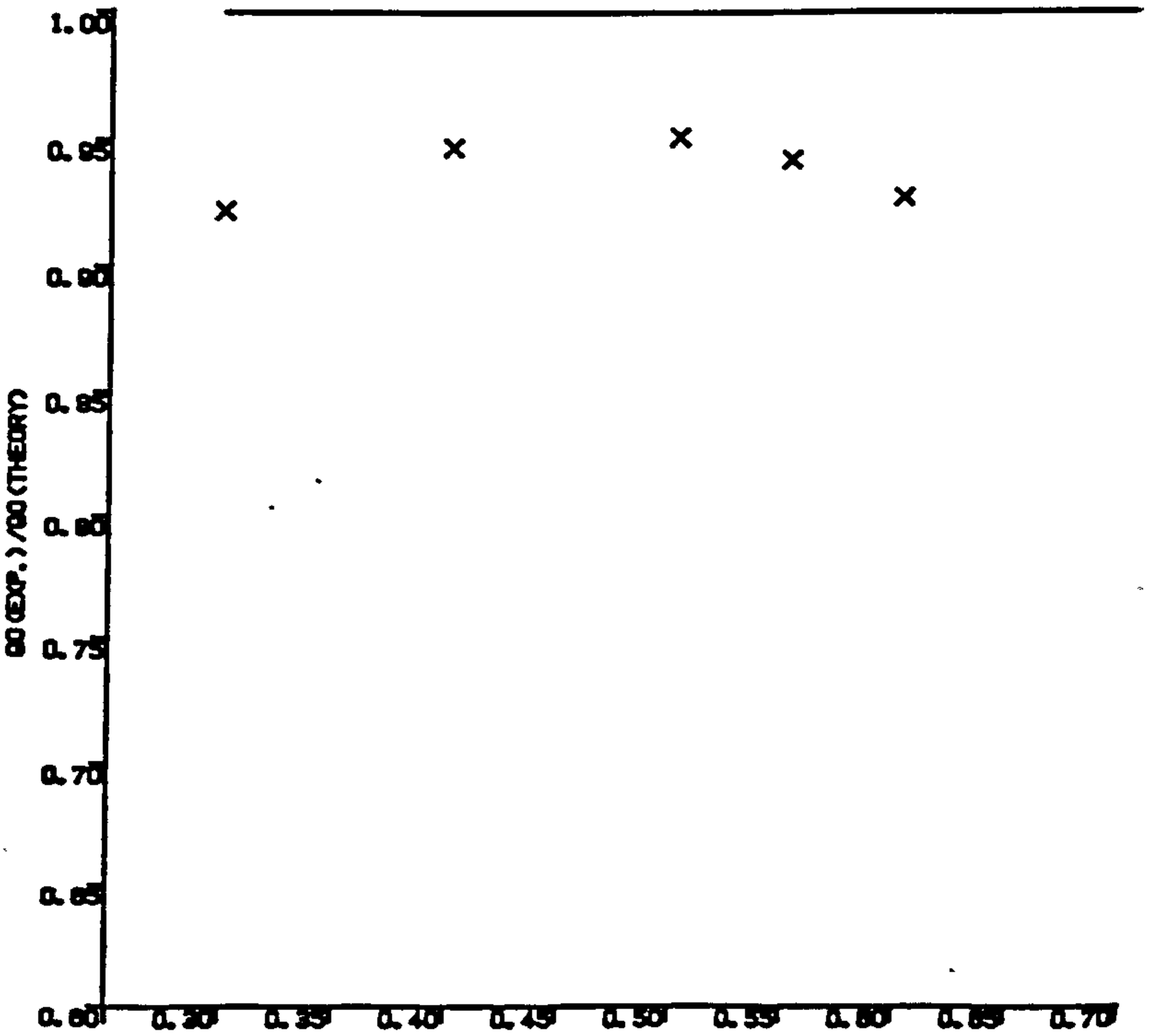

(d) Normalised Q

(Q_o = 15200)

CHAPTER THREE

TUNABLE RESONANT CAVITIES

(COAXIAL REENTRANT AND MULTICYLINDRICAL TYPES)

3.1 Introduction

The requirement for tunable resonant cavities with simple mechanical construction may be necessary in some applications in the VHF and UHF frequency bands. It may also be necessary to consider the size of the cavity especially at frequencies below 1.0GHz. Unlike waveguide cavities with tuning problems (mechanically and analytically), reentrant cavities have wide tuning range using simple mechanical means and quite a low resonant frequency can be achieved with a small size. The difficulty encountered is mainly in the development of a general and effective analytical method for solution to its complex geometrical shape.

Theoretical analysis of a reentrant cavity is an old attempt. Notable among these works were those of Hansen[1], Hahn[2], Mayer[5], Kihara[6], Fujisawa[7], Orlov[8,9], Uenakada[10], Williamson[13], Jaworski[14] and recently Sen[18]. Some of these works have found useful applications in the study of solid state devices. While some attempts are basically too involved analytically[1,2,5,13,14], some others lack in concise analysis of all types of reentrant cavities because higher order modes in the vicinity of the open end of the inner conductor are unaccounted for[8,9,17]. The simplest attempt considered the cavity as supporting TEM-mode with the gap represented by a lumped capacitance[8,9]. For some applications, this is sufficient. In our case, this is found not to be sufficiently accurate for design purposes. In general, more sophisticated methods are needed in order

to evaluate the resonant frequency with reasonable accuracy and for design purposes to predict accurately the design parameters.

The resonant frequency alone does not totally specify resonance requirements. The knowledge of filter quality factor is a vital requirement when considering the resonant cavity for application in mobile radio and radio base stations. For this particular reason, most of the theories, even with accurate predictions of the resonant frequencies, are found inadequate in this consideration. The empirical formulations are found to be unacceptable when geometrical dimensions are altered. The necessity for an acceptable analytical method calls for solution to the field equations of the cavity. This is essential in that the stored energies and the loss in the walls can only be determined when the fields are known. If the field equations can be obtained, it is believed that application to other types of reentrant cavities would become simpler.

To solve the wave equations, various methods have been proposed and in some cases tested with good agreement between theory and practice. Of all these methods, the most appealing are due to Hansen (1939), Hahns (1941), Motz (1946), Mayer (1946), Williamson (1976) and Jaworski (1978). The inclusion of an unknown aperture field is the main disadvantage of Hansen's and Williamson's methods. Those of Jaworski, Motz and Mayer have disadvantages in that they do not give the fields in concise forms. Hahn's method provides the field in a rather compact form and there is no need using arbitrary functions. Before now, Hahn's method has been referenced by many authors and applied by Karpova[11] in the study of solid state dielectric materials. However, no literature has been found to apply it fully to filter networks employing hybrid mode cavities except perhaps narrow gap coaxial reentrant cavity types.

Because of its reported close agreement in dielectric constant computation to practice, the knowledge of the field equation, even though infinite series is expected to be useful generally in the study of all types of reentrant cavities inasmuch as it would be found useful in structures with cylindrical symmetry.

3.2.1 Hahn's Method and Coaxial Reentrant Cavities

One could say that the exact mathematical analysis of cavities of the reentrant type is a complex problem due to the effects of the fringing field surrounding the gap region. However, if the Maxwell's equations can be sufficiently analysed and balanced over the entire space and boundary walls of the cavity, reasonably accurate results can be obtained. Essentially, the entire cavity can be divided into two separate regions, Fig. 1(a), each representing geometry of known closed field equations[2]. It does not matter how it is divided for solution once closed field equations can be defined for each region[20]. In other words, it is necessary to find solutions of the wave equations for both regions separately and then use the continuity of the tangential components of the electromagnetic field across the boundary between the two regions denoted as A and B in Fig. 1(a). Hahn considered the symmetrical solutions of the wave equation in cylindrical coordinates with only the field components E_z, E_r and H_ϕ (TM-mode) not equal to zero. The method is briefly outlined below.

The components of field in region A assume the form:

$$E_z^A = A_o Z_o(k_o r) + \sum_{n=1}^{\infty} A_n Z_o(k_n r)\cos(\gamma_n z) \quad , \tag{1a}$$

$$E_r^A = \sum_{n=1}^{\infty} \frac{\gamma_n}{k_n} A_n Z_1(k_n r)\sin(\gamma_n z) \quad , \tag{1b}$$

and

$$H_\phi = j\frac{A_o}{k_o} Z_1(k_o r) + j\sum_{n=1}^{\infty} \frac{A_n}{k_n} Z_1(k_n r)\cos(\gamma_n z) \quad , \tag{1c}$$

for which the first set of boundary conditions

$$E_r^A = 0, \text{ for } Z = 0 \text{ and } Z = L$$

and

$$E_z^A = 0, \quad \text{for } r = r_2 \text{ must be satisfied.}$$

Therefore

$$Z_o(k_o r) = J_o(k_o r) - \frac{J_o(k_o r_2)}{N_o(k_o r_2)} N_o(k_o r) \quad ,$$

$$Z_1(k_o r) = J_1(k_o r) - \frac{J_o(k_o r_2)}{N_o(k_o r_2)} N_1(k_o r) \quad ,$$

$$Z_o(k_n r) = J_o(k_n r) - \frac{J_o(k_n r_2)}{N_o(k_n r_2)} N_o(k_n r),$$

and

$$Z_1(k_n r) = J_1(k_n r_2) - \frac{J_o(k_n r_2)}{N_o(k_n r_2)} N_1(k_n r).$$

In these equations,

$$j = \sqrt{-1} \quad ,$$

$$\gamma_n = \frac{n\pi}{L} \quad , \; n = 1,2,3,\ldots \quad ,$$

$$k_n = \sqrt{k_o^2 - \gamma_n^2} \quad ,$$

$k_o = 2\pi/\lambda$ - phase constant of free space ,

L is the cavity length,

r_2 is the outer conductor radius ,

and A_o, A_n are constants.

When k_n is imaginary, J_o, N_o, J_1, N_1 are replaced by I_o, K_o, I_1, $-K_1$ respectively.

In a similar way, the field components in region B are given by:

$$E_z^B = B_o J_o(k_o r) + \sum_{m=1}^{\infty} B_m J_o(k'_m r)\cos(\alpha_m z) \quad , \tag{2a}$$

$$E_r^B = \sum_{m=1}^{\infty} \frac{\alpha_m}{k'_m} B_m J_1(k'_m r)\sin(\alpha_m z) \quad , \tag{2b}$$

and

$$H_\phi^B = j\frac{B_o}{k_o} J_1(k_o r) + j\sum_{m=1}^{\infty} \frac{B_m}{k'_m} J_1(k'_m r)\cos(\alpha_m z) \quad . \tag{2c}$$

For which $E_r^B = 0$ for $Z = 0$ and $Z = s$, where

$$k'_m = \sqrt{k_o^2 - \alpha_m^2} \quad , \; m = 1,2,3,\ldots \quad ,$$

$$\alpha_m = \frac{m\pi}{s} \quad ,$$

s is the gap length

and B_o, B_m are constants to be determined.

When $k'^2_m < 0$, J_o, J_1 are replaced by I_o, I_1 respectively.

The other boundary condition is at the surface $r=r_1$. We can write for this condition

$$E_z^{AB} = \begin{cases} D_o + \sum_{m=1}^{\infty} D_m \cos(\frac{m\pi}{s} z) & \text{for } 0 \leq Z \leq s \\ 0 & \text{for } s \leq z \leq L \end{cases} \tag{3a}$$

In region A this can be expanded in cosine Fourier series as:

$$E_z^A = C_o + \sum_{n=1}^{\infty} C_n \cos(\frac{n\pi}{L} z) \tag{3b}$$

where

$$C_o = \frac{1}{L}\int_0^L [D_o + \sum_{m=1}^{\infty} D_m \cos(\frac{m\pi}{s} z)]\,dz$$

$$= \frac{1}{L}\int_0^s [D_o + \sum_{m=1}^{\infty} D_m \cos(\frac{m\pi}{s} z)]\,dz$$

$$= \frac{s}{L} D_o = aD_o \tag{4a}$$

$$C_n = \frac{2}{L}\int_0^L [D_o + \sum_{m=1}^{\infty} D_m \cos(\frac{m\pi}{s} z)]\cos(\frac{n\pi}{L} z)\, dz$$

$$= \frac{2D_o \sin(n\pi a)}{n\pi} + \frac{2}{\pi}\sum_{m=1}^{\infty} (-1)^m D_m \frac{a^2 \sin(n\pi a)}{(a^2 n^2 - m^2)} \qquad (4b)$$

and $a = \frac{s}{L}$.

To make the field in region A satisfy the condition of equation (3a) the following equalities must be satisfied by substituting $r=r_1$:

$$C_o = A_o Z_o(k_o r_1) \qquad (5a)$$

$$C_n = A_n Z_o(k_n r_1) \qquad (5b)$$

By substituting for A_o, A_n in equations 1(a-c), we can write for the field in region A

$$E_z^A = C_o \frac{Z_o(k_o r)}{Z_o(k_o r_1)} + \sum_{n=1}^{\infty} C_n \frac{Z_o(k_n r)}{Z_o(k_n r_1)} \cos(\frac{n\pi}{L} z)\ , \qquad (6a)$$

$$E_r^A = \sum_{n=1}^{\infty} \frac{n\pi}{Lk_n} C_n \frac{Z_1(k_n r)}{Z_o(k_n r_1)} \sin(\frac{n\pi}{L} z)\ , \qquad (6b)$$

$$H_\phi^A = j\frac{C_o}{K_o}\frac{Z_1(k_o r)}{Z_o(k_o r_1)} + j\sum_{n=1}^{\infty} \frac{C_n}{k_n}\frac{Z_1(k_n r)}{Z_o(k_n r_1)} \cos(\frac{n\pi}{L} z) \qquad (6c)$$

for which C_o, C_n can be expressed in terms of D_o, D_m.

In the second region, B, it is observed that the remaining boundary condition can be satisfied by considering the component E_z^B at $r=r_1$. In a similar fashion to the way this was done for region A we can infer

$$D_o = B_o J_o(k_o r_1)$$

and

$$D_m = B_m J_m(k'_m r_1)$$

The field in region B can be expressed in terms of D_o, D_m as

$$E_z^B = D_o \frac{J_o(k_o r)}{J_o(k_o r_1)} + \sum_{m=1}^{\infty} D_m \frac{J_o(k'_m r)}{J_o(k'_m r_1)} \cos(\frac{m\pi}{s} z)\ , \qquad (7a)$$

$$E_r^B = \sum_{m=1}^{\infty} \frac{m\pi}{sk'_m} D_m \frac{J_1(k'_m r)}{J_o(k'_m r_1)} \sin\left(\frac{m\pi}{s} z\right) ,$$

$$H_\phi^B = j \frac{D_o}{k_o} \frac{J_1(k_o r)}{J_o(k_o r_1)} + j \sum_{m=1}^{\infty} \frac{D_m}{k'_m} \frac{J_1(k'_m r)}{J_o(k'_m r_1)} \cos\left(\frac{m\pi}{s} z\right) .$$

At the boundary surface between the regions A and B, the tangential components of the field must balance. That is

(1) $$(E_z^A)_{r=r_1} = (E_z^B)_{r=r_1}$$

(2) $$(H_\phi^A)_{r=r_1} = (H_\phi^B)_{r=r_1}$$

Condition (1) has been satisfied. Condition (2) is satisfied by expanding $(H_\phi^A)_{r=r_1}$ in cosine Fourier series for $0 \leq z \leq s$ and then equating coefficients of the expansion. We therefore have the following equalities:

$$\frac{D_o}{k_o} \frac{J_1(k_o r_1)}{J_o(k_o r_1)} = \frac{1}{s} \int_0^s \left[\frac{C_o}{k_o} \frac{Z_1(k_o r_1)}{Z_o(k_o r_1)} + \sum_{n=1}^{\infty} \frac{C_n}{k_n} \frac{Z_1(k_n r_1)}{Z_o(k_n r_1)} \cos\left(\frac{n\pi}{L} z\right)\right] dz$$

$$= \frac{C_o}{k_o} \frac{Z_1(k_o r_1)}{Z_o(k_o r_1)} + \frac{1}{\pi a} \sum_{n=1}^{\infty} \frac{C_n}{k_n} \frac{Z_1(k_n r_1)}{Z_o(k_n r_1)} \frac{\sin(n\pi a)}{n} \qquad (8)$$

$$\frac{D_m}{k'_m} \frac{J_1(k'_m r_1)}{J_o(k'_m r_1)} = \frac{2}{s} \int_0^s \left[\frac{C_o}{k_o} \frac{Z_1(k_o r_1)}{Z_o(k_o r_1)} + \sum_{n=1}^{\infty} \frac{C_n}{k_n} \frac{Z_1(k_n r_1)}{Z_o(k_n r_1)} \cos\left(\frac{n\pi}{L} z\right)\right] \cos\left(\frac{m\pi}{s} z\right) dz$$

$$= \frac{2}{\pi a} (-1)^m \sum_{n=1}^{\infty} \frac{C_n}{k_n} \frac{Z_1(k_n r_1)}{Z_o(k_n r_1)} \qquad (9)$$

Substituting values of C_o and C_n, we can re-write equations (8) and (9) as

$$D_o R_o = aD_o G_o + \frac{1}{\pi a} \sum_{n=1}^{\infty} G_n \frac{\sin(n\pi a)}{n} \left[\frac{2D_o \sin(n\pi a)}{n} + \frac{2}{\pi} \sum_{m=1}^{\infty} (-1)^m D_m \frac{a^2 \sin(n\pi a)}{a^2 n^2 - m^2}\right]$$

$$= aG_o D_o + \frac{2}{\pi a} \sum_{n=1}^{\infty} \frac{G_n \sin^2(n\pi a)}{n} \left[\frac{D_o}{n} + \sum_{m=1}^{\infty} (-1)^m D_m \cdot \frac{a^2}{a^2 n^2 - m^2}\right] \qquad (10)$$

$$D_t R_t = \frac{2}{\pi a}(-1)^t \sum_{n=1}^{\infty} G_n \frac{2\sin(n\pi a)}{\pi}\left[\frac{D_o}{n} + \sum_{m=1}^{\infty}(-1)^m D_m \frac{a^2}{a^2 n^2 - m^2}\right] \qquad (11)$$

where

$$n,t,m = 1,2,3,4,\ldots.$$

and

$$R_o = \frac{J_1(k_o r_1)}{J_o(k_o r_1)}\ ,\quad R_m = \frac{k_o}{k'_m}\frac{J_1(k'_m r_1)}{J_o(k'_m r_1)}\ ,$$

$$G_o = \frac{Z_1(k_o r_1)}{Z_o(k_o r_1)}\ ,\quad G_n = \frac{k_o}{k_n}\frac{Z_1(k_n r_1)}{Z_o(k_n r_1)}\ .$$

We can normalise the coefficients by tentatively putting $D_o = 1$. The set then becomes

$$R_o = aG_o + \frac{2}{\pi a}\sum_{n=1}^{\infty} G_n \frac{\sin^2(n\pi a)}{n^2\pi} + \frac{2}{\pi a}\sum_{n=1}^{\infty}\frac{G_n \sin^2(n\pi a)}{n\pi} a^2 \sum_{m=1}^{\infty}(-1)^m D_m \frac{a^2}{a^2 n^2 - m^2} \qquad (12)$$

$$D_t R_t = \frac{4}{\pi a}(-1)^t \sum_{n=1}^{\infty} G_n \frac{2\sin(n\pi a)}{n\pi} + \frac{4}{\pi a}\sum_{n=1}^{\infty} G_n \frac{\sin(n\pi a)}{\pi}\sum_{m=1}^{\infty}(-1)^m D_m \frac{a^2}{a^2 n^2 - m^2} \qquad (13)$$

Equation (13), a linearly dependent equation, would, on solution, give the coefficients D_i, $i=1,2,3,\ldots$. This can be done by means of matrix algebra employing Gaussian reduction[21]. The reduction to only two equations with just a set of coefficients is necessary because inclusion of zeroes and both infinitesimally small and large elements in the matrix would result in computational errors. This will be discussed later in the application of this method to more complex geometrical surfaces. Equation (12) is the resonance equation.

The problem of this method is convergence. Under certain dimensional situations, the convergence is very rapid after which the slowness in convergence makes it difficult for an unchecked application. For a narrow gap cavity, the convergence is very rapid and to determine the resonant

frequency a numerical solution of the equations above is performed.

3.2.2 Numerical solution to the resonance equation and computation of coefficients

The main difficulty in designing all types of reentrant cavity is that the relevant design formulae are implicit relationships. Thus, to determine the natural frequencies of a structure like this, we have to solve the resonance equation on finding the coefficients of the expansion. The drawback in the application of this equation is that it is not direct and cannot be analysed without the extensive use of a computer. Hence, a computer solution to equations (12) and (13) was undertaken. A finite number of terms was taken. The trade-offs between accuracy and number of terms used would depend on the intended accuracy of the theoretical data compared with practice. For wide gap cavity type,it would be difficult to get easily converging coefficients. The number of terms before the convergence can be noticed depends on the gap/length,(S/L),ratio. As this approaches 1, the convergence is rapid and waveform approaches a waveguide mode. In the same manner, as the ratio approaches zero, the convergence becomes rapid with the waveform approaching coaxial cavity mode. The problem is therefore between the two limits especially when

$$0.1 \leq (L-S)/L \leq 0.90$$

However, for all cases, the error should be kept below 0.25%. For this accuracy it could prove helpful if the termination is made after the nth term for which the nth term resonant frequency have a difference a small fraction of the (n-1)th term frequency. This could well be achieved for the first 6 or 10 terms depending on the fraction chosen or the intended accuracy. It should be noted however that as the number of terms increases the resonant frequency is found to decrease. But, generally,

the final result is found to be close to the experimental value. The computer program developed allows for the calculation of the resonant frequency and the coefficients of expansion (Appendix II).

For clarification, the experimental results of Uenakada for various cavity dimensions operating at 2.0GHz frequency band are tabulated below to compare accuracies by taking 6 and 10 terms in the series. Even though the frequencies of interest are lower than any of these values but they provide a baseline by which the results may be judged. However the effect of mechanical deviation on the resonant frequency is unknown. Nevertheless the method can, therefore, be said to give a good prediction.

Cavity No.	L (mm)	S (mm)	r_1 (mm)	r_2 (mm)	Uenakada Expt.Freq. (GHz)	F(N=6) (GHz)	F(N=10) (GHz)
1	22.792	7.958	6.004	42.29	2.135	2.134	2.130
2	34.826	8.028	5.992	13.80	2.326	2.344	2.338
3	31.806	7.984	5.9935	20.99	2.280	2.294	2.286
4	28.019	7.999	5.999	29.988	2.2264	2.238	2.230
5	31.806	7.980	3.495	20.99	2.394	2.416	2.406
6	33.806	10.000	8.405	20.99	2.3027	2.301	2.292
7	33.806	10.000	4.206	20.99	2.4018	2.423	2.410

TABLE 1 Comparing taking n=6 and n=10 and experimental results of Uenakada

3.2.3 Computation of the quality factor, Q_o

Once the coefficients and the resonant frequency are obtained, the stored electric and magnetic energies can be determined. Since the definition of resonance holds for any electrical network, it is easy to establish that at resonance, the total stored electric and magnetic energies are equal. The total stored energy is the sum of energies stored in each region. The stored magnetic energy appears to be the easiest to calculate for the cavity since there is only one component of the magnetic field in each region. The losses are calculated for each conductor surface in each region. The total loss is the sum of all the losses in the walls.

The stored magnetic energy is given as

$$W_H = \frac{\mu}{4} \iiint_v |\vec{H}|^2 \, d\tau$$

where $d\tau$ is an element of volume and v is the volume of the region. For each region, the stored magnetic energy is given as

$$W_{TR} = \frac{\mu}{4} \iiint_{v_R} |\vec{H}_\phi|^2 \, d\tau$$

By employing Bessel's integral equations of Appendix I, the following expressions represent the total stored magnetic energy in each region as shown in Fig. 1(b).

Region A

$$W_A = \frac{\pi}{2} \mu L \left\{ \frac{r_2^2}{2} \left[\left[\frac{A_o}{k_o} Z_1(k_o r_2) \right]^2 - \frac{A_o^2}{k_o^2} Z_o(k_o r_2) Z_2(k_o r_2) \right] + \right.$$

$$+ \frac{r_2^2}{4} \sum_{n=1}^{\infty} \frac{A_n^2}{k_n^2} \left[[Z_1(k_n r_2)]^2 - Z_c(k_n r_2) Z_2(k_n r_2) \right] -$$

$$\left. - \frac{r_1^2}{2} \frac{A_o^2}{k_o^2} \left[[Z_1(k_o r_1)]^2 - Z_o(k_o r_1) Z_2(k_o r_1) \right] - \right.$$

$$- \frac{r_1^2}{4} \sum_{n=1}^{\infty} \frac{A_n^2}{k_n^2} [[Z_1(k_n r_1)]^2 - Z_o(k_n r_1) Z_2(k_n r_1)] \} \qquad (14)$$

and region B

$$W_B = \frac{\pi}{2} \mu S \{ \frac{B_o^2}{k_o^2} \frac{r_1^2}{2} [[J_1(k_o r_1)]^2 - J_o(k_o r_1) J_2(k_o r_1)] +$$

$$+ \frac{r_1^2}{4} \sum_{n=1}^{\infty} \frac{B_n^2}{k'^2_n} [[J_1(k'_n r_1)]^2 - J_o(k'_n r_1) J_2(k'_n r_1)] \} \qquad (15)$$

The total stored energy W_T in the cavity is therefore

$$W_T = 2(W_A + W_B)$$

The power dissipated in the nth wall (see Fig. 1(b)) is given as

$$P_n = \frac{R_s}{2} \iint_S |\vec{H}_t|^2 \, dS$$

where H_t is the tangential magnetic field to surface S_A and R_s is the skin resistance of the surface at the resonant frequency.

$$\vec{H}_t = H_\phi \quad \text{for all the surfaces.}$$

By employing Appendix I, these are given as:

$$P_1 = \pi R_s r_2 L \{ \frac{A_o^2}{k_o^2} [Z_1(k_o r_2)]^2 + \frac{1}{2} \sum_n [\frac{A_n}{k_n} Z_1(k_n r_2)]^2 \} \qquad (16a)$$

$$P_2 = \pi R_s \{ \sum_{\substack{m=0 \\ m \neq n}}^{\infty} \sum_{n=0}^{\infty} (-1)^{m+n} \frac{A_n A_m}{k_n k_m} [\frac{k_m r_2 Z_1(k_n r_2) Z_o(k_m r_2) - k_n r_2 Z_o(k_m r_2) Z_1(k_m r_2)}{k_n^2 - k_m^2}$$

$$- \frac{k_m r_1 Z_1(k_n r_1) Z_o(k_m r_1) - k_n r_1 Z_o(k_n r_1) Z_1(k_m r_1)}{k_n^2 - k_m^2}] \} \qquad (16b)$$

$$P_3 = R_s r_1 \quad (L-S)\left[\left[\frac{A_o}{k_o} Z_1(k_o r_1)\right]^2 + \frac{1}{2} \sum_{n=1} \left[\frac{A_n}{k_n} Z_1(k_n r_1)\right]^2 +\right.$$

$$+ \frac{1}{4} \sum_{n=1} \frac{A_n^2}{k_n^2} [Z_1(k_n r_1)]^2 \frac{\sin(2k_{Zn}S)}{k_{zn}} - 2 \frac{A_o}{k_o} Z_1(k_o r_1) \sum_{n=1} \frac{A_n}{k_n} Z_1(k_n r_1)$$

$$\left.\frac{\sin(k_{zn}S)}{k_{zn}} - \frac{1}{2} \sum_{\substack{m=1 \\ m\neq n}} \sum_{n=1} \frac{A_n A_m}{k_n k_m} Z_1(k_m r_1) Z_1(k_n r_1) \left[\frac{\sin(k_{zm}-k_{zn})S}{k_{zm}-k_{zn}} + \right.\right.$$

$$\left.\left. + \frac{\sin(k_{zm}+k_{zn})S}{k_{zm}+k_{zn}}\right]\right. \qquad (16c)$$

$$P_4 = \pi R_s \left\{ \frac{r_1^2}{2} \sum_{n=0} \frac{B_n^2}{k_n'^2} \left[\left[J_1(k_n' r_1)\right]^2 - \left[J_o(k_n' r_1) J_2(k_n' r_1)\right] + \right.\right.$$

$$\left.\left. + \sum_{\substack{m=0 \\ m\neq n}} \sum_{n=0} (-1)^{m+n} \frac{B_n B_m}{k_n' k_m'} \frac{k_n' r_1 J_1(k_m' r_1) J_o(k_n' r_1) - k_m' r_1 J_1(k_n' r_1) J_o(k_m' r_1)}{k_m'^2 - k_n'^2} \right\}\right.$$

(16d)

$$P_5 = \pi R_s \left\{ \frac{r_1^2}{2} \sum_{n=0} \frac{B_n^2}{k_n'^2} \left[\left[J_1(k_n' r_1)\right]^2 - J_o(k_n' r_1) J_2(k_n' r_1)\right] + \right.$$

$$\left. + \sum_{\substack{m=0 \\ m\neq n}} \sum_{n=0} \frac{B_n B_m}{k_n' k_m'} \frac{k_n' r_1 J_1(k_m' r_1) J_o(k_n' r_1) - k_m' r_1 J_1(k_n' r_1) J_o(k_m' r_1)}{k_n'^2 - k_m'^2} \right\} \qquad (16e)$$

$$P_6 = \pi R_s \left\{ \sum_{\substack{m=0 \\ m\neq n}} \sum_{n=0} \frac{A_n A_m}{k_n k_m} \left[\frac{k_m r_2 Z_1(k_o r_2) Z_o(k_m r_2) - k_n r_1 Z_1(k_m r_2) Z_o(k_n r_2)}{k_n^2 - k_m^2} - \right.\right.$$

$$\left. - \frac{k_m r_1 Z_1(k_n r_1) Z_o(k_m r_1) - k_n r_1 Z_o(k_n r_1) Z_1(k_m r_1)}{k_n^2 - k_m^2} \right] +$$

$$+ \frac{r_2^2}{2} \sum_{n=0} \frac{A_n^2}{k_n^2} \left[\left[\left[Z_1(k_n r_2)\right]^2 - Z_o(k_n r_2) Z_2(k_n r_2)\right] - \left[\left[Z_1(k_n r_1]\right]^2 - \right.\right.$$

$$\left.\left. - Z_o(k_n r_1) Z_2(k_n r_1)\right]\right] \right\} \qquad (16f)$$

where

$$k_{zm} = \frac{m\pi}{L}$$

and

$$k_{zn} = \frac{n\pi}{L}$$

In these expressions it should be noted that $Z_o(k_n r_2) = 0$ for all n.

The quality factor Q_o is expressed in terms of the stored energy and dissipated power as

$$Q_o = \frac{\omega_o W_T}{P} \qquad (17)$$

where

$$P = P_1 + P_2 + P_3 + P_4 + P_5 + P_6$$

and ω_o is the resonant angular frequency.

3.3 Hybrid Mode Cavities

The term 'Hybrid' as used here will be restricted to qualify very wide gap reentrant cavities for which the centre conductor length (L-S) is very much smaller than a quarter of resonant wavelength. Generally, the term refers to all types of reentrant cavities supporting both coaxial and waveguide modes.

Without loss of generality, narrow gap reentrant cavities are not useful for application in filter related networks because of their general low quality factors. Their applications are only inevitable when the application of other types of resonators with much higher values of Q-factcrsis prohibited for dimensional reasons. This is the case for frequencies below 1GHz. What is therefore found is that the Q's are generally low for the volume when compared with waveguide cavities of similar dimensions. However the reentrant cavities have

been found to give almost linear tuning over a wide frequency range. This advantage has placed much importance on its application in microwave communication networks. The need for high Q-factor combined with wide range linear tuning has therefore led to the development of resonant cavities for which the high Q-factor known for waveguide cavities is combined with wide tuning range known for reentrant or coaxial types. The high degree combination of the two types can be obtained in hybrid mode cavity for which the length of the inner conductor of a reentrant cavity is less than ½ the length of the cavity,

$$\frac{L}{2} < S < L$$

For this cavity, there have been many attempts to find a simple solution through the use of an empirically derived equivalent lumped impedance[7,10]. However, a general method derived from the wave equations has been found most desirable since the design work must be able to predict accurately enough the design parameters. The direct application of Hahn's method has been found most useful for this since hybrid mode cavities are wide gap versions of general reentrant coaxial cavities.

3.4.1 Experiments with general coaxial reentrant cavity

Appendix II is a computer program for the numerical solution of equations (12) and (13) modified to incorporate equations (14), (15), (16) and (17).for the evaluation of the cavity unloaded Q. This was used to predetermine the expected resonant frequency and quality factor of a cavity whose dimensions were conveniently chosen arbitrarily. The cavity, length L = 13.68cm, outer radius $r_2 \cong 3.81$cm, was to resonate, if particularly designed as waveguide cavity supporting fundamental TM_{010} mode, at 3GHz. By incorporating an adjustable

centrally placed inner conductor, radius r_1= 1.07cm, to form a reentrant coaxial cavity, as shown in Fig. 1(c), this was used as the first practical check on the theory. The length of the centre conductor was adjusted to cover most of the cavity length. Fig. 3(a) is the plot of the resonant frequency against (L-S)/L. Fig. 3(b) summarises the variation of the unloaded Q with the length of the centre conductor.By scaling down the theoretical curve (the solid line) by a factor of 1/7 (the broken line), the cavity Q_o showed a close agreement between theory and practice. This close agreement could be observed further for the same cavity from the plot of $Q_o(f)/Q_o(1.02GHz)$ vs. frequency in Fig. 3(c).

The mechanical and geometrical deviations of the resonator are known to affect the resonant frequency. Ironically, there is no means by which this can be deduced because the computed result itself contains errors from the series termination and the numerical analysis. However it is easy to settle on a particular choice of the number of terms between 6 and 10 when the length of the centre conductor is less than half the length of the outer conductor.

Close observation of the tuning curve, Fig. 3(a), shows that it is approximately linear over a wide frequency range especially within the region $0.1 \leq \frac{L-S}{L} \leq 0.4$. However, for us, it is of importance to investigate the properties not only through frequency range but also the degradation of cavity Q_o with frequency. Fig. 3(c) shows that for about 10% frequency change, the quality factor variation is about 10%.

3.4.2 Design techniques and optimisation of design parameters

The design work follows the numerical solution to the resonant equation. For an hybrid mode coaxial reentrant cavity, the outer conductor radius is decided by the maximum resonant frequency and the length by the maximum Q_o. The maximum resonant frequency represents the fundamental resonant frequency of a cylindrical cavity supporting TM_{010} mode and is always higher than the maximum frequency expected of the hybrid mode cavity. Thus the cavity has upper bounds of a pure cylindrical cavity, TM_{010} mode, resonant characteristics.

Fig. 4 presents a summary of how the unloaded Q, Q_o, varies with the ratio r_1/r_2 for a cavity having dimensions r_2 = 6.67cm and L = 7.62cm for frequencies of 1.6, 1.5, 1.4 and 1.3GHz employing the same computer program. It could be observed that for a known length L and outer radius r_2 of a reentrant cavity, that is for a nominal cavity volume, the highest Q factors can be obtained for any desired frequency range when the centre conductor radius is about a quarter of the outer conductor radius. The exact ratio depends on the desired frequency. Table 2 shows how closely theory and practice agree.

r_1/r_2	Q_o at 1.6GHz		Q_o at 1.5GHz		Q_o at 1.4GHz	
	Theory	Practice	Theory	Practice	Theory	Practice
0.316	19257	15168	17268	13844	15794	12969
0.263	19477	15782	17494	14369	15985	13682
0.19	19600	15860	17508	14300	15932	13518

TABLE 2

Tunable reentrant cavities, like other tunable cavities, are expected to incorporate movable parts. This is where its construction becomes more difficult than the construction of a waveguide cavity. If an open gap exists within the periphery of the movable member, low resonant Q_o would result. Usually, therefore, spring fingers are used to block the gap between the centre conductor and the cavity plate while it, in addition, holds the centre conductor in position. An illustration of this can be seen on Plate 1.

3.5 Experimental Results (Hybrid Mode Cavity)

Fig. 5(a) relates the plots of modified theoretical Q_o against frequency with practice. Fig. 5(b) is a tuning curve for the same cavity, dimensions $L = 7.62cm$, $r_2 \cong 6.67cm$ and $r_1 \cong 2.22cm$. The tuning curve shows quite a close agreement between theory and practice. Another cavity having the same outer conductor dimensions but with $r_1 = 2.1cm$ was tested. Fig. 6 shows how the plot of $Q_o(f)/Q_o(1.5GHz)$ against frequency followed the same trend as the one obtained for the test resonator. It further shows that there is a very close agreement between relative values of Q_o obtained theoretically and those obtained from practice.

Because of increased geometrical and boundary surface imperfections, the resonance loss can be observed to increase in comparison with that observed in Chapter Two. From Figs. 3(b) and (c) and Fig. 5 for a hybrid mode cavity, it is possible to establish the average expected resonance loss in Q of reentrant cavities to a minimum of 14%.

3.6 Hahn's Method Applied to Multicylindrical Cavity

Theory and Practice

At frequencies around 100MHz, the use of ordinary reentrant cavity is confronted by the volume of the cavity. At this stage what matters most may not be Q_o but the resonant frequency, that is, very high value of Q_o may not be all that is necessary. For such a case, a new idea has to come in. This is found in multicylindrical coaxial cavities[5,7]. We shall consider the case of two inner coaxial cylinders as shown in Fig. 2.

The cavity is divided into sections having closed field equations just the same way coaxial cavities were divided. The first requirement is that cylinder b has a thickness a multiple of the skin depth of the conductor. Fields in the sections are found as modal expansions of the fields in identical resonators with closed field waveforms.

In Region I

$$E_z^I = A_o J_o(k_o r) + \sum_{n=1}^{\infty} A_n J_o(k'_n r) \cos(\frac{n\pi}{S} z) \quad , \tag{18a}$$

$$E_r^I = \sum_{n=1}^{\infty} \frac{n\pi}{Sk'_n} A_n J_1(k'_n r) \sin(\frac{n\pi}{S} z) \tag{18b}$$

and

$$H_\phi^I = j \frac{A_o}{k_o} J_1(k_o r) + j \sum_{n=1}^{\infty} \frac{A_n}{k'_n} J_1(k'_n r) \sin(\frac{n\pi}{S} z). \tag{18c}$$

In Region II

$$E_z^{II} = B_o J_o(k_o r) + C_o N_o(k_o r) + \sum_{m=1}^{\infty} [B_m J_o(k_m r) + C_m N_o(k_m r)] \cos(\frac{m\pi}{L} z), \tag{19a}$$

$$E_r^{II} = \sum_{m=1}^{\infty} \frac{m\pi}{Lk_m} [B_m J_1(k_m r) + C_m N_1(k_m r)] \sin(\frac{m\pi}{L} z) \tag{19b}$$

and

$$H_\phi^{II} = j[\frac{B_o}{k_o} J_1(k_o r) + \frac{C_o}{k_o} N_1(k_o r)] + j \sum_{m=1}^{\infty} \frac{1}{k_m} [B_m J_1(k_m r) + C_m N_1(k_m r)] \cos(\frac{m\pi}{L} z). \tag{19c}$$

In Region III

$$E_z^{III} = E_o J_o(k_o r) + F_o N_o(k_o r) + \sum_{t=1}^{\infty} [E_t J_o(\dot{k}_t r) + F_t N_o(\dot{k}_t r)] \cos(\frac{t\pi}{d} z'), \quad (20a)$$

$$E_r^{III} = \sum_{t=1} \frac{t\pi}{d\dot{k}_t} [E_t J_1(\dot{k}_t r) + F_t N_1(\dot{k}_t r)] \sin(\frac{t\pi}{d} z') \quad (20b)$$

and

$$H_\phi^{III} = j \frac{1}{k_o} [E_o J_1(k_o r) + F_o N_1(k_o r)] + j \sum_{t=1}^{\infty} \frac{1}{\dot{k}_t} [E_t J_1(\dot{k}_t r) + F_t N_1(\dot{k}_t r)] \cos(\frac{t\pi}{d} z') \quad (20c)$$

Finally in Region IV, the fields are expressed as

$$E_z^{IV} = D_o Z_o(k_o r) + \sum_{q=1} D_q Z_o(k_q r) \cos(\frac{q\pi}{L} z), \quad (21a)$$

$$E_r^{IV} = \sum \frac{q\pi}{bk_q} Z_1(k_q r) \sin(\frac{q\pi}{L} z) \quad (21b)$$

and

$$H_\phi^{IV} = j \frac{D_o}{k_o} Z_1(k_o r) + j \sum \frac{D_q}{k_q} Z_1(k_q r) \cos(\frac{q\pi}{L} z) \quad (21c)$$

where

$$Z_o(k_o r) = J_o(k_o r) - \frac{J_o(k_o r_4)}{N_o(k_o r_4)} N_o(k_o r),$$

$$Z_o(k_q r) = J_o(k_q r) - \frac{J_o(k_q r_4)}{N_o(k_q r_4)} N_o(k_q r),$$

$$Z_1(k_o r) = J_1(k_o r) - \frac{J_o(k_o r_4)}{N_o(k_o r_4)} N_1(k_o r),$$

$$Z_1(k_q r) = J_1(k_q r) - \frac{J_o(k_q r_4)}{N_o(k_q r_4)} N_1(k_q r),$$

for which

$$k_q = \sqrt{k_o^2 - (\frac{q\pi}{L})^2},$$

$$\dot{k}_n = \sqrt{k_o^2 - (\frac{n\pi}{S})^2},$$

$$k_m = \sqrt{k_o^2 - (\frac{m\pi}{L})^2},$$

$$k'_t = \sqrt{k_o^2 - (\frac{t\pi}{d})^2}$$

and

$$z' = z + d - L$$

When any of k_q, k'_n, k_m, or k'_t is imaginary, the corresponding Bessel function J_o, J_1, N_o, N_1 should be replaced by I_o, I_1, K_o, $-K_1$ as performed earlier. By matching the tangential fields at the common surfaces between regions I & II, II & III, III & IV, the following equalities can be derived:

$$B_o J_o(k_o r_1) + C_o N_o(k_o r_1) = aA_o J_o(k_o r_1) \qquad (22)$$

$$B_m J_o(k_m r_1) + C_m N_o(k_m r_1) = \frac{2A_o J_o(k_o r_1)}{m\pi} \sin(m\pi a) +$$

$$+ \sum_{n=1}^{\infty} (-1)^n A_n J_o(k'_n r_1) \frac{2ma^2}{\pi} \frac{\sin(m\pi a)}{m^2 a^2 - n^2} \qquad (23)$$

$$A_o J_1(k_o r_1) = B_o J_1(k_o r_1) + C_o N_1(k_o r_1) + \frac{1}{\pi a} \sum_{m=1}^{\infty} \frac{k_o}{mk_m} [B_m J_1(k_m r_1) +$$

$$+ C_m N_1(k_m r_1)] \sin(m\pi a) \qquad (24)$$

$$\frac{1}{k'_n} A_n J_1(k'_n r_1) = (-1)^n 2 \sum_{m=1}^{\infty} \frac{ma}{\pi} \frac{1}{k_m} [B_m J_1(k_m r) + C_m N_1(k_m r_1)] \frac{\sin(m\pi a)}{m^2 a^2 - n^2} \qquad (25)$$

$$B_o J_o(k_o r_2) + C_o N_o(k_o r_2) = [E_o J_o(k_o r_2) + F_o N_o(k_o r_2)] b \qquad (26)$$

$$B_m J_o(k_m r_2) + C_m N_o(k_m r_2) = 2\{[E_o J_o(k_o r_2) + F_o N_o(k_o r_2)] \frac{\sin(m\pi b)}{m\pi} +$$

$$+ \sum_{t}^{\infty} (-1)^t [E_t J_o(k'_t r_2) + F_t N_o(k'_t r_2)] \frac{mb^2}{\pi} \frac{\sin(m\pi b)}{m^2 b^2 - t^2} \qquad (27)$$

$$D_o Z_o(k_o r_3) = [E_o J_o(k_o r_3) + F_o N_o(k_o r_2)] b \qquad (28)$$

$$D_q Z_o(k_q r_3) = 2\{[E_o J_o(k_o r_3) + F_o N_o(k_o r_3)] \frac{1}{q\pi} \sin(q\pi b) +$$

$$+ \sum_t^{\infty} (-1)^t [E_t J_o(\dot{k}_t r_3) + F_t N_o(\dot{k}_t r_3)] \frac{qb^2}{\pi} \frac{\sin(q\pi b)}{q^2 b^2 - t^2} \} \quad (29)$$

$$E_o J_1(k_o r_3) + F_o N_1(k_o r_3) = D_o Z_1(k_o r_3) + \frac{1}{\pi b} \sum_{q=1}^{\infty} \frac{k_o}{q k_q} D_q Z_1(k_q r_3) \sin q\pi b \quad (30)$$

$$\frac{1}{\dot{k}_t} [E_t J_1(\dot{k}_t r_3) + F_t N_1(\dot{k}_t r_3)] = (-1)^t/2 \sum_q^{\infty} \frac{qb}{\pi} \frac{D_q}{k_q} Z_1(k_q r_3) \frac{\sin(q\pi b)}{q^2 b^2 - t^2} \quad (31)$$

$$E_o J_1(k_o r_2) + F_o N_1(k_o r_2) = B_o J_1(k_o r_2) + C_o N_1(k_o r_2) +$$

$$+ \frac{1}{\pi b} \sum_m^{\infty} \frac{k_o}{m k_m} [B_m J_1(k_m r_2) + C_m N_1(k_m r_2)] \sin(m\pi b) \quad (32)$$

$$\frac{1}{\dot{k}_t} [E_t J_1(\dot{k}_t r_2) + F_t N_1(\dot{k}_t r_2)] = (-1)^t . 2 \sum_m^{\infty} \frac{mb}{\pi} \frac{1}{k_m} [B_m J_1(k_m r_2) + C_m N_1(k_m r_2)] .$$

$$\cdot \frac{\sin(m\pi b)}{m^2 b^2 - t^2} \quad (33)$$

where n,m,q,t = 1,2,3,...

We have got twelve dependent linear equations in which equations (23)-(33) can be used for the computation of coefficients. Equation (22) on substitution of the coefficients B_o, C_o, A_o forms the resonance equation. Since it is an implicit function, it can only be solved numerically. Normally one of the coefficients A_o and D_o is put as unity thereby normalising other coefficients. The easiest way to approach the eleven simultaneous equations is through matrix algebra. However, much problem was encountered in this direction, as will be outlined shortly. The computed results were found complicated.

The eleven equations were reduced to four with four unknown sets of coefficients by partially solving the linear equations. The four remaining expressions are lengthy and would not be included here. However, the steps followed included: B_o, C_o, E_o, F_o, and D_o were expressed in terms of B_m, C_m by solving equations (22),(24),(26), (32) and (28). D_q was also obtained from equation (29) in terms of B_m, C_m, E_t, F_t. By substituting A_n in equation (25) into equation (23) and B_o, C_o, E_o, F_o, D_o, D_n into equations (27) and (31), we will be left with the five essential equations of which equation (30) constitutes the resonance equation. The five equations contain sets of coefficients in B_m, C_m, E_t and F_t. If 10 terms are chosen from each series, we will have to solve 40 x 40 matrix algebra to obtain

B_n, C_n, E_n, F_n for n = 1,2,... 10.

By means of FORTRAN Library for Matrices and Function Minimisation, this amounts to a minor problem.

The major problem with the numerical solution arises as a result of terms in I_o, I_1, K_o, K_1, the modified Bessel functions. The modified Bessel functions I_o, I_1 increase exponentially in contrast to the second kind K_o, K_1 which exponentially approach zero. The inclusion of these will definitely result, as elements of the matrix with the use of Gaussian reduction, in truncation errors. If only we can reduce the four dependent linear equations to one with only one unknown coefficient set, we could then have 'normalised' arguments with terms in I_o/I_1, K_o/K_1, I_1/I_o, K_1/K_o replacing terms in I_o, K_o, I_1, K_1. This same problem has been checked on equations (4), (8) and (6) with convincing satisfaction.

Table 3 compares theoretical results, obtained by reduction to 4 linearly dependent equations of the 11 simultaneous equations and taking 10 terms in each set of coefficients, with experimental results. (Appendix III contains the computer program for the computation of the resonant

frequency). The error introduced into the numerical solution was between 1.0 and 6% comparing theory with practice. With further reduction of the linear equations one hopes the error would reduce to that of termination of the infinite series. This method would therefore be an effective way to analyse the resonant parameters, especially Q_o, of cavities having cylindrical symmetry. Meanwhile, for the frequency analysis of this present cavity, a simpler method has been reported with good accuracy[15]. But, the present method is one of the best available methods for even more complicated boundaries characterised by cylindrical symmetry provided the matrix algebra can be operated upon effectively in view of the complicating transcendental functions.

TABLE 3: The theoretical and practical results of a multicylindrical cavity compared. The dimensions of the cavity are L ≅ 13.7cm, d ≅ 8.76cm, r_1 ≅ 1.07cm, r_2 ≅ 1.94cm, r_3 ≅ 2.03cm, r_4 ≅ 3.81cm. See Fig. 6(b).

Gap Length (cm)	Expt. Frequency F_e (MHz)	Theoretical Freq. F_ϕ	% Error $\lvert f_e - f_o \rvert \times 100 / f_e$
1.0	330.515	340.228	2.94
2.0	351.839	363.630	3.35
3.0	383.086	407.128	5.7
4.0	403.67	408.513	1.2
5.0	438.847	415.456	5.33
6.0	475.952	451.696	5.37

3.7 Discussion and Conclusion

The hybrid mode, cylindrical reentrant cavity has been investigated together with the narrow gap type and we have seen that over the years a number of different formulations have been published from which the properties of the cavity, in particular the resonant frequency, can be calculated. Hahn's formulation has been found particularly useful because it gives a general idea of the waveform in the cavity and thus provides an easy means by which other resonant parameters can be computed. The development of the technique for application in the design of hybrid mode cavities is basically superior to other forms of approach in existence.

In view of experimental and numerical errors, it has been found that resonant frequency can be predicted with error less than 0.2% in the case of hybrid mode cavities. In addition, with proper choice of scaling factors, the cavity quality factor can be predicted with high degree of accuracy. A probable scaling factor has been found here to be about 0.86. However, such closeness can only be inferred in the case of multicylindrical types provided such an hectic algebraic substitution as suggested earlier could be performed. If this can be done, such resonant characteristics as the quality factor can be obtained employing Appendix I. Such a solution would be a stepping-stone to the analysis of more complicated structures and the subsequent miniaturisation of resonant cavities.

Generally, the Q-factor of coaxial reentrant cavity decreases with increasing insertion depth of the centre conductor. Although the Q factor is known to depend on the volume-to-surface area ratio of a cavity, there is usually an optimum value of the ratio of inner conductor radius to outer conductor radius for the highest probable Q-factor obtainable from a cavity of known outer conductor dimensions. This ratio has been

found centred on 1/4.

It can be concluded that if by checking the computed resonant frequency with practice, the number of terms to be taken in the series is established, the method deviation introduced in this way would not exceed 0.2% for hybrid mode cavities and 6% for multi-cylindrical types. The computation of the resonant parameters by employing different metals in the construction of the cavity would not analytically amount to any additional problems whatsoever.

3.8 References

1. Hansen, W W: 'On the resonant frequencies of closed concentric lines', J. Appl. Phys., Vol. 1o, pp. 38-45, 1939

2. Hahn, W C: 'A new method for the calculation of cavity resonators', J. Appl. Phys., Vol. 12, pp. 62-68, 1941.

3. Marcuvitz, E: 'Waveguide Handbook', (MIT Rad. Lab. Series Vol. 10), New York: McGraw Hill, 1951, p. 178.

4. Motz, H: 'Calculation of the electromagnetic field, frequency and circuit parameters of high frequency resonator cavity', JIEE, Vol. 93, Pt. III, p. 335-43, 1946.

5. Mayer, E: 'Resonant frequencies of nosed-in cavity', J. Appl. Phys., Vol. 17, pp. 1046-1055, 1946.

6. Kihara, T: 'Approximate methods regarding electromagnetic waves in hollow pipes and cavities', J. Physical Soc. Japan, Vol. 2, pp.65-90, 1947.

7. Fujisawa, K: 'General treatment of klystron resonant cavities', IRE Trans. MTT, Vol. 6, pp. 344-358, Oct. 1958.

8. Orlov, S I: 'Calculation of the Q of a coaxial resonant circuit', Radio Engineering, Vol. 23, No. 1, 1968, pp. 65-68.

9. Orlov, S I: 'Optimising the wave impedance of a coaxial resonant circuit', Telec. & Radio Eng., Vol. 21, No. 10, p. 68-90.

10. Uenakada, K: 'LCR equivalent circuit of reentrant cavity resonator', Trans. Inst. Electron. Commun. Eng., Japan, Vol. 53B, pp. 51-58, 1970.

11. Karpova, O V: 'On an absolute method of measurement of dielectric properties of a solid using a π-shaped resonator', Sov. Physics (Solid State), Vol. 1, pp. 220-228, 1959/60.

12. Rivier, E & Verge-Lapisardi, M: 'Lumped parameters of a reentering cylindrical cavity', IEEE Trans. MTT, Vol. MTT-19, pp. 309-314, March 1971.

13. Williamson, A G: 'The resonant frequency and tuning characteristics of a narrow gap reentrant cylindrical cavity', IEEE Trans. MTT, Vol. 24, No. 4, April 1976, pp. 182-187.

14. Jaworski, M: 'On the resonant frequency of a reentrant cylindrical cavity', IEEE Trans. MTT, Vol. 26, No. 4, April 1978, pp. 256-266.

15. Anvari, K: PhD Thesis, University of Bradford, 1980.

16. Howson, D P: 'The design and performance of a hybrid mode coaxial cavity resonator', (University of Bradford), Unpublished.

17. Kuznetsova, A M: 'A practical method of designing multicylinder microwave resonators', Telecom. & Radio Eng., Pt. 2 (USA), Vol. 29, No. 4, pp. 114-117, 1972.

18. Sen, S et al: 'Resonant modes in reentrant cavities', Radio & Electronic Engr., Vol. 50, No. 3, pp. 113-116, March 1980.

19. Bruyevich, A N et al: 'Simple formulas for the parameters of circuits which replace coaxial resonators', Radio Eng. (USA), Vol. 23, No. 8, 1968, pp. 138-141.

20. Kline, M: 'Some Bessel equations and their application to guide and cavity theory', J. Maths & Phys., Vol. 27, pp. 37-48, 1948

21. Barnett, S: Matrix methods for engineers and scientists , McGraw Hill Co., pp. 34-44

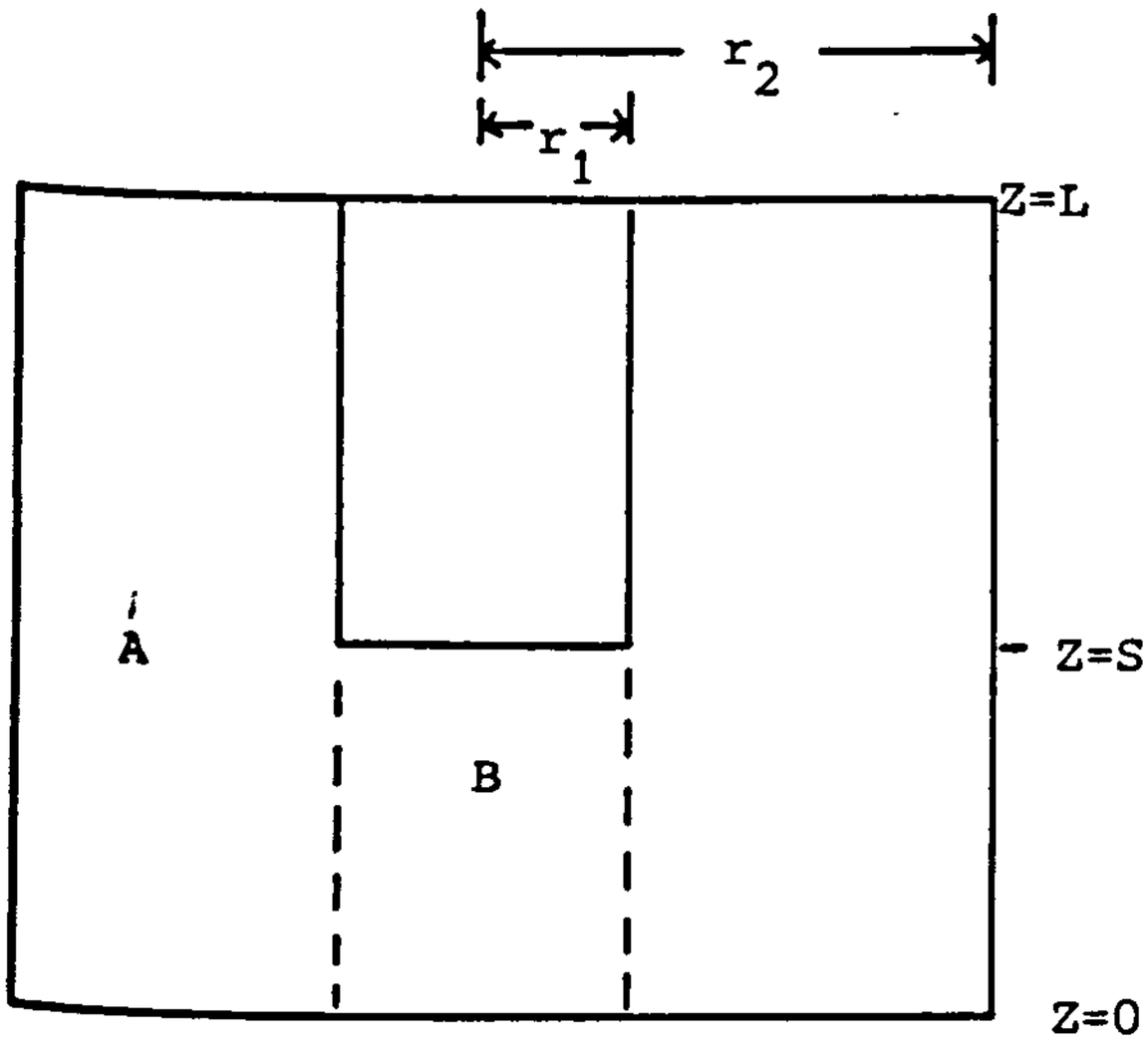

(a) Division into analytic geometries

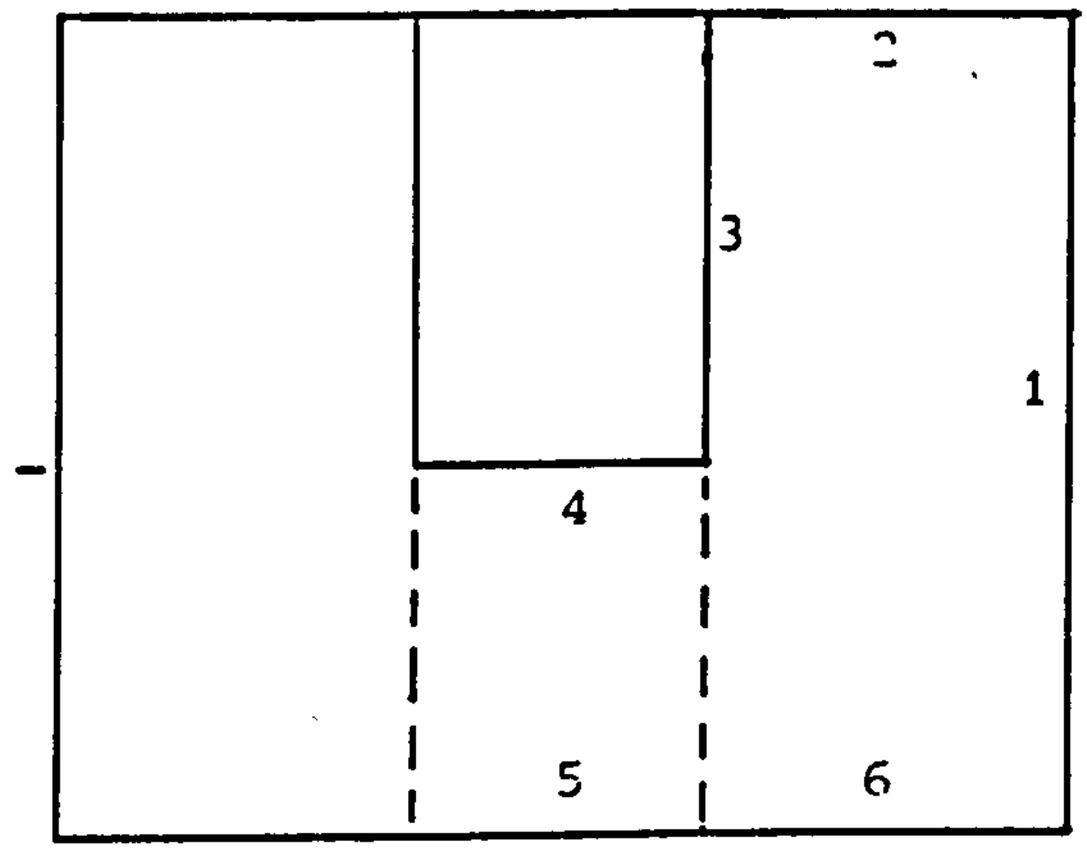

(b) Wall identifications for the calculation of Q

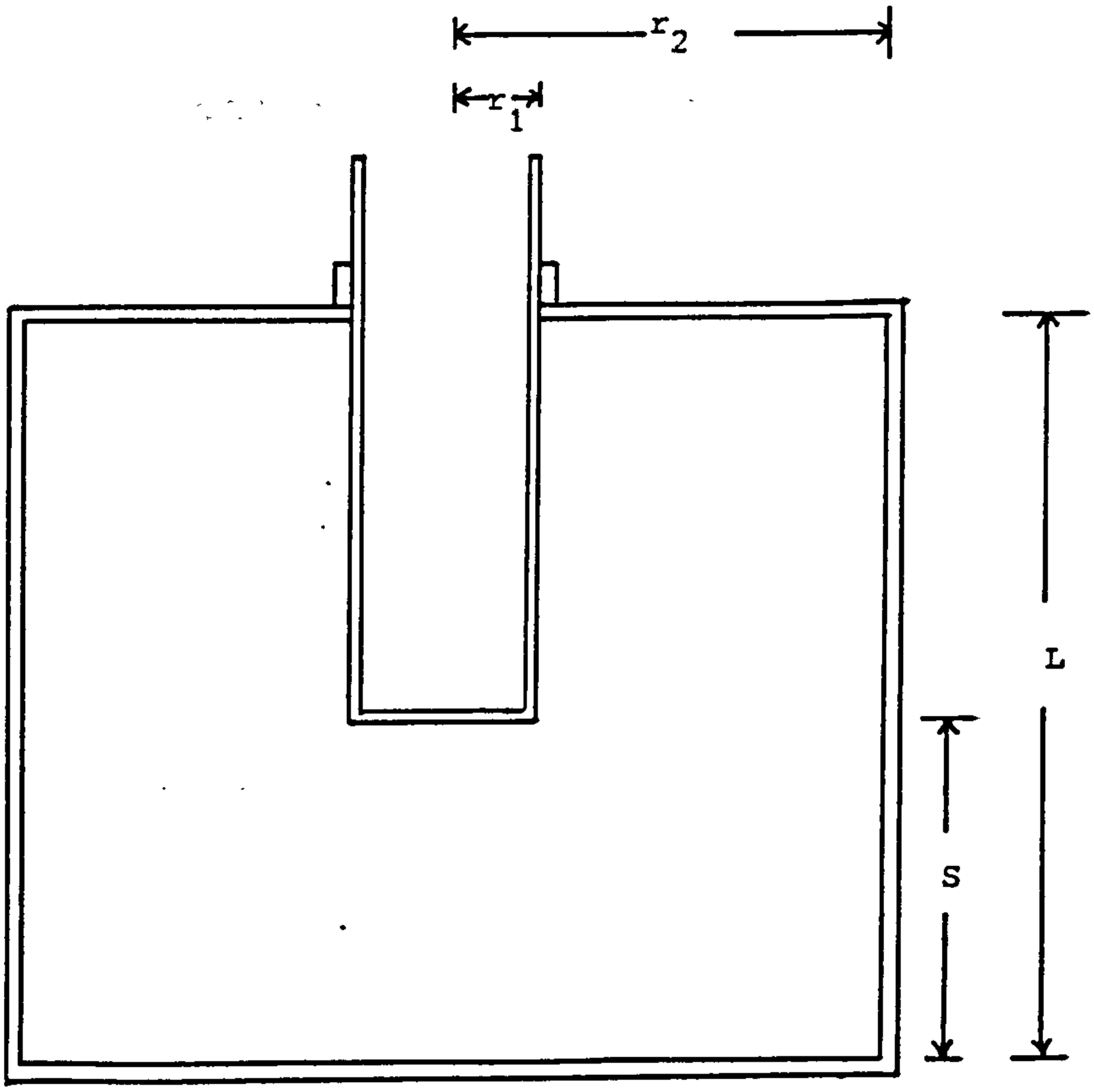

(c) An experimental cavity

Figure 1 Coaxial resonant cavity

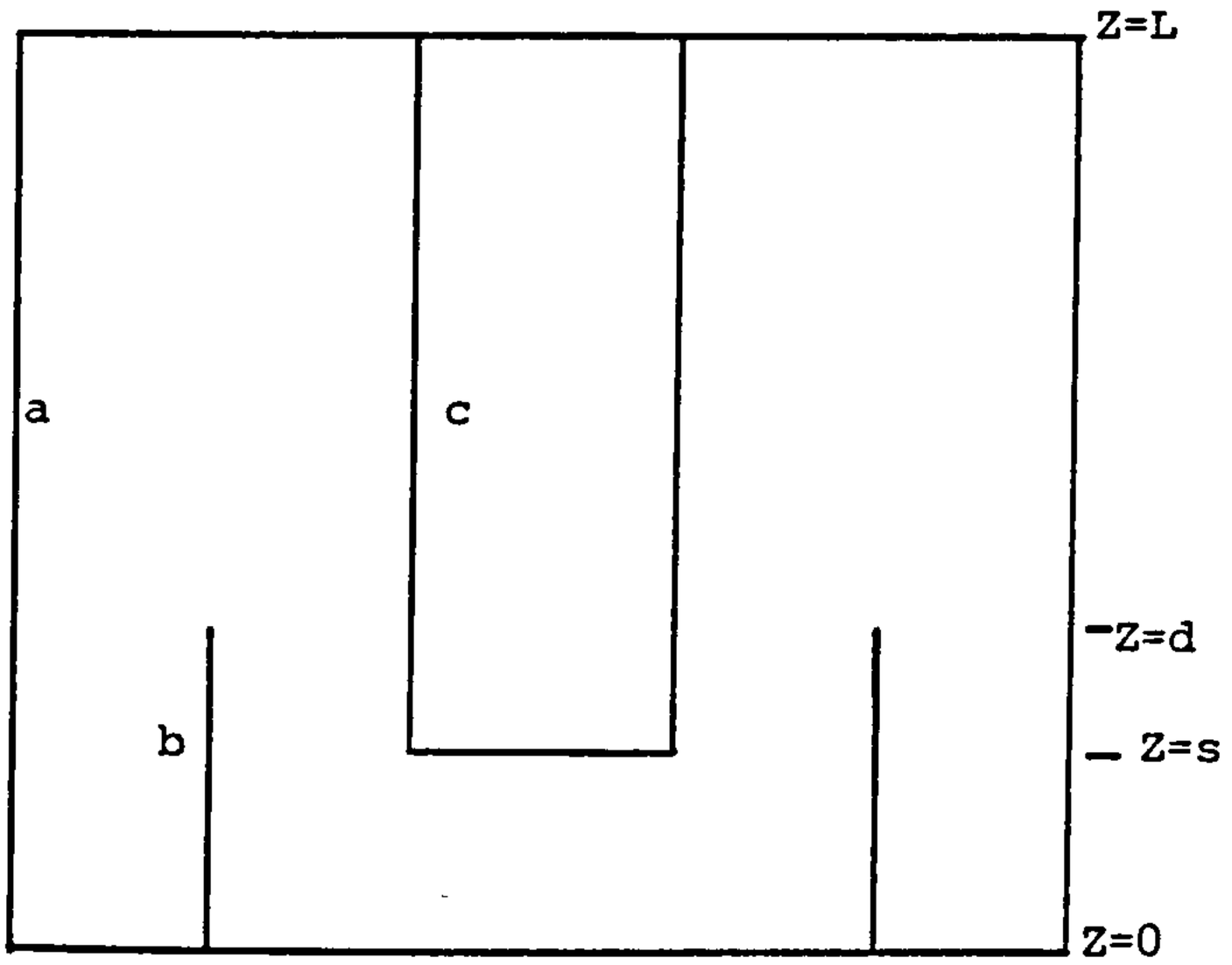

(a) A two-dimensional view of the three cylinders

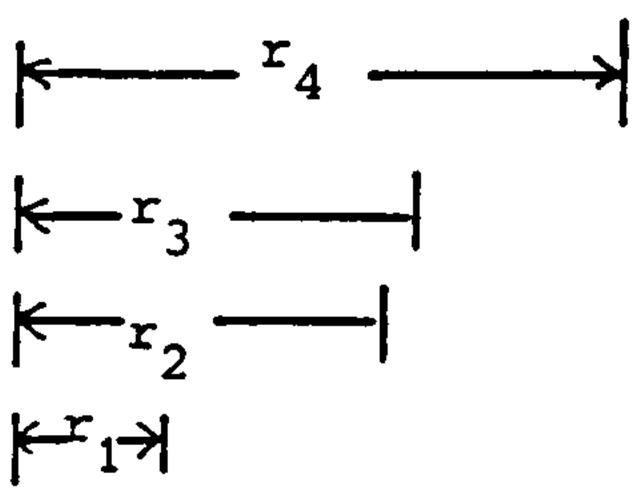

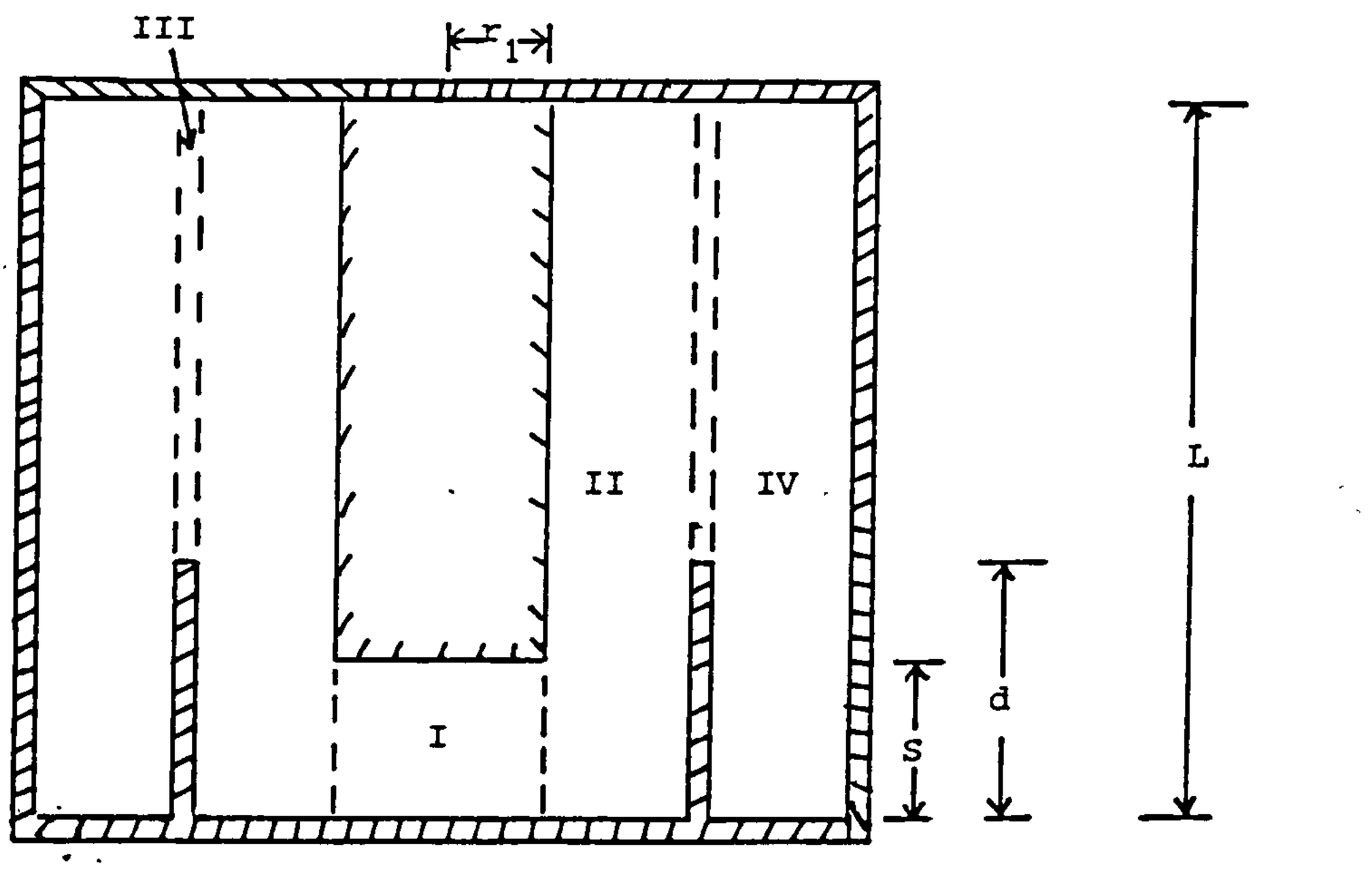

(b) Division into analytical regions showing various dimensions

Figure 2 A multicylindrical cavity

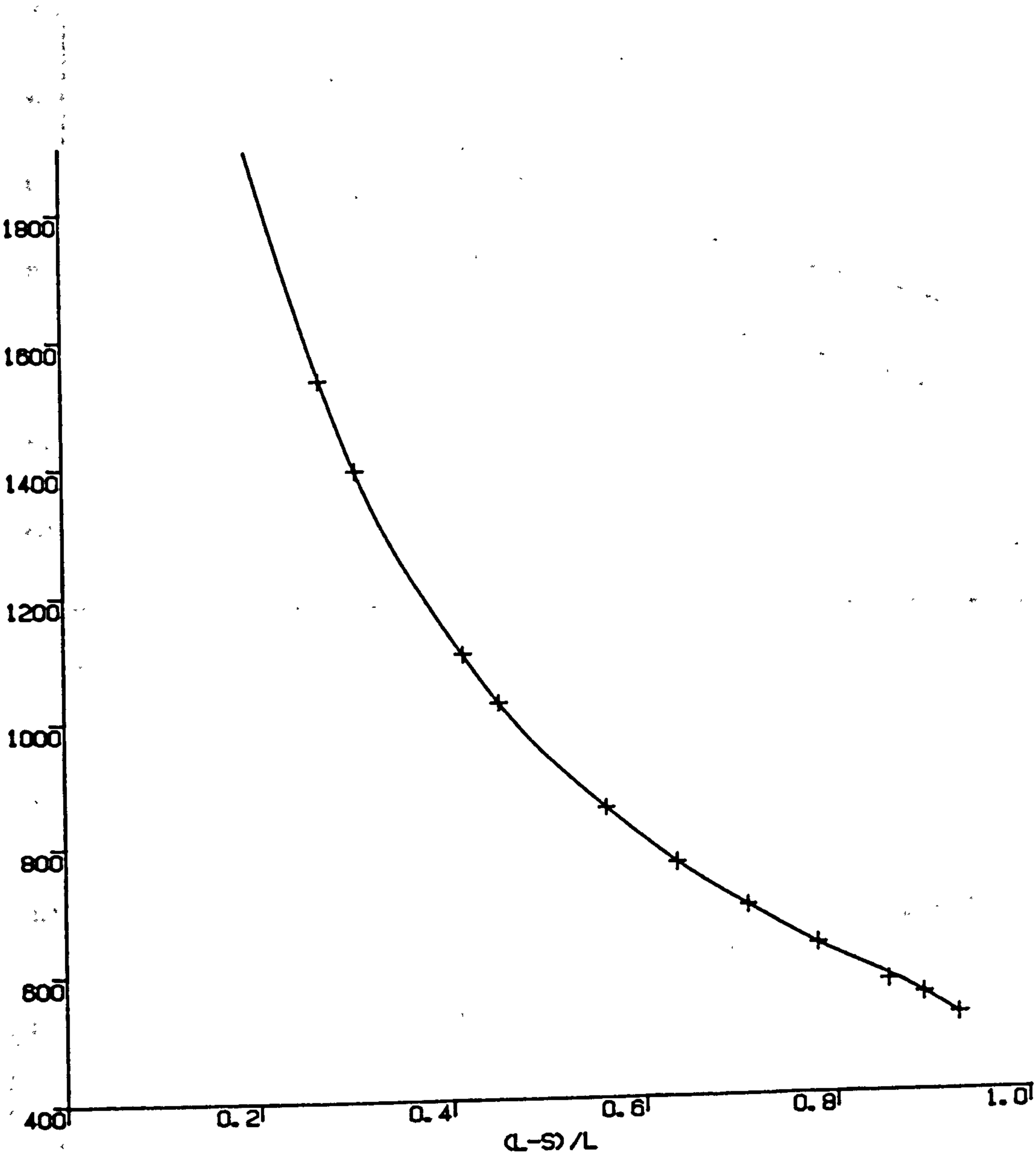

Figure 3(a) Tuning curve for the test cavity

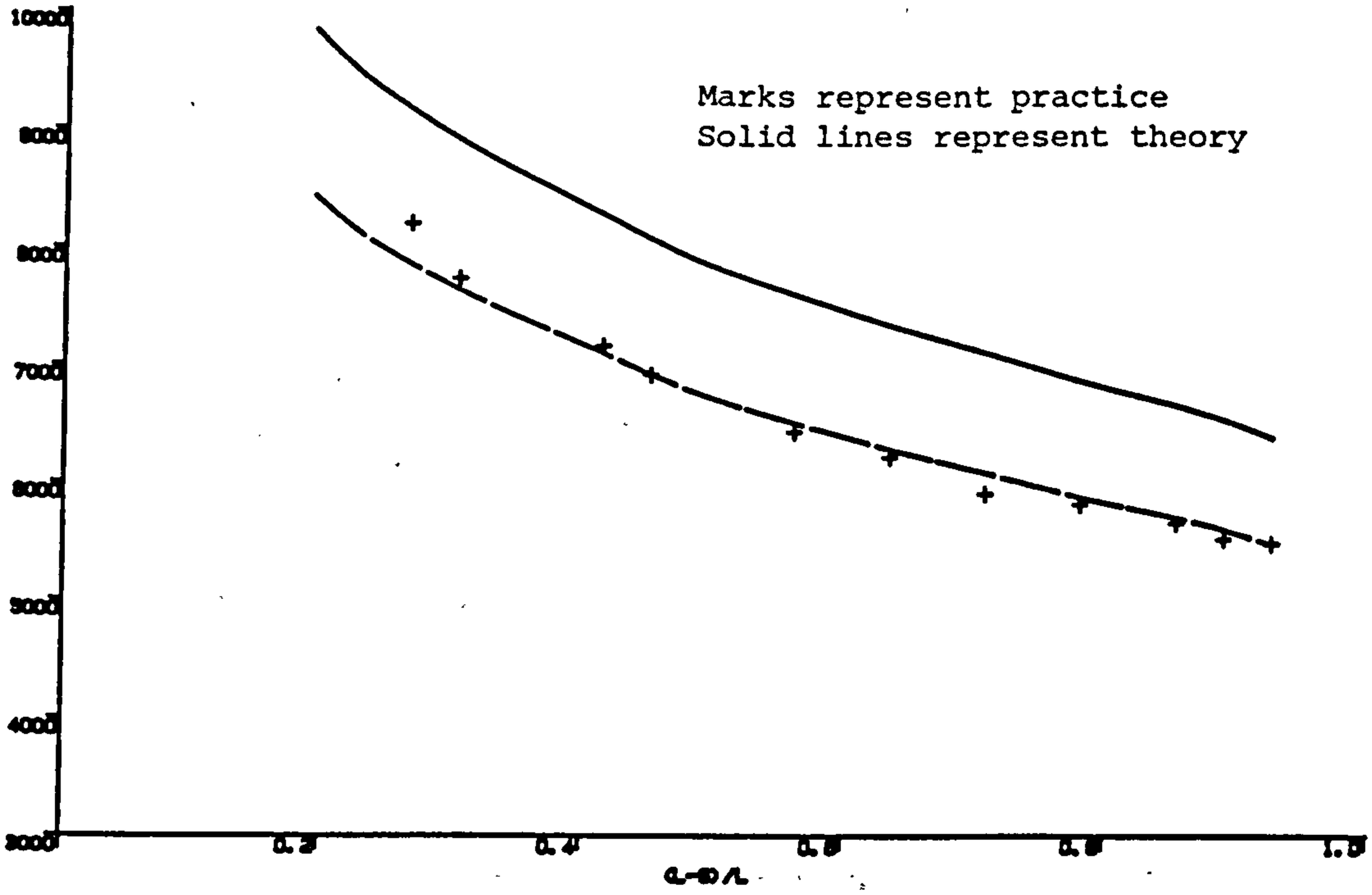

(b) Q_o vs. (L-S)

Broken line represents the theoretical Q scaled by 6/7

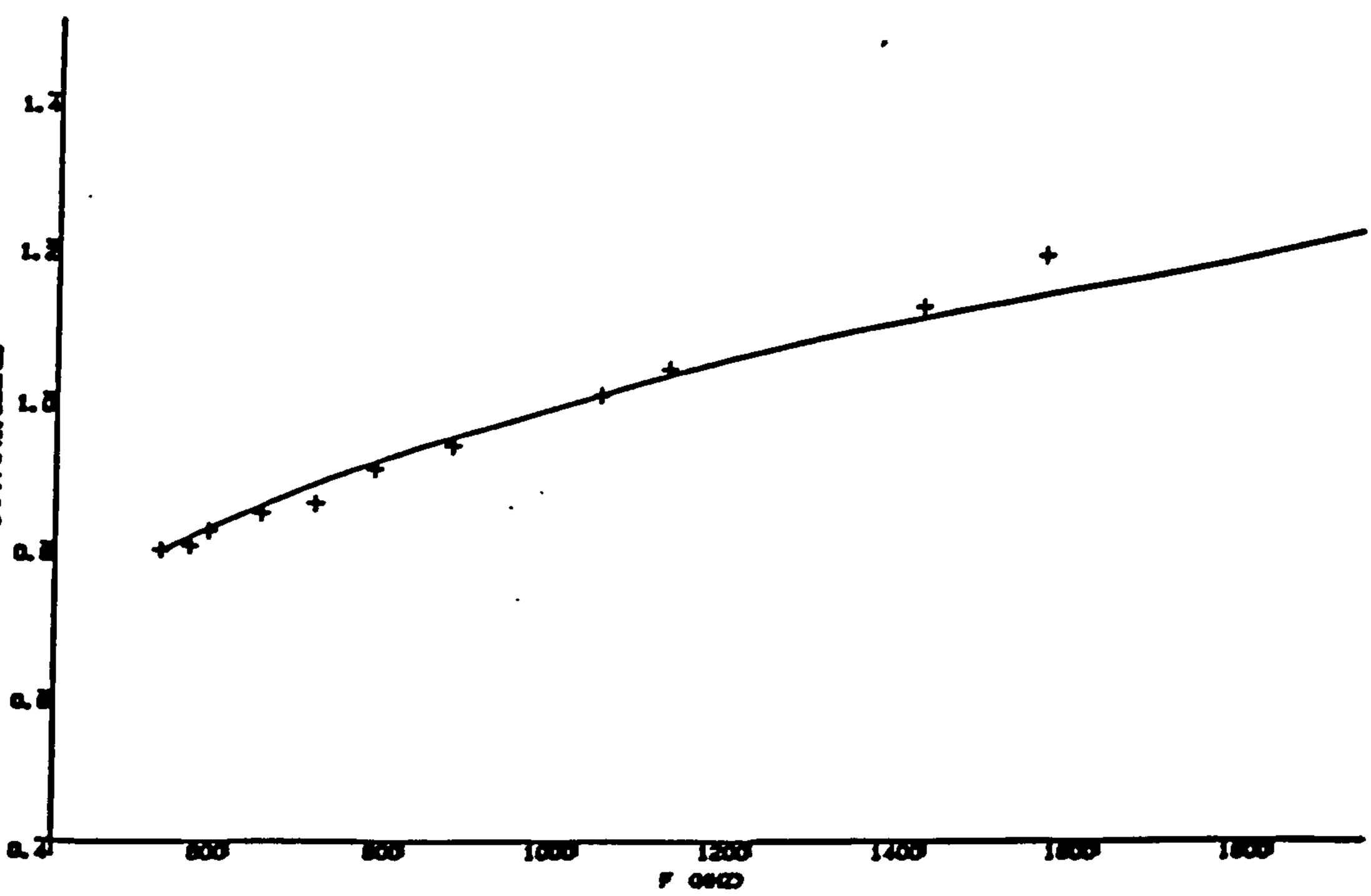

(c) $Q(f)/Q_o(1.02GHz)$ vs. frequency

Figure 3 Resonant characteristics plot

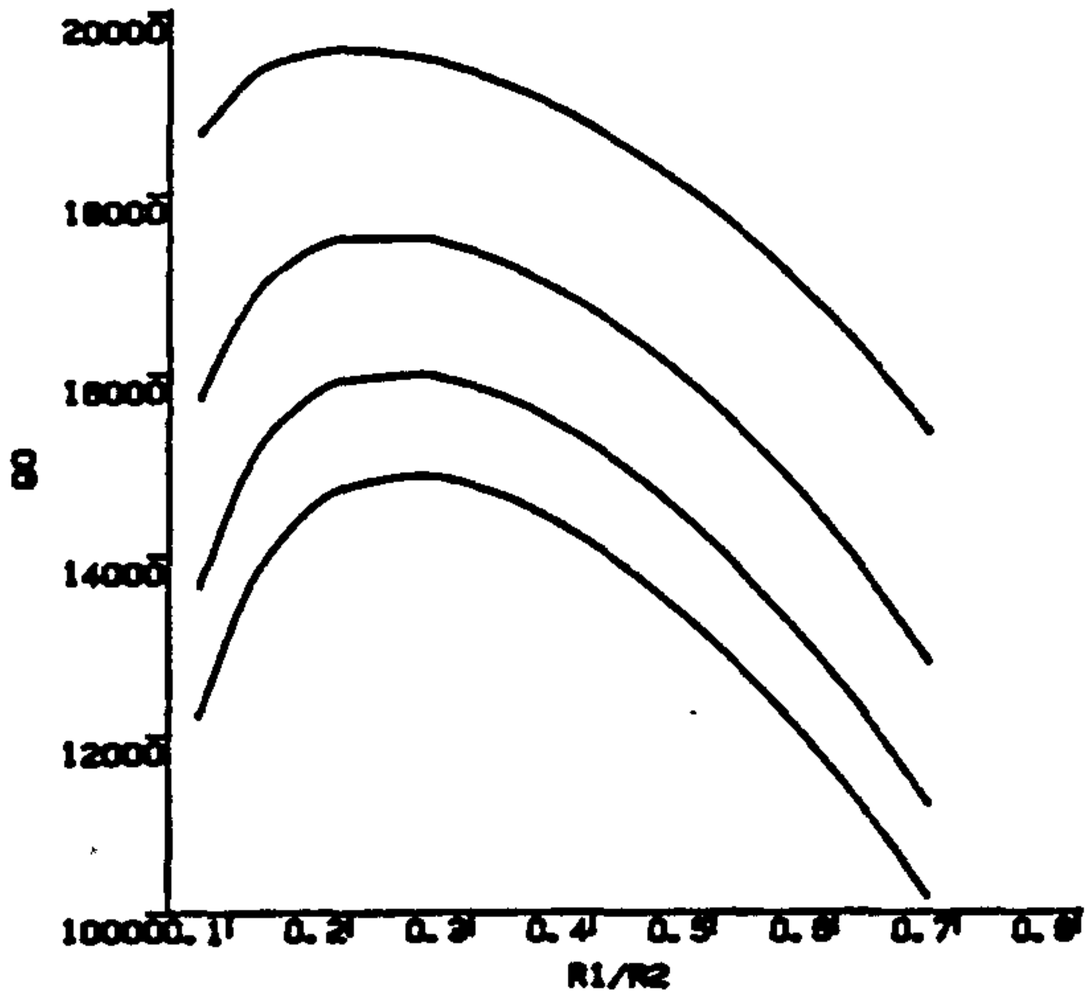

Figure 4 Variation of Q with the ratio $\frac{\text{inner conductor radius}}{\text{outer conductor radius}}$ for selected frequencies

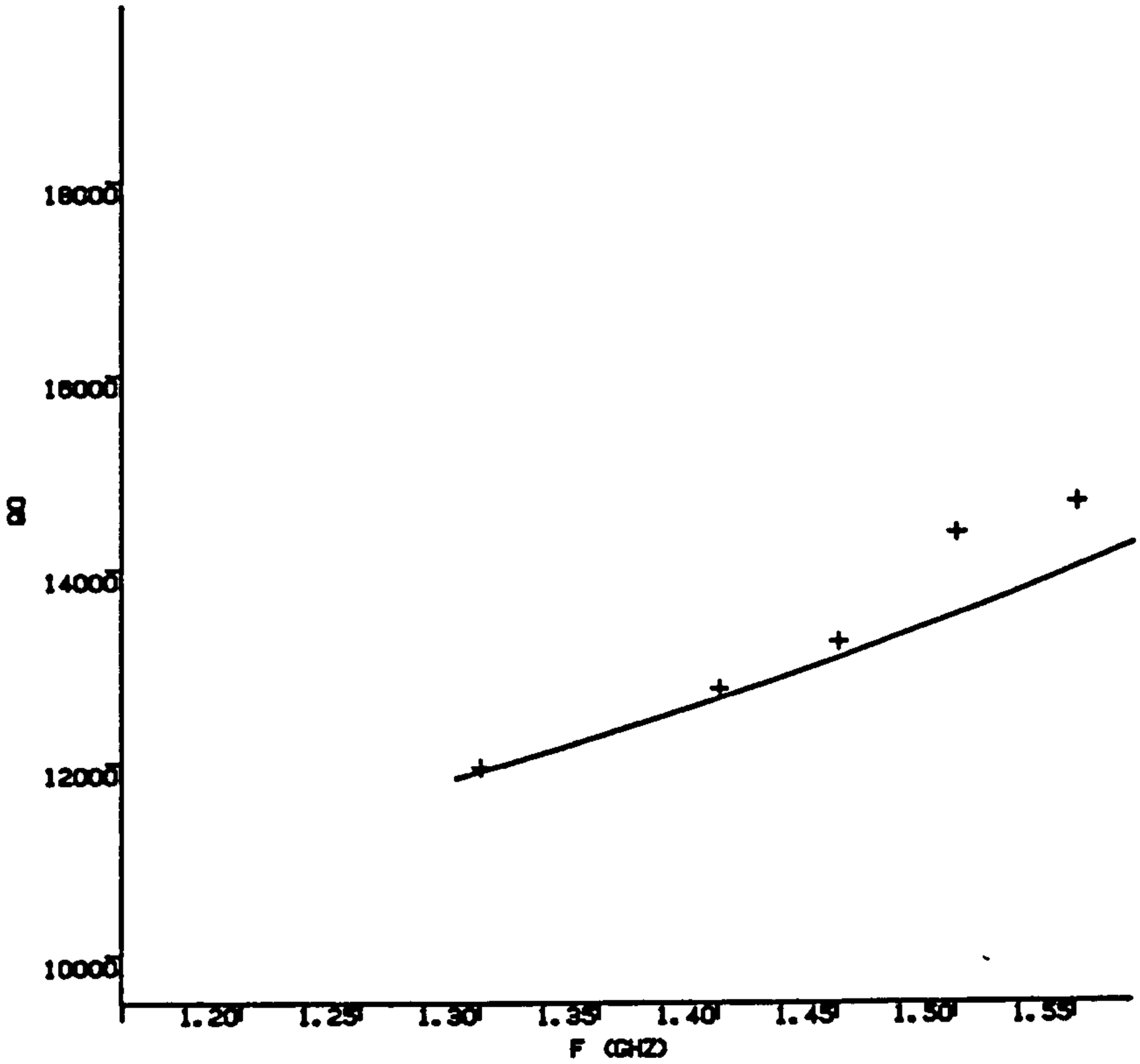

(a) Q_o vs. frequency (theory and practice)
(scaling factor 6/7)

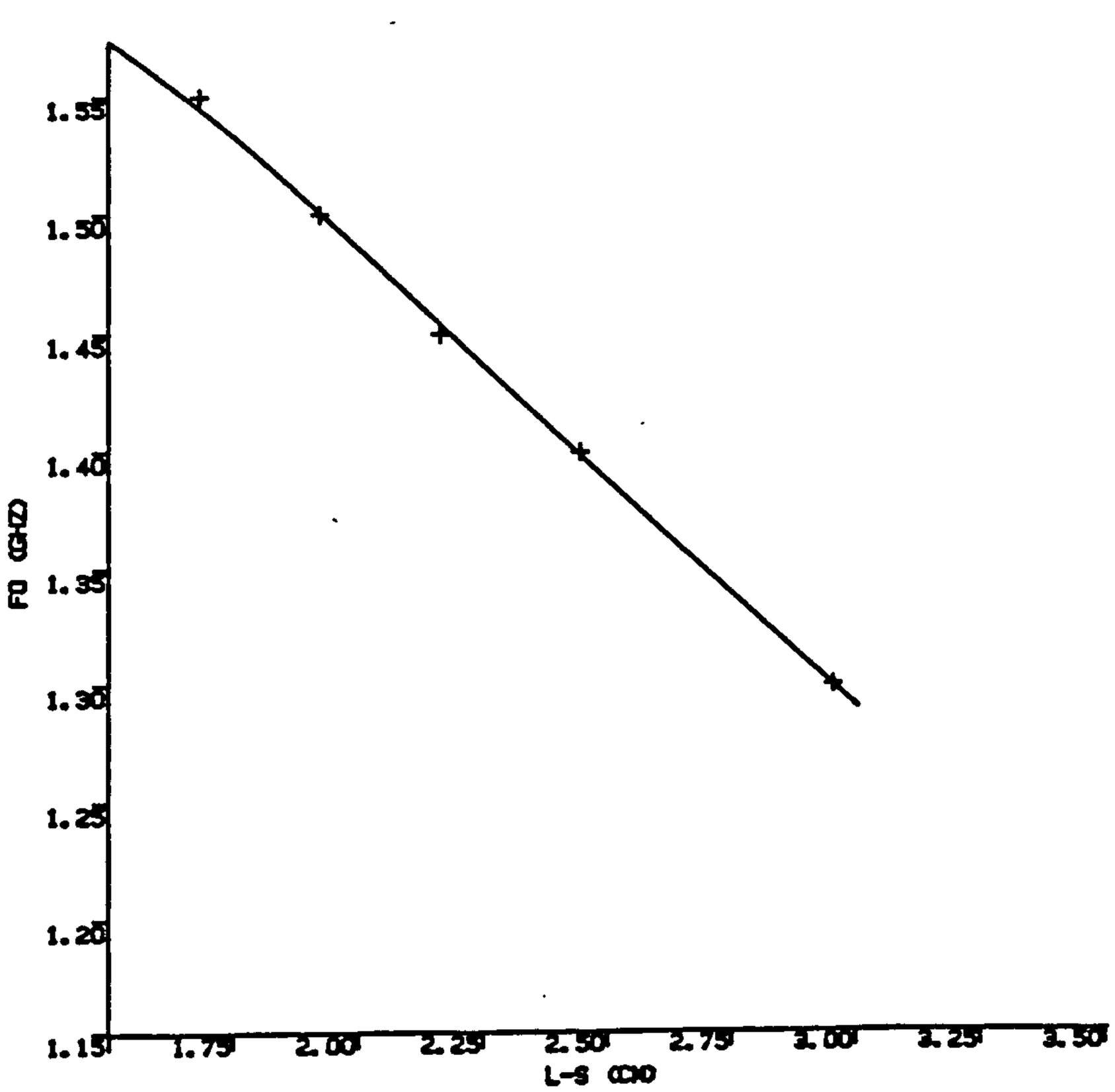

(b) Frequency vs. length of inner conductor

Figure 5

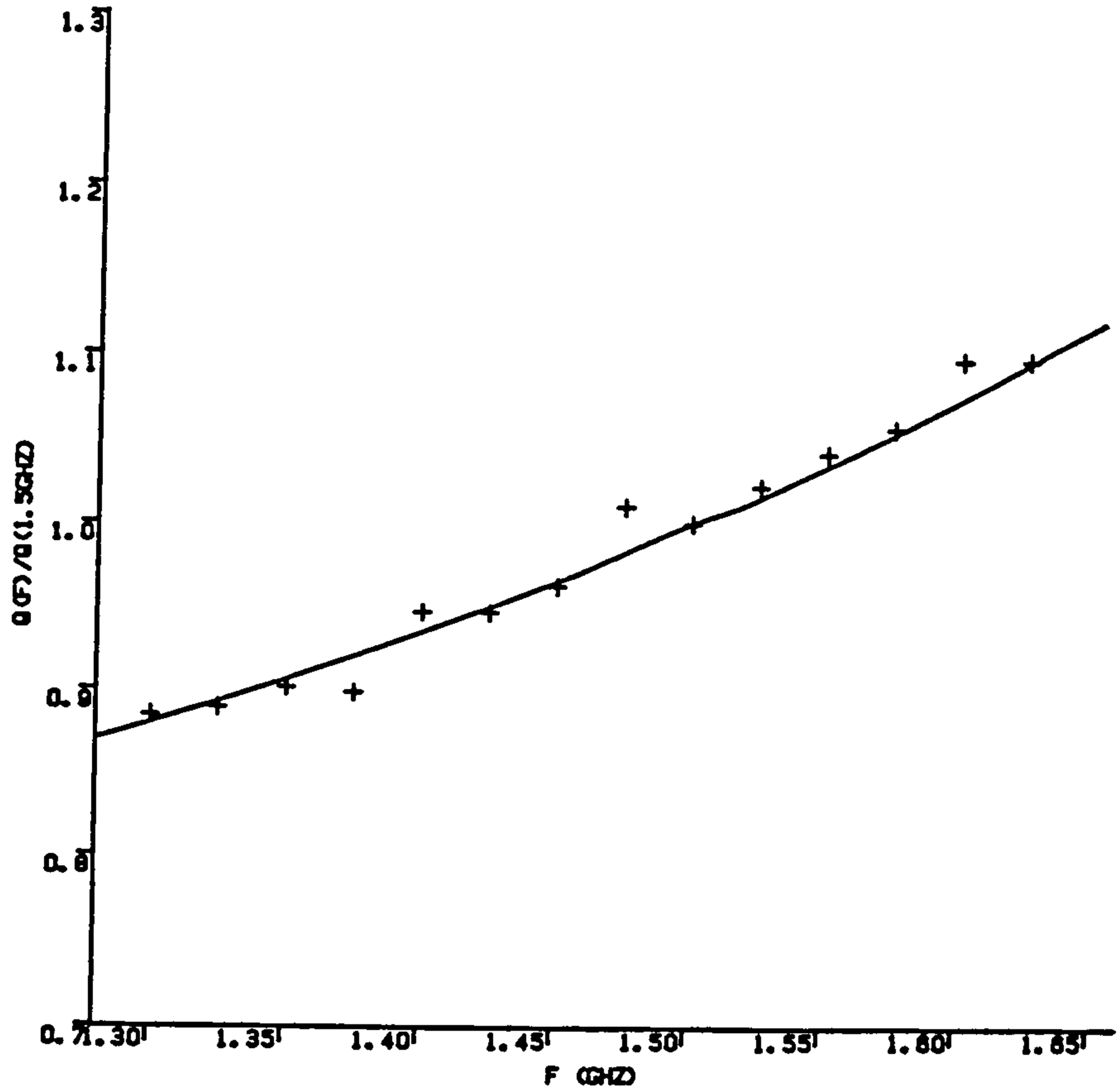

Figure 6 Q(f)/Q (1.5GHz) vs resonant frequency

CHAPTER FOUR

FREQUENCY TUNING AND TEMPERATURE COMPENSATION

4.1 Introduction

A resonant cavity designed for communication system use is meant to operate at the frequency of the source or load. However, in spite of the theory and design procedures available for resonant cavities, the resonant frequencies obtained in practice may differ slightly from the desired frequencies, the reason being the approximations in theory, mechanical imperfection and various design uncertainties. Quite often a communication system may not only be required to operate at a single centre frequency but over a range of frequencies. For these reasons, a tunable resonant cavity is required for which the range of tuning would depend on the requirement and application. Two types of such cavities have been discussed in Chapter Three

When the weather conditions vary, the resonant parameters of a resonant cavity would vary. Of all the possible variations, changing temperature and humidity would exert the most adverse effect. If the cavity is hermetically sealed like those discussed in Chapters Two and Three, the effect of humidity can be neglected. Since the cavity is constructed from metallic conductor and because the dimensions of the conductor would vary with temperature, temperature changes would affect the resonant frequency most drastically. And to reduce the resonant frequency change with temperature variation, a temperature compensation means is needed. Compensating for frequency changes may take different dimensions, but essentially the methods are based on frequency tuning techniques. If, therefore, the tuning problem can be adequately solved,

the method for compensation would have been solved in addition.

Many useful methods have been developed over the years for the frequency tuning and stabilisation of most commonly employed resonant cavities[1-13]. To achieve highly stable resonant cavities, conductors having small thermal coefficients of expansion like super-invar and ordinary invar have been employed[10]. Though this reduces the temperature dependency of the cavity it may drastically lower the cavity quality factor. It would be more expensive and heavier. Because of the low thermal conductivity associated with invar, transient effects may be prolonged when compared with similar cavities constructed from copper, aluminium and brass.

The cavities to be considered are those constructed from copper, brass or aluminium. And the techniques discussed here include an economic method for compensation.

4.2 General Theory and Analysis

If the inner wall of a cavity deforms as depicted in Fig. 1, its resonant frequency will change. Then if the deformation is extremely small, the resonant frequency changes according to perturbation theory[1]. This is expressed as:

$$\frac{\Delta f_o}{f_o} = \frac{\int_{\Delta V}(\mu H^2 - eE^2)}{4W} , \qquad (1)$$

where

$$W = \tfrac{1}{2}\int_V \mu H^2\, dV = \tfrac{1}{2}\int_V eE^2\, dV ,$$

V = Total volume of cavity, and

ΔV = Deformation in terms of volume.

The perturbing material can be a conducting material introduced into the cavity or side wall of the cavity bulging in or out. The equation

says that if we insert a metal piece in the electric field region of the cavity, the resonant frequency would fall and if we do so in the magnetic field portion the frequency rises. It also shows that the rate of frequency change per volume of the perturbing material depends on the stored energy distribution at the point of perturbation. Actually this equation, though limited to extremely small perturbation can be found to give insight into most frequency changes resulting from large perturbing materials for which the equation does not sufficiently apply. Regarding temperature compensation, this equation may be found sufficient in that for some metal walls the frequency deviation for limited temperature excursion would permit its direct application[10]. For all types of cavities for which frequency stability is to be achieved with wide tuning range, a different analytical method would be necessary. The reason is that the tuning material amounts to an additional boundary which completely modifies the field in the cavity and to adequately account for such extra boundary condition, a complicated mathematical function would have to be solved. In all, the major problems encountered with tuning can be divided into two categories representing cases for which the field is unchanged and where the field is completely modified.

The first category includes all types of coaxial reentrant cavities for which by simple variation of the inner conductor length, the frequency can be varied proportionately. The technique of varying the inner conductor length amounts to virtually no extra boundary condition, thereby leaving the field structure unchanged. It has been observed that over quite a wide range of frequencies, the tuning curve is reasonably linear as shown in Fig. 5 (Ch. Three).However,like other types of resonators, decrease of the cavity volume also decreases the cavity Q_o. To keep the quality factor reasonably constant over the tuning range, other

tuning mechanisms have been described[12]. This method[12] is only limited to very narrow frequency range in addition to complication of the theoretical knowledge of the cavity field equations. The use of the centre conductors is found to be the most effective method for the frequency tuning of all types of reentrant cavities either over narrow or very wide frequency range because it is simpler both mechanically and analytically.

The second category where the fields take different forms from the original waveforms is found in the waveguide cavities. However, if the tuning plunger is inserted at the centre of a circular cavity we can treat it like a coaxial reentrant cavity. If the plunger is extremely thin, solutions similar to rectangular cavity's could be applied as will be outlined later. Alternatively, the procedure due to Barinova et al[13] could be followed.

The perturbation formula has shown two directions in which the resonant frequency can be changed: positive increment by perturbing at high magnetic field region or negative increment by inserting material at high electric field region. The method to be employed would depend on the resonant cavity mode we are considering. In other words, the point at which perturbation is made would depend on the field components and distribution and the rate at which tuning would be effected per unit volume of the material. For rectangular cavity TE_{101} mode for example, there is only one electric field component with one antinode compared with the magnetic field's four antinodes. It is therefore necessary for an effective frequency change to perturb the cavity at high electric field region. Whichever method is chosen, an arrangement which would cause the frequency to change either way

can be made as will be explained later.

Usually the metal piece, the plunger, is cylindrical in shape for easy fabrication and of course makes solution to the problem simpler. Since it is extremely difficult to obtain exact solution of electromagnetic field distribution in the perturbed rectangular cavity, a different approach as outlined below is necessary for the solution.

Fig. 2 shows a cross-section of a rectangular cavity with a thin circular plunger inserted at the mid-point of the end plate at y=0. We shall consider the case of the TE_{101} fundamental mode for which the plunger is in the position of highest electric field region of the unperturbed cavity. In this way, the magnetic field is taken to be zero within the region of perturbation and the electric field is thus assumed constant over the region occupied by the plunger. The plunger therefore constitutes a capacitive post. The result is that the resonant frequency is proportional to the change in capacitance resulting from the post. The capacitance change depends on:

(a) the field intensity at the point of insertion,

and (b) the electric energy in the cavity relative to that of the post considered as a capacitor.

The change in capacitance can therefore be written as

$$\Delta C = PK_f \tag{2}$$

where P has been defined by (b) and K_f defined by (a) above. To find K_f, we have to consider and solve for the stored electric energy in the cavity and an equivalent lumped capacitance. For this reason, we can define for a cavity the stored electric energy W_ε by

$$W_\varepsilon = \frac{\varepsilon}{4} \int_v |E|^2 \, d\tau \tag{3}$$

where v is the volume of the cavity and $\vec{E}$ is the electric field intensity.

From lumped impedance concept,

$$W_\varepsilon = \frac{1}{2} C_f V^2 \tag{4}$$

where C_f, V are the equivalent capacitance and voltage respectively.

Differentiating equations (3) and (4) with respect to the volume

$$\frac{dW_\varepsilon}{d\tau} = \frac{\varepsilon}{4} |\vec{E}|^2 \tag{5}$$

and

$$\frac{dW_\varepsilon}{d\tau} = \frac{1}{2} V^2 \frac{dC_f}{d\tau} + CV \frac{dV}{d\tau} \tag{6}$$

The equivalent voltage V for the cavity is defined as

$$V = \text{average} \int \vec{E}.\vec{d\ell}$$

$$= \frac{\int |\vec{E}| d\tau}{A_n}$$

where A_n is the surface area normal to the E-component, therefore

$$\frac{dV}{d\tau} = \frac{|E|}{A_n}$$

For TE_{101} mode, the equivalent voltage is given as

$$V = \frac{4|E_o|}{\pi^2} b \tag{7}$$

Equation (6) therefore reduces to

$$\frac{dW_\varepsilon}{d\tau} = \frac{8E_o^2 b^2}{\pi^4} \frac{dC_f}{d\tau} + C_f \frac{4E^2}{\pi^2 A_n} \tag{8}$$

Equating (4) and (8), we have

$$\frac{\varepsilon}{4} |E|^2 = \frac{8E_o^2 b^2}{\pi^4} \frac{dC_f}{d\tau} + \frac{4E^2 b}{\pi^2 A_n} C_f \tag{9}$$

Equation (9) is the general capacitance function in the cavity.

Since the initial electric field intensity is assumed to be constant over the region displaced by the plunger, we can approximate the field displaced to the field strength at the centre of the region. That is,

$$E \cong E(\frac{a}{2}, y, \frac{d}{2}) = E_o.$$

Therefore

$$\therefore \quad |E| = E_o .$$

Substituting this into equation (9) and by simple transformation we can re-write equation (9) as

$$\frac{\varepsilon}{4} = \frac{8b^2}{\pi^2} \frac{dK_f}{d\tau} + \frac{4b}{\pi^2 A_n} K_f , \qquad (10)$$

where K_f now indicates the capacitance function within the region displaced by the plunger for which K_f vanishes with the plunger.

Therefore

$$\frac{\pi^2 \varepsilon A_n}{16b} - K_f = \frac{2A_n b}{\pi^2} \frac{dK_f}{d\tau}$$

The differential equation on separation of variables and integration becomes

$$- \ln(\frac{\pi^2 \varepsilon A_n}{16b} - K_f) = \frac{\pi^2 r_1^2 b_1}{2A_n b} + P$$

where P is a constant. Therefore

$$\frac{\pi^2 \varepsilon A_n}{16b} - K_f = B \exp(- \frac{\pi^2 r_1^2 b_1}{2A_n b}) \qquad (11)$$

Since $K_c = 0$ when the plunger is withdrawn,

$$B = \frac{\pi^2 \varepsilon A_n}{16b}$$

Hence, K_f can be written, on substitution of B, as

$$K_f = \frac{\pi^2 \varepsilon A_n}{16b} \left[1 - \exp\left(-\frac{\pi^2 r_o^2 b_1}{2A_n b}\right)\right] \qquad (12)$$

Using equations (3) and (4), the cavity equivalent lumped capacitance C_o in line with the definitions above is

$$C_o = \frac{\pi^4 \varepsilon ad}{128b} \qquad (13)$$

From (6) P can be written as

$$P = \frac{C_{st}}{\varepsilon r_1}$$

where C_{st} is the static capacitance of the region due to the insertion of the plunger and εr_1 is the static capacitance of the post assumed by itself as a capacitance such that as $r_1 \to 0$, $P \to \infty$. This is because with r_1 considered as infinitesimally small and for b'=b, the electric field is completely earthed for the TE_{101} mode. The static capacitance C_{st} for the case of a square surface for which $A_n = a^2$ is given as

$$C_{st} = \frac{8\pi\varepsilon b_1}{\ln(a/r_1)} + C_{fr_1} + C_{fr_2} \qquad (14)$$

where the first term on the RHS of the equality sign is the static capacitance of a cylinder parallel to a rectangular cylinder and located at the centre of the rectangle.. C_{fr_1} is due to fringing field and C_{fr_2} due to proximity of the end of the plunger to the end plates of the cavity. The latter is therefore due to excess fringing effect. C_{fr_1}, C_{fr_2} can only be derived empirically. Both are assumed proportional to the distance between the side walls and the plunger, the circumference and the length of the plunger and the separation from any of the end plates. They are given as

$$C_{fr_1} = \frac{2\pi r_1 a^2}{b} \frac{b_1}{s} \tanh \frac{b_1}{s} \qquad (15)$$

$$C_{fr_2} = \begin{cases} \dfrac{2\pi r_1 a\varepsilon}{b} \cdot \dfrac{3b_1}{b} \tanh\left(\dfrac{2b_1 - b'}{s}\right) & \text{for } 0 \leq b' \leq \dfrac{b}{2} \\ \dfrac{2\pi r_1 a\varepsilon}{b} \cdot b_1 \tanh\left(\dfrac{2b_1 - b'}{2s}\right) \cdot \left(\dfrac{1}{b} + \dfrac{1}{b+b_1}\right) & \text{for } \dfrac{b}{2} \leq b' \leq b \end{cases} \qquad (16)$$

For rectangular cavity for which the two faces at y=0, y=b are not squares, one can substitute

$\frac{a+d}{2}$ for a and ad for a^2

For a cylindrical cavity, a is replaced by 2R where R is the radius of the cylinder.

The total equivalent capacitance for the perturbed cavity is therefore

$$C_{eq} = C_o + C$$

$$= C_o\left(1 + \frac{C}{C_o}\right)$$

$$= C_o[1 + F(c)]$$

F(c) is a ratio now found independent of any other form the definition of C_o assumes for the cavity.

Since the plunger does not interfere with the magnetic field region or is assumed not to interfere with it, the equivalent lumped inductance, L_o, of the cavity remains unchanged. The resonant frequency, f_o', is therefore

$$f_o' = \frac{\omega_o'}{2\pi} = \frac{1}{2\pi} \frac{1}{\sqrt{L_o C_{eq}}}$$

$$= \frac{1}{2\pi} \cdot \frac{1}{\sqrt{L_o C_o [1+F(c)]}}$$

But $f_o = \frac{1}{2\pi} \cdot \frac{1}{L_o C_o}$,

$$\therefore \quad f'_o = \frac{1}{1+F(c)}$$

The normalised frequency change is therefore

$$f_{norm} = \frac{f_o - f'_o}{f_o} = 1 - \frac{1}{1+F(c)} \qquad (18)$$

By substituting the known expressions in equation (17), the change in frequency can be found. Figure 3 is a plot of frequency deviation against g where g is given as b_1/b. The dimensions of the cavity are given as

a = 13.754cm c = 13.7338 cm b = 3.5179cm

r_1 = 0.1378 cm

It can be observed that theory - the solid line - is very close to practice - the marks.

Actually, this formulation applies only to relatively thin plungers inserted at the region of the cavity where the magnetic field completely vanishes. Fig. 3 (b) shows what happens when r_1 is only doubled. Even though theory and practice closely agree for small b_1, this completely breaks down as b_1 increases.

4.3 Temperature Compensation

The tuning techniques described above would only lower the resonant frequencies from the unperturbed values as the insertion depths increase. If the centre frequency is well chosen within the tuning range, frequency changes can be effected either way.

Since the cavity is made of metal, the temperature coefficient of the resonant frequency is negative. That is, when the temperature rises, the metal expands and the resonant frequency tends to lower. To reduce

the resonant frequency change to temperature variation, a temperature compensation technique is needed. An exact compensation may be hard to achieve because in some cases it may not be possible to have a linear frequency dependency on the temperature. Even where this is so, because of mechanical deviation in the design work at least a slight deviation from an exact compensation would be inevitable. The major aim for compensation is therefore to beat down the frequency dependency on the ambient temperature.

It has been said earlier that extension of the relationship between the centre conductor of a coaxial cavity and the outer conductor still applies to the tunable circular cavity perturbed centrally except that the centre conductor is relatively small. However, since coaxial reentrant cavities have been explored theoretically and practically, this constitutes no problem extending the same theory to the cylindrical cavity tunable by insertion of a metallic rod. In all the considerations so far, variation of centre conductor lengths are used to vary the frequencies. Essentially the tuning procedures follow the same technique, therefore one expects the temperature compensation to follow the same technique for analytical simplicity and unique constructional method. However, the need for linear tuning curve places certain reconsideration of this method for rectangular cavities.

Since the design motives are always to keep the cost low, any common material could be used but the overall outlook of the final product would depend on the selected materials and the designer's own objectives. In some other cases, the compensation can be made by varying the centre conductor electronically. The latter is very necessary when precision is required in the compensation especially because of transient effects. This would however cause additional cost and periodical

checking on the system. The compensation procedure to be described here would be unique for the coaxial and rectangular cavities. It is my belief that using the same technique, it would apply equally to any form of cavity tunable by post or plunger. The cavity is described for cheap and common conductors such as copper, brass or aluminium.

4.4 Design Technique for Temperature Compensation

4.4.1 Coaxial cavity

It is difficult with the theory developed in Chapter Three to study the temperature effect directly . However, it is possible to draw inferences from the wave equations. To determine the exact dependency of the resonant frequency on temperature, numerical evaluation would be necessary.

Fig. 5(a) is a typical temperature characteristic of a hybrid mode reentrant cavity. The cavity has a frequency range centred on 1.5GHz. The dimensions of the cavity have been taken as that of the experimental copper cavity given as follows:

$2r_1$ = 4.1275 cm, $2r_2$ = 13.335 cm, L = 7.62 cm, d = 1.9106 cm.

These dimensions at 22°C would set the resonant frequency at 1501.769MHz. It could be observed that the curve, the solid line, is reasonably linear. If the length d of the centre conductor is kept constant over the temperature range, the frequency deviation gradient is found to decrease by about 20%. This is shown by the broken line. To achieve this in practice, the centre conductor is attached to any material D_1 of zero thermal coefficient of expansion. The arrangement is depicted in Fig. 4. The conductor marked A is the compensator. The method follows:

When the temperature rises, the metal conductors expand. The

effective height, L_e, of aluminium compensator increases and since it is fixed firmly with material D_1, D_1 experiences an outward movement which in turn retracts the centre conductor from the cavity. This on its own causes an increase in the resonant frequency. Fig. 5b shows a plot of the length of the centre conductor which needs to be retracted or inserted to keep the frequency relatively constant at 1501.769MHz. The gradient, ℓ_α, is defined as the length of inner conductor which needs to be retracted or inserted for every degree rise or fall in temperature as to keep the frequency constant. The compensator A has for every rise in temperature from 22°C a gradient given as $L_e\alpha_{al}$. The compensator should be able to retract a length $\ell_\alpha \Delta T$ for a temperature rise ΔT. For this to be satisfied therefore

$$L_e\alpha_{al}\Delta T = \ell_\alpha \Delta T$$

$$\text{i.e. } L_e = \frac{\ell_\alpha}{\alpha_{al}} \qquad (19)$$

where α_{al} is the thermal coefficient of the compensator.

However, this is found insufficient when the end plate containing the device has got a considerable thickness. If the thickness of the plate is t_1, on expansion with temperature rise of ΔT, the change in thickness would be $t_1\alpha_1\Delta T$. This constitutes a further reduction in the length of the plunger within the cavity. This tends to increase the resonant frequency. It can be corrected if the thickness t_2 of the end plate of the centre conductor is made to compensate for this such that

$$t_2\alpha_2 = t_1\alpha_1$$

where α_1, α_2 are the thermal coefficients of expansion of the cavity's and the centre conductor's end plates respectively. Alternatively, the

compensating metal length, L_e, can be readjusted. Thus, if ℓ'_α is the new gradient, we have

$$\ell'_\alpha = \ell_\alpha - t_1\alpha_1 \qquad (20)$$

The compensator length L becomes

$$L_e = \frac{\ell'_\alpha}{\alpha_{al}} \quad \text{at } 22°C$$

For a coaxial reentrant cavity, it can be observed from plots of Figs. 6(a) and 6(b) that the frequency deviation per degree Centigrade for fixed centre frequency does not depend on the normalised values of r_1 and d. For this reason, quite a wide choice of design parameters can be obtained without any effect on the compensator length. The choice however depends on the allowable minimum Q-factor.

The gradient ℓ_α for this particular case is 0.001 mm/°C. The compensator was made from aluminium metal for which the coefficient of thermal expansion is $\alpha_{al} \cong 24 \times 10^{-6}$/°C. From equation (21), the compensator length L_e is computed to be 4.25cm approximately. Fig. 7 shows how theory and practice agree for the compensated cavity. As can be seen from the Figure, there is a slight deviation in the way theory and practice agree. This is obvious at an ambient temperature range of 35°C to 45°C. The deviation can be attributed to experimental error

4.4.2 Rectangular cavity

The procedure is similar to the one described above except for some few alterations. The centre conductor, that is the plunger, is so thin that no provision can be made for attachment of material of zero thermal coefficient of expansion. Therefore, we cannot keep the

i:

insertion depth constant for temperature deviation. In place of this, however, invar with coefficient of expansion much less than the compensators thermal coefficient of expansion is employed. This appears to keep the length relatively constant when compared with copper, brass or aluminium plunger. A plot of temperature characteristic of the cavity with plunger is shown in Fig. 8a. The compensator arrangement is similar to that of Fig. 4. L_e is the length of the compensator, and b_1 the insertion depth of the plunger. The initial condition is set at 22°C ambient temperature. For a temperature change, ΔT, the insertion depth of the plungerbecomes

$$b_1(1+ \alpha_1\Delta T) - L_e(\alpha_2- \alpha_1)\ \Delta T$$

where α_1, α_2 are the thermal coefficients of expansion of the plunger and compensator materials respectively. The effect of the end plate of the cavity could be neglected. This would be found justified when it is compared with the length L of the compensator. Fig.8(b) shows a plot of the length of the inner conductor which must be retracted or inserted to keep the frequency constant. Let the gradient of the curve be e_α. Then

$$e_\alpha\Delta T = b_1 - b_1(1+ \alpha_1\Delta T) + L_e\Delta T(\alpha_2- \alpha_1)$$

$$e_\alpha = -b_1\alpha_1 + L_e\alpha_2 - L_e\alpha_1$$

$$\therefore \quad L_e = \frac{e_\alpha + b_1\alpha_1}{\alpha_2- \alpha_1}$$

For the experimental model, the compensator was constructed from aluminium and the plunger from invar. The cavity is a copper cavity with dimensions a = 13.754 cm, c ≅ 13.7338 cm, b ≅ 3.5179 cm and r_1= 0.1378 cm. The gradient e_α of the curve in Fig. 8b is approximately 0.003mm/°C. For a resonant frequency of 1501.769 at 22°C, b_1= 1.75 cm

and L_e = 14.5 cm. Fig.8(c) shows a plot of frequency deviation against temperature with compensation. The plot shows that within the limit of experimental and numerical errors, theory and practice closely agree.

4.5 Conclusion

So far we have discussed qualitatively the tuning and temperature compensation techniques for the common resonant cavities often employed in communication systems. We have done this upon the background theories of Chapter Three and earlier sections of this chapter. It has been observed that theory and practice do agree reasonably well and highly stable resonant cavities can be constructed from such common and cheap metals like aluminium, brass and copper. In all these considerations, if the required resonant frequency varies, optimum compensation is accomplished by simply changing the lengths of the inner conductor. This method has been found cheaper in cost and design. However, because of the tuning rate the compensator may be too long for practical application when the method is applied to rectangular cavities. Because the technique is such that if the resonant frequency varies, compensation is accomplished by simple variation of the length of the compensator only, highly stable tunable resonant cavities can be constructed. It is possible to calibrate the cavity or follow a standard design chart.

However this compensation technique cannot take care of the transient effect. But, any transient effect can be reduced by employing thin conductors such that the thermal transmission through the cavity and compensator walls is rapid. This would however jeopardise the cavity's resistance to vibrations, especially in the case of cavities employed in mobile communications systems. By employing copper or aluminium conductors, this effect can be reduced considerably. In this

way less expensive cavities can be constructed without sacrificing the stabilisation characteristic. The method is particularly valuable because tolerance of machining, construction and thermal expansion coefficient of the cavity and compensator metals exert less influence on the temperature characteristics at least over the lower range of the ambient temperature.

4.6 References

1. Slater, J C: 'Microwave electronics', Rev. Mod. Phys., Vol. 18, 1946, pp. 467-512.

2. Hansen, W W & Post, R F: 'On the measurement of cavity impedance', J. Appl. Phys., Vol. 19, 1948, pp. 1059-1061.

3. Sedykh, V M: 'A two frequency cavity resonator with independent tuning', Soviet Radio Engng (USA), Vol. 8, 1965, pp. 451-2.

4. Spencer, N A: 'Cavity resonators design charts', Electronics, May 1954, pp. 186-8.

5. Atia, A E & WIlliams, A E: 'Temperature compensation of TE_{011} mode circular cavities', IEEE MTT-24, Oct. 1976, pp. 668-9.

6. Goud, P A: 'Cavity frequency stabilisation with compound tuning mechanisms', Microwave Journal, March 1971, pp. 55,56,58.

7. Bogucki, J & Szklarczyk, Z: 'Temperature compensated cavity resonators for TE_{011} type oscillations', Wiad Telekomm. (Poland), Vol. 18, pt. 3, 1978, pp. 86-7.

8. Brady, M M: 'Simple temperature compensation of large rectangular waveguide resonant cavities', Electronic Engineering, Feb. 1969, p. 198-9.

9. Macdonald, J R: 'Tuning of a rectangular parallelopiped cavity resonator with a circular metallic post', Review of Sc. Instr., Vol. 26, No. 5, May 1955, pp. 433-4.

10. Satto, T; Arai, Y & Iwakumi, M: 'Temperature stabilisation method in a reentrant cavity', Fujitsu Sci. & Tech. Journal (Japan), Vol. 12, 1976, pp. 27-55.

11. Mandel'Shtam, M Ya: 'Rectangular waveguide resonators with capacitive tuning post, tunable over wide limits', Radio Eng., Vol. 23, No. 7, 1968, pp. 63-67.

12. Stephenson, J G: 'Resonant cavity tuning now made easy', Electronics Jan. 1963, pp. 46-51.

13. Barinova, V F; Rayezskiy, S B & Rudoyasova. L G: 'Design of a waveguide resonator which is tunable by inserting a metallic rod', Radio Eng. Electron. Physics (USA), Vol. 20, No. 12, pp. 126-129.

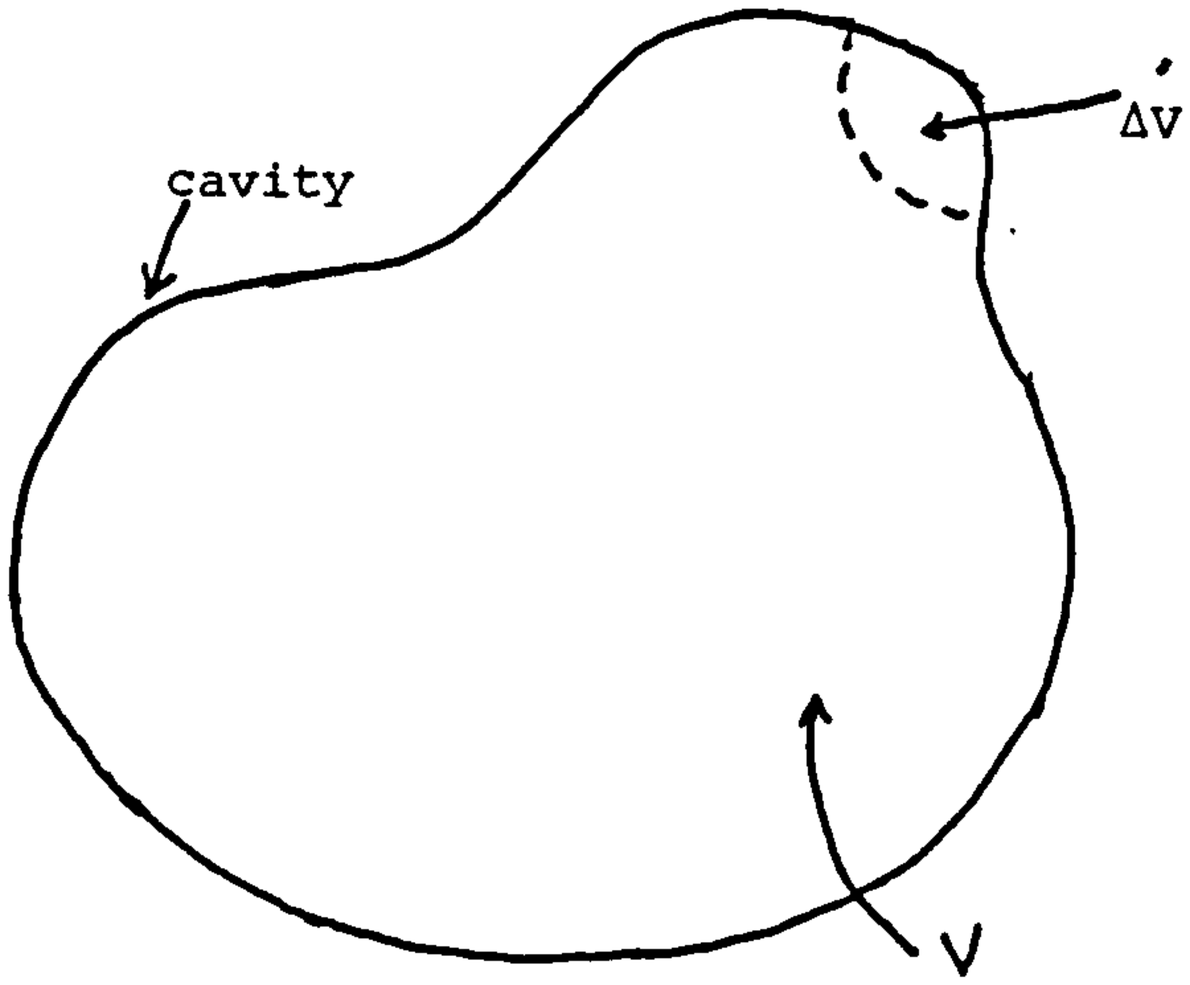

Figure 1 Cross-section of an arbitrary cavity resonator perturbed by means of a material of volume ΔV

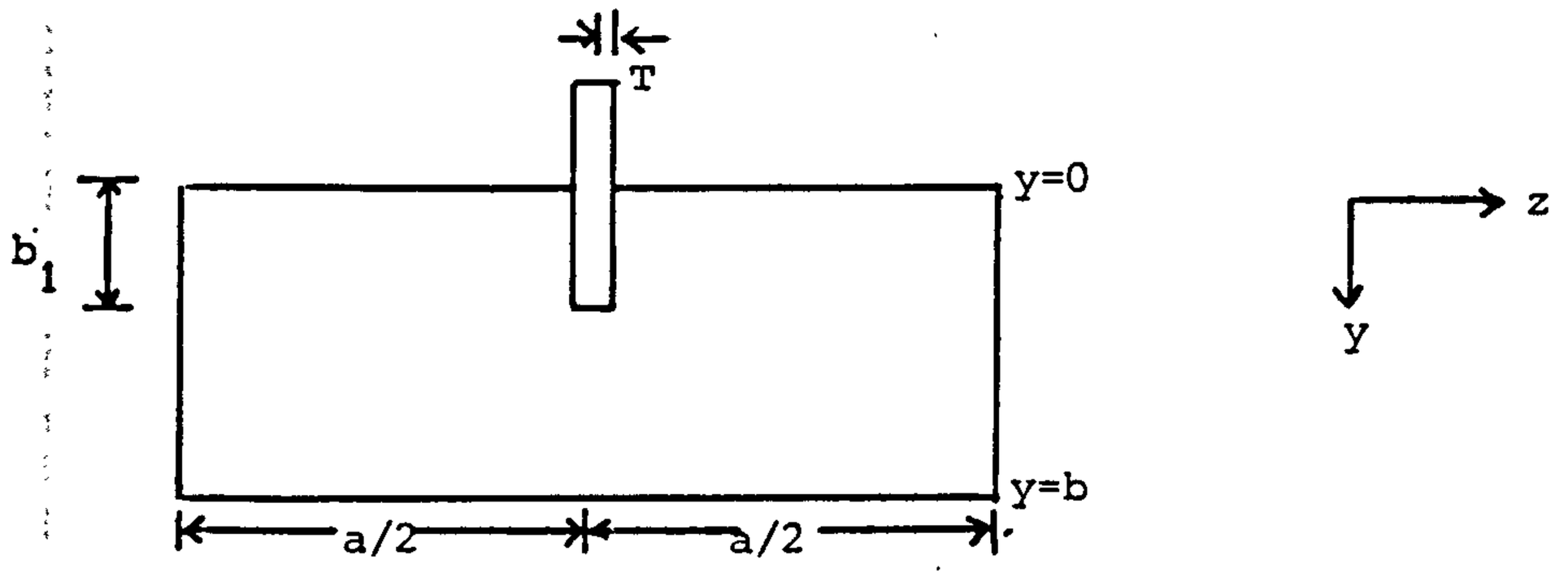

Figure 2 Cross-section of a rectangular cavity showing position of the plunger

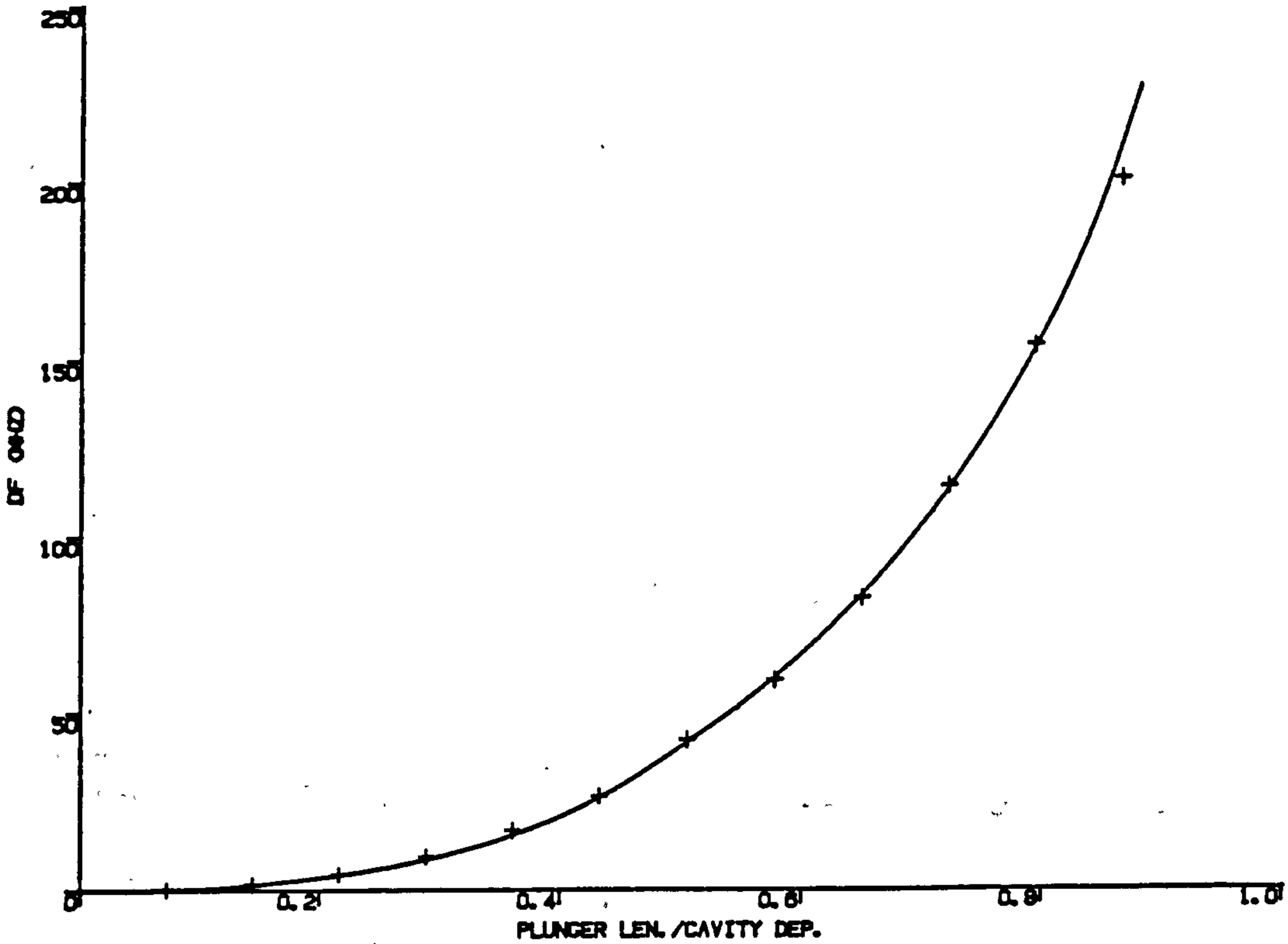

(a) with thin plunger

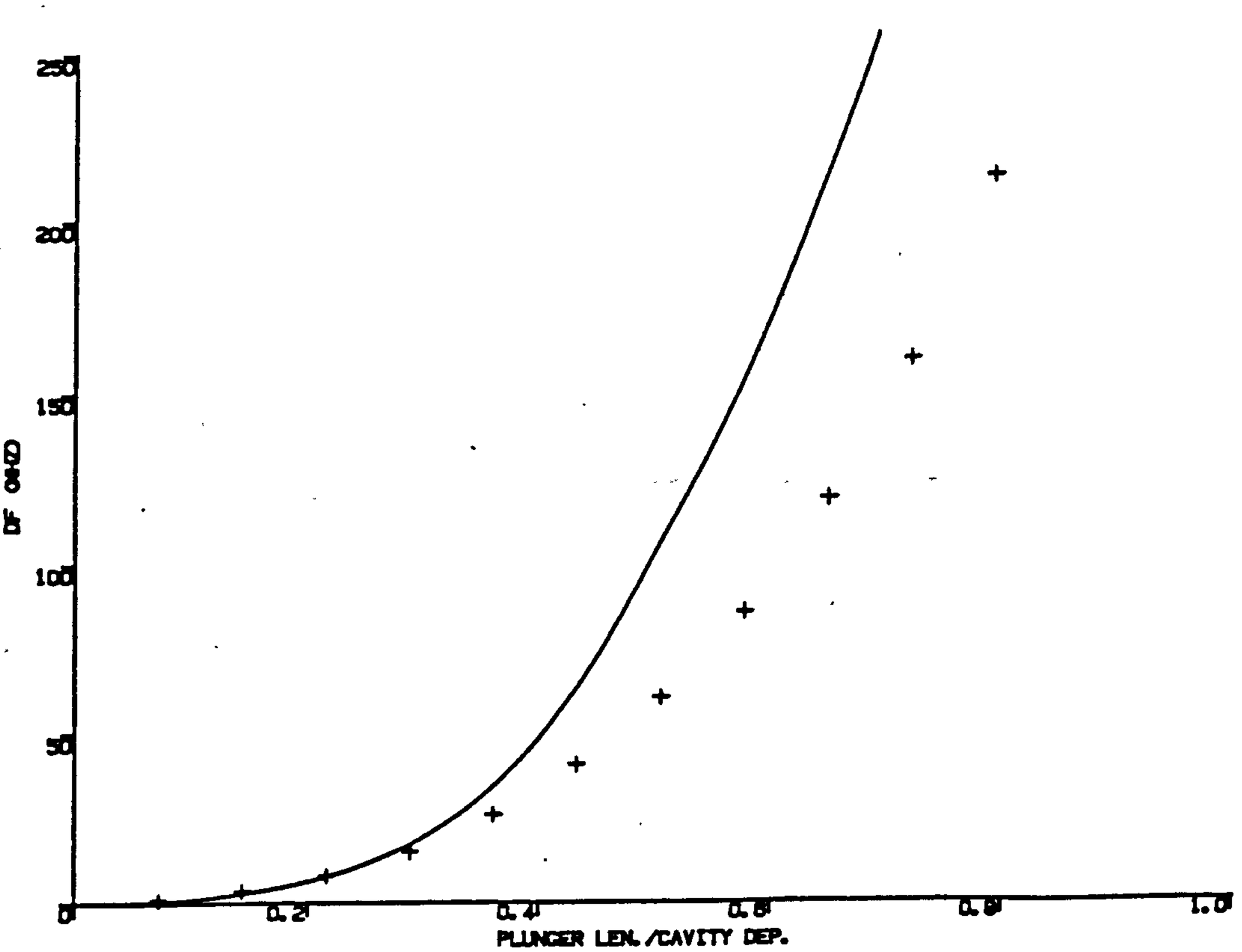

(b) with bigger plunger

Figure 3 Tuning curves for a rectangular cavity

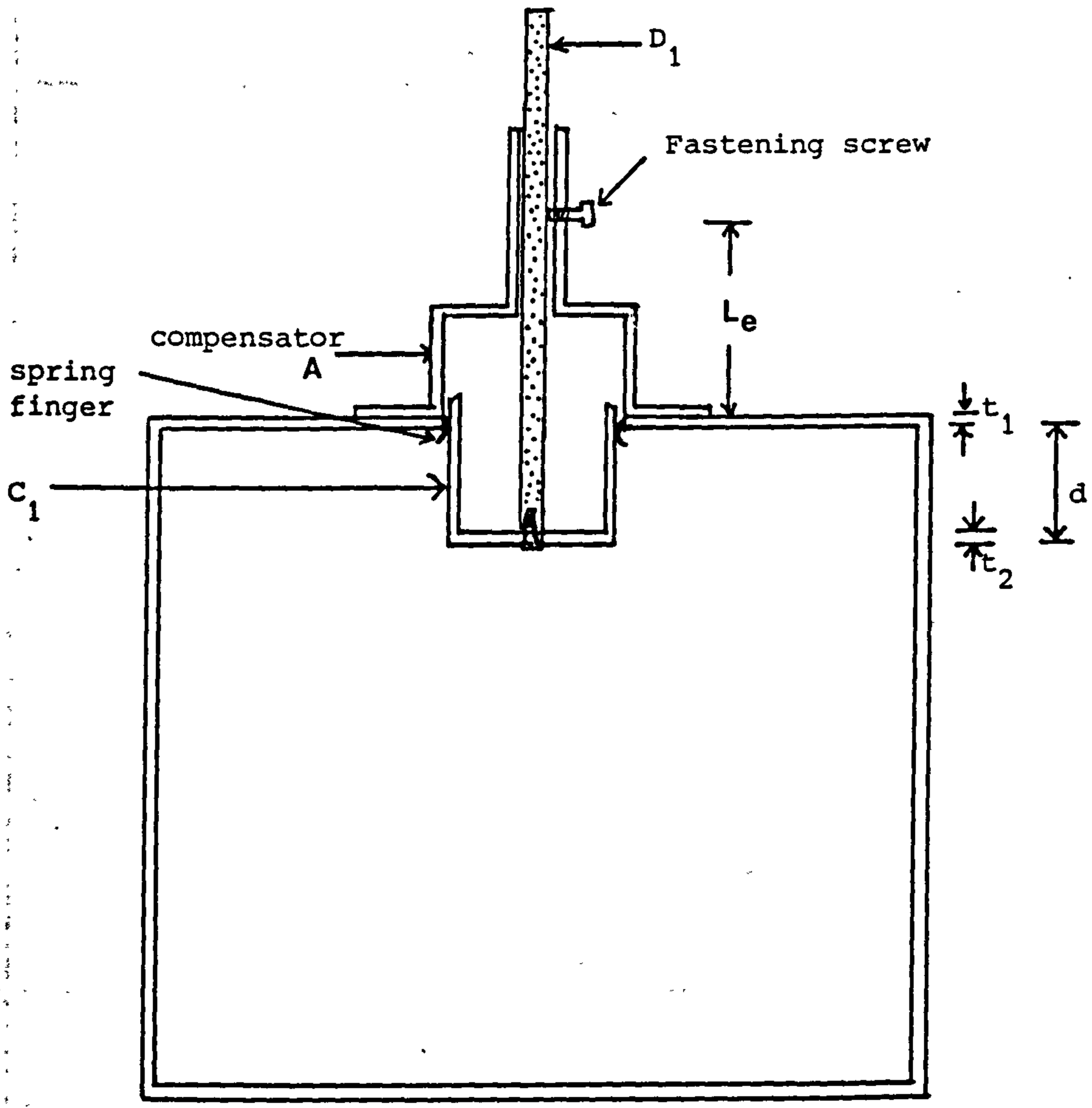

Figure 4 Cross-section of a temperature compensated hybrid mode cavity

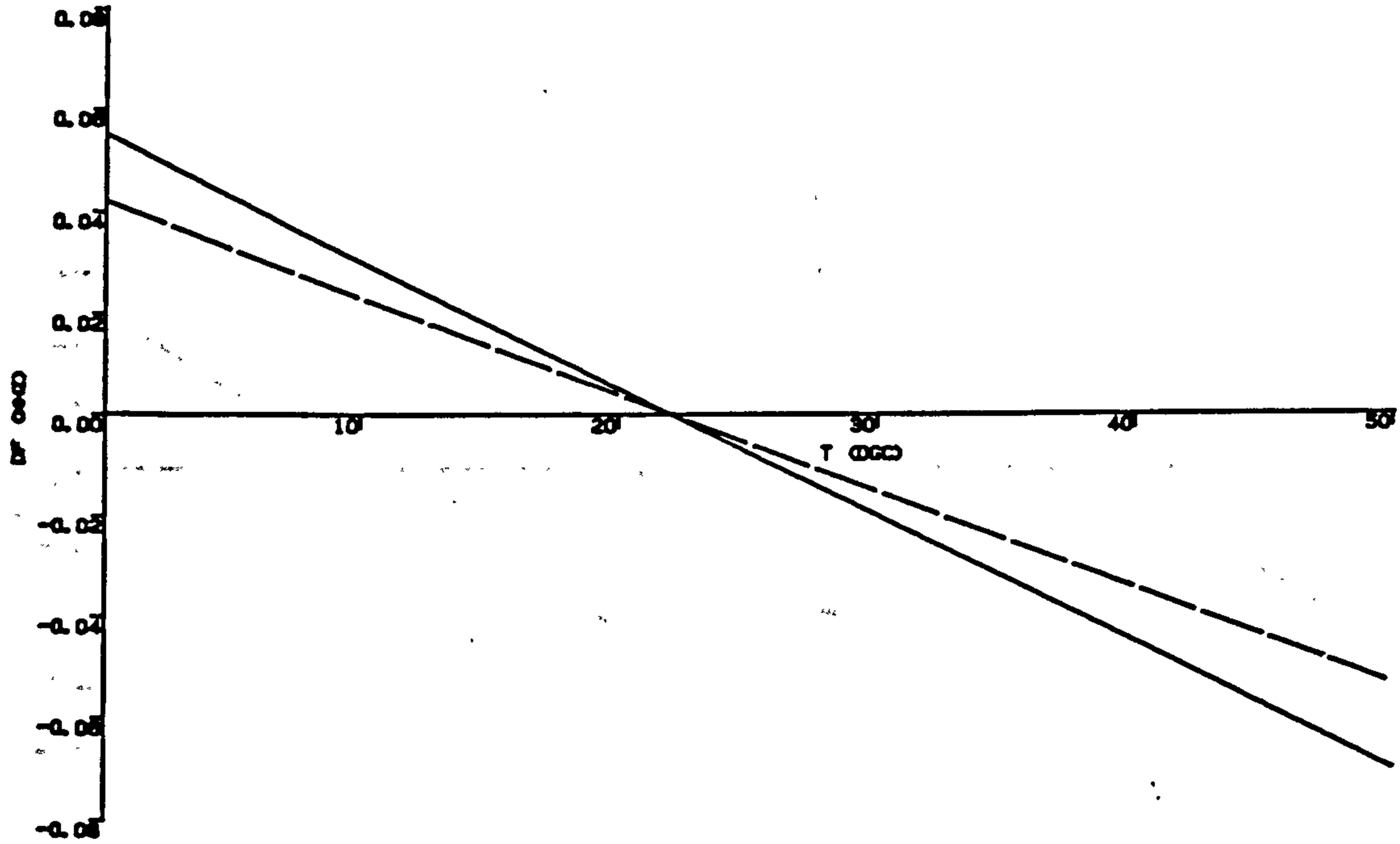

(a) Temperature characteristic without compensation:
(Frequency deviation vs. temperature)

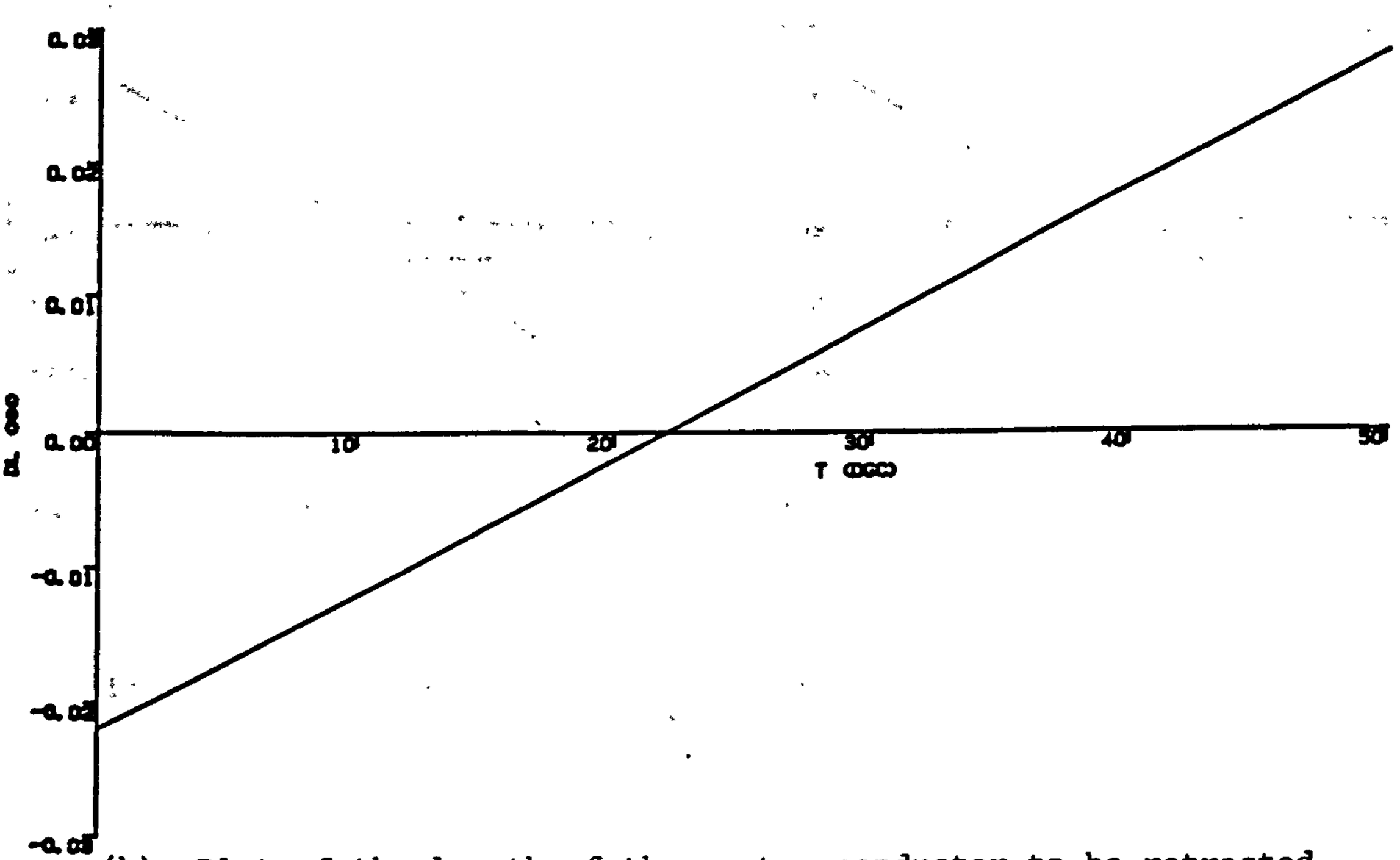

(b) Plot of the length of the centre conductor to be retracted against temperature for a resonant frequency of 1501.769MHz

Figure 5

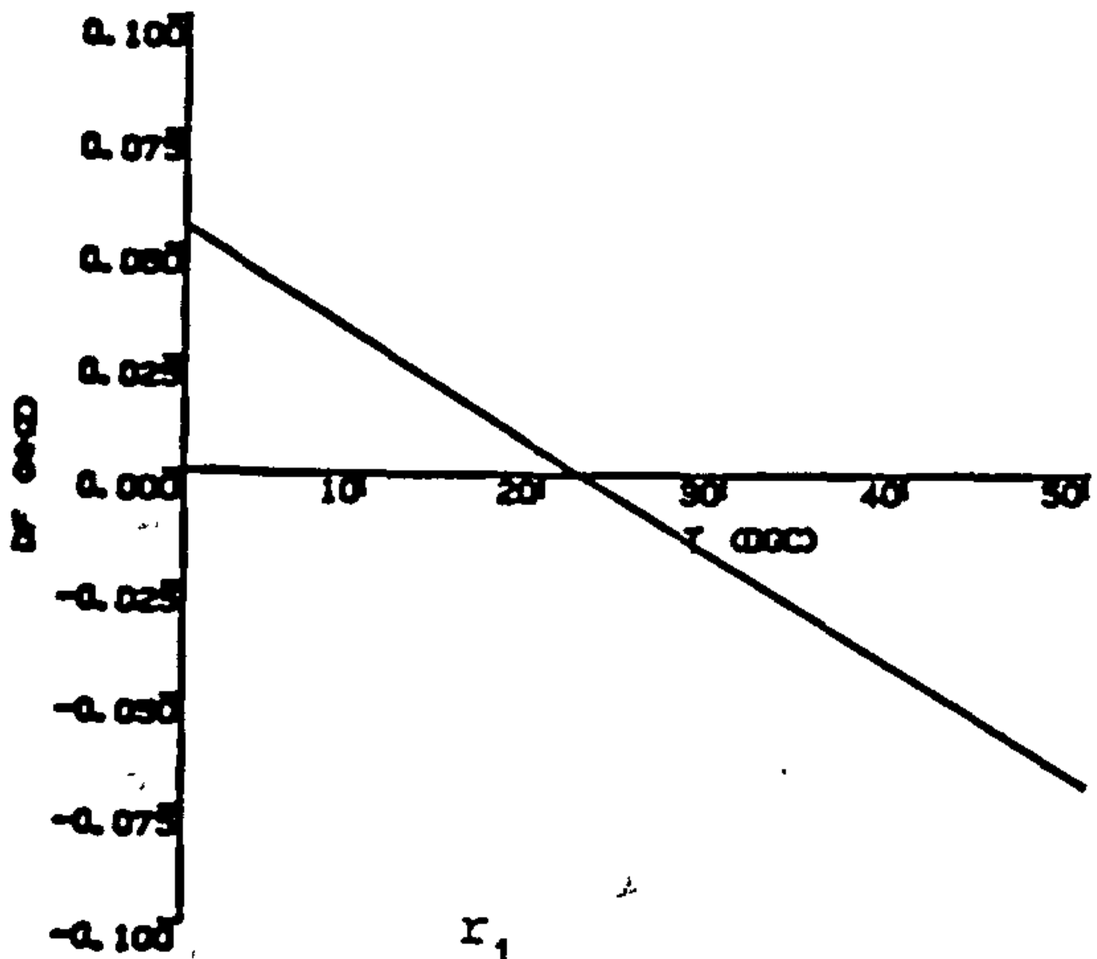

$\frac{r_1}{r_2} = 0.2$

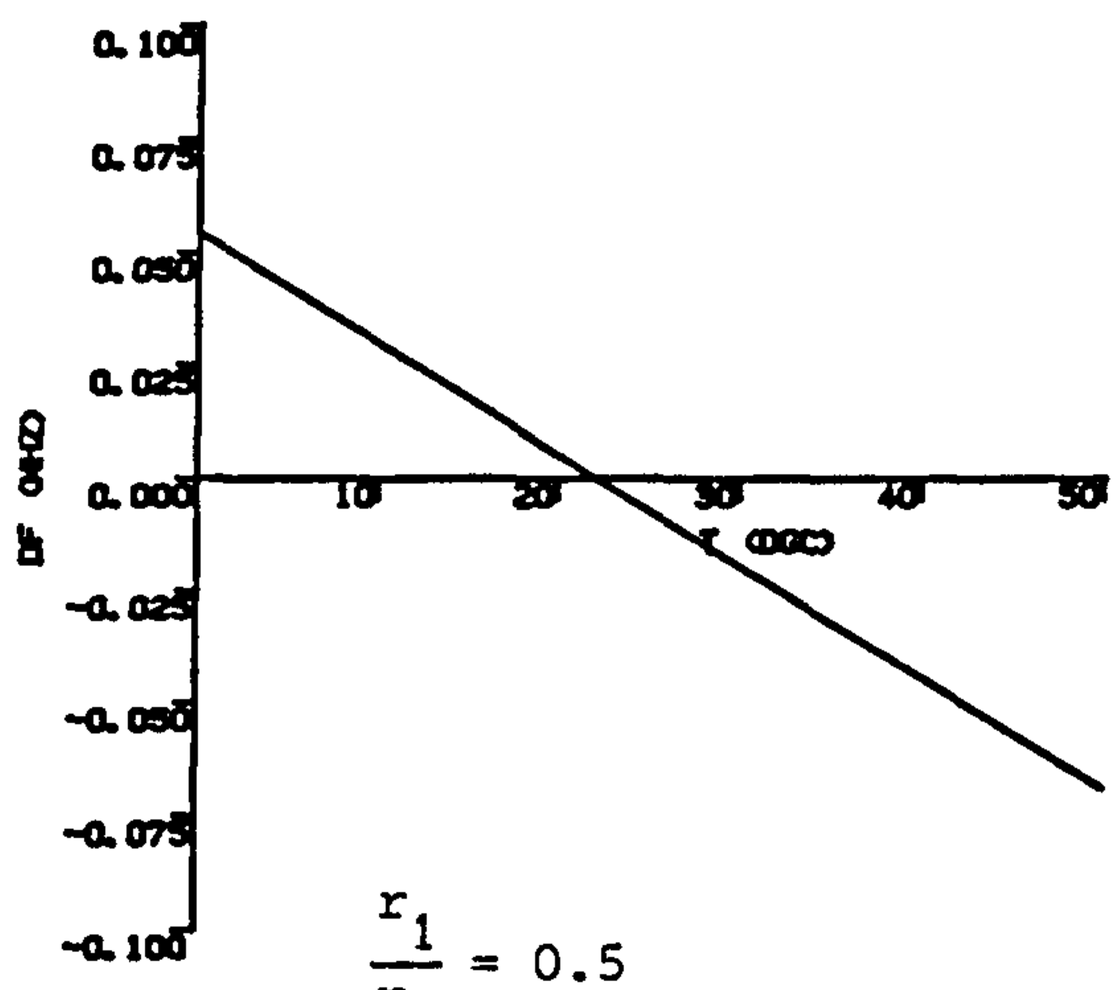

$\frac{r_1}{r_2} = 0.5$

$\frac{r_1}{r_2} = 0.7$

$\frac{r_1}{r_2} = 0.8$

Figure 6(a) Theoretical curves of temperature characteristics of uncompensated cavity for a resonant frequency of 1.5GHz

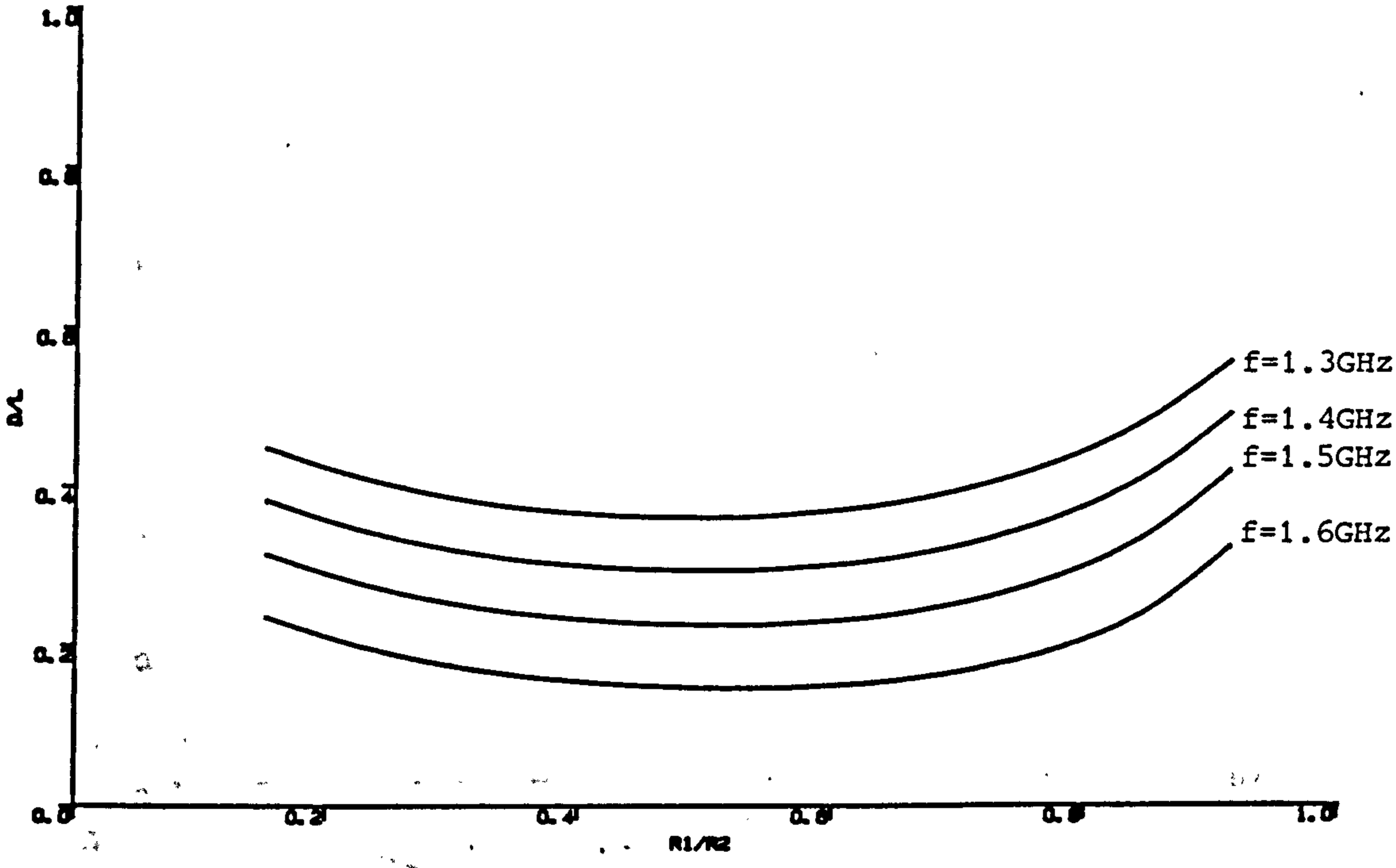

Figure 6(b) Plot of normalised insertion depth against normalised centre conductor radius (r_2=6.6675, L = 7.62cm)

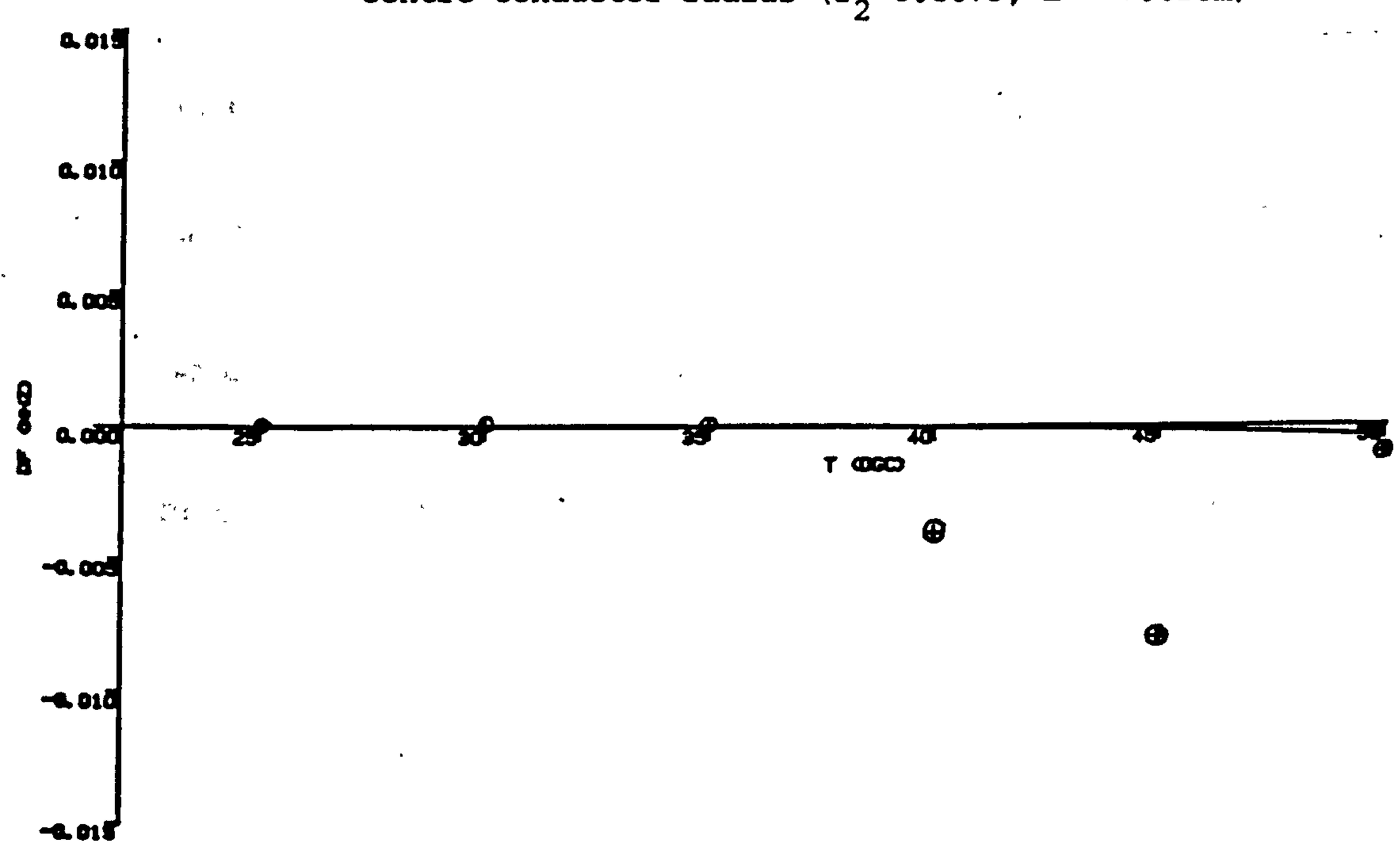

Figure 7 Temperature characteristic with compensation (hybrid mode cavity)
(Frequency deviation vs. temperature)
Solid line overlapping the temperature coordinate represents theory, marks represent practice

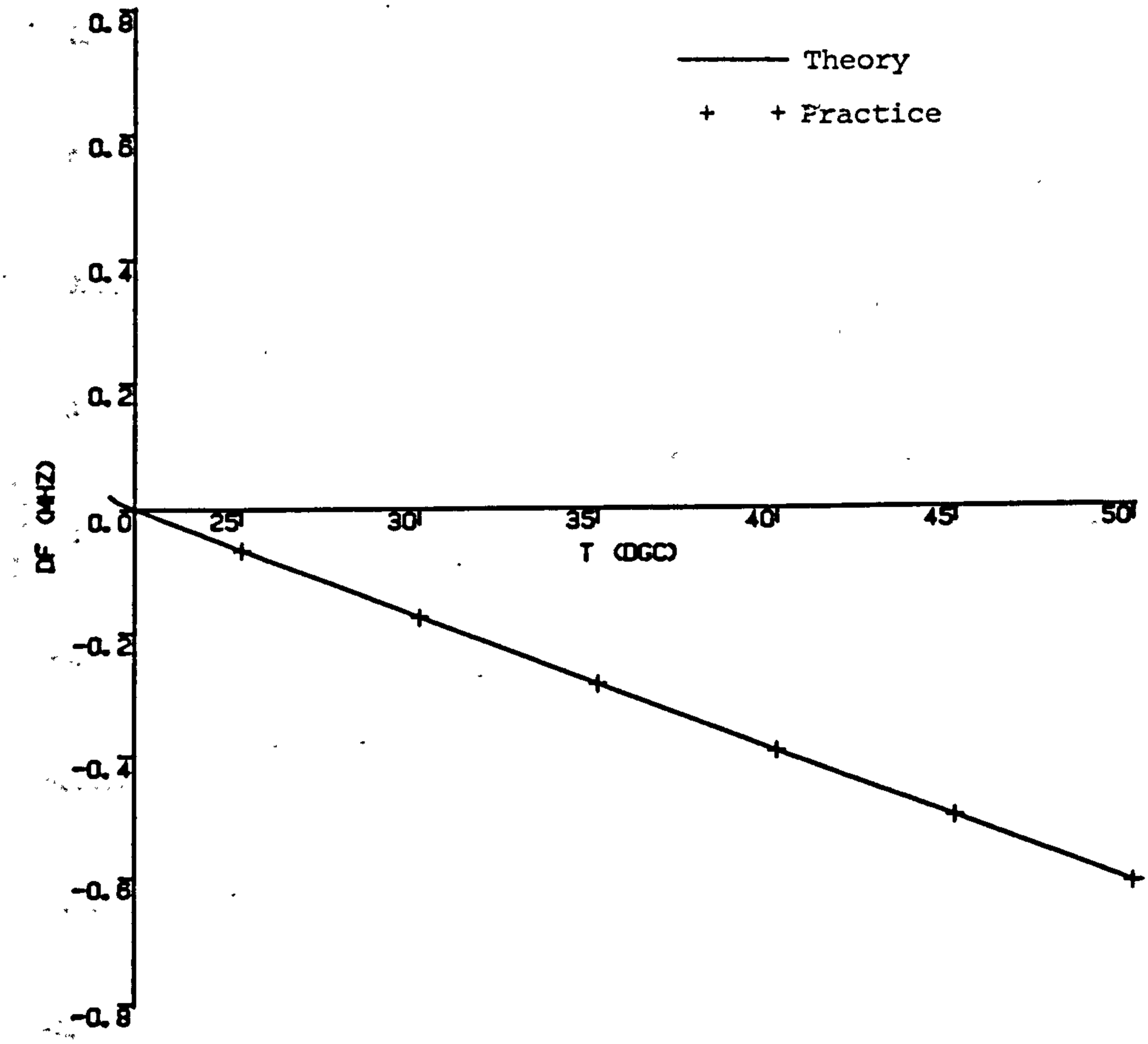

Figure 8(a) Temperature characteristic without compensation (rectangular cavity)

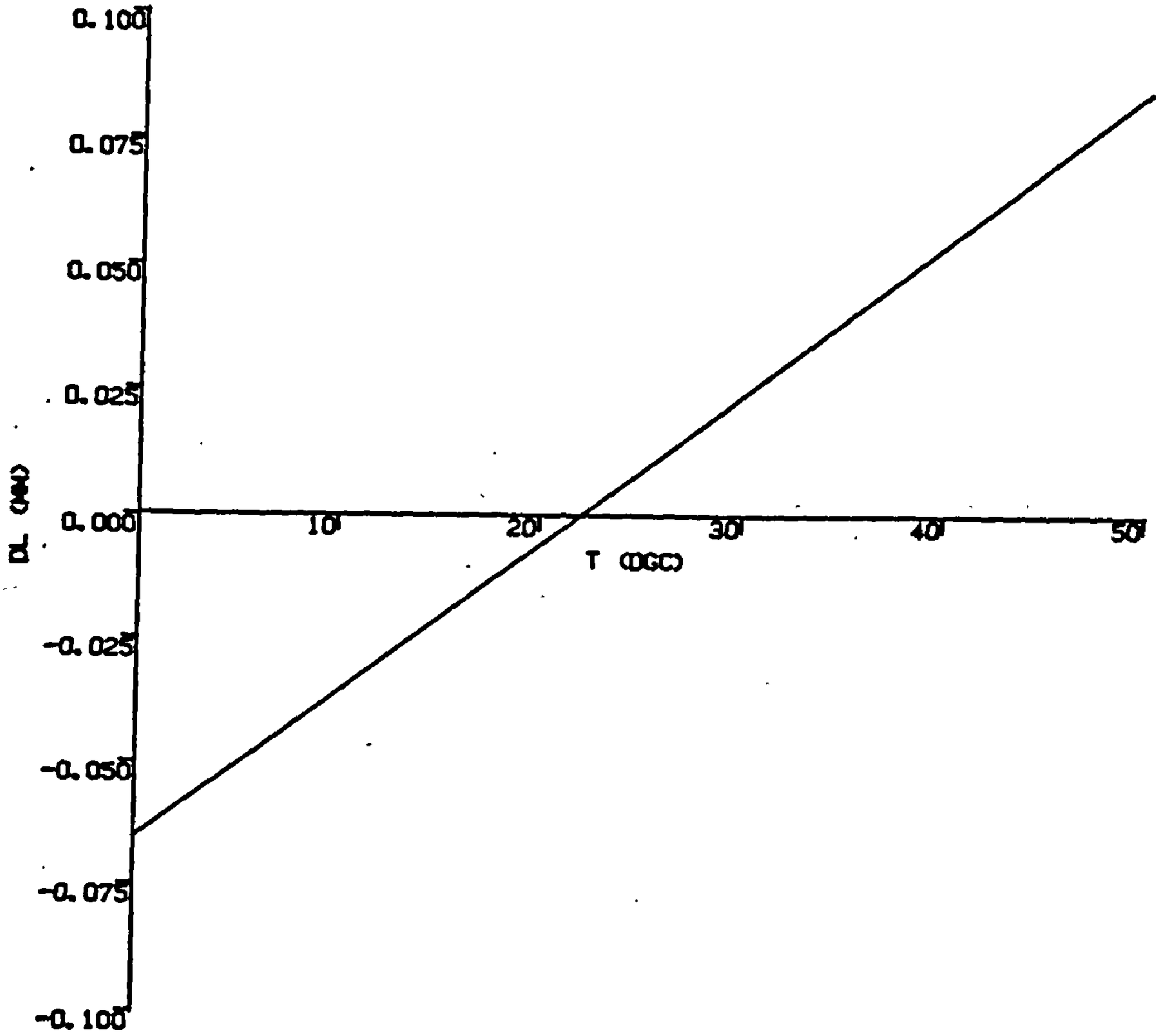

Figure 8(b) Plot of the plunger length to be retracted against temperature for a fixed resonant frequency of 1501.769MHz

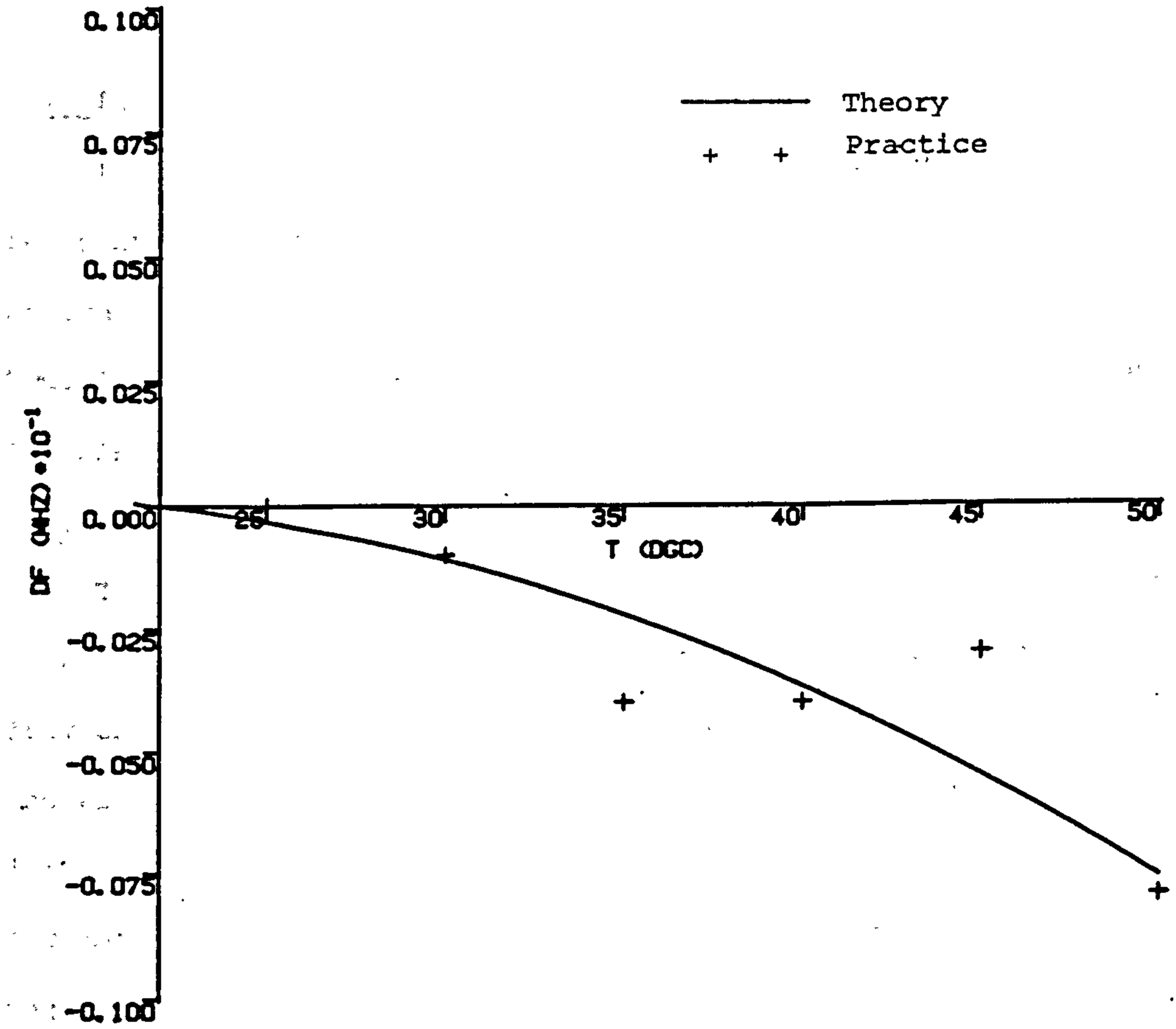

Figure 8(c) Temperature characteristic with compensation (rectangular cavity
(Frequency deviation vs. ambient temperature)

CHAPTER FIVE

EFFECTS OF GAPS AND HOLES IN THE CAVITY WALLS ON THE COUPLED CAVITY QUALITY FACTOR

5.1 Introduction

In Chapters Two and Three we found that coupled cavities have resonant parameters significantly different from theory even with design optimisation. In characterisation of coupled cavity in Chapter Two, it has been mentioned how resonant parameters vary with coupling In this chapter we shall expand this further to include the exact sources of disparities and distribute the losses accordingly.

The usual difference between theory and practice has been known to be attributable to geometrical and mechanical deviations, leakages from the cavity and the perturbing influence of 'foreign' materials and wall imperfections. In other words, the losses depend on many influencing sources. Of the main cavity parameters, the Q factors are most affected by defects in resonant structures. Resonant frequency variation has been found deviated from theory by less than 0.5% and this can always be tuned to the required value. For most practical resonant cavities the degradation in Q has been found to lie between 4 and 16%. And, with reference to Chapters Two and Three, the Q loss would increase with increased leakage or perturbation. This analysis is therefore intended to determine the losses arising from gaps, holes, cracks and perturbing materials and surfaces.

An exact determination of the properties of a perturbed or coupled cavity poses a problem because although the empty cavity is well understood, the same claim cannot be made for the cases in which the interior and interior surface are perturbed. The knowledge of the

fields in a cavity provides the means of determining the cavity's resonant parameters and where the field cannot be obtained it is a difficult task solving for the resonant parameters. Moreover, apart from fields in the original cavity fields in the other regions connected to the cavity are required. The aim is that if the exact effect of any perturbance can be determined from its influence on the fields, then,by proper interpretation of the results, it is possible to estimate how the effective unloaded Q varies as a function of the dimensions and positions of the discontinuity, gap or hole in the cavity wall or the material.

In the first part of this analysis, a theoretical attempt was made at determining the fields in the cavity and the hole or gap region. Such an approach, though difficult, provides a better insight into the study of perturbed cavities. An empirical solution was found inevitable more so since a resonator designed for practical engineering applications often leads to tractable shapes; the results of which can be scaled down to the operative frequency or cavity dimensions. Once the general phenomenon is understood, it is easy to produce desired resonant parameters by trial, with little error. Hence the results to be discussed here are based on simple modelling of the original problem aimed specifically at providing information which can be used to predict and minimise the various forms of Q losses in a coupled resonant cavity.

5.2 Theoretical Review

In dealing with material or boundary wall perturbations, one of the factors that has to be taken into account is whether the distortion of internal electric or magnetic field caused by the hole or gap in the cavity wall is sufficiently small to be tolerable. Or, on the other hand, whether the perturbation would permit the application of Slater's perturbation criterion[1]. In all aspects, the criterion usually advanced for the validity of the perturbation method is too strong and in reality most practical phenomena violate this condition. Moreover, if the criterion can be employed, in most cases, it would only be useful obtaining the frequency shift which is not the actual content of this analysis. A complete theoretical solution would involve the knowledge of the electromagnetic fields in the region bounded by the original boundary walls and the region backing the surface of the discontinuity, or the new surface on introduction of the perturbing material.

However, the fields in the cavity could only be determined when the cavity and perturbance can be described by a known geometrical shape - rectangular, cylindrical, coaxial or spherical - for which known trigonometric, hyperbolic or transcendental functions can be applied to obtain solutions that approximate the boundary conditions everywhere in the composite structure. Or, better still, when a hybrid geometrical configuration can be defined as found in re-entrant cavities (Chapter Three) for which a hybrid field configuration can possibly be defined. In other words, the composite structure must be able to undergo non-vanishing regional divisibility of known geometries. The Lorentz Reciprocity Theorem[8,9], the Schelkunoff's Equivalence Principle[3,9] and general field expansion method formulated by Hahn[2] can all be

used as the basis for the approximation and it is in this formulation that the expansion coefficients are found. Calculations can then be made on small (non-zero or non-vanishing) surfaces.

5.3 Area of Investigation

The major discontinuities encountered in practice have been categorised into three major sources:

a) the hole made for coupling coaxial line to be referred to in the course of analysis as 'hole'

b) the gap left for the free movement of a tuning plunger to be referred to as 'gap', and

c) the imperfection at joint due to either inaccessibility for proper finishing or total 'disregard' for such joint as found in detachable end-plate cavities. This would be referred to as 'edge-gap'.

Typical examples of holes and gaps are shown schematically in Figs. 1(a) and 1(b) respectively.

While holes and gaps may produce measurable surfaces of discontinuity in the cavity, edge gaps would in many cases have irregular surfaces. However, edge gap amounts to only an integral current path increase, except where it results in partial wall current cut-off, the effect on the resonant parameters is usually negligible. In all cases where there is no current flow between the two adjacent plates at the joint, any discontinuity at the joint would have negligible effect on the resonant parameters. A hole, for all coaxial coupling lines, can be taken as an aperture-like discontinuity backed by a coaxial waveguide. The gap surrounding the tuning member is a circular slot when the plunger is circular. We could assume the gap to be a perfect coaxial cavity, as shown in Fig. 1(b), bounded by conducting walls except at

the surface of discontinuity.

5.3.1 Formulation of the problem

Consider Fig. 2(a) depicting an aperture backed by an arbitrary structure. An incident electromagnetic wave $[\vec{E}_o, \vec{H}_o]$ impinges normally on the plane and the aperture. The problem is to determine the field in the cavity and the field penetrated through the surface of discontinuity into the arbitrary region. To obtain these fields we shall consider two major methods:

1) Field expansion method - Hahn's formulation[2,4], and

2) Equivalent current principle[3,5,6].

A. Field Expansion Method

In Chapter Three, simple forms of microwave resonant cavity with complicated boundary walls were analysed employing Hahn's formulation[2] of the problem. It was concluded, because of the analytical effectiveness of the method, that it opens the way for the solution to other complicated boundary conditions. Such structures can be found in cavities perturbed by holes and gaps in the boundary walls.

As usual, the method consists of dividing the structure into two or more regions with known closed field equations, finding series solutions which fulfil the boundary conditions in each region separately and then matching the solution at their common surface - surface of discontinuity. By expanding the fields in series of normal modes in each region, the influence of all modes is respected.

B. Equivalent Current Principle

Fig. 2(b) represents a simplified 2-dimensional view of the original problem. It is known that a prescribed field distribution at a surface of discontinuity can be used to calculate the fields elsewhere connected by the discontinuity by employing Green's functions for the region[3,5]. The approach most commonly used for such calculations was developed by Schelkunoff[9] and is known as Schelkunoff's equivalence theorem.

The equivalence principle, derived from Maxwell's equations, states that when the surface of discontinuity, S_a, is closed by a perfectly conducting wall, an equivalent electric or magnetic current flows on the surface. The current flowing in this wall is given as

$$\vec{J}_{es} = \hat{n} \times \vec{H}_o$$

representing the equivalent electric current, and

$$\vec{J}_{ms} = \vec{E}_o \times \hat{n}$$

representing the equivalent magnetic current, where $\hat{n}$ is a unit vector normal to S_a directed outwards. When the wall is removed, these sources radiate a field $(\vec{E}_a, \vec{H}_a)$ into the hole or gap, region $Z<0$, and a field $(\vec{E}_s, \vec{H}_s)$ into the cavity. Thus the total field in the perturbed cavity is the sum of the original field in the region $(\vec{E}_o, \vec{H}_o)$ and the scattered field $(\vec{E}_s, \vec{H}_s)$. It is known that the scattered field must satisfy all the boundary conditions in the cavity. It is obvious that if $\vec{E}_o$ and $\vec{H}_o$ are known functions of the cavity coordinate, the equivalent currents at the surface of discontinuity can be obtained.

To find the fields radiated into both regions, Green's functions appropriate to the region and the original problem are employed. This

method is outlined in Chapters Five and Seven of reference 3. The field radiated to the original cavity and the hole are therefore found expressible as expansions of the normal cavity or waveguide modes in the regions. However, the necessary and sufficient condition for the solution to the field distribution in the two regions, cavity and gap (or hole) is the continuity of the tangential field components along the surface of discontinuity.

When two sources (electric and magnetic current sources) are provided, the electric and magnetic fields are determined for each of these current sources and added vectorially. Thus the total fields in each region can be obtained irrespective of the number or positions of the discontinuities.

5.3.2 Analytical problems

Whichever of the methods is chosen, there is no means of avoiding fields expressed as infinite series expansion of normal modes in the separate regions. The solution methods as presented here and in the literature pose simplified analytical features. The major drawbacks in their applications to the treatment of perturbed cavities are two-fold:

1) In certain categories of resonant cavities, the determination of equivalent current may be impossible or difficult because the region itself may not possess known definite field equations. For instance, the calculation of wall current would be difficult to handle for a coaxial reentrant cavity for which the field is represented by an infinite series of normal modes. On the other hand, expansion of fields in series of yet another series expansion of normal modes would amount to an insolvable mathematical equation otherwise a probably time consuming computation.

2) The surface of discontinuities are vanishly small and so, in most other cases, is the gap or hole region itself, especially the gap or hole width. It is therefore an impracticable approach applying either analytical method.

Most gaps and holes are also found asymmetrically related to the original cavity structure. Therefore, the expansion cannot take the advantage of symmetry common with most analytical structures. Inside the gap the fields are represented by piecewise, continuous functions and these methods can only be applied to obtain solutions that approximate the boundary conditions and determine the coefficients which would converge the series expansion. Since vanishingly small holes and gaps have been found to present mathematical difficulties and bigger ones have been found impractical, modelling have been found best analysed by empirical means. Moreover, detailed computations are very complicated and time consuming.

5.4 Effects of Major Design Defects

The results obtained earlier and in the referred chapters, Chapters Two and Three, are strictly for well designed coupled cavities. To furnish us with more information we shall now examine the case when various major defects are progressively introduced. The cavity for investigation is a tunable 1.5GHz cavity with a theoretical unloaded Q of 12000. Fig. 7 is a schematic diagram of the test piece used to simulate a defective coupling terminal. The loop size was calculated for d=0, UR 72 cable and loop diameter 1.0cm. One end-plate carried the coupling devices and tuning plunger while the other one was made detachable (only fastened to the cavity with screws). The design would thus permit such likely design defects in the coupling terminals, tuning plunger and joints between cavity and end plates (or joints) to be

introduced progressively.

Table 2 shows the effect of introducing major constructional errors. It was observed, as is obvious from the table, that when d=0 and the detachable end-plate was firmly joined, the loss in Q_o was in the range of 14%. Further observations showed that as defects were introduced in progression, the error increased. However, it is difficult to assert linearity in this case because of lack of exactness in the extent to which individual defects were introduced. For instance, the adjustment of the detachable plate was by slackening screws.

TABLE 2

t (mm)	d (mm)	Q_o	Approximate Percentage Loss	Comment
0	0	10316	14	(1)
0	0	9876	18	(2)
5	5	9432	21	(2)
0	0	9618	20	(3)
0	0	8346	30	(2)+(3)
5	5	8020	33	(2)+(3)

Keys to comment:

(1) Fastened end-plate

(2) Slackened end-plate

(3) Loose plunger and gap width 1mm

Further observation revealed that the material which makes the walls of the gap has little or no effect on the loss for practicable gap width. This is because the amount of leakage into the gap would only depend on the gap width and for the gaps we refer to here, the

leaking energy would be an energy loss.

5.5 Experimental

The experimental procedure consisted of measuring the unloaded Q and resonant frequency of a cavity without test holes or gaps and then repeating these measurements on the same cavity for a series of different hole positions andprogressively larger gaps. Furthermore, various combinations of holes were measured to establish that the process is essentially linear; that is, the net Q shifts are the sum of those obtained with the discontinuities separately.

5.5.1 Aperture-like discontinuities backed by a coaxial waveguide

It has been shown in Chapter Two how the effective coupled cavity Q_o varies as function of coupling position for a transmission line cavity. Practice and theory have also been compared. However, the amount of loss due to the leakage to the coaxial line through the surface of the discontinuity is unknown.

The work reported here involves experiments with TE_{101} rectangular resonant cavity. Typical experimental results indicated the effects on Q and the trends of this commonest form of perturbation. A rectangular resonator shown in Fig. 3(a) and having the dimensions x = z = 14.1cm and y = 3.2cm was set into oscillation at its lowest frequency - TE_{101} mode. The electric field is therefore wholly in the y-direction with the antinode located at the mid-point of the x-z side. The current antinodes are located at the 'vertical sides' (y-axis). The advantage of the choice of cavity and mode was that x and z axes can be interchanged without any difference in the field and coupling. The coupling positions and axis are therefore rotatable. The coupling loops were located half-way along the x-axis at z = 1.19cm and z = 12.91cm, thus making a symmetrical

coupling. Four pairs of test holes similar in dimensions to the coupling holes were positioned half way along the z-axis and spaced on the x-axis at 1.27cm from each other with the first pair located at x = 1.19 and x = 12.91cm. By selectively covering three pairs of holes and constructing 50 ohm coaxial lines similar to the coupling line for the other pair, measurements of resonant frequency and the unloaded Q were taken. An empirical curve 'a' was constructed as shown in Fig. 4. This figure represents the approximate percentage loss in Q as a function of coupling position. By increasing the sizes of the test holes, hence the surfaces of discontinuity, curve 'b' shows that with increased coupling line diameter Q loss would increase. The resonant frequency remained almost constant for small coupling holes and the deviation became larger as the surface of the discontinuity increased. The deviation also increased towards the electric field antinode. Fig. 5 shows a plot of the approximate frequency deviation against coupling position.

The power leakage to the coupling line was measured. Observation revealed the existence of another mode, a 'parasitic mode', having a lower resonant frequency and almost within the noise level. When the diameter of the coupling line was increased, the leakage to the line increased and the frequency separation decreased. The isolation between the parasitic mode and the coupled cavity resonance decreased relatively. As the coupling position approached the electric field antinode, the frequency separation and isolation were found decreased as shown in Fig. 6.

Since it is easier to find the separate effect of each hole on the resonant parameters, it is necessary to find what effect super-positioning individual effects have on the total effect of the discontinuities. Table 1 shows clearly that the effect of all the

discontinuities is nearly the algebraic sum of the loss incurred by individual discontinuity. It shows further that the discontinuities are almost independent of one another.

Table 1 Linearity Test

	Set	1st hole	2nd hole	Total	Both Pair
Percentage change in Q	1st	0.55	0.567	1.117	1.1
	2nd	0.96	0.795	1.755	1.71

5.5.2 Slot-like perturbance

Resonant structures having slot-like discontinuities backed by cavity or waveguide structures have varying influence on the resonant parameters. A model cavity shown in Fig. 3 provides a better method for investigation. The dimensions of the structure backing the surface of the discontinuity depend on the designer's choice. Since the effect on resonant parameter would also depend on these dimensions, care should be taken to separate the resonant frequency of the structure widely from the resonant frequency of the unperturbed cavity. This would ensure the optimum condition of operation with less energy contained in or dissipated on the surface walls of the perturbance.

The presence of the tuning plunger has been observed to tend to divide the coupled cavity resonance into two[4]. There is no means of ruling out completely the excitation of 'parasitic' mode(s). However, energy is exchanged between the parasitic mode and the actual resonance mode. Sometimes, the effe ct could be as to suppress both parasitic and actual modes below the noise level. Observation has revealed that there is increased loss when the parasitic mode is well above noise level, the resonance loss is high. It is essential, for such reasons,

to guard against any accentuated resonance degeneracy hence reduced gap width. Any excitation of undesired modes in the gap causes much loss for the desired resonance mode.

Fig. 8 represents the percentage change in unloaded Q as a function of gap width for the resonant cavity shown in Fig. 3. It is observed that the loss in Q increased with increased gap width. This has been attributed to the increased energy coupled into the cavity backing the discontinuity by virtue of the increased surface of discontinuity. This energy is mostly dissipated on the surface wall in the gap. If the gap takes the form of waveguide, part of the coupled energy would be propagated out while the rest is dissipated. Further observation revealed that as the gap width and depth increased, the resonance loss increased and the loaded Q approached Q_o, the unloaded Q factor. By carefully exciting the parasitic mode, the loss in the actual resonance mode was found for the 2mm gap as 3.8dB. The general loss could be more depending on the excitation level of the parasitic mode. When this is excited, one mode is always above and one below the exact resonance of the 'unperturbed' mode. With the parasitic mode suppressed within the noise level, the resonance loss was just 0.64dB. Another inhibit action of a parasitic mode is that the frequency spacing is always small.

5.6 Loss Budget for a Coupled Cavity

It follows from the earlier analysis that the extent to which measured Q_o differs from theory depends on the number of sources directly linked with energy leakages from and perturbation of fields in the cavity. Thus as a first step towards estimation of Q_o, a list of these sources would be helpful. We can only talk of estimation which is purely

approximate and for which the experimental Q_o would differ from predicted Q_o by less than 2%. The results obtained above and earlier in Chapters Two and Three can be used to establish a loss budget for coupled cavities.

With reference to Chapter Three, for a tunable and detachable end-plate coaxial cavity, the average loss was found close to 14%. In Chapter Two a coupled cavity without tuning mechanism or detachable end plate has been found having loss between 4% and 7% but more of an average expectation of 6%. From Fig. 4, it was observed that the loss arising through direct leakage from the cavity to the coupling lines, for all practicable loop positions, would not be more than 2% of the total theoretical Q_o. Thus a minimum Q loss of 4% can be linked with other unavoidable sources like leakages through direct coupling between loops and lines, various perturbation effects and internal holes and slots. Fig. 8 shows that the loss arising through the slot surrounding the tuning plunger for a gap of 1mm width is between 4% and 6%. With larger gaps, there is always attending additional loss. In practice, larger gaps could be used but with spring fingers blocking the gap (or rather reducing the average gap width) and holding the plunger firmly. Thus we can expect an average 1mm gap width; hence an average 4% loss for thin plungers and 6% for bigger plungers. Here we shall assume a tentative loss of 6%. Summing up, it is obvious that when one end-plate is detachable no matter how the plate is fastened, unless the loose joint so created does not interfere with normal wall current flow, there would be leakages. By virtue of this a tentative minimum additional loss of 2% would be most appropriate. Table 3 is a possible loss budget constructed for an average minimum loss. By considering it for resonant cavity design, with proper scaling and deleting which-

ever does not apply, one can arrive at close agreement with practical values.

One thing concerning the use of this budget is that it is better to over-estimate the loss than under-estimate it for fear of falling below the design specification. Where the estimate is found much below experimental, a quick check on the sources as listed in the budget would be appropriate.

Table 3: Loss Budget Table for a typical resonant cavity

Source	Average allowable percentage of the theoretical value	Comment
Slots (plunger)	6	
Coupling hole	2	Leakages directly from cavity
Detachable plate	2	Minimum average value
Unavoidable influences	4	Includes direct coupling between loop and line
Percentage Gross Loss (Average)	14	

5.7 Conclusion

For the cases mentioned above the following assertions hold:

1) Aperture-like discontinuities have more influence in electric field regions while slot-like holes are found most sensitive in magnetic field regions.

2) The effects on Q diminish as the aperture decreases in diameter and as either or both of the slot's width and depth decreases.

The losses in Q_o are therefore found to increase with increased gap

width and aperture diameters and their proximities to regions where they are most sensitive. Leaking energy into the gap always amounts to extra losses from the cavity for all practicable gaps.

5.8 References

1. Slater, : 'Microwave electronics', Rev. Mod. Phys., Vol. 18, 1946, pp. 467-512.

2. Hahn, W C: 'A new method for the calculation of cavity resonators', J. Appl. Phys., Vol. 12, 1941, pp. 62-68.

3. Collin, R E: Field theory of guided waves , McGraw Hill, 1960.

4. Loncar, G: 'Methods of field identification in a resonator with an azimuthal perturbation, Part II', Acta Tech. CSAV., Vol. 13, Pt. 4, 1968, pp. 559-589.

5. Ghandi, Om P: Microwave Engineering and Applications , Pergamon Press, 1981.

6. Cheng, D K & Chen, C A: 'On transient electromagnetic excitation of a rectangular cavity.... etc', Report No. AD-A030 364, June 1976.

7. Wilton, D R & Dunaway, O C: 'Electromagnetic penetration through apertures of arbitrary shape... etc', Report No. AD-A021 988, Aug. 1975.

8. Harrington, R F: Time-Harmonic electromagnetic fields , McGraw Hill, 1961.

9. Schelkunoff, S A: 'Some equivalent theorems of electromagnetics and their applications to radiation problems', BSTJ, Vol. 15, 1936, pp. 92-112.

10. Schelkunoff, S A: Electromagnetic waves , D Van Nostrand Company, 1960.

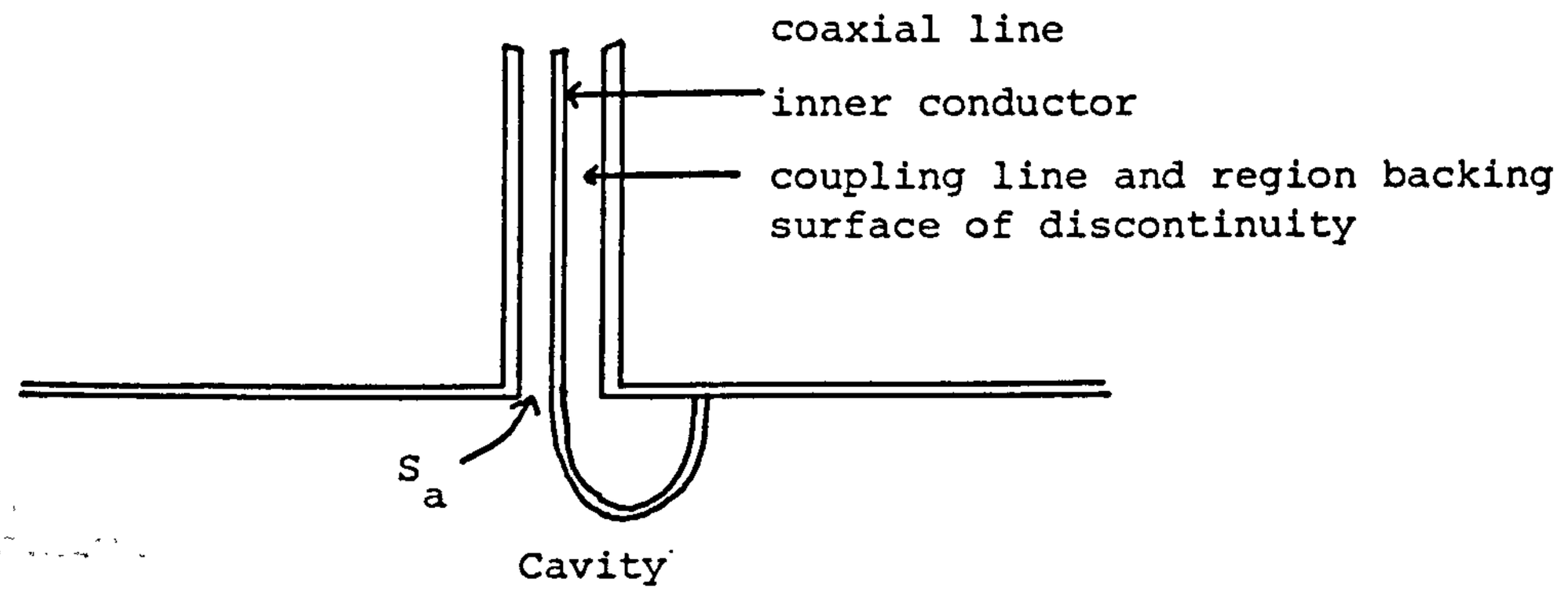

(a) A coupling terminal showing surface of discontinuity (S_a), the coupling loop and the coaxial line

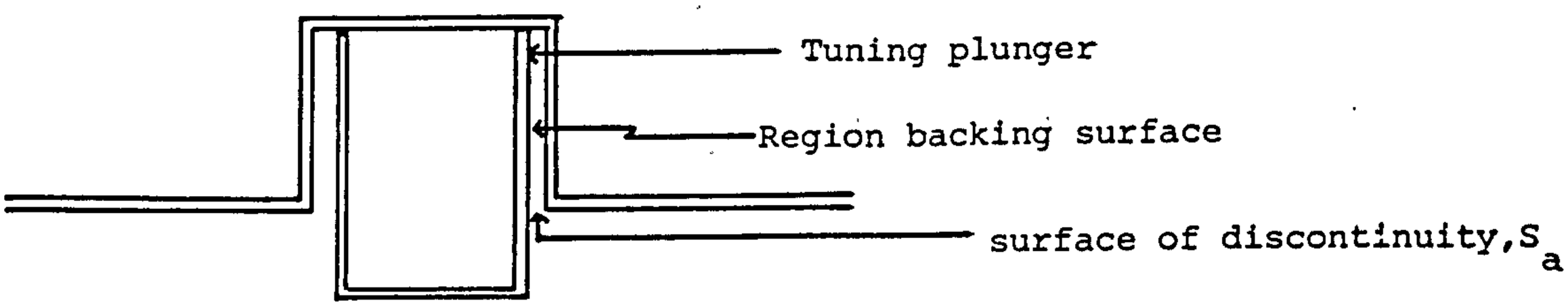

(b) Tuning mechanism showing the gap and the surface of discontinuity

Figure 1

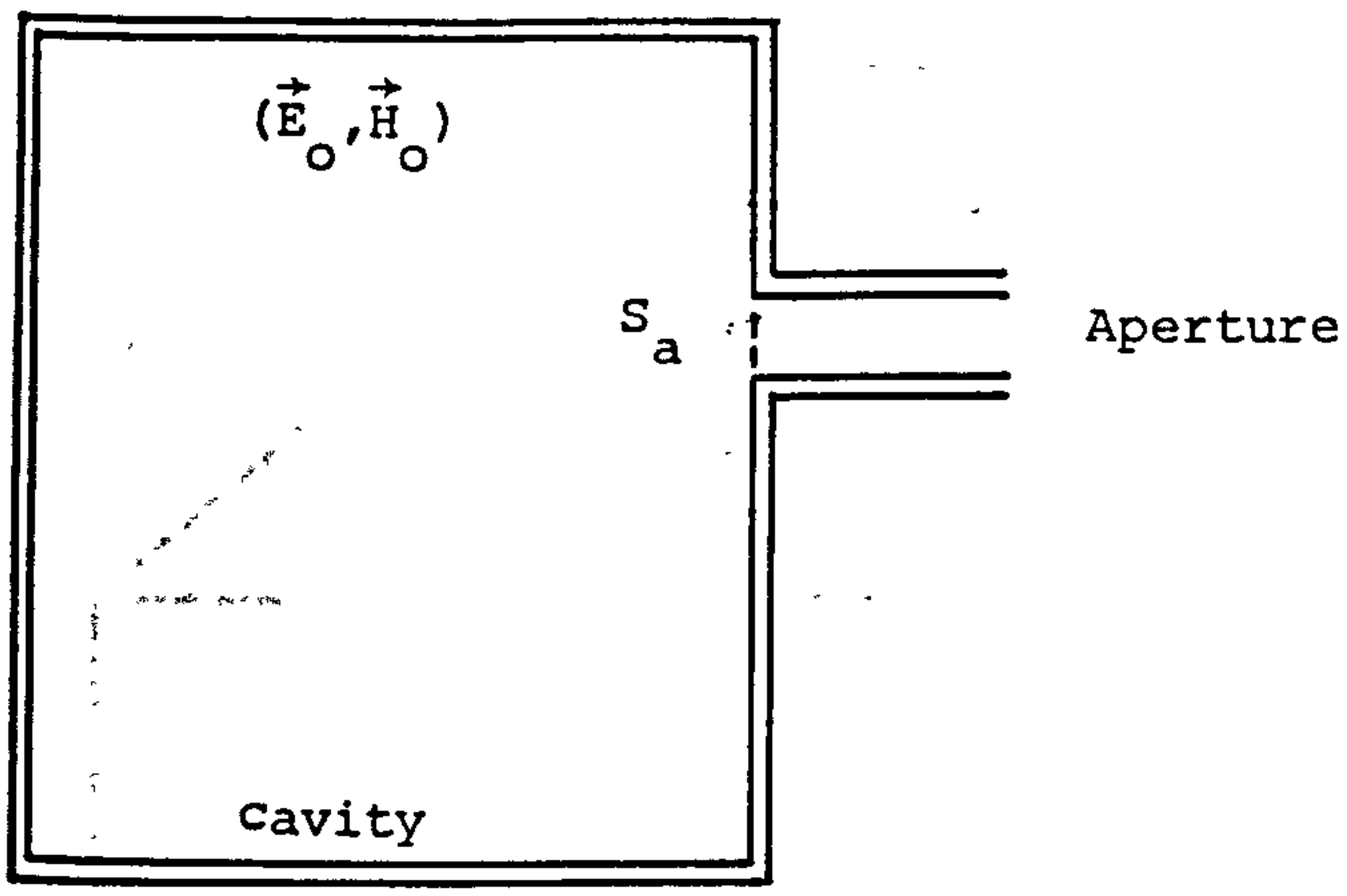

(a) A schematic diagram of a cavity and an aperture

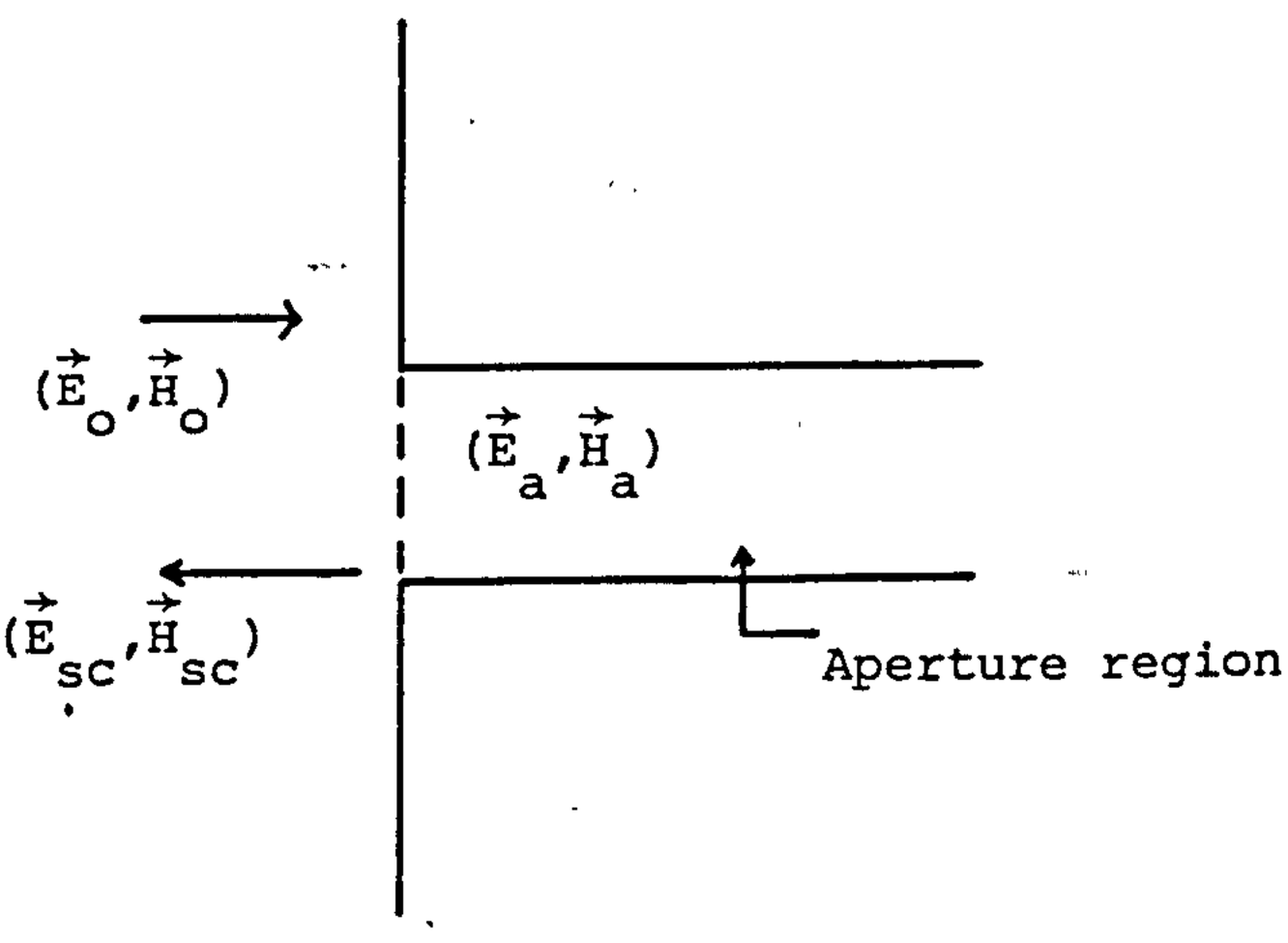

(b) A two-dimensional view of the plane containing the aperture

Figure 2

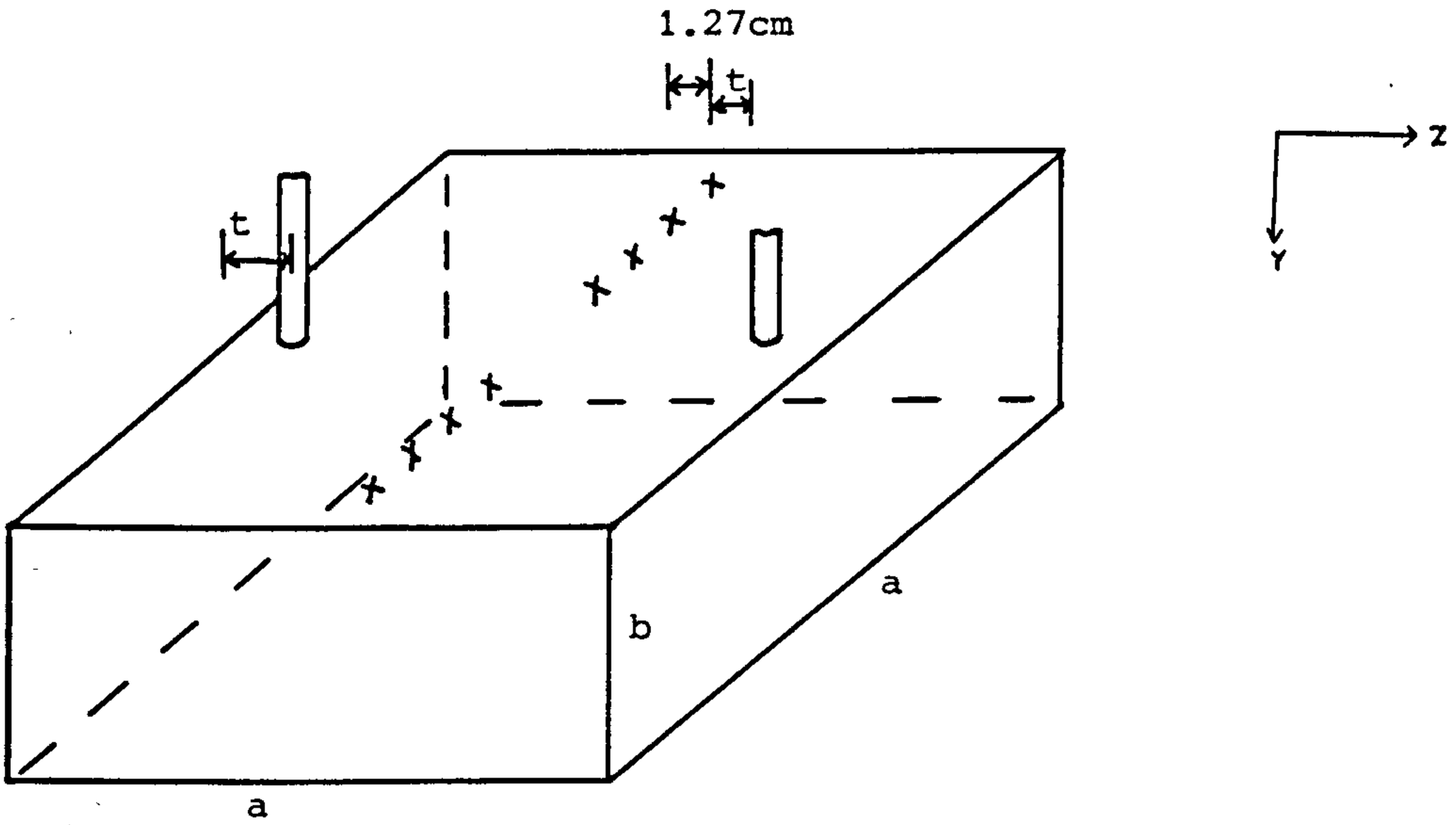

(a) Experimental cavity showing test hole positions

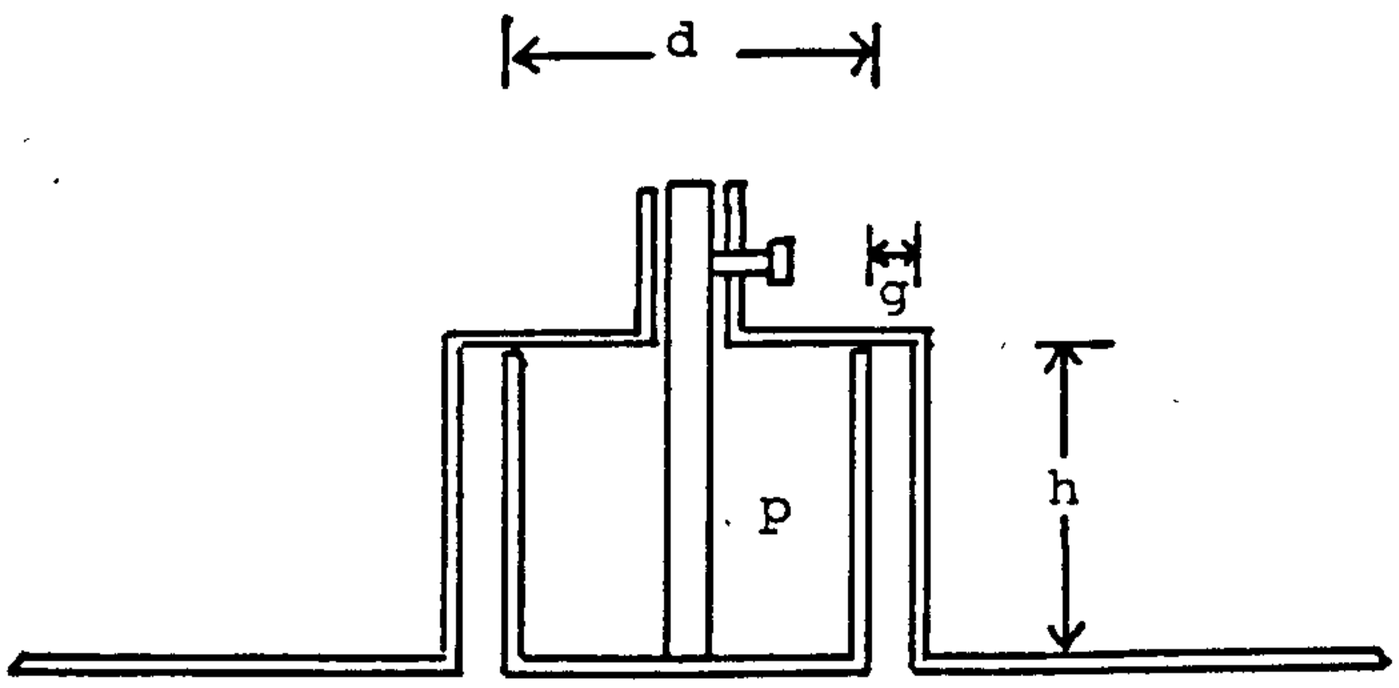

Figure 3 (b) A test gap

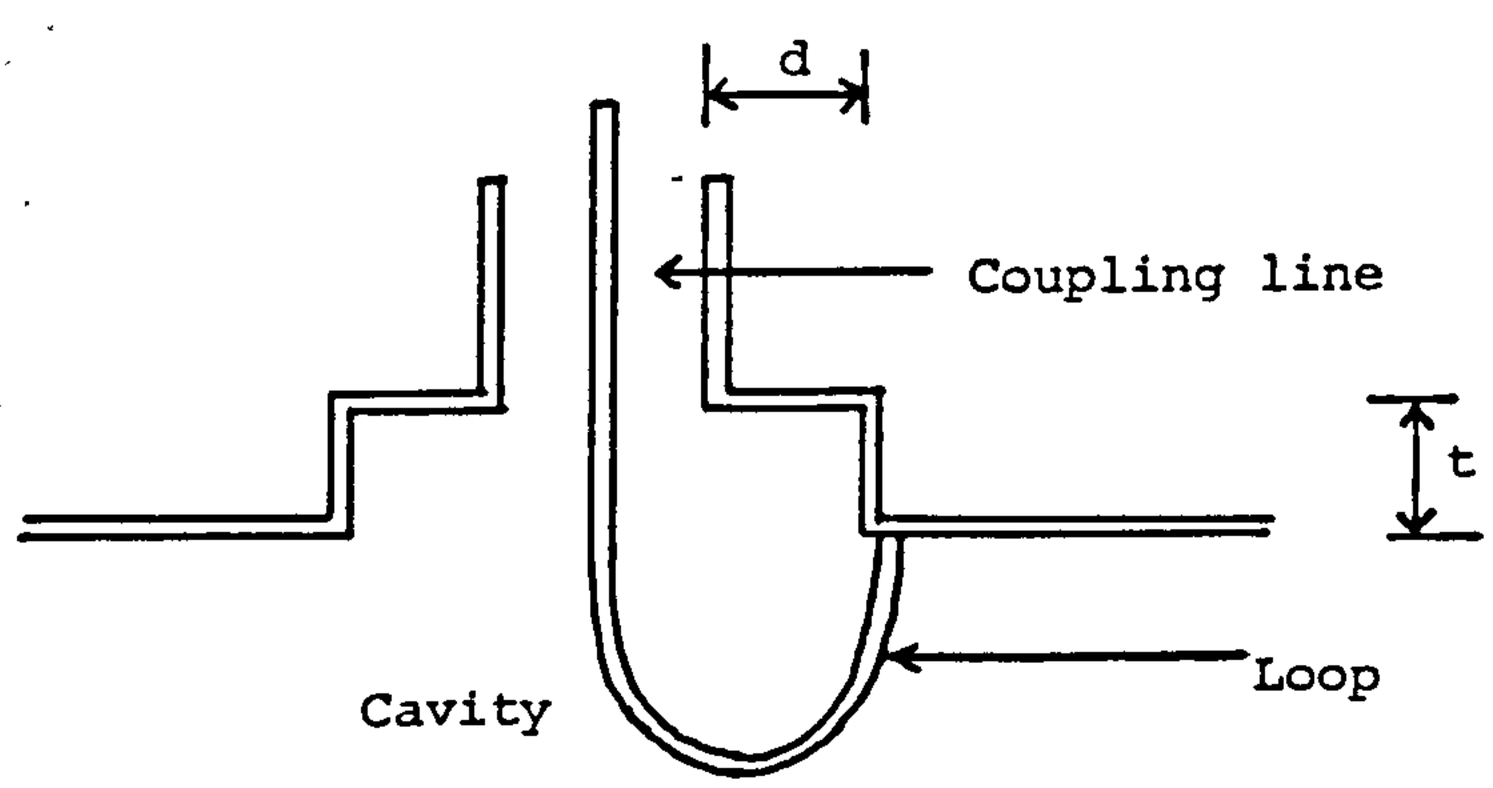

Figure 7 The test piece used to simulate coupling terminal faults

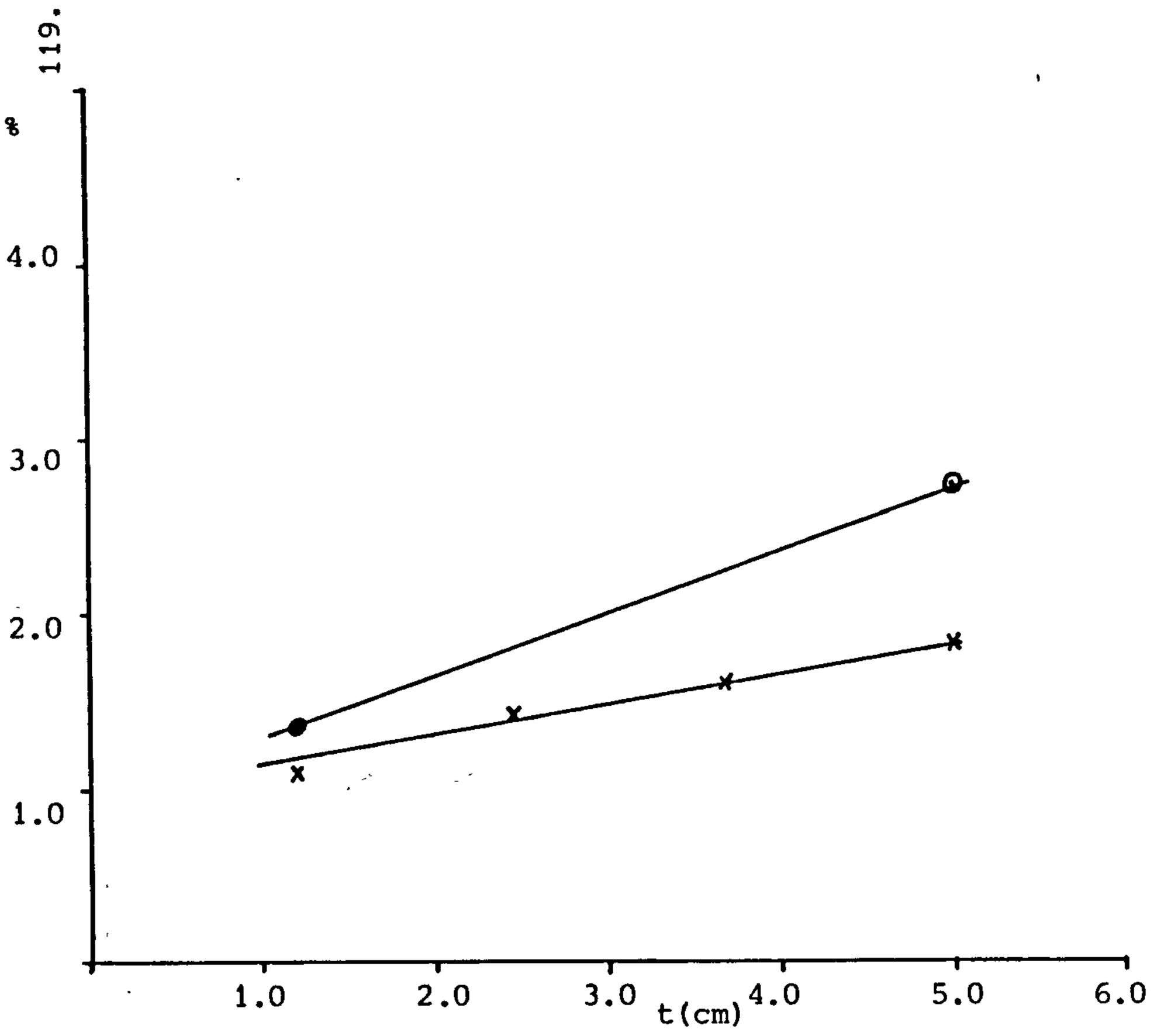

Figure 4 Plot of percentage loss against coupling position

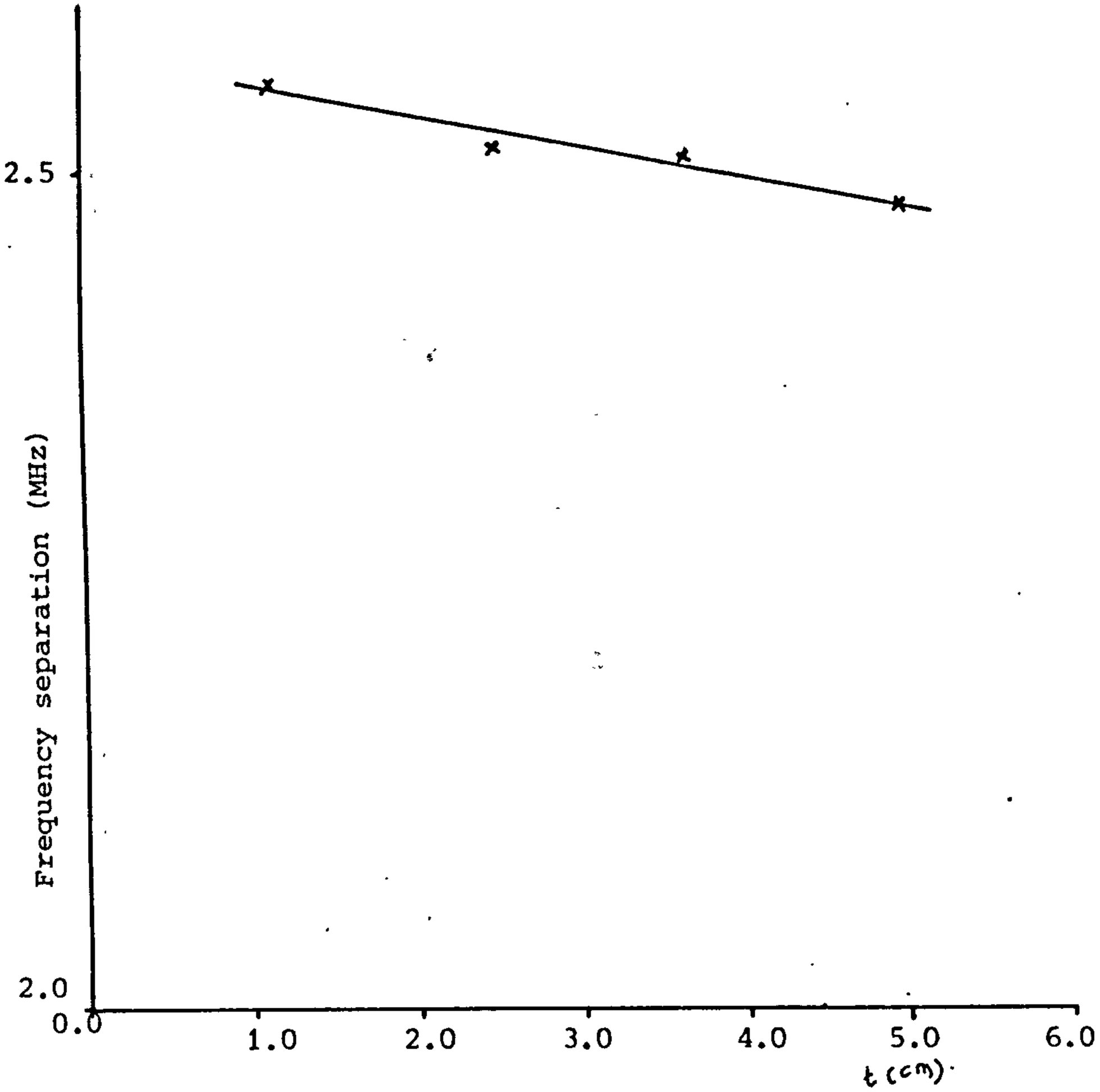

Figure 5 Frequency separation vs. coupling position

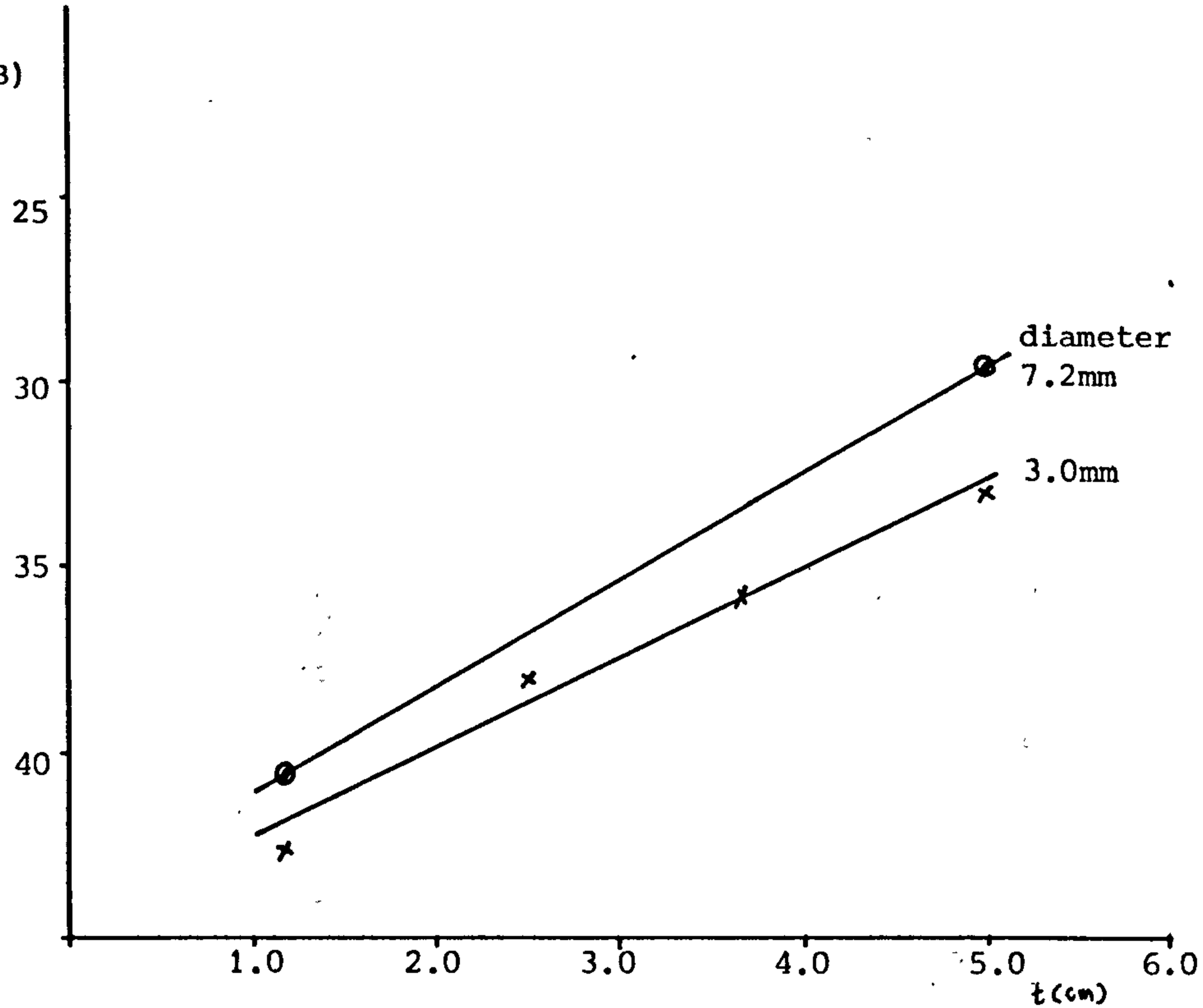

Figure 6 Isolation between the 'parasitic' line mode and coupled cavity mode (isolation vs. position)

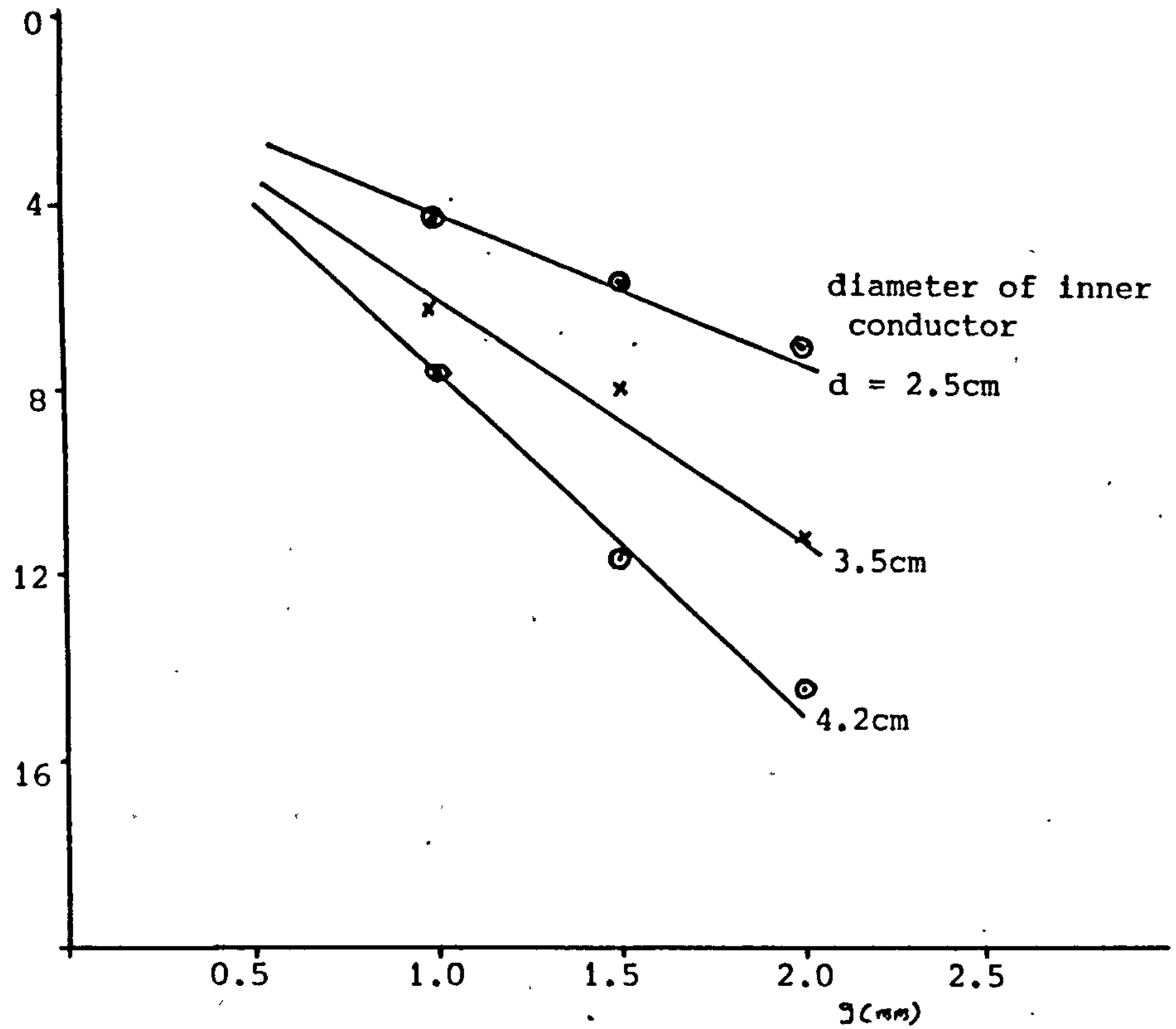

Figure 8 Percentage loss vs. gap width (g) for test gap of Fig. 3(b) with h=3cm and the average radius of outer conductor is .8cm

CHAPTER SIX

TECHNIQUES FOR COMMUNICATION NETWORKS DESIGN AND DEVELOPMENT

6.1 Introduction

The major usefulness of resonant cavities in a communication system is found in their frequency discriminating abilities. Hence, cavities are usually employed as complex filter networks in a communication system. It is also possible in microwave engineering, as it is in low frequency engineering, to increase the frequency selectivity by inter-connection of resonant cavities. Basically, the design procedure is almost the same as for low frequency circuits especially when the component cavities are interpreted in terms of lumped element parameters.

The multicavity filters are, in general, of two basic types: the narrow band and the wide band. The wide band networks are in addition of two categories. In the first, cavities are coupled to give a filter with high rejection outside the passband but with dips or ripples in the passband. This is referred to as Tchebyshev filter. The number of ripples depends on the number of cavities. The second category is the maximally flat type designed to eliminate the ripples within the passband. These have been discussed elsewhere in the literature[1,2].

In communication systems, it is often necessary to operate at least a receiver-transmitter combination on a common antenna[3]. For such a purpose, the necessity for matching filter network for narrow or wide band communication channel has been recognised and various analytical procedures with varying degrees of difficulty and simplicity

can be found in the literature[4-16]. Usually, each transmitter or receiver is connected through a filter arm to a single junction with each filter arm consisting of at least a resonant cavity. When there is more than one cavity in an arm, probably because of wide channel bandwidth or the demand for increased selectivity or rejection, the problem becomes that of coupling together the cavities and deciding the individual cavity expected resonance characteristics.

This chapter has a two-fold purpose. First it interprets measured resonant parameters of a cavity to an equivalent simple LCR shunt or series circuit. This would ensure application of the present analysis to a wide variety of coupled cavities. Secondly, it describes the development of each unit of multicavity networks with particular emphasis on the two-cavity networks for application in duplexers. It further shows the effect of each cavity and coupling line on the complex network parameters. Thus, prior to assembly, each cavity resonance parameters can be optimised and each can be tuned to the required frequency. Because of difficulty in designing temperature compensated cavities with absolute frequency stability, we shall briefly examine cases whereby the cavities in each arm are tuned to different frequencies within a narrow range. On the final analysis the idea is that if we can design a duplexer from expected resonant parameters of component cavity resonators it would be easy to design individual resonant cavity to meet the specifications expected of it. And, if this is possible for a duplexer, the same analytical method would hold for other microwave communication systems. Furthermore, numerous experiments in industry and elsewhere have shown that the good agreement between theory and practice actually depends almost completely on how close the actual length of the coupling line is to the real length. It is because of this that the work reported here has been designed to consider the theoretical aspect of interconnected

6.2 Cavity Filters

The exact impedance functions of most coupled resonant cavities are hard to obtain. Where these can be obtained, there is usually a need for empirical adjustment of theoretical values to closely conform with practice. The need for common approach to all filters employing resonant cavities with known or unknown theoretical equivalent circuit becomes of practical importance in view of continued increasing use of various resonant cavities with or without analytic geometries. For complex filter circuits, it is also important to use simplified equivalent network configurations and impedance expressions for individual resonant cavities. In other words, it is better to represent a cavity by an equivalent lumped impedance or shunt admittance without making any reference to the mode of coupling or other design parameters that usually complicate the exact coupled cavity equivalent network.

Two major filter responses possible from a cavity resonator are bandpass and bandstop filter responses. In the ensuing analysis, we shall approach the equivalent circuit parameters through the cavity in-circuit unloaded quality factor, the resonant frequency and the midband attenuation.

6.2.1 Bandpass filter

A bandpass filter and resonator has input and output ports distinct from one another. Such resonators have been discussed earlier in Chapters Two and Three.

Consider the bandpass filter network shown in Fig. 1. The source and load impedances or admittances are normalised to unity and so are the equivalent network elements. The source and load impedances or admittances are equal for the usual measuring equipments in the laboratory. Moreover, earlier computations and laboratory measurements were based on

equal source and load impedances (or admittances). From fundamental network theory,

$$Q_o = \frac{\omega_o L_s}{R} = \frac{\omega_o C_p}{G} \qquad (1)$$

and

$$Q_L = \frac{\omega_o L_s}{R+2} = \frac{\omega_o C_p}{G+2} \qquad (2)$$

where ω_o, Q_o, Q_L are the angular resonant frequency, the unloaded in-circuit quality factor and the loaded quality factors respectively. Let

$$A = 10^{L_A(dB)/20} \qquad (3)$$

where $L_A(dB)$ is the midband attenuation (insertion loss).

$$\frac{Q_o}{Q_L} = \frac{A}{A-1} \qquad (3)$$

So, if Q_o and $L_A(dB)$ are known, the value of loaded Q can be computed. In general, the knowledge of any two of Q_o, Q_L and $L_A(dB)$ could be used to determine the third.

From Fig. 1(a), the insertion loss function L_A is

$$L_A = \left(\frac{R+2}{2}\right)^2 \qquad (5)$$

where $L_A = 10^{L_A(dB)/10}$

i.e. $L_A = A^2$

$$\therefore \quad A = \frac{R+2}{2}$$

$$R = 2A - 2 = 2(A-1) \qquad (6)$$

Alternatively, from Fig. 1(b)

$$G = 2(A-1) \qquad (7)$$

Hence

$$L_s = \frac{Q_o R}{\omega_o} \qquad (8)$$

$$C_p = \frac{Q_o G}{\omega_o} \tag{9}$$

The equation representing the resonators equivalent impedance Z_c and admittance Y_c are

$$Z_c = 2(A-1)\left[1 + jQ_o\left(\frac{\omega}{\omega_o} - \frac{\omega_o}{\omega}\right)\right] \tag{10}$$

and

$$Y_c = 2(A-1)\left[1 + jQ_o\left(\frac{\omega}{\omega_o} - \frac{\omega_o}{\omega}\right)\right] \tag{11}$$

6.2.2 Bandstop filters

A cavity bandstop filter has only one coupling terminal connected to the through line by a quarter wavelength or odd multiples of a quarter wavelength line. Its operation is such that at the cavity's resonant frequency, the filter reflects all the signal. In a series circuit representation, it is equivalent to an open circuit, and in a shunt circuit, a short circuit at resonance. Figs. 2(a) and 2(c) are the series and shunt forms of typical bandstop filter respectively. The unloaded Q factor could be obtained by considering resonance losses or by measurement. All impedances and admittances are normalised. R_s, L_s, C_s and G_p, L_p, C_p are the transformed equivalent network elements of the resonant cavity. Let R_{cs}, L_{cs}, C_{cs} and G_{cs}, L_{cp}, C_{cp} be the equivalent circuit elements of the cavity, if the quarter wavelength line is loss free and unity normalised characteristic impedance, then

$$\frac{L_p}{R_p} = \frac{L_{cp}}{R_{cp}}$$

and

$$\frac{L_s}{R_s} = \frac{L_{cs}}{R_{cs}}$$

The quality factor, Q_o of the cavity is given, from Fig. 2(a), as

$$Q_o = \frac{\omega_o C_p}{G_p} = \omega_o C_p R_p = \omega_o C_{cp} R_{cp} \qquad (12)$$

where ω_o is the mid-stopband frequency. If the maximum attenuation is L_A(dB), then the following can be deduced:

Let

$$A = 10^{L_A(dB)/20}$$

But

$$A = \frac{2+R_p}{2}$$

$$\therefore \quad R_p = 2(A-1) \qquad (13a)$$

or

$$G_p = \frac{1}{2(A-1)} \qquad (13b)$$

Thus, Z, the impedance of the notch section, is given as

$$Z_p = \frac{R_p}{1+jQ_o(\frac{\omega}{\omega_o} - \frac{\omega_o}{\omega})}$$

$$= \frac{2(A-1)}{1+jQ_o(\frac{\omega}{\omega_o} - \frac{\omega_o}{\omega})} \qquad (14)$$

Alternatively, from Fig. 2(b),

$$Y_s = \frac{1}{R_s(1+jQ_o(\frac{\omega}{\omega_o} - \frac{\omega_o}{\omega})}$$

$$= \frac{2(A-1)}{1+jQ_o(\frac{\omega}{\omega_o} - \frac{\omega_o}{\omega})} \qquad (15)$$

The maximum VSWR can be obtained from the notch filter and it is given as

$$VSWR(max) = 2A-1 \tag{16}$$

The cavity equivalent circuit elements can be obtained even if the exact length of the line is not a quarter wavelength but known. If the measurement is taken for a quarter wavelength of line at the mid stopband, then

$$R_{cp} = \frac{1}{R_p}$$

$$R_{cs} = \frac{1}{R_s}$$

If the length of line is different from a quarter wavelength, the attenuation would be affected and the impedance seen from the input to the notch assuming no line loss is rather

$$Z'_p = \frac{j \sin\theta + Z_{cp}\cos\theta}{\cos\theta + jZ_{cp}\sin\theta} \tag{17}$$

or the admittance,

$$Y'_s = \frac{j \sin\theta + Y_{cs}\cos\theta}{\cos\theta + jY_{cs}\sin\theta} \tag{18}$$

where

$$Z_{cp} = \frac{1}{Z_p}$$

$$Y_{cs} = \frac{1}{Y_s}$$

and

$$\theta = \frac{l_n}{\lambda} \cdot 2\pi$$

l_n being the length of line connecting the one port cavity to the through line.

We can re-write these two equations as

$$Z'_p = \frac{jZ_p \sin\theta + \cos\theta}{Z_p \cos\theta + j \sin\theta} \quad (19)$$

and

$$Y'_s = \frac{jY_s \sin\theta + \cos\theta}{Y_s \cos\theta + j \sin\theta} \quad (20)$$

6.3.1 Design theory and analysis

Two major and basic filter responses possible from a cavity resonator have been discussed viz bandpass and bandstop. The criterion for the application of individual unit is a dependent factor of what are the expected inband slope and system characteristics. Quite a variety of responses can be obtained by various combinations of these basic units.

The above derivations have considered the cavities as equivalence of simple LCR series or shunt circuits for which the elements are independent of frequency. These can be considered as approximate representations and without much practical and theoretical differences. However, it should be noted that R, L and C are frequency dependent because the energy stored in and power dissipated in the walls of a resonator vary with field and therefore the frequency. Actually, the resonance curve is not symmetrical as these derivations would make us believe. For most cavity resonators off band attenuation for frequencies higher than the midband frequency is slightly steeper than for lower frequencies. The measured values are therefore average of the two slopes, measured in terms of half-power bandwidth. This frequency dependency can only be known to a certain extent if the complex reflection coefficients can be measured over a wide range of frequencies centred on the midband resonant frequency. All admittances and impedances are usually normalised assuming the line characteristic impedance or

admittance is unity. If, therefore, on measurement, two cavities have the same insertion loss or midband attenuation and unloaded Q at the same frequency, to a first approximation, their behaviours, in all aspects, are very similar at that frequency.

6.3.2 General multi-cavity filter network

We shall first consider the general case of a filter network consisting of n numbers of interconnected cavities. Fig. 3(a) shows a section of two port multi-cavity network with the ith cavity coupled to the (i+1)th cavity by a line length l_i. All admittances are normalised assuming the coupling line characteristic admittance is unity. The ith cavity has a normalised admittance Y_i. For an n interconnected cavities we can write the following transfer matrix for the network:

$$[A] = \begin{bmatrix} 1 & 0 \\ Y_1 & 1 \end{bmatrix} \begin{bmatrix} p_1 & jq_1 \\ jq_1 & p_1 \end{bmatrix} \begin{bmatrix} 1 & 0 \\ Y_2 & 1 \end{bmatrix} \begin{bmatrix} p_2 & jq_2 \\ jq_2 & p_2 \end{bmatrix} \cdots \begin{bmatrix} 1 & 0 \\ Y_i & 1 \end{bmatrix} \begin{bmatrix} p_i & jq_i \\ jq_i & p_i \end{bmatrix} \cdots \begin{bmatrix} 1 & 0 \\ Y_n & 1 \end{bmatrix}$$

$$= \prod_{i=1}^{n-1} \begin{bmatrix} 1 & 0 \\ Y_i & 1 \end{bmatrix} \begin{bmatrix} p_i & jq_i \\ jq_i & p_i \end{bmatrix} \times \begin{bmatrix} 1 & 0 \\ Y_n & 1 \end{bmatrix} \qquad (21)$$

where

$$p_i = \cos \beta l_i$$

and $$q_i = \sin \beta l_i$$

$$\beta = \frac{2\pi}{\lambda}$$

In a more general form we can re-represent the circuit by the form shown in Fig. 3(b). Let

$$[A] = \begin{bmatrix} A_{11} & A_{12} \\ A_{21} & A_{22} \end{bmatrix} \qquad (22)$$

For this representation, the transmission loss function, L, is given from the current ratio

$$R' = \frac{1}{1+Y_L}\,[A_{11} + A_{21} + A_{22}Y_L + A_{12}Y_L]$$

as

$$L = \left| \frac{1}{1+Y_L}\,(A_{11} + A_{21} + A_{22}Y_L + A_{12}Y_L) \right|^2 \qquad (23)$$

$$\therefore \quad L(dB) = 20 \log_{10} \left\{ \left| \frac{1}{1+Y_L}(A_{11} + A_{21} + A_{22}Y_L + A_{12}Y_L) \right| \right\} \qquad (24)$$

A solution to obtain the system resonant frequency and resonance attenuation is by numerical means if perchance Y_L represents a complex impedance function at the passband of the network or when any of the cavities in the network has resonant frequency distinct from others. Special cases where the coupled structures are not resonant at frequencies of operation and for which the actual length of coupling lines would be different from quarter wavelength have been characterised. This subject is taken up in Appendix IV. The response curve can be obtained by substituting numerically in the equations.

Whatever number of basic cavities interconnection, the resulting two port network will possess a transmission matrix [A] which is the product of the individual matrices as they appear in the cascade.

6.3.3 Two-cavity interconnections[1,3]

Consider a set of 1.5GHz resonant cavities designed with in-circuit unloaded Q of 14000 and insertion loss of 0.7dB, and also a cavity bandstop filter with 25dB maximum attenuation and unloaded Q factor of 14000. Consider further Fig. 4 showing symbolically an equivalent network representing interconnected two-cavity filter network. θ_1 represents, in electrical degrees, the length of the coupling line l_1. Y_1, Y_2 represent the impedance functions of the two cavities as observed

from the through line where each could represent any of bandpass and bandstop basic filters. We shall now consider cases where

1. Y_1, Y_2 are both bandpass network admittances.
2. Y_1 is a bandstop filter admittance and Y_2 a bandpass filter admittance.

We shall assume the line to be lossless. This would be especially true for cases when the line length is short[8]. This circuit can be transformed into Fig. 3(a) where the transfer matrix [A] is given as

$$[A] = \begin{bmatrix} 1 & 0 \\ Y_1 & 1 \end{bmatrix} \begin{bmatrix} \cos\theta_1 & j\sin\theta_1 \\ j\sin\theta_1 & \cos\theta_1 \end{bmatrix} \begin{bmatrix} 1 & 0 \\ Y_2 & 1 \end{bmatrix} \quad (25)$$

Y_1 and Y_2 are obtained from equations (11) or (19) as presented in sections 6.2.1 and 6.2.2. By substituting in equation (24), such parameters as isolation, attenuation and midband insertion loss can be deduced.

Two-cavity Bandpass Filter

Fig. 5(a) compares the frequency responses of the network when both cavities are tuned to the same frequency, curve 1, and when one is slightly tuned to a different frequency 4MHz below the other, curve 2. The coupling line is exactly a quarter wavelength long at 1.5GHz. It could be observed that the insertion loss increased considerably. In coupled resonant cavities, such response as obtained in curve 2 always has the resulting resonance dip tracing the original curve, curve 1, in such a way that the difference between their resonance peaks is approximately the difference between the peaks of the ripples. Increased insertion loss in this case does not correspond to increased off-band isolation, rather a degradation. The ripple observed in this case is characterised by Tchebyshev filters. Fig. 5(b) is a plot of insertion loss and attenuation against the length l_1 when both cavities are tuned to the same frequency.

The attenuation is obtained for a frequency of 1.481GHz i.e. 19MHz below the midband resonant frequency. It is observed that as the coupling line length differs from a quarter wavelength long, the insertion loss decreases as well as the attenuation. A closer examination shows that the isolation between the passband and the offband frequencies decreases as the length differs further from a quarter wavelength.

Two-Cavity Bandstop-Bandpass Network

The two major problems with a two-cavity bandpass filter is that the insertion loss cannot be less than the sum of individual cavity insertion loss under matched input and output loads; and there is general degradation of resonance response when the coupling line differs from a quarter wavelength long.

One advantage of interconnecting cavity-bandpass and -bandstop units is because of the reduction in the insertion loss. It also offers the possibility of trading attenuation rates at both sides of the passband. The following analysis would show further advantages and disadvantages of the interconnection.

Equations (13), (14), (15) and (16) have been derived from a possible maximum attenuation of a cavity notch filter and any length of line l_t connecting the cavity to the through line. Equations (17)-(20) show that the impedance function for any length l_t can still be derived from the earlier knowledge. Let Y_1 represent Y'_s (section 6.2.2) in equation (25) and Y_2 represent a cavity bandpass impedance. From theory, the length θ_1 must be multiples of half the wavelength at mid-stopband or zero. For design purposes, $l_1 = 0$. θ, equation (19) (or (20)), is given as

$$\theta = \frac{l_t}{\lambda} .2\pi$$

Consider the notch filter for maximum attenuation of 25dB and midband frequency of 1.481GHz when $l_t = \frac{\lambda_t}{4}$, where λ_t is the resonant wavelength of the cavity notch filter. Substituting in equations (15), (20), (24) and (25), we can obtain the transmission loss function. By numerical solution to equation (24), the frequency shifts at passband and reject band, attenuation etc. can be obtained. Fig. 6(c) presents the response curves of the network for various values of l_t. It is obvious that by changing the line length the midband frequencies can be altered. However the shift in the centre frequency of the stopband is more affected than at the passband. When the line length differs from a quarter wavelength long, midband attenuations increase but with improved isolation between passband and reject band. However, if the filter is to be considered for midband frequency at f_t, it follows from Fig. 6(a) that changing the line length would inhibit the performance. Figs. 6(b) and (c) summarise the various effects caused by changing l_t and frequency separation between the notch and bandpass cavity resonances.

It is deducible from the plots that by decreasing the frequency separation between cavity notch filter and bandpass filter, there is generally increased insertion loss and decreased attenuation at the reject band. With θ above $\frac{\pi}{2}$, the isolation between passband and reject band increased but the frequency separation increased accordingly with attendant increased insertion loss. It could be observed further that as θ decreases below $\frac{\pi}{2}$, the resonance curve compresses while with θ above $\frac{\pi}{2}$, the curve expands. In essence if the desired maximum isolation is demanded for a known frequency separation and for the exact separate resonant frequencies of Y_1 and Y_2, the best resonance achievement would only be possible for $l_t = \frac{\lambda_t}{4}$. Anyway, there exists flexibility in any

design procedure in this line and it is very possible and effective to trade isolation and insertion loss better than the two cavity bandpass network.

A disadvantage is that the expected network response can be marred by slight variation in the coupling line length. Thus while complete cavity bandpass filter network would be inflexible to slight coupling line variations, such may shift the desired resonance performance of a combination of cavity notch and bandpass filters. Other advantages are that sharper cut-off can be obtained between the passband and stopband; however at the expense of less steep cut-off on the other side of the passband. Secondly, the fear of any abnormal resonance dip resulting from off-tuning any of the cavities is eliminated. The notch, under critical length l_t, would exert insignificant effect on both the insertion loss of the passband and the midband frequency.

6.4.1 A Resonant Cavity Frequency Duplexer

So far we have discussed the responses of two major filter networks namely a bandpass and bandstop as well as complex networks derived from the two basic units. We have observed the quality of each of these networks. It is now left to develop this basic idea into a suitable communication network as found in duplexers, multiplexers, etc. A good number of literature has been quoted earlier and the work here includes further analysis.

6.4.2 Design requirements and basic configuration

Each filter unit was to be developed and tuned for the required specification. Actually this practice, the individual unit development, cannot be foregone despite the fact that by connecting it to the load with appendage networks, the in-circuit characteristics are expected to be affected. The last stage in the development program is thus the assessment of the effectiveness and behaviour of individual units in the multi-circuit system, at least to furnish us with such idea as to how much allowance should be provided in the basic units. It is however a reasonable expectation that no fundamental changes do occur. This, admittedly, would be yet a dependent factor of channel spacing - none of the channels, as is usually the case, may be allowed to overlap within the same system or station. Thus we do not envisage any pitfalls whatsoeve

Let us consider a two unit interconnection of filters as often obtained in two-branch duplexers common with land mobile communications. The receive power is much lower than the transmit power. Thus, the function of the network in the receive arm of the duplexer would be to protect the receiver from the transmitter by limiting the amount of power coupled to the receiver to below the receive power level. So in essence, the isolation demanded from the receiver filter unit would depend on the relative magnitudes of the transmitted and received power levels. The basic function of the filter in the transmit path is to match the transmitter to the load. In view of these reasons, it is always necessary to employ more than one cavity in the receive path while a single cavity may perform the function required of the transmit path circuit. Further analytical requirements have been outlined in the literature. We shall approach the analysis through the two basic units already discussed and compare their performance in a two branch,

narrow band duplexer. A bandpass filter is provided for the transmit path while the receive path has two cavities connected as discussed in section 6.3.3. We shall consider this for a frequency separation between receiver and transmitter of 19MHz where the receiver and transmitter are operating at 1500MHz and 1481MHz respectively. Fig. 7 shows the filter networks interconnection. Each arm is coupled to the common junction through a quarter wavelength line at the individual arms operating midband frequency. This permits the use of any length of line to connect the load to the junction without offsetting the responses of the duplexer arms[10].

The observed response from the receiver side is given by the transmission loss equation (24), where [A] is given as:

$$[A] = \begin{bmatrix} 1 & 0 \\ Y_{r_1} & 1 \end{bmatrix} \begin{bmatrix} p_1 & jq_1 \\ jq_1 & p_1 \end{bmatrix} \begin{bmatrix} 1 & 0 \\ Y_{r_2} & 1 \end{bmatrix} \begin{bmatrix} p_2 & jq_2 \\ jq_2 & p_2 \end{bmatrix} \begin{bmatrix} p_t & jq_t \\ jY_t & p_t \end{bmatrix} \begin{bmatrix} 1 & 0 \\ Y_t+Y_L & 1 \end{bmatrix} \quad (26)$$

and

$$\beta_1 = \cos\theta_{r_1}, \quad q_1 = \sin\theta_{r_1}, \quad p_2 = \cos\theta_{r_2}, \quad q_2 = \sin\theta_{r_2}$$
$$p_t = \cos\theta_t, \quad q_t = \sin\theta_t$$

as defined for equation (24).

In Fig. 7(a), $\theta_{r_1} = \theta_{r_2}$ and are both quarter wavelength long at the receiver's frequency of 1.5GHz. Here, each cavity bandpass filter was to be designed for an in-circuit unloaded Q factor of 14000 and insertion loss of 0.7dB. Then, by following the previous analysis, the observed response at the receiver side is shown in Fig. 8(a). Fig. 8(b) summarises the effect of changing the line length on attenuation and insertion loss. The isolation between the receiver and transmitter is the difference of the two. However, there is quite a limited room for trade-offs between isolation and insertion loss. As the insertion loss

decreases, the reject band attenuation but not the general off-band attenuation decreases as to decrease the isolation. Compared with responses and curves of Fig. 5, the insertion loss of the arm is little affected by the other arm network but the isolation is very much affected. In other words, we may not expect an overall characteristic changes of any basic unit on interconnection in a multi-unit network. The insertion loss observed between transmitter and the load is obtained by reversing the order of matrix multiplication i.e.

$$A = \begin{bmatrix} 1 & 0 \\ Y_t & 1 \end{bmatrix} \begin{bmatrix} p_t & jq_t \\ jq_t & p_t \end{bmatrix} \begin{bmatrix} p_{r_2} & jq_{r_2} \\ jq_{r_2} & p_{r_2} \end{bmatrix} \begin{bmatrix} 1 & 0 \\ Y_{r_2} & 1 \end{bmatrix} \begin{bmatrix} p_{r_1} & jq_{r_1} \\ jq_{r_1} & p_{r_1} \end{bmatrix} \begin{bmatrix} 1 & 0 \\ Y_{r_1}+Y_o & 1 \end{bmatrix} \quad (27)$$

By substituting this in equation (24), we can obtain both the insertion loss and response observed from the load side. Generally, the incircuit effect on the separate unit is not all that severe if we compare Figs. 5 and 8.

Consider Fig. 7(b) with the notch filter designed for a maximum attenuation of 25dB at f_t. In simplified form Y_{r_1} represents a bandstop filter impedance in lieu of the bandpass filter. l_1 is zero and l_2 kept as a quarter wavelength. Fig. 9(a) presents a summary of the response for a 19MHz separation and for various values of l_t. In comparison with Fig. 6(a) there is unnoticeable difference between resonant peaks but a slight increase in attenuation could be observed in the reject band. By comparing Figs. 6(c,d) and 9(c,d), one can observe that the insertion loss is little affected by external network while the isolation between reject band and passband is most influenced by any of l_t and frequency separation changes. However, any of these has little or no recognisable effect on the frequency shifts. Generally, a lot of improvement in isolation does occur for multi-unit filter interconnections, an assertion

which may fail to hold when reject band and passband are very close.

6.5 Conclusion

One major objective of the analysis has been to develop an effective analytical technique which would allow such routine as predetermination of individual resonant cavity characteristics from the general communication network specification. This has been made possible by the two basic and fundamental analysis of sections 6.2.1 and 6.2.2 which allows for the use of resonant cavities with measured or accurately predicted resonant parameters. In other words, resonant cavities can be designed and the response optimised prior to the final assembly.

Performance of combinations of cavities was generally good. The analysis has shown the possibilities of trading off various resonance characteristics such as attenuation and insertion loss. It follows that a combination of cavity bandstop and bandpass in a filter unit would allow flexibility in trade-offs between reject band attenuation and insertion loss. Generally, the passband is little affected by variations in the reject band. However, while variations in the length of coupling lines exert less influence on the insertion loss and off-band attenuation of all cavity bandpass filter units, such would alter the off-band response of a cavity bandstop-bandpass filter combination; which may circumvent its flexibility.

Finally, the effect of connecting many filter units to a common junction or load amounts to less inhibiting effect on each branch insertion loss while a general improvement may take place in the reject band attenuation provided none of the channels intersects with the other.

6.6 References

1. Matthaei, G L et al: 'Microwave filters, impedances,....', McGraw Hill, New York, 1964.

2. Mumford, W W: 'Maximally flat filters', BSTJ, Vol. 27, 684, 1946.

3. Shepherd, N H: 'Analysing interference in FM communication systems', Electron Ind., pp. 15-29, March 1958.

4. Matthaei, G L: 'Design of wideband (and narrow band) bandpass microwave filters on the insertion loss basis', IEEE Trans. MTT-8, pp. 580-593, 1960.

5. Pritchard, W L: 'Quarter wave coupled waveguide filters', J. Appl. Phys., Vol. 18, pp. 862, Oct. 1947.

6. Crosby, D R: 'Duplexing filters design at 2000M/cs', IRE Trans. MTT, Vol. 1, pp. 31-38, 1953.

7. Potok, M H N: 'The design of inductive post type microwave filters', J. Brit. IRE, p.263, May 1958.

8a Howson, D P: 'The performance of two .....', Univ. Bradford PGEEE Report No. 245, 1978.

8b. Howson, D P: PGEEE Report No. 246, 1978.

9. Bryson, W B: 'Design of high isolation duplexers and a new antenna for duplex systems', IEEE Trans. Veh. Comm., (USA), Vol. 14, No. 1, p.34, Mar. 1965.

10. Uenishi, K et al: 'Transmitter multiplexing system in UHF mobile radio', IEEE Trans. Veh. Tech., Vol. 18, p.1-11, May 1969.

11. Bowers, E O & Curtis, C W: 'A resonant cavity frequency duplexer', Nat. Conv. Rec., IRE, 1956, Pt. 5, p. 113-8.

12. Russell, R L: 'Cavity resonators as VHF radio system elements', MSc Thesis, Univ. Bradford, 1976.

13. Strangmann, D & Pichler, K: 'Cavity resonators for UHF-TV transmitters', Microwave J., Vol. 20, No. 11, p.63, 1977.

14. McGladelery, B: 'Applying multicouplers to the assignment of base station frequencies', Canadian Electron Eng., Vol. 19, No. 10, pp. 23-25, Oct. 1975.

15. Hessel, J et al: 'Microwave filter theory and design', Proc. IRE, Vol. 37, p.651, 1949.

16. Carlin, H J: 'UHF multiplexer uses selective couplers', Electronics, Vol. 28, pp. 152-155, Nov. 1955.

17. Fraisse, H J: 'A bandstop filter for VHF and UHF', Rundfunktech. Mitt., Vol. 6, No. 5, p.209, May 1962.

18. Young, L et al: 'Microwave bandstop filters with narrow stopbands', IRE Trans. MTT. Vol. 10, pp. 416-427, No. 1, 1962.

19. Kurzro, R M: 'Comments on loaded Q of a waveguide cavity resonator', IEEE Trans. MTT Vol. 15, No. 3, Mar. 1967.

20. Aston, R: 'Techniques for increasing the bandwidth of TM_{010}-mode power combiner', IEEE MTT-Vol. 27, No. 5, p.479, May 1979.

21. Marcuvitz, N: Waveguide Handbook .

22. Guillemin, E A: Communication Networks , Vol. 2, John Wiley & Sons Inc., NY, 1935.

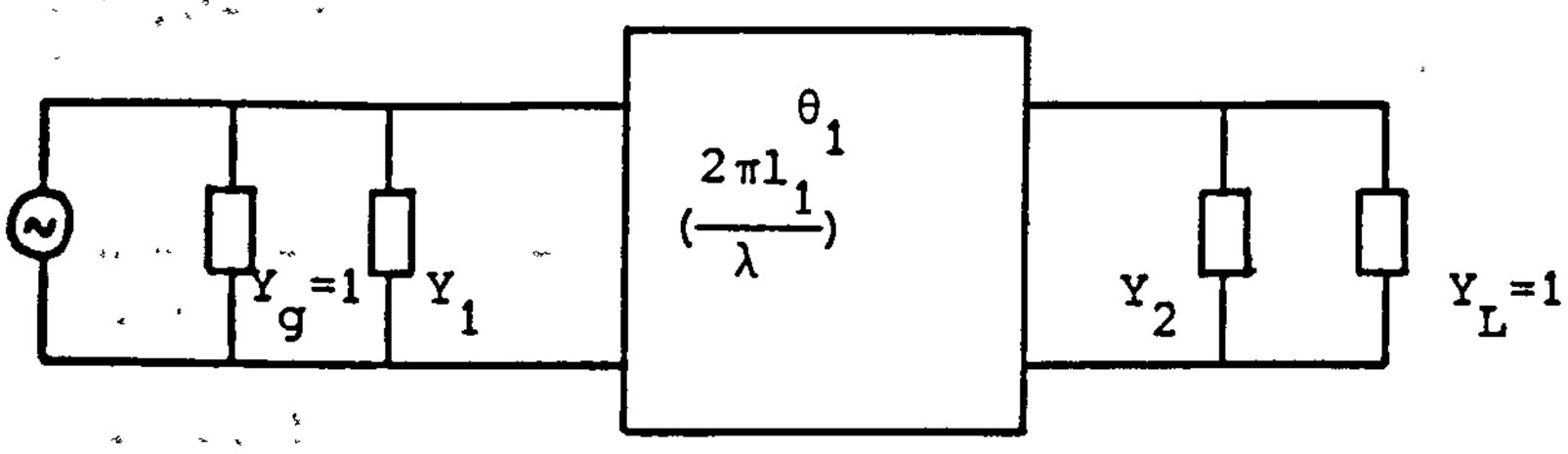

Figure 4 An equivalent impedance representation of a two-cavity filter

(a) All cavity bandpass arrangement

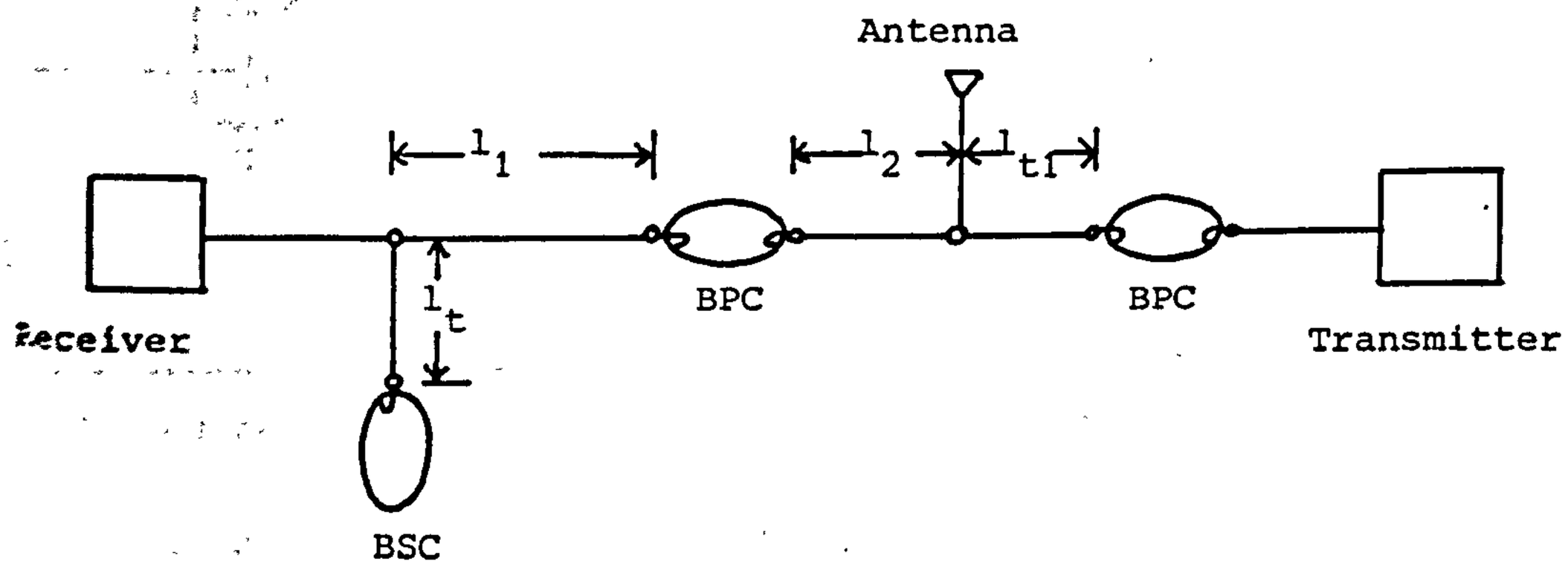

(b) Cavity bandpass-bandstop arrangement

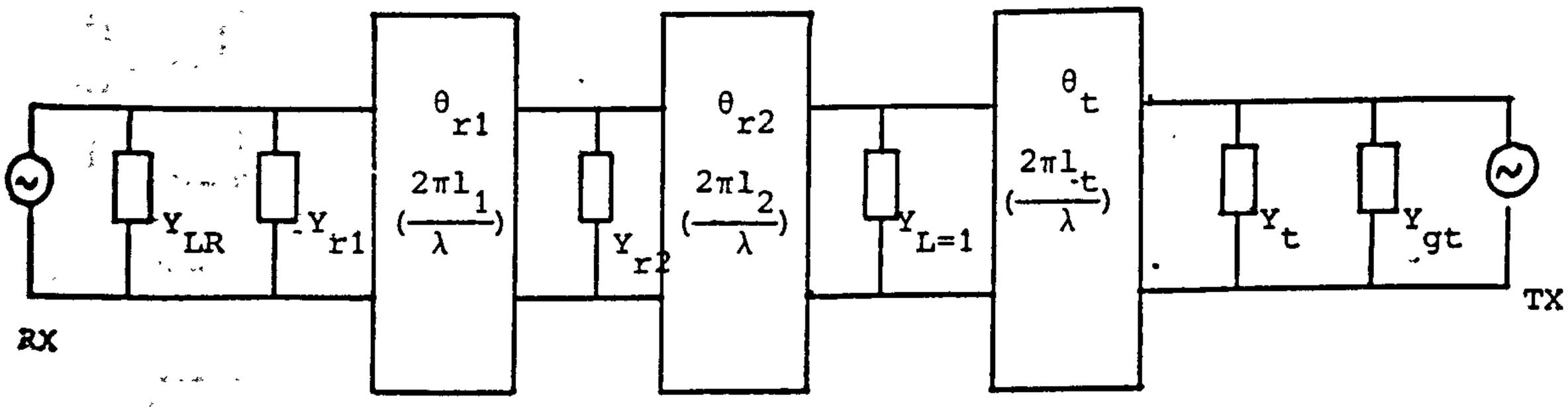

(c) Equivalent admittance representation of (a) and (b)

Figure 7 Duplexer networks

(Notation: BPC - bandpass cavity
BSC - bandstop cavity)

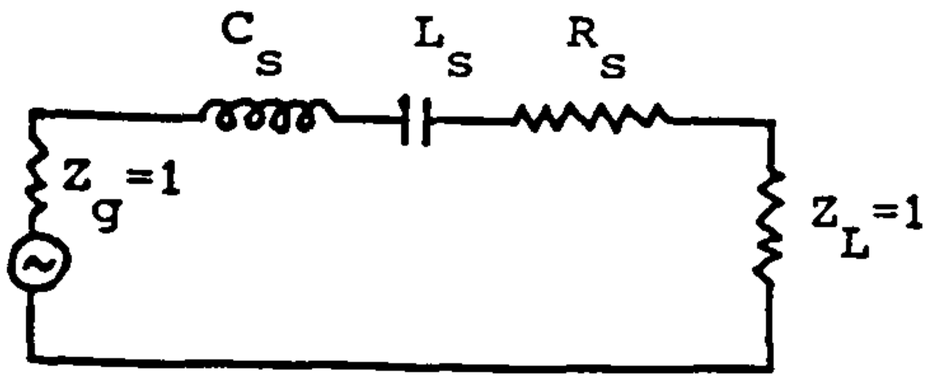

(a) Series representation

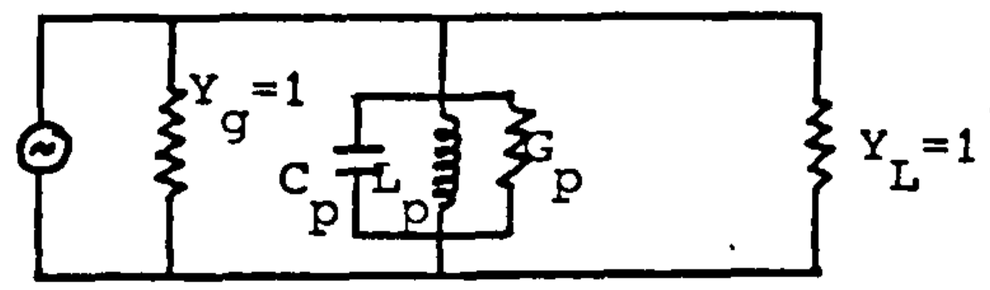

(b) Shunt representation

Figure 1 Typical bandpass filter network

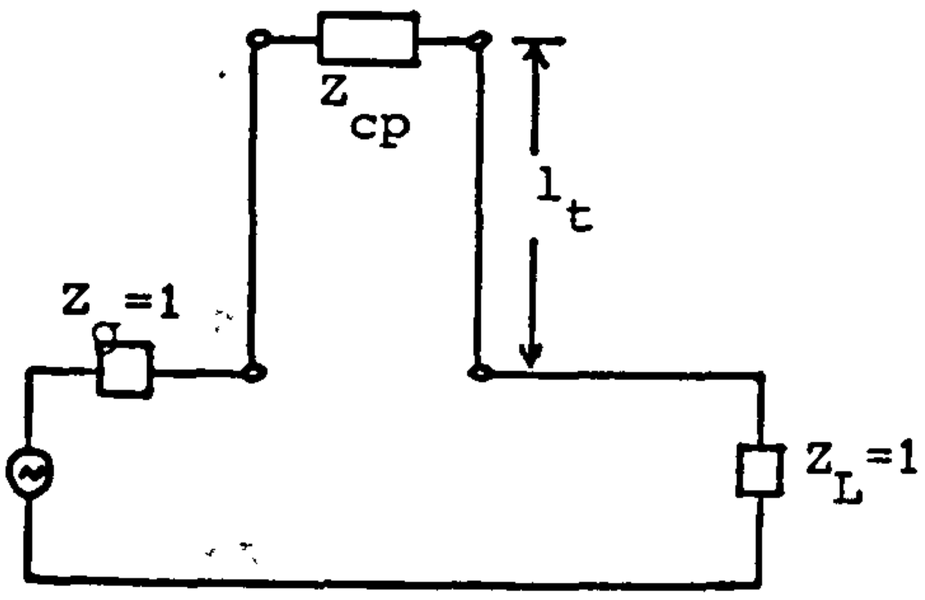

(a) Series representation

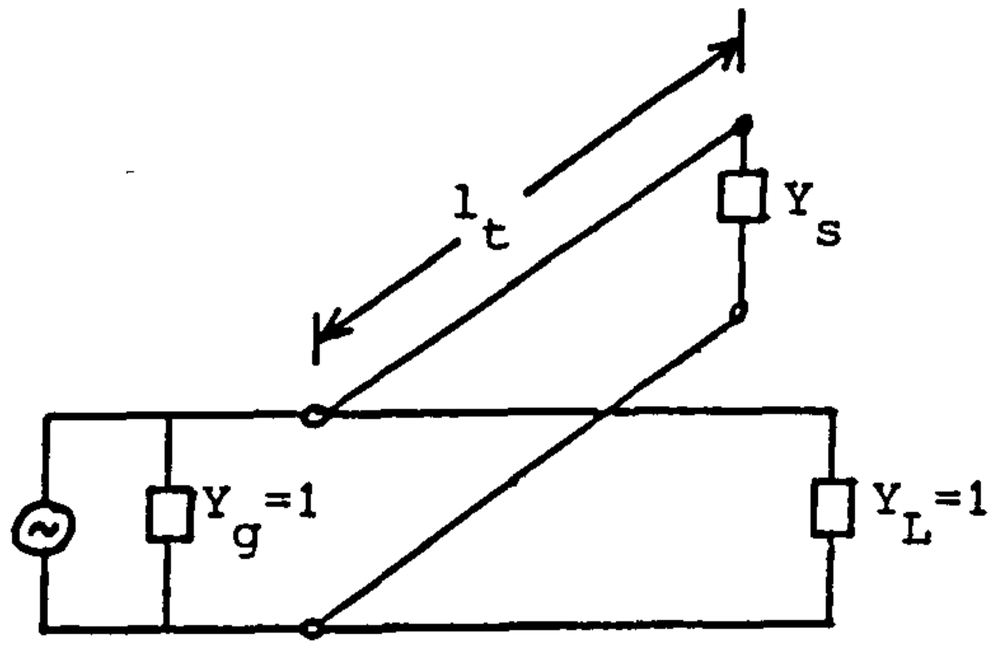

(b) Shunt representation

Figure 2 Typical bandstop filter network

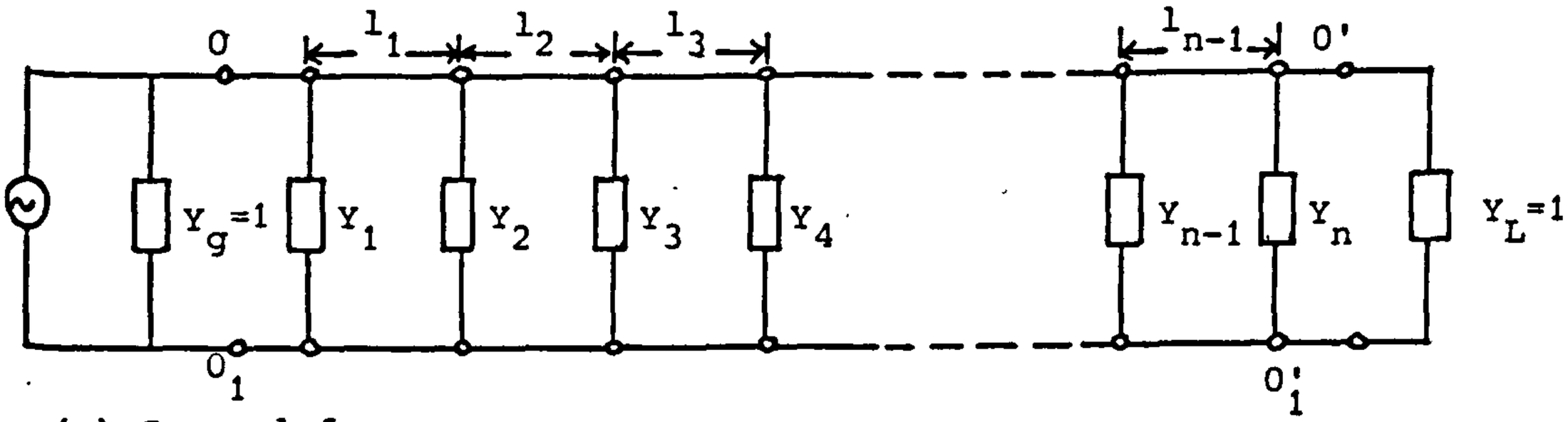

(a) General form

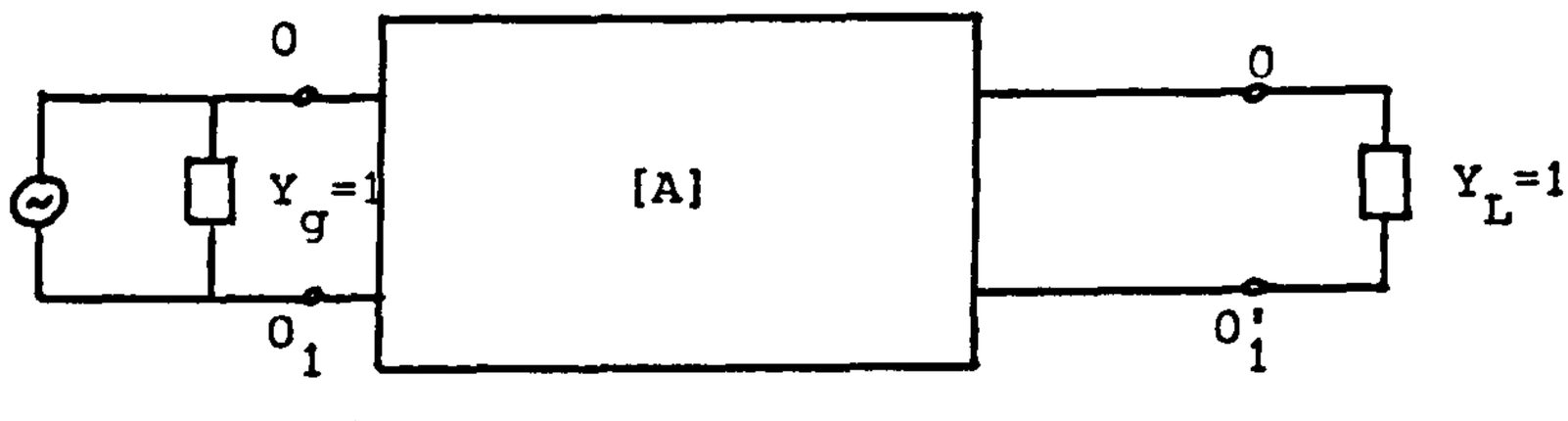

(b) Simplified form

Figure 3 General representation of multi-element filter network

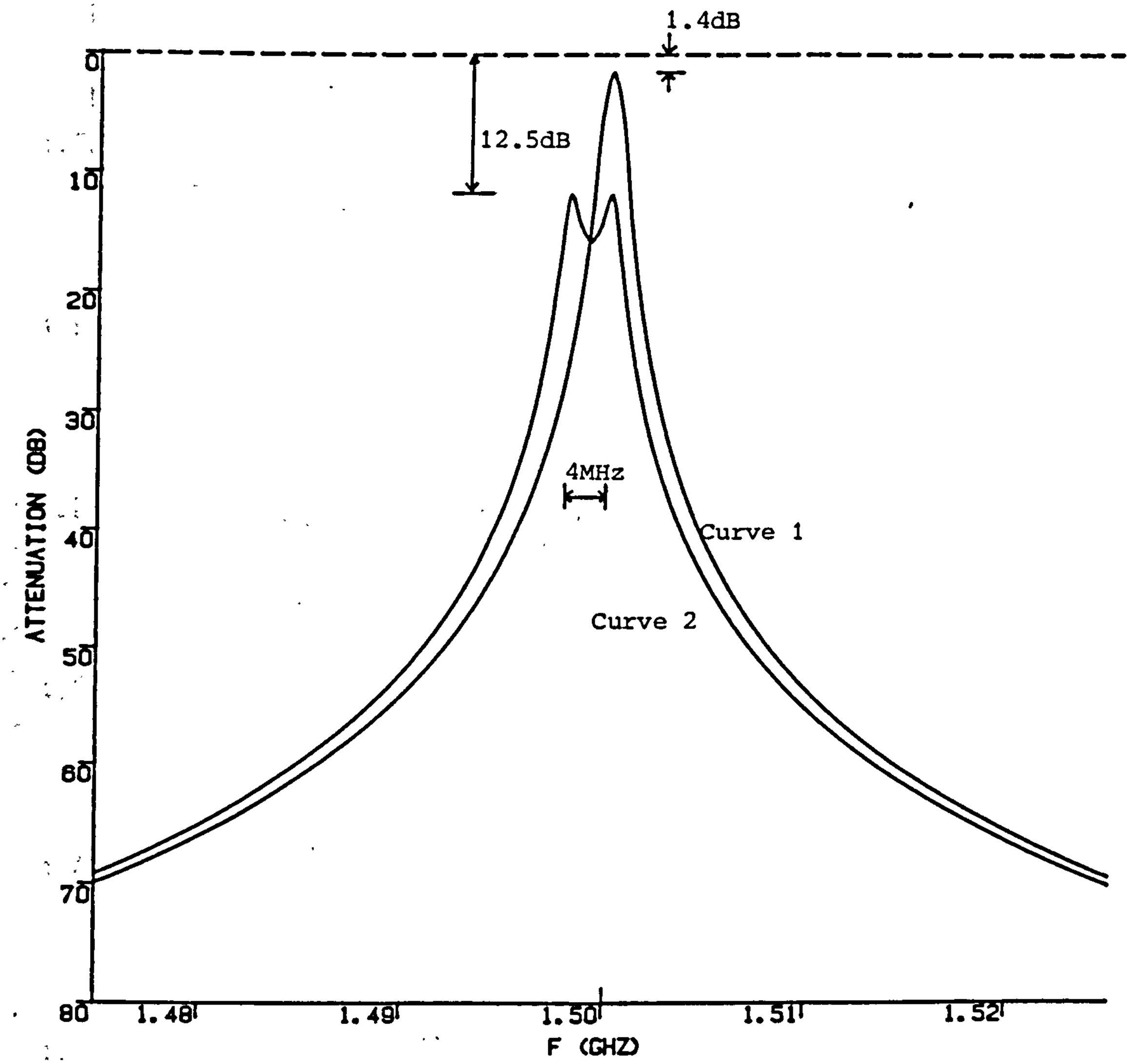

Figure 5(a) Frequency response of a two-cavity bandpass filter
(a) When both cavities are tuned to the same frequency
(b) When one is detuned by 4MHz below the other

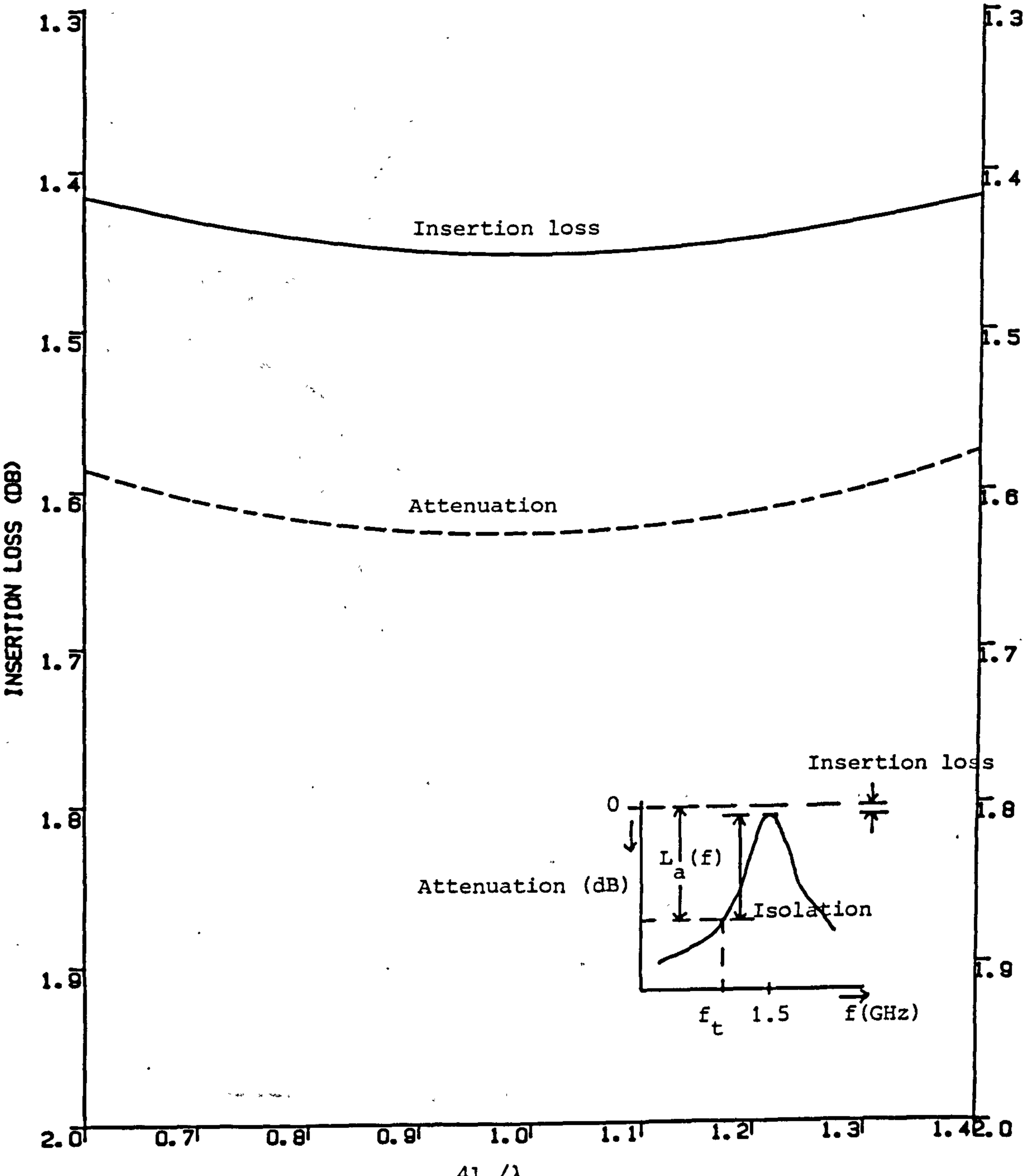

$41_i/\lambda_f$

Figure 5(b) Plots of insertion loss and attenuation against l_1

$\lambda_f = \frac{2.998}{15}$ (f = 1.5GHz)

Attenuation is obtained for f_t = 1.481GHz

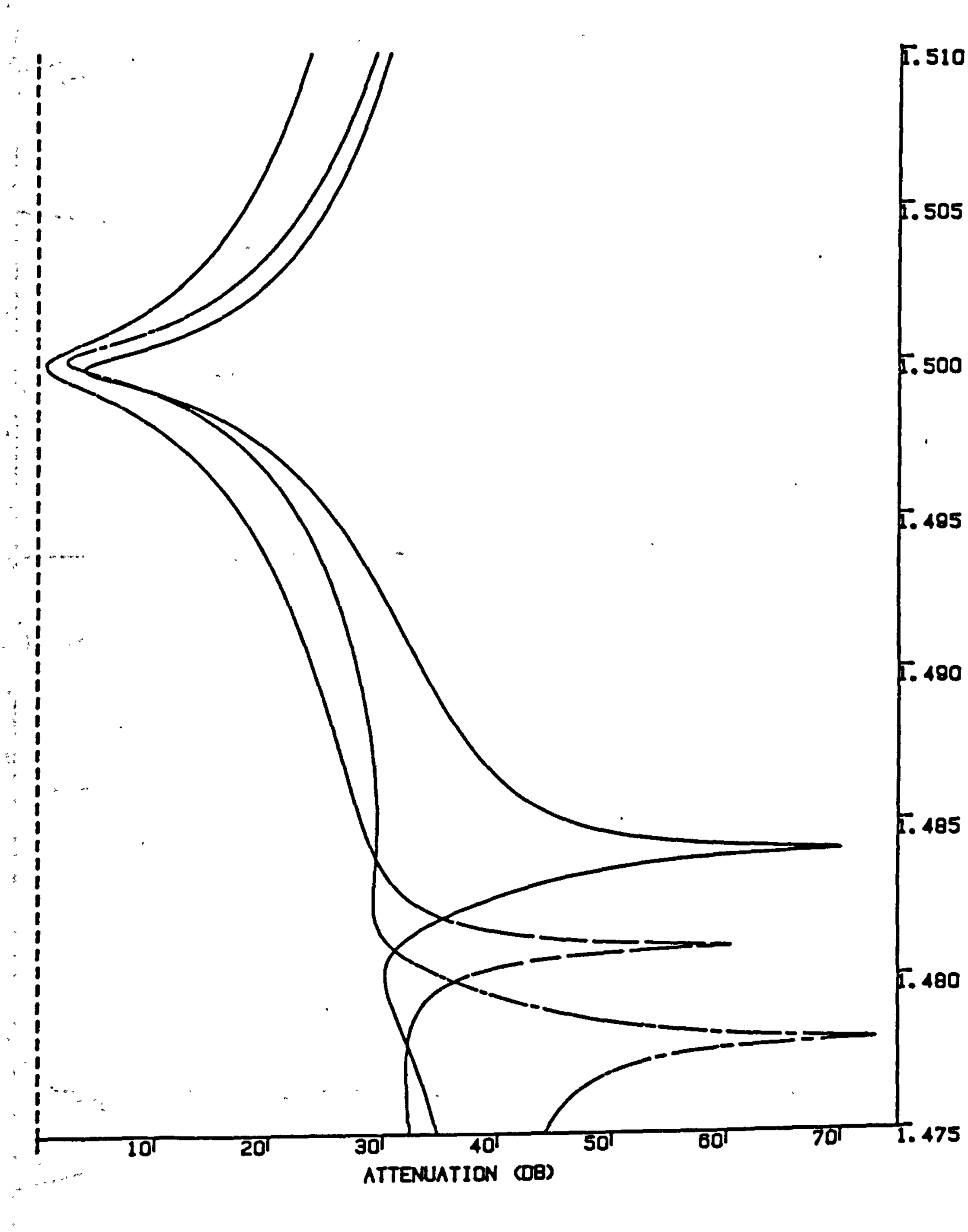

Figure 6(a) Response curves for various l_t

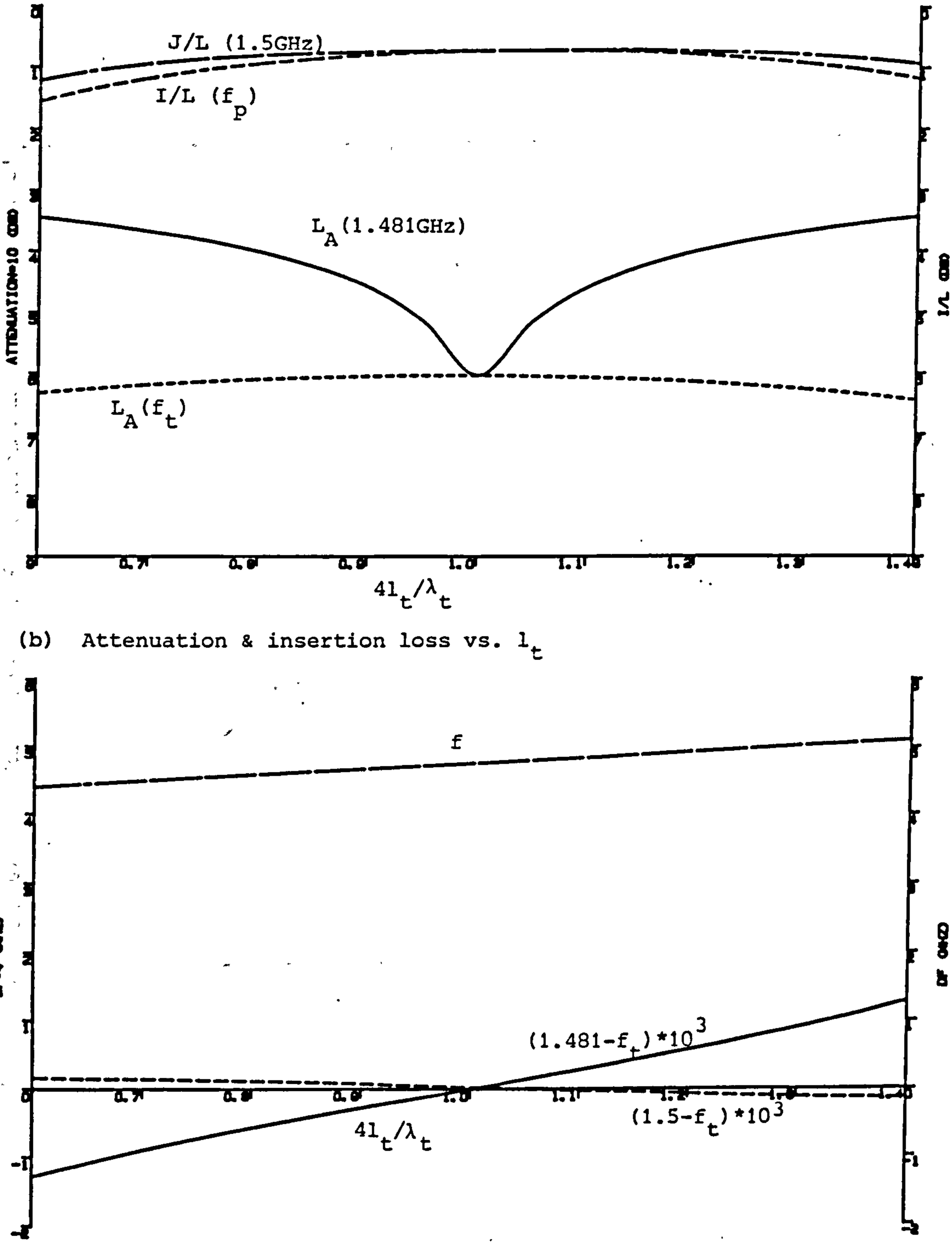

(b) Attenuation & insertion loss vs. l_t

(c) frequency shifts vs. l_t

Figure 6

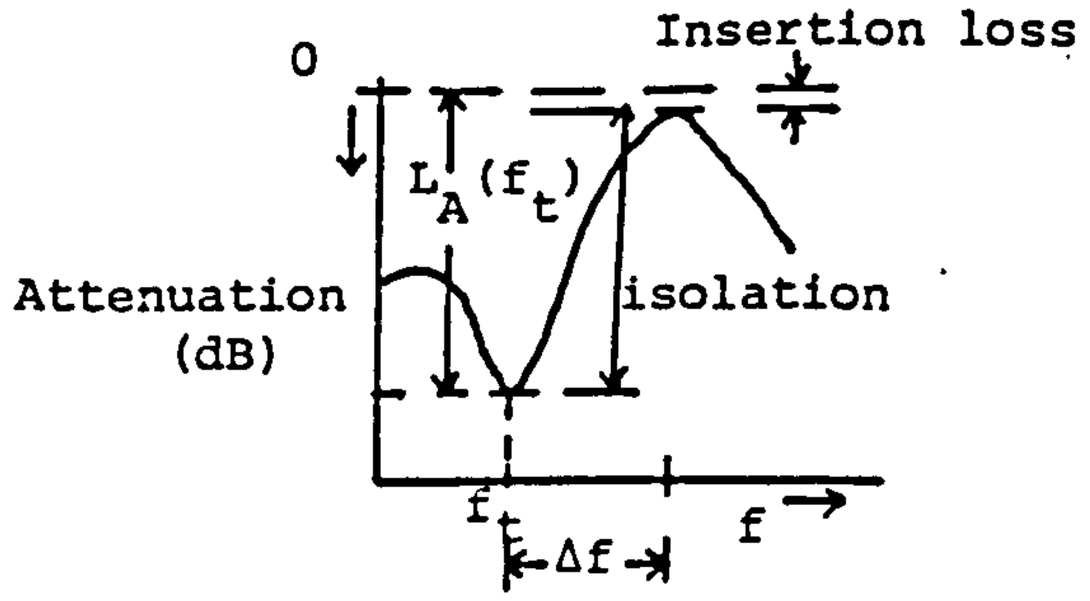

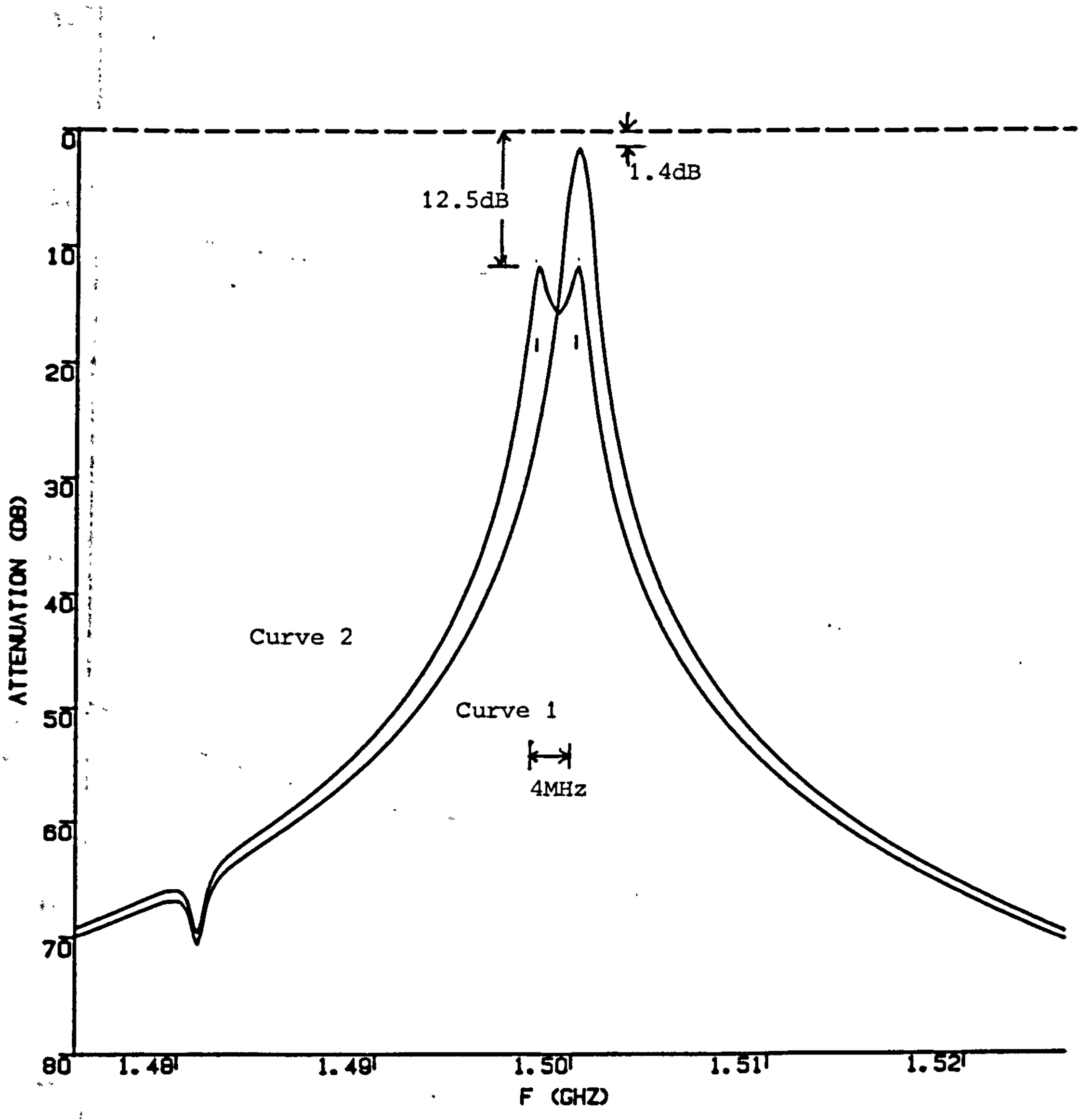

Figure 8 (a) Frequency response of a three-cavity bandpass duplexer
(1) When both are tuned to the same frequency
(2) When one is detuned by 4MHz below the other

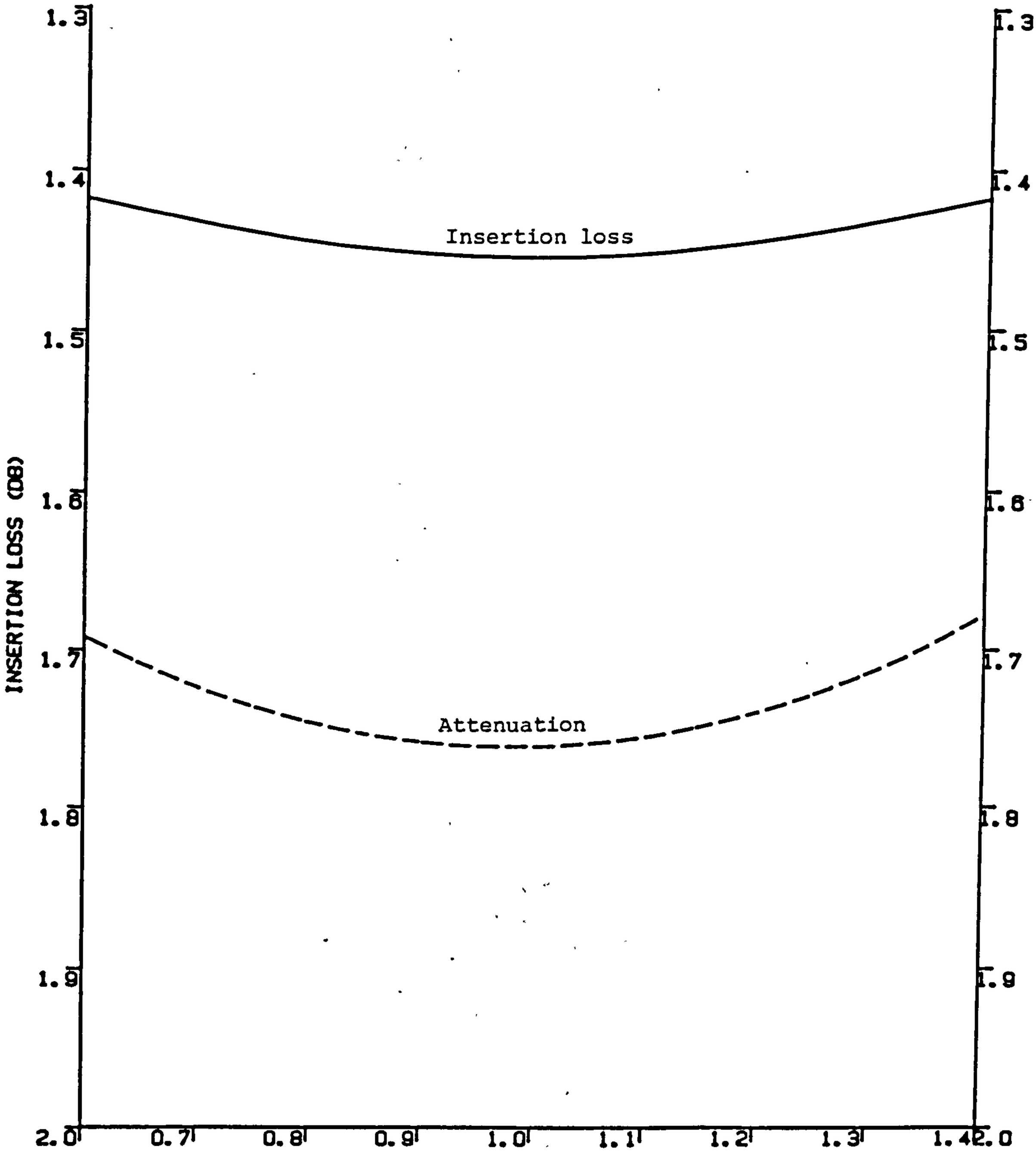

Figure 8(b) Plots of insertion loss and attenuation against l_1

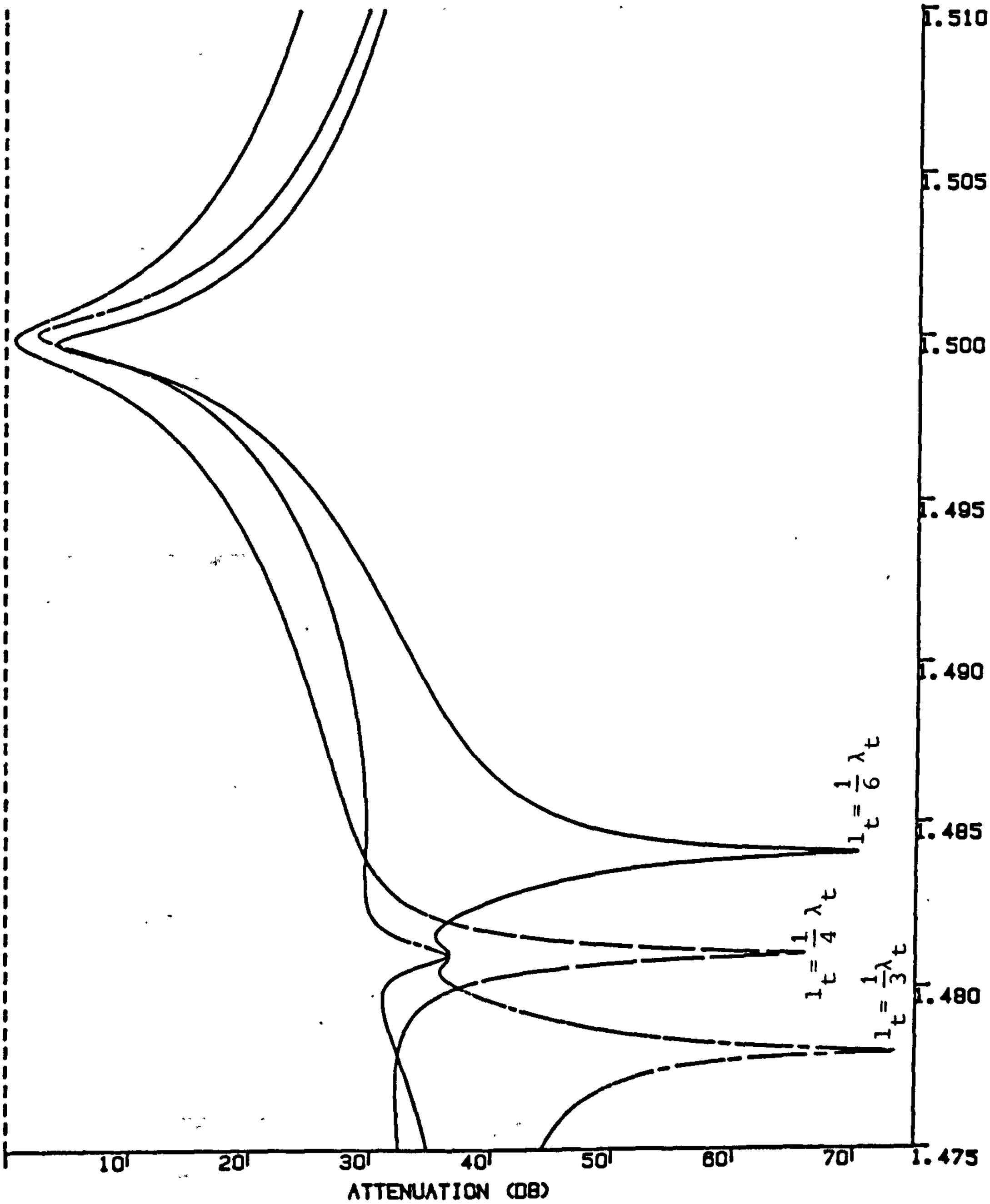

Figure 9(a) Response curves for various 1_t

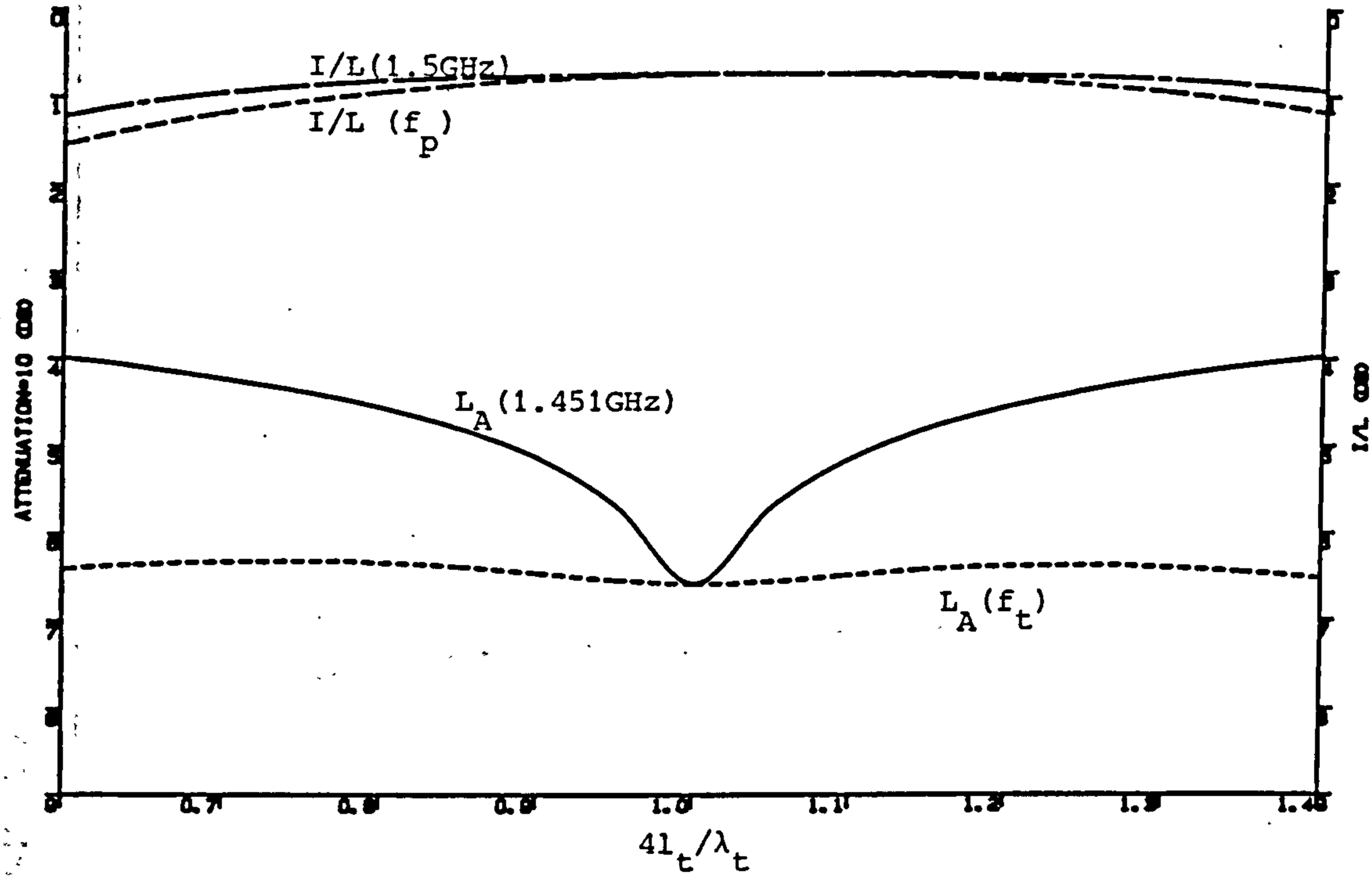

(b) Attenuation & insertion loss vs. coupling line length

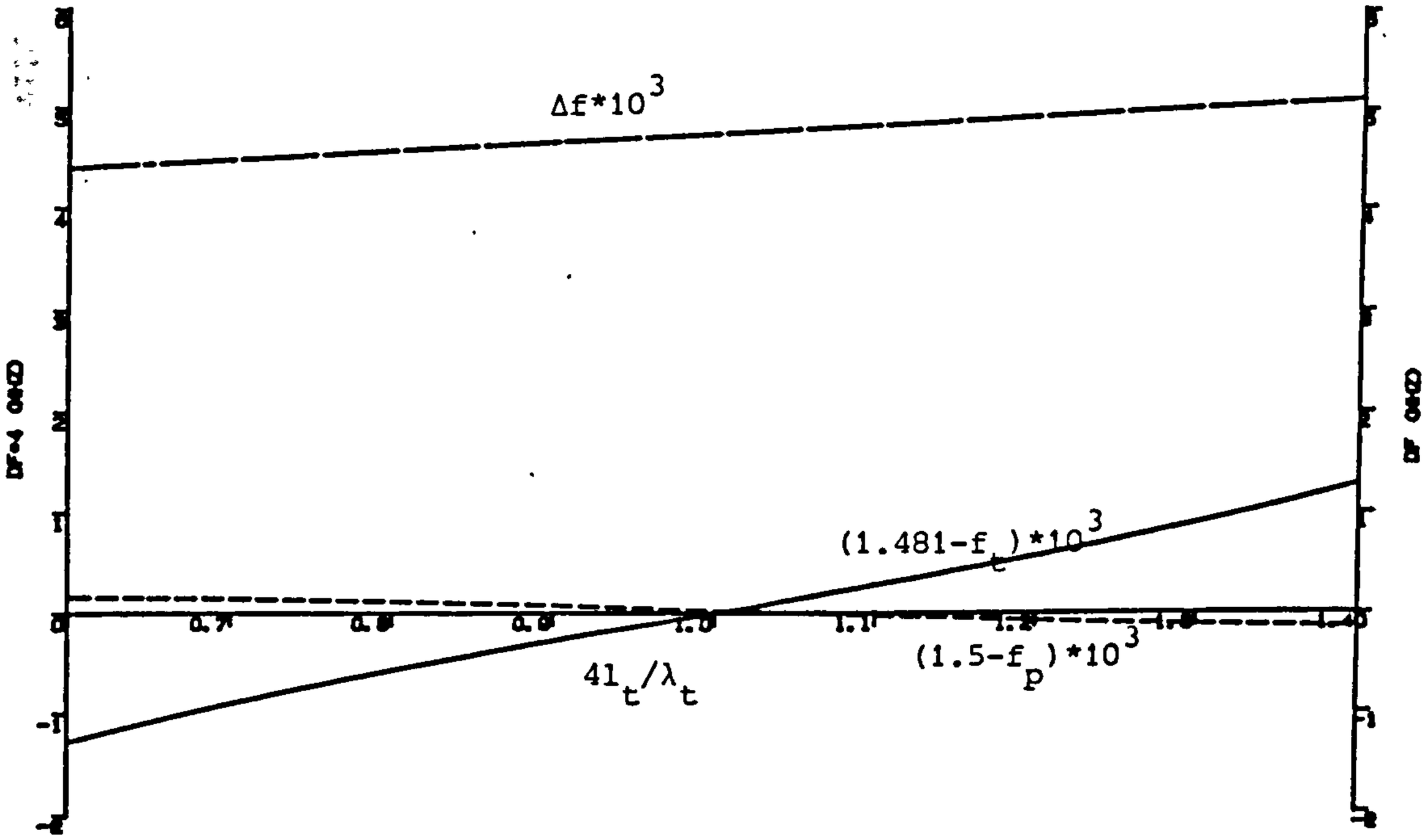

(c) Frequency shifts vs. coupling line length

Figure 9

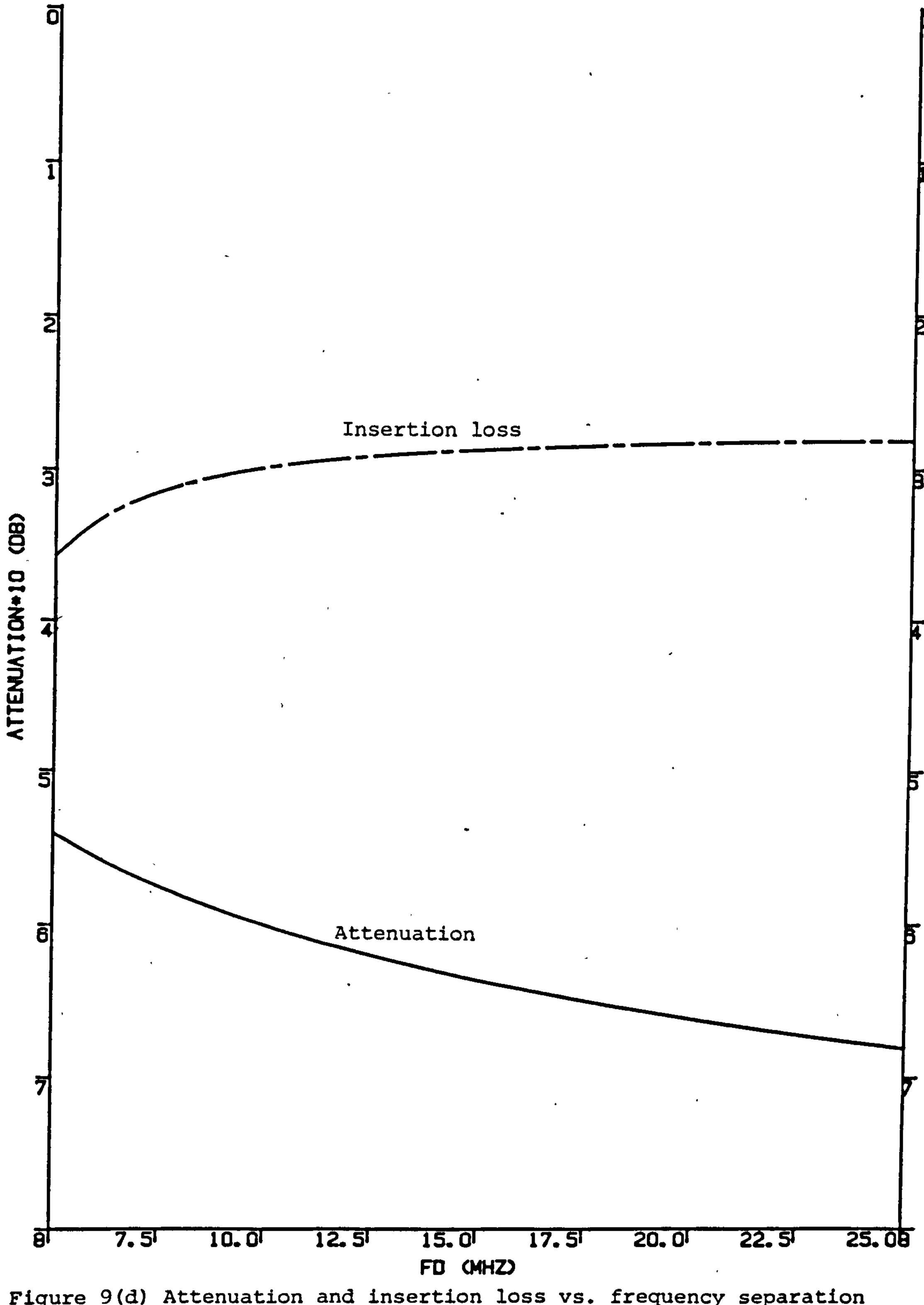

Figure 9(d) Attenuation and insertion loss vs. frequency separation between receiver and transmitter

CHAPTER SEVEN

C O N C L U S I O N S

The case of loop-coupled cavity has been treated in Chapter Two. Loops were found to exert varying influences on the resonant parameters. It was found possible to optimise the performance of a loop coupled cavity, not without losses, and predict the resonant parameters with high accuracy. The chapter has further demonstrated that Q_L and insertion loss can be traded, one for the other, by mere alteration of loop positions or sizes. Observations showed that it is virtually impossible to keep Q_o invariant for variations of Q_L and insertion loss over wide or narrow range. This has been attributed to either varying perturbing influence of the loop wire or the changing positions of discontinuities. However, it is possible to keep the variation of Q_o as low as 2% over limited but useful range of Q_L and insertion loss trading.

In Chapter Three, Hahn's original formulation for fields in reentrant coaxial cavities was found most appropriate for the computation of the resonant frequency and Q of all types of reentrant coaxial cavities. However, a lot of numerical analysis has been involved. The accuracy demonstrated by the method was quite appealing. Moreover the method can be applied to virtually all cavities with cylindrical symmetry. Deviation in frequencies between theory and practice was found below 0.2% while relative values of Q_o were found close to within 3% of the theoretical results for a coaxial reentrant type. For multi-cylindrical cavities a complete study, even if we take into consideration only two inner cylinders, is an enormous task unless the linear

dependent equations are reduced to single implicit linear equation.

Generally, the resonant frequency obtained in practice usually differs from theoretical values and that it is always necessary to include a tuning screw for the family of cavities for which resonant properties do not include tunability. To this end, an elaborate and qualitative analysis of tuning with thin screws inserted in the electric field antinode was undertaken. The result has shown a good agreement between theory and practice not only for short screws or plungers but also, by modification of the tuning equation, for very long tuning plungers.

An analysis of temperature compensation has included another method for an effective and cheap temperature compensation technique. This technique seeks for linearity in tuning curves and therefore would be applicable to other tunable resonant cavities which demonstrate such linearity at least over a range of frequencies followed during temperature excursion. If the required resonant frequency varies, optimum compensation can still be accomplished by changing the length L_e of the compensating material (see Chapter Four). By calibration, this can be done with little or no difficulty. In most cases, it is possible to reduce the temperature dependency of the resonant frequency to less than 10 parts in a million on the average.

Later analysis and investigations of Chapter Five showed how a cavity resonant parameter can be assessed in terms of losses, in particular losses in Q_o. The assessment was based on earlier observations from analysis and experiments. It further showed the dependency of Q_o on perturbing surfaces such as holes and gaps in the cavity walls and any perturbing materials such as loops. Tangential magnetic fields were observed to be most sensitive to slots while the electric fields

were observed to be most sensitive to aperture-like holes. The results obtained have been found to be generally representative of losses in resonant cavities. A loss budget has been constructed based on individual hole or crack effects. The loss budget will help a designer to 'accurately' estimate the likely Q_o obtainable from a coupled cavity. Furthermore, potentially troublesome discontinuities or perturbing materials can be located quickly and an appropriate remedial action can be taken.

The use of all cavity bandpass filters in a two-port filter network unit is not particularly encouraged because by slightly off-tuning any of the member-cavities, the fluctuation of the insertion loss in the passband may become too much to be tolerated in most communication applications. However, all cavity-bandpass filter inter-coupling is not very sensitive to variations in the coupling line lengths. In the aggregate, individual unit characteristics usually improve on connection to a common junction of many network units.

Finally, the theoretical and the experimental results obtained for the characteristics of UHF cavities have shown a very satisfactory agreement. Hence there are sufficient grounds for the belief that the same holds for VHF cavities. In general, the good agreement between expected and actual results has indicated that filters can be designed entirely on paper with performances close to those predicted.

ADDITIONAL REFERENCES

Adlam, J H et al: 'A method of measuring the Q-factors of an electromagnetic mode in a resonator ....', AERE G/R 767, August 1951.

Argence, E & Kahan, T: Theory of waveguide and cavity resonators , Blackie & Sons Ltd, 1967.

Bethe, H A: 'Theory of diffraction by small holes', The Phys. Rev., Vol. 66, No.s 7&8, pp. 163-182, 1944.

Chisholm, R M: 'Boundary conditions and ohmic losses in conducting wedges', IRE Trans. MTT, Vol. 8, pp. 189-198, Mar. 1960.

Craven, G F & Mok, C K: 'The design of evanescent mode waveguide bandpass filters for a prescribed insertion loss characteristic', IEEE Trans. MTT, Vol. 19, No. 3, p.295, Mar. 1971.

Davies, J B: 'Review of methods for numerical solution of the hollow waveguide problem', Proc. IEE, Vol. 119, No. 1, Jan. 1972.

Green, P E, 'General purpise programs for the frequency domain analysis of microwave circuits', IEEE Trans. MTT, Vol. 17, p.506, 1969.

Grunan, W C & Mason, C R: 'A simplified solution for tapered transformer lines', Microwaves, p.82, Oct. 1981.

Hoyt, H C: 'Designing resonant cavities with LALA computer program', Los Alamos Sc. Lba., N.Mex., LA-DC-8255.

Jackson, J D: Classical Electrodynamics , John Wiley & Sons Inc., 1962.

Johnson, W A: 'Exterior-interior aperture coupling of a rectangular cavity.....', Arizona Univ., Tucson Eng. Exper. Station, AD-A084 258, Mar. 1980.

Kanthar, Z: 'Cascade synthesis of .... two-port cavities', AD-749 199, p.24-25, 1972.

King, R W P: Fundamental Electromagnetic Theory , Dover. Publ. Inc., New York, 1963.

Konrad, A & Silvester, P: 'A finite element program package for axisymmetric scalar field problems', Computer Physics Comm., Vol. 5, pp. 437-455, 1973.

Kurokawa, K: An introduction to the theory of microwave circuits , Academic Press, New York, 1969.

---- 'The expansions of electromagnetic fields in cavities', IRE Trans., MTT, Vol. 6, pp. 178-187, April 1955.

Lebowitz, R A: 'Determination of the parameters of cavities terminating transmission lines', IRE Trans. MTT, Vol. 4, pp. 51-53, 1956.

Lewin, L: Theory of waveguides , Newnes & Butterworth, 1975.

Lin, W: 'Microwave filters employing a single cavity....', J. Appl. Phys., Vol. 22, No. 8, Aug. 1951.

Lytle, R J & Lager, D L: 'Solutions of the scalar Helmholtz equation in the elliptic-cylinder co-ordinate system', California Univ., Livermore, Lawrence Livermore Labs., URCL-S7420, 1973.

Mayes, P E: 'The equivalence of electric and magnetic sources', IRE Trans. Antenna & Prop., Vol. 6, pp. 295-296, 1958.

Mittra, R & Lee, S W: 'Analytical techniques in the theory of guided waves', The Macmillan Company, NY, 1971.

Moon, P & Spencer, D E: Foundations of Electrodynamics , D Van Nostrand Company Inc., 1960.

Moore, W S: 'The Design, analysis, and performance of resonant and non-resonant microwave ....', The Rev. Sci. Inst., Vol. 44, No. 2, pp. 158-164, Feb. 1973.

Pipes, L A: 'Matrix theory of skin effect in laminations', J. Franklin Inst., p.127-138, Aug. 1956.

Ramo, S; Whinnery, J R & Van Düzer, T: 'Fields and waves in communication electronics , John Wiley, NY, 1965.

Reiter, Gy: 'The properties of the equivalent network for the coupling hole of cavity resonators', Proc. 3rd Colloq. on Mic. Comm., Budapest, April 1966, pp. 503-511.

Risley, E W Jr: 'Discontinuity capacitance of a coaxial line .....: pt. II-lower bound solution', IEEE Trans. MTT, Vol. 22, p.564-566, 1973.

Seely, S L & Poularikas, A D: 'Electromagnetics: classical and modern theory and applications , Marcel Dekker Inc., NY, 1979.

Stratton, J A: Electromagnetic Theory , McGraw Hill Book Co., 1941.

Van Bladel, J: Electromagnetic Fields , McGraw Hill Book Co., 1964.

Whiteside, H: 'Electromagnetic field probes', Cruff Lab. Hav. Univ., Cambridge, Mass., Tech. Rpt. No. 377, 1962.

Wheeler, H A: 'Formulas for the skin effect', Proc. IRE, Vol. 30, p.412, Sept. 1942.

APPENDIX I

Consider the product

$$P(x) = C_n(hx)\overline{C}_n(kx)$$

where, for $h^2, k^2 > 0$

$$C_n(hx) = AJ_n(hx) + BN_n(hx)$$
$$\overline{C}_n(hx) = \overline{A}J_n(kx) + \overline{B}N_n(kx)$$

and for $h^2, k^2 < 0$

$$C_n(hx) = AI_n(hx) - BK_n(hx)$$
$$\overline{C}_n(kx) = \overline{A}I_n(kx) - \overline{B}K_n(kx)$$

A, B, $\overline{A}$, $\overline{B}$ are arbitrary constants.

The following indefinite integrals, omitting constants of integration, can be deduced:

For $h^2, k^2 > 0$

$$\int_x xP(x)_{h\neq k}dx = \int_x xC_n(hx)\overline{C}_n(kx) = (h^2-k^2)^{-1}x[hC_{n-1}(hx)\overline{C}_n(kx) - kC_n(hx)\overline{C}_{n+1}(kx)]$$

$$\int_x xP(x)_{h=k}dx = \int_x xC_n(hx)C_n(hx) = -\frac{1}{4}x^2[C_{n-1}(hx)\overline{C}_{n+1}(hx) - 2C_n(hx)\overline{C}_n(hx) + C_{n+1}(hx)\overline{C}_{n-1}(hx)]$$

$$\int_x xP(x)_{h=k}dx = \int x^{-1}C_m(hx)C_n(hx)dx = (m^2-n^2)^{-1}[(m-n)C_m(hx)\overline{C}_n(hx) - (hx)C_{m+1}(hx)\overline{C}_n(hx) + (hx)C_{m+1}(hx)\overline{C}_n(hx) + hxC_m(hx)\overline{C}_{n+1}(hx)]$$

For $k^2<0$, $h^2>0$

$$\int xP(x)_{h\neq k} = \int xC_n(hx)\bar{C}(kx)dx = (h^2+k^2)x[-hC_{n-1}(hx)\bar{C}_n(kx) + KC_n(hx)C_{n-1}(kx)]$$

For $k^2, h^2<0$

$$\int xP(x)_{h\neq k}dx = \int xC_n(hx)\bar{C}_n(kx)dx = (k^2-h^2)^{-1}x[KC_{n-1}(kx)C_n(hx) - hC_{n-1}(hx)\bar{C}_n(kx)]$$

$$\int_x P(x)_{h=k}dx = \int x[C_n(hx)]^2 = \frac{x}{2}\{[C_n(hx)]^2 - C_{n-1}(hx)C_{n+1}(hx)]\}$$

Functions in n+1 and m+1 can be reduced to lower functions on application of Recurrence Formulae[1,2].

References

1. Dwight, H B: 'Tables of integrals and other mathematical data', 4th Ed., 1961, McMillan Co., NY.

2. Spiegel, M R: 'Mathematical handbook of formulas and tables', Schaum's Outline Series, McGraw Hill Bk. Co., 1968.

```
      PROGRAM CCOAX
C     THIS PROGRAM COMPUTES THE RESONANT FREQUENCY AND
C     Q OF A REENTRANT COAXIAL CAVITY
      COMMON/DATA/L,S,R1,R2,N,PI,CORD,RLP
C     WHERE L, R2, R1 AND S REPRESENT THE CAVITY OUTER
C     CONDUCTOR LENGTH AND RADIUS, THE INNER CONDUCTOR
C     RADIUS AND THE SEPARATION BETWEEN THE INNER AND OUTER
C     CONDUCTORS END PLATES RESPECTIVELY
C     N IS THE NUMBER OF TERMS TAKEN IN THE SERIES
      INTEGER IBOUND,IFAIL1,LIW,LW,J
      REAL L,AM(6),AN(0:6),CN(0:6)
      REAL BL(1),BU(1),W(13),X(1)
      INTEGER IW(3)
      OPEN(81)
      N=6
      CV=2.998E8
      CORD=5.0E-2
      RLP=0.5E-2
      L=3.0*2.54E-2
      R1=1.75*2.54E-2/2.0
      R2=5.25*2.54E-2/2.0
      DO 92 JJ=9,14
      PD=0.9+JJ*0.15
      IF(JJ.EQ.7)PD=1.866451
      S=L-PD*1E-2
      D=S/L
      A=PD*1E-2/L
      J=1
      X(1)=1.0
      IBOUND=0
      BL(1)=0.8
      BU(1)=2.0
      LIW=3
      LW=13
      IFAIL1=1
      CALL E04JAF(J,IBOUND,BL,BU,X,F,IW,LIW,W,LW,IFAIL1)
      CALL COEFF(AM,X,AN,CN)
      CALL ENRGY(Q,AN,CN,X)
      WRITE(81,*)Q,X
92    CONTINUE
      END
      SUBROUTINE FUNCT1(J,XC,FC)
      COMMON/DATA/L,S,R1,R2,IM,PI,CORD,RLP
      DIMENSION X(6),QH(6),BSS(4,2)
      REAL KO,KN,K,L
      PI=3.14159
      CV=2.998E8
      KO=2*PI*XC/CV*1E9
      CALL ANALY(KO,X,QH)
      K=KO**2
      AL=S/L
      CALL BSF(2,K,BSS,0)
```

```
      RO=BSS(2,1)/BSS(1,1)
      FO=BSS(2,1)-BSS(1,2)*BSS(4,1)/BSS(3,2)
      GO=BSS(1,1)-BSS(1,2)*BSS(3,1)/BSS(3,2)
      QO=FO/GO
      DU1=0.0
      DU2=0.0
      DO 23 JM=1,IM
      DU1=DU1+QH(JM)/JM**2
      PZ=0.0
      Z=(JM*AL)**2
      DO 22 IJ=1,IM
      PZ=PZ+(-1)**IJ*X(IJ)/(Z-IJ**2)
   22 CONTINUE
      DU2=DU2+QH(JM)*PZ
   23 CONTINUE
      PIA=PI**2*AL/2.0
      PC=DU1+AL**2*DU2+PIA*AL*QO-PIA*RO
      FC=ABS(PC)
      RETURN
      END
      SUBROUTINE ANALY(KO,X,QH)
C     COMPUTATION OF A SET OF COEFFICIENTS OF THE EXPANSION
      COMMON/DATA/L,S,R1,R2,IM,PI,CORD,RLP
      DIMENSION X(6),QH(6)
      COMMON A(6,6),B(6,6),BSS(4,2),
     1CON(6),W1(6),W2(6)
      REAL KO,KN,K,L
      INTEGER IFAIL,IM
           AL=S/L
      DO 50 KI=1,IM
      DO 51 KJ=1,IM
      A(KI,KJ)=0.0
   51 CONTINUE
      CON(KI)=0.0
   50 CONTINUE
      DO 90 IT=1,IM
      TI=IT**2
      DO 89 IN=1,IM
      K=KO**2-(IN*PI/L)**2
      KN=SQRT(ABS(K))
      CALL BSF(2,K,BSS,0)
      IF(K.LT.0.0)BSS(4,1)=-BSS(4,1)
      F=BSS(2,1)-BSS(4,1)*BSS(1,2)/BSS(3,2)
      G=BSS(1,1)-BSS(1,2)*BSS(3,1)/BSS(3,2)
      Q=KO*F/(G*KN)
      H=IN*PI*AL
      Z=(IN*AL)**2
      H1=(SIN(H))**2
      QH(IN)=Q*H1
      QZ=Q*AL*Z*H1
      QA=-Q*AL*H1
      DO 88 IQ=1,IM
      QI=IQ**2
      A(IT,IQ)=A(IT,IQ)+(-1)**IQ*QZ/((Z-TI)*(Z-QI))
   88 CONTINUE
```

```
      CON(IT)=CON(IT)+QA/(Z-TI)
   89 CONTINUE
      K=KO**2-(IT*PI/S)**2
      KN=SQRT(ABS(K))
      CALL BSF(1,K,BSS,0)
      R=BSS(2,1)*KO/(BSS(1,1)*KN)
      A(IT,IT)=A(IT,IT)-(-1)**IT*PI**2*R/4.0
   90 CONTINUE
      IFAIL=0
      CALL F04ATF(A,IM,CON,IM,X,B,IM,W1,W2,IFAIL)
      RETURN
      END
      SUBROUTINE BSF(IOUT,K,BSS,IT)
C     SUBROUTINE FOR THE EVALUATION OF BESSEL'S FUNCTIONS
      COMMON/DATA/L,S,R1,R2,N,PI,CORD,RLP
      REAL K,BSS(4,2),V(2),L
      AK=SQRT(ABS(K))
      IFAIL=0
      V(1)=AK*R1
      V(2)=AK*R2
      IF(IT.EQ.1)V(1)=AK*CORD
      IF(K.GE.0.0)THEN
      DO 40 I=1,IOUT
      BSS(1,I)=S17AEF(V(I),IFAIL)
      BSS(2,I)=S17AFF(V(I),IFAIL)
      IF(IOUT.EQ.1)RETURN
      BSS(3,I)=S17ACF(V(I),IFAIL)
      BSS(4,I)=S17ADF(V(I),IFAIL)
   40 CONTINUE
      ELSE
      DO 50 I=1,IOUT
      BSS(1,I)=S18AEF(V(I),IFAIL)
      BSS(2,I)=S18AFF(V(I),IFAIL)
      IF(IOUT.EQ.1)RETURN
      BSS(3,I)=S18ACF(V(I),IFAIL)
      BSS(4,I)=S18ADF(V(I),IFAIL)
   50 CONTINUE
      END IF
      RETURN
      END
      SUBROUTINE COEFF(AM,X,AN,CN)
C     COMPUTATION OF THE REMAINING SETS OF COEFFICIENTS
C     OF THE EXPANSION
      COMMON/DATA/L,S,R1,R2,IM,PI,CORD,RLP
      DIMENSION AM(6),AN(0:6),CN(0:6),QH(6)
      REAL L,K,KO,BSS(4,2)
      KO=2*PI*X*1E9/2.998E8
      CALL ANALY(KO,AM,QH)
      K=KO**2
      CALL BSF(2,K,BSS,0)
      AN(0)=1/BSS(1,1)
      AL=S/L
      FO=BSS(1,1)-BSS(1,2)*BSS(3,1)/BSS(3,2)
      CN(0)=AL/FO
      DO 20 I=1,IM
```

```
      K=K0**2-(I*PI/L)**2
      CALL BSF(2,K,BSS,0)
      FT=BSS(1,1)-BSS(1,2)*BSS(3,1)/BSS(3,2)
      SINT=SIN(I*PI*AL)
      TA=(I*AL)**2
      K=K0**2-(I*PI/S)**2
      CALL BSF(1,K,BSS,0)
      AN(I)=AM(I)/BSS(1,1)
      SAT=0.0
      DO 21 J=1,IM
      AJ=J**2
      SAT=SAT+AM(J)*SINT*(-1)**J/(TA-AJ)
   21 CONTINUE
      CN(I)=2*(SINT/I+AL**2*I*SAT)/(PI*FT)
   20 CONTINUE
      RETURN
      END
      SUBROUTINE SECH(K0,Z,BSA)
C     SUBROUTINE FOR EVALUATION OF THE INTEGRALS OF
C     EQUATIONS INVOLVING BESSEL'S FUNCTIONS
      COMMON/DATA/L,S,R1,R2,N,PI,CORD,RLP
      DIMENSION Z(0:6,3,2),BSS(4,2),BSA(0:6,3)
      REAL K0,L
      DO 10 IN=0,N
      WK1=K0**2-(PI*IN/S)**2
      WK2=K0**2-(PI*IN/L)**2
      ZK1=SQRT(ABS(WK1))
      ZK2=SQRT(ABS(WK2))
      CALL BSF(1,WK1,BSS,0)
      BSA(IN,1)=BSS(1,1)
      BSA(IN,2)=BSS(2,1)
      BSA(IN,3)=2*BSS(2,1)/(ZK1*R1)-BSS(1,1)
      IF(WK1.LT.0.0)BSA(IN,3)=-BSA(IN,3)
      V1=ZK2*R1
      V2=ZK2*R2
      CALL BSF(2,WK2,BSS,0)
      FAC=BSS(1,2)/BSS(3,2)
      IF(WK2.GE.0.0)THEN
      Z(IN,1,1)=BSS(1,1)-FAC*BSS(3,1)
      Z(IN,1,2)=0.0
      Z(IN,2,1)=BSS(2,1)-FAC*BSS(4,1)
      Z(IN,2,2)=BSS(2,2)-FAC*BSS(4,2)
      Z(IN,3,1)=2*Z(IN,2,1)/V1-Z(IN,1,1)
      Z(IN,3,2)=2*Z(IN,2,2)/V2-Z(IN,1,2)
      ELSE
      FAC=-FAC
      BI1=BSS(1,1)-2*BSS(2,1)/V1
      BI2=BSS(1,2)-2*BSS(2,2)/V2
      BK1=BSS(3,1)-2*BSS(4,1)/V1
      BK2=BSS(3,2)-2*BSS(4,2)/V2
      Z(IN,1,1)=BSS(1,1)+FAC*BSS(3,1)
      Z(IN,1,2)=BSS(1,2)+FAC*BSS(3,2)
      Z(IN,2,1)=BSS(2,1)-FAC*BSS(4,1)
      Z(IN,2,2)=BSS(2,2)-FAC*BSS(4,2)
      Z(IN,3,1)=BI1+FAC*BK1
```

```
      Z(IN,3,2)=BI2+FAC*BK2
      END IF
   10 CONTINUE
      RETURN
      END
      SUBROUTINE ENRGY(QO,AN,BN,X)
C     SUBROUTINE FOR EVALUATION OF THE CAVITY UNLOADED Q.
      COMMON/DATA/L,S,R1,R2,N,PI,CORD,RLP
      DIMENSION Z(0:6,3,2),BSA(0:6,3),AN(0:6),BN(0:6),
     1BSS(4,2)
      REAL K,KI,KJ,KO,L,MU
      KO=2*PI*X*1E9/2.998E8
      MU=4E-7*PI
      SIGMA=5.8E7
      SGMA1=1.57E7
      CALL SECH(KO,Z,BSA)
      W=2E9*PI*X
      ZLO=W*MU*RLP*(ALOG(8*RLP/5E-4)-1.75)
      RS=SQRT(PI*X*1E9*MU/SIGMA)
      RS1=SQRT(PI*X*1E9*MU/SGMA1)
      FACT21=0.0
      FACT32=0.0
      FACT1=(BN(0)*Z(0,2,2)/KO)**2
      FACT3=(BN(0)*Z(0,2,1)/KO)**2
      FACT31=0.0
      FACT4=0.0
      P3=0.0
      P2=0.0
      P6=0.0
      P4=0.0
      P5=0.0
      PACT4=(AN(0)/KO)**2*(BSA(0,2)**2-BSA(0,1)*BSA(0,3))
      K=KO**2
      CALL BSF(2,K,BSS,1)
      Z1=(BN(0)/KO)*(BSS(2,1)-BSS(1,2)*BSS(4,1)/BSS(3,2))
      VOLT=Z1*PI*RLP**2/2
      FACT22=0.0
      DO 41 I=0,N
      AK=KO**2-(PI*I/S)**2
      AKI=SQRT(ABS(AK))
      K=KO**2-(PI*I/L)**2
      KI=SQRT(ABS(K))
      ZKI=I*PI/L
      SNC2=SIN(2*ZKI*S)/ZKI
      SNC1=SIN(ZKI*S)/ZKI
      IF(I.EQ.0)GOTO 39
      IFAIL=0
      V1=ZKI*RLP
      BS=S17AFF(V1,IFAIL)
      CALL BSF(2,K,BSS,1)
      IF(K.LT.0.0)BSS(4,1)=-BSS(4,1)
      Z1=(BN(I)/KI)*(BSS(2,1)-BSS(1,2)*BSS(4,1)/BSS(3,2))
      VOLT=VOLT+(-1)**I*PI*Z1*RLP*BS/ZKI
      FACT1=FACT1+(BN(I)/KI*Z(I,2,2))**2/2.0
      FACT21=FACT21+(Z(I,2,1)**2-Z(I,1,1)*Z(I,3,1))*(BN(I)/KI)**2
```

```
      FACT22=FACT22+(Z(I,2,2)**2-Z(I,1,2)*Z(I,3,2))*(BN(I)/KI)**2
      FACT3=FACT3+((BN(I)/KI)*Z(I,2,1))**2/2.0
      FACT31=FACT31+((BN(I)/KI)*Z(I,2,1))**2*SNC2
      FACT32=FACT32+(BN(I)/KI)*Z(I,2,1)*SNC1
      FACT4=FACT4+(BSA(I,2)**2-BSA(I,1)*BSA(I,3))*(AN(I)/AKI)**2
   39 DO 40 J=0,N
      AK1=K0**2-(PI*J/S)**2
      AKJ=SQRT(ABS(AK1))
      ZKJ=PI*J/L
      BK=K0**2-ZKJ**2
      KJ=SQRT(ABS(BK))
      SNA=SIN((ZKJ+ZKI)*S)/(ZKJ+ZKI)
       IF(J.EQ.I)GOTO 40
       PRA=K-BK
       PRB=AK-AK1
       PM=(KJ*R2*Z(I,2,2)*Z(J,1,2)-KI*R2*Z(I,1,2)*Z(J,2,2))*
     1(BN(I)/KI)*(BN(J)/KJ)
       PT=(KJ*R1*Z(I,2,1)*Z(J,1,1)-KI*R1*Z(I,1,1)*Z(J,2,1))*
     1(BN(I)/KI)*(BN(J)/KJ)
       PZ=AKJ*R1*BSA(I,2)*BSA(J,1)-AKI*R1*BSA(J,2)*BSA(I,1)
       SNB=SIN((ZKJ-ZKI)*S)/(ZKJ-ZKI)
       IJ=I+J
       P2=P2+(-1)**IJ*(PM-PT)/PRA
       P6=P6+(PM-PT)/PRA
       P4=P4+(AN(I)/AKI)*(AN(J)/AKJ)*PZ/PRB*(-1)**(I+J)
      P5=P5+(AN(I)/AKI)*(AN(J)/AKJ)*PZ/PRB
      IF(I.EQ.0)GOTO 40
      IF(J.EQ.0)GOTO 40
      P3=P3-Z(J,2,1)*Z(I,2,1)*(SNB+SNA)*(BN(I)/KI)*(BN(J)/KJ)
   40 CONTINUE
   41 CONTINUE
      Z1=(BN(0)/K0)**2*(Z(0,2,1)**2-Z(0,1,1)*Z(0,3,1))
      Z2=(Z(0,2,2)**2-Z(0,1,2)*Z(0,3,2))*(BN(0)/K0)**2
      FACT=FACT21+Z1
      P1=PI*RS*R2*L*FACT1
      FAC=FACT22+Z2
      P2=PI*RS*(P2+FAC*R2**2/2-FACT*R1**2/2)
      P3=PI*RS*R1*((L-S)*FACT3-FACT31/4-FACT32*2*(BN(0)/K0)*
     1Z(0,2,1)+P3/2)
      PACT=PACT4+FACT4
      P4=PI*RS1*(PACT*R1**2/2+P4)
      P5=PI*RS1*(PACT*R1**2/2+P5)
      P6=PI*RS1*(P6+FAC*R2**2/2-FACT*R1**2/2)
      WA=0.5*PI*W*MU*L*(R2**2*(FACT22/2+Z2)-R1**2*(Z1+FACT21/2))
      WB=PI*W*MU*S*R1**2*(PACT4/2+FACT4/4)
      P=ABS(P1)+ABS(P2)+ABS(P3)+ABS(P4)+ABS(P5)+ABS(P6)
      WT=ABS(WA)+ABS(WB)
      Q0=WT/P
      RETURN
      END
```

```
      PROGRAM THRCYLS
C     COMPUTES THE RESONANT FREQUENCY OF MULTICYLINDRICAL
C     RESONANT CAVITY
      COMMON L,B,A,D,S,R1,R2,R3,R4,N
C      L : LENGTH OF OUTER CONDUCTOR
C      R4 : RADIUS OF OUTER CONDUCTOR
C      R3 : OUTER RADIUS OF THE MIDDLE CONDUCTOR
C      R2 : INNER RADIUS OF THE MIDDLE CONDUCTOR
C      L-D : LENGTH OF THE MIDDLE CONDUCTOR
C      R1 : THE INNER CONDUCTOR RADIUS
C      S : SEPARATION BETWEEN THE END PLATES OF THE
C       INNER AND OUTER CONDUCTORS
C      N : NUMBER OF TERMS TAKEN IN THE EXPANSION
      INTEGER IBOUND,IFAIL,LIW,LW,JJ
      REAL L,BL(1),BU(1),W(13),X(1)
      INTEGER N,IW(3)
      OPEN(3,FILE='KOT1')
      N=6
      L=13.7E-2
      D=8.76E-2
      R1=1.06934E-2
      R2=1.9357E-2
      R3=2.025E-2
      R4=3.81E-2
      B=(L-D)/L
      JJ=1
      DO 21 I=1,6
      S=1E-2*I
      A=S/L
      X(1)=0.32
      IBOUND=0
      BL(1)=0.1
      BU(1)=1.5
      LIW=3
      LW=13
      IFAIL=1
      CALL E04JAF(JJ,IBOUND,BL,BU,X,F,IW,LIW,W,LW,IFAIL)
      WRITE(3,*)S*1E2,'    ',X(1)

   21 CONTINUE
      END
      SUBROUTINE SECT(K,R,I,N,BSS)
C     EVALUATES BESSEL'S FUNCTIONS
      REAL BSS(4,4),K,R(4)
      AK=SQRT(ABS(K))
      IFAIL=0
      DO 40 J=N,I
      V=AK*R(J)
      IF(K.GE.0.0)THEN
      IF(I.EQ.1)THEN
      BSS(1,J)=S17AEF(V,IFAIL)
      BSS(2,J)=S17AFF(V,IFAIL)
```

```
      GOTO 40
      END IF
      BSS(1,J)=S17AEF(V,IFAIL)
      BSS(2,J)=S17AFF(V,IFAIL)
      BSS(3,J)=S17ACF(V,IFAIL)
      IF(J.EQ.4)GOTO 40
      BSS(4,J)=S17ADF(V,IFAIL)
      ELSE
      IF(I.EQ.1)THEN
      BSS(1,J)=S18AEF(V,IFAIL)
      BSS(2,J)=S18AFF(V,IFAIL)
      GOTO 40
      END IF
      BSS(1,J)=S18AEF(V,IFAIL)
      BSS(2,J)=S18AFF(V,IFAIL)
      BSS(3,J)=S18ACF(V,IFAIL)
      IF(J.EQ.4)GOTO 40
      BSS(4,J)=-S18ADF(V,IFAIL)
      END IF
   40 CONTINUE
      RETURN
      END
      SUBROUTINE FUNCT1(JJ,XC,FC)
      COMMON L,B,A,D,S,R1,R2,R3,R4,N
      DIMENSION CON(6,5),BSS(4,4),DN(6),D1(6,5,6),WRK(1),
     1AN(6),BN(6),CN(6),EN(6),FN(6),B2(6,6),C2(6,6)
      DIMENSION B1(6,5,6),C(6,5,6),E(6,5,6),F(6,5,6),AA(6)
      DIMENSION W(30,30),Z(30,1),WINV(30,30),WORK(30),ACON(30,1)
      EQUIVALENCE (B1(1,1,1),W(1,1)),(C(1,1,1),W(1,7)),
     1(E(1,1,1),W(1,13)),(F(1,1,1),W(1,19)),(D1(1,1,1),W(1,25)),
     1(BN(1),Z(1,1)),(CN(1),Z(7,1)),(EN(1),Z(13,1)),(FN(1),Z(19,1)),
     1(DN(1),Z(25,1)),(CON(1,1),ACON(1,1))
      INTEGER IFAIL,N,I
      REAL KO,KI,K,KT,L,R(4)
      PI=3.14159
      VCL=2.998E8
      KO=2*PI*XC*1E9/VCL
      R(1)=R1
      R(2)=R2
      R(3)=R3
      R(4)=R4
      K=KO**2
      CALL SECT(K,R,4,1,BSS)
      FA=BSS(3,3)*BSS(2,3)-BSS(4,3)*BSS(1,3)
      TO=BSS(1,3)-BSS(1,4)*BSS(3,3)/BSS(3,4)
      T10=BSS(2,3)-BSS(1,4)*BSS(4,3)/BSS(3,4)
      T01=BSS(3,2)*BSS(2,2)-BSS(4,2)*BSS(1,2)
      ZO=(T10*BSS(3,3)-TO*BSS(4,3)/B)/FA
      YO=(TO*BSS(2,3)/B-T10*BSS(1,3))/FA
      S1=BSS(3,3)/(FA*PI*B)
      S2=-BSS(1,3)/(FA*PI*B)
      AT1=BSS(3,2)*(ZO*BSS(2,2)+YO*BSS(4,2))
      Z10=(AT1-BSS(4,2)*(ZO*BSS(1,2)+YO*BSS(3,2))*B)/T01
      AT2=BSS(2,2)*(ZO*BSS(1,2)+YO*BSS(3,2))*B
      Y10=(AT2-BSS(1,2)*(ZO*BSS(2,2)+YO*BSS(4,2)))/T01
```

```
      AT3=BSS(3,2)*(BSS(2,2)*S1+BSS(4,2)*S2)
      S11=(AT3-BSS(4,2)*B*(BSS(1,2)*S1+BSS(3,2)*S2))/T01
      S10=-BSS(3,2)/(PI*B*T01)
      AT4=BSS(2,2)*(BSS(1,2)*S1+BSS(3,2)*S2)*B
      S22=(AT4-BSS(1,2)*(BSS(2,2)*S1+BSS(4,2)*S2))/T01
      S20=BSS(1,2)/(PI*B*T01)
      Z30=BSS(1,1)*Z10+BSS(3,1)*Y10
      S30=BSS(1,1)*S11+BSS(3,1)*S22
      S31=BSS(1,1)*S10+BSS(3,1)*S20
      Z20=Z0*BSS(1,2)+BSS(3,2)*Y0
      S00=S1*BSS(1,2)+BSS(3,2)*S2
      DO 28 II=1,N
      DO 28 IM=1,5
      CON(II,IM)=0.0
      DO 28 IK=1,N
      B1(II,IM,IK)=0.0
      C(II,IM,IK)=0.0
      D1(II,IM,IK)=0.0
      E(II,IM,IK)=0.0
      F(II,IM,IK)=0.0
   28 CONTINUE
      DO 43 IN=1,N
      B1N=(IN*B)**2
      A1N=(IN*A)**2
      K=K0**2-(IN*PI/(L-D))**2
      KI=SQRT(ABS(K))
      CALL SECT(K,R,3,2,BSS)
      E(IN,1,IN)=(-1)**IN*BSS(2,2)/KI
      F(IN,1,IN)=(-1)**IN*BSS(4,2)/KI
      E(IN,2,IN)=(-1)**IN*BSS(2,3)/KI
      F(IN,2,IN)=(-1)**IN*BSS(4,3)/KI
      K=K0**2-(IN*PI/S)**2
      KI=SQRT(ABS(K))
      CALL SECT(K,R,1,1,BSS)
      AA(IN)=BSS(2,1)/KI
      K=K0**2-(IN*PI/L)**2
      KI=SQRT(ABS(K))
      CALL SECT(K,R,4,1,BSS)
      B1(IN,4,IN)=BSS(1,2)
      C(IN,4,IN)=BSS(3,2)
      D1(IN,3,IN)=BSS(1,3)-BSS(1,4)*BSS(3,3)/BSS(3,4)
      B1(IN,5,IN)=(-1)**IN*BSS(1,1)
      C(IN,5,IN)=(-1)**IN*BSS(3,1)
      SIMA=SIN(IN*PI*A)
      SIMB=SIN(IN*PI*B)
      TA=2*SIMA/(IN*PI*A)
      CON(IN,5)=TA*Z30
      TB=2*SIMB/(IN*PI)
      CON(IN,4)=TB*Z20
      CON(IN,3)=T0*TB/B
      QJ=IN*B**2*SIMB/PI
      DO 42 IJ=1,N
      AT=(IJ*A)**2
      BT=(IJ*B)**2
      K=K0**2-(IJ*PI/S)**2
```

```
      AKN=SQRT(ABS(K))
      CALL SECT(K,R,1,1,BSS)
      AST=4*AKN*IN*A**2*SIMA*BSS(1,1)/(PI*BSS(2,1)*(AIN-IJ**2))
      K=KO**2-(IJ*PI/(L-D))**2
      KT=SQRT(ABS(K))
      CALL SECT(K,R,3,2,BSS)
      E34=-2*(-1)**IJ*QJ/(BIN-IJ**2)
      E(IN,3,IJ)=E34*BSS(1,3)
      F(IN,3,IJ)=E34*BSS(3,3)
      E(IN,4,IJ)=E34*BSS(1,2)
      F(IN,4,IJ)=E34*BSS(3,2)
      K=KO**2-(IJ*PI/L)**2
      KI=SQRT(ABS(K))
      CALL SECT(K,R,4,1,BSS)
      SINB=SIN(IJ*PI*B)
      SINA=SIN(IJ*PI*A)
      BC5=-2*IJ*A*(-1)**IJ*SINA/(PI*KI*(AT-IN**2))
      BC1=-2*IJ*B*SINB/(PI*KI*(BT-IN**2))
      B1(IN,1,IJ)=BC1*BSS(2,2)
      C(IN,1,IJ)=BC1*BSS(4,2)
      B2(IN,IJ)=BC5*BSS(2,1)
      C2(IN,IJ)=BC5*BSS(4,1)
      T1Q=BSS(2,3)-BSS(1,4)*BSS(4,3)/BSS(3,4)
      PT=KO*SINB/(IJ*KI)
      D1(IN,2,IJ)=-2*IJ*B*T1Q*SINB/(PI*KI*(AT-IN**2))
      D1(IN,4,IJ)=-TB*S00*T1Q*PT
      D1(IN,5,IJ)=-TA*S30*T1Q*PT
      B1(IN,5,IJ)=B1(IN,5,IJ)-TA*S31*PT*BSS(2,2)
      C(IN,5,IJ)=C(IN,5,IJ)-TA*S31*PT*BSS(4,2)
      DO 41 IK=1,N
      K=KO**2-(IK*PI/L)**2
      KT=SQRT(ABS(K))
      CALL SECT(K,R,1,1,BSS)
      ATA=(IK*A)**2
      PAT=(-1)**IK*IK*A*SIN(IK*PI*A)/(PI*KT*(ATA-IJ**2))
      B1(IN,5,IK)=B1(IN,5,IK)-AST*PAT*BSS(2,1)
      C(IN,5,IK)=C(IN,5,IK)-AST*PAT*BSS(4,1)
   41 CONTINUE
   42 CONTINUE
   43 CONTINUE
      NEQ=N*5
      IFAIL=0
      CALL F01AAF(W,NEQ,NEQ,WINV,NEQ,WORK,IFAIL)
      CALL F01CKF(Z,WINV,ACON,NEQ,1,NEQ,WRK,1,1,IFAIL)
      SR=0.0
      BO=Z10
      CO=Y10
      DO 45 I=1,N
      K=KO**2-(I*PI/L)**2
      KI=SQRT(ABS(K))
      CALL SECT(K,R,4,1,BSS)
      T1Q=BSS(2,3)-BSS(1,4)*BSS(4,3)/BSS(3,4)
      SINB=SIN(PI*I*B)
      ABT=KO*DN(I)*T1Q*SINB/(I*KI)
      ST=BN(I)*BSS(2,2)+CN(I)*BSS(4,2)
```

```
      TS=ST*K0*SINB/(I*KI)
      B0=B0+S11*ABT+S10*TS
      C0=C0+S22*ABT+S20*TS
      RS=(BN(I)*BSS(2,1)+CN(I)*BSS(4,1))*SIN(PI*I*A)
      SR=SR+RS*(-1)**I*K0/(I*KI)
      DO 44 IL=1,N
   44 BCM=BN(IL)*B2(I,IL)+CN(IL)*C2(I,IL)
      AN(I)=BCM/AA(I)
   45 CONTINUE
      K=K0**2
      CALL SECT(K,R,4,1,BSS)
      A0=(B0*BSS(1,1)+C0*BSS(3,1))/(A*BSS(1,1))
      AFC=A0*BSS(2,1)-B0*BSS(2,1)-C0*BSS(4,1)-SR/(PI*A)
      FC=ABS(AFC)
      RETURN
      END
```

APPENDIX IV

Characterisation Procedure for Coupling Line Length using a Circular Loop in Free Space

The analysis has been designed to determine the effect of a non-resonant reactive element on the coupling line length. For this, a circular loop in free space has been characterised on a length of line connected to a through-line as shown in Fig. 1. The impedance of the loop is given as

$$Z_l = R_r + j\omega L \tag{1}$$

where R_r is the radiation resistance of the loop and L is the loop's self-inductance. The admittance function is therefore given as

$$Y'_l = \frac{R}{R_r^2+\omega^2 L^2} - j\frac{\omega L}{R_r^2+\omega^2 L^2} \tag{2}$$

$$= G_l + jB_l$$

The admittance seen looking towards the loop from the T-junction, Fig. 2, is

$$Y_l = \frac{\sinh(\alpha+j\beta)_l + Y'_l\cosh(\alpha+j\beta)_l}{\cosh(\alpha+j\beta)l + Y'_d\sinh(\alpha+j\beta)_l} \tag{3}$$

where the characteristic impedance of the line has been normalised to unity. Expanding this, and equating the imaginary part to zero (at resonance) we have

$$B_l[1-(\alpha l)^2]\tan^2\theta + B_l[(\alpha l)^2-1] + \{G_l^2[1-(\alpha l)^2] + B_l^2[1-(\alpha l)^2]-1\}\tan\theta = 0 \tag{4}$$

where $\theta = \beta l$, β is the phase constant of the line and α the attenuation constant.

Equation (4) gives us a quadratic equation in tan θ. For short

stub and small α, $(\alpha l)^2 << 1$. Equation (4) reduces to

$$B_1 \tan^2\theta - B_1 + (G_1^2 + B_1^2 - 1)\tan\theta = 0 \qquad (5)$$

Hence

$$\theta_1 = \frac{n\pi}{2} + \tan^{-1}\frac{B_1 + \sqrt{[(1-B_1^2-G_1^2)+4B_1^2]}}{-2B_1} \qquad (6)$$

and

$$\theta_2 = \frac{m\pi}{2} + \tan^{-1}\frac{B_1 - \sqrt{[(1-B_1^2-G_1^2)+4B_1^2]}}{-2B_1}$$

It can be shown that at resonance,

$$\tan^{-1}\frac{B_1 + \sqrt{[1-B_1^2-G_1^2]+4B_1^2}}{-2B_1} - \tan^{-1}\frac{B_1 - \sqrt{[1-B_1^2-G_1^2]+4B_1^2}}{-2B_1}$$

$$= \frac{i\pi}{2} \qquad (8)$$

where i = 1,3,5,....

Equation (8) is an implicit function of frequency and the resonant frequency can be obtained by numerical methods. The length l of the stub is given as

$$l = \frac{\theta_1}{\beta} = \frac{\theta_2}{\beta} \qquad (9)$$

By numerically solving equation (8), the length l can be obtained from equation (9).

Table 1 compares theory and practice and shows that theory and practice are in close agreement; and that the actual length of line required is different from a quarter wavelength at the operating resonant frequency for this particular case. It should be noted, as obvious from equations (5),(6) and (9) that this statement would be true only when B_1 is not exactly zero at the resonant frequency at which l is exactly a quarter wavelength long otherwise the resonant frequency would change when

l is different from a quarter wavelength long.

Table 1

Loop radius d = 0.6cm
Loop wire diameter, 2r = 0.9144mm
Cable - RG58C/U 50Ω

Resonant Frequency (GHz)	Quarter Wavelength $\lambda_g/4$ (cm)	l	
		Theory	Practice
1.40	3.72	4.145	4.146
1.44	3.60	4.018	4.046
1.48	3.50	3.899	4.001
1.55	3.35	3.71	3.723

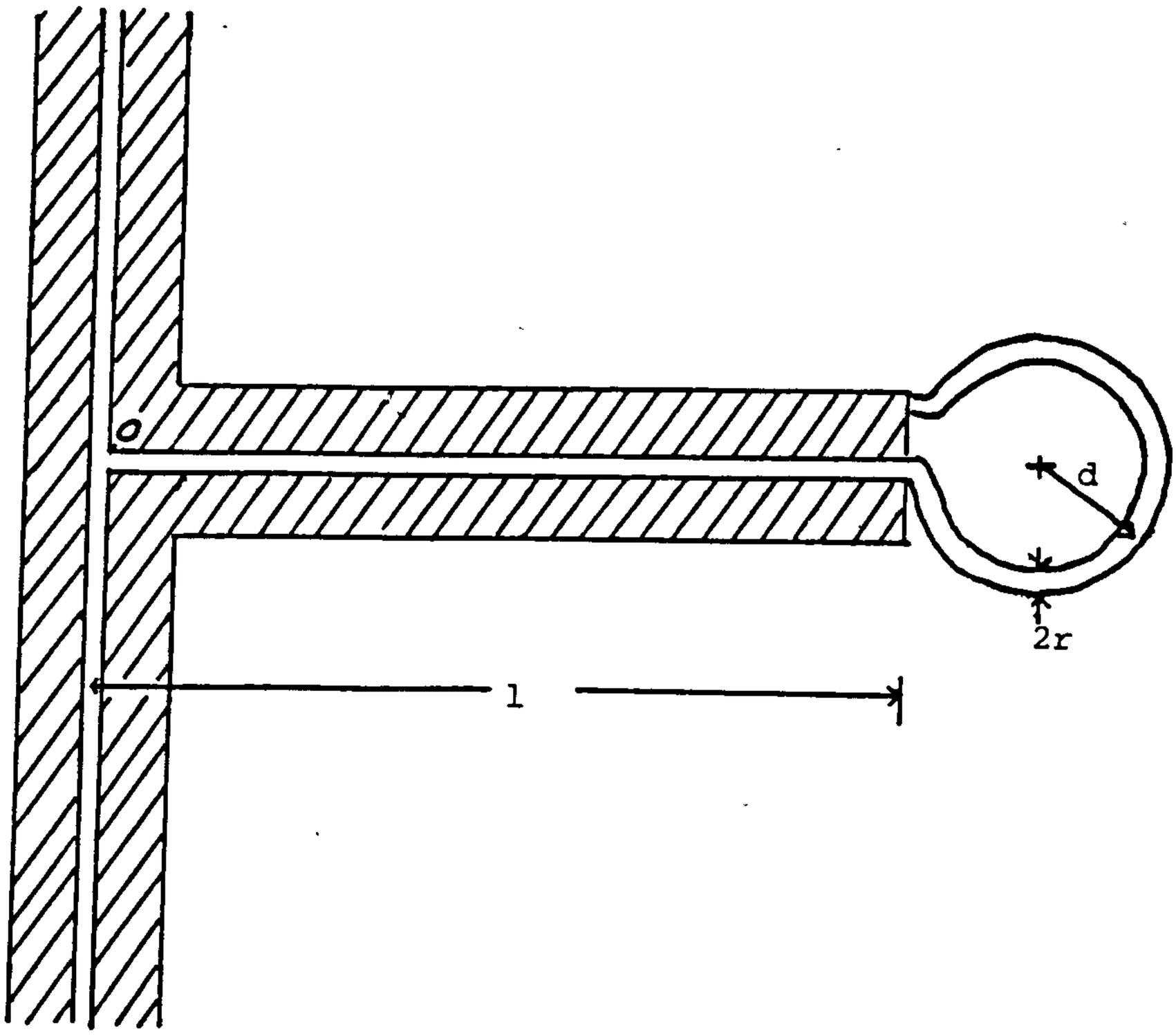

Figure 1

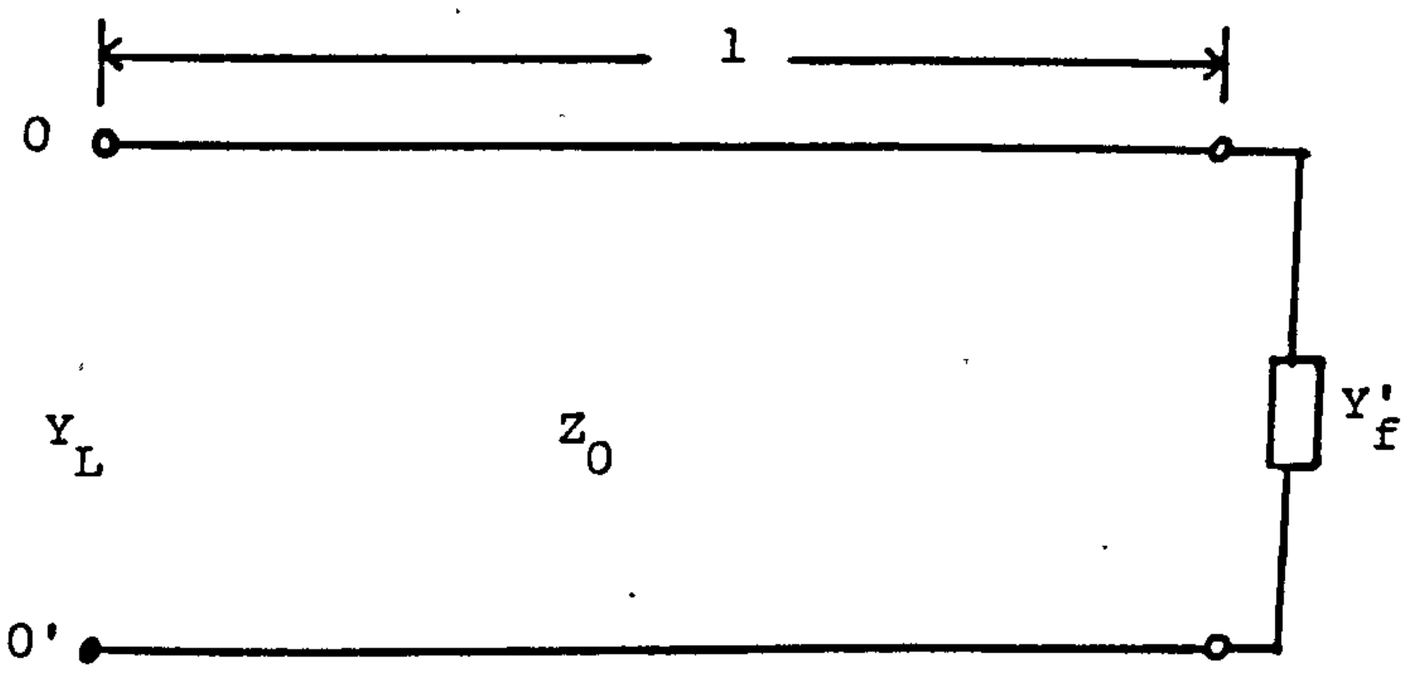

Figure 2

Notes on Measurements and Equipments

In the practical aspects of this work, three measuring equipments were used and the individual equipment employed depended on the technology of the day. The earliest equipment was the HP 8410B Network Analyser. This was used partly for the results presented in Chapter Two and Appendix IV. Measurements with the Kikusi Alignment Scope (Model 5122A) made the work easier and this was used for the later stage of the work. The Takeda Riken Spectrum Analyser (TR4172), the latest equipment in the course of the work, provided a more accurate measuring technique and was used for the remaining aspects of the work reported here. It is therefore the author's contention that even though there are measurement errors in the results presented here and may vary from one chapter to the other, but because readings were taken repeatedly over a long time, errors resulting from reading uncertainties have been reduced to the least possible level.

The major measurement in the laboratory, and as reported here, involved taking resonant peak frequency (the resonant frequency, f_o), the 3dB bandwidth (Δf) and the insertion loss (I/L). From these three resonant characteristics, it has been possible to calculate the unloaded quality factor, Q_o, employing the general relationship

$$Q_o = \frac{f_o}{\Delta f} \left(\frac{10^{\frac{I/L}{20}}}{10^{\frac{I/L}{20}} - 1} \right)$$

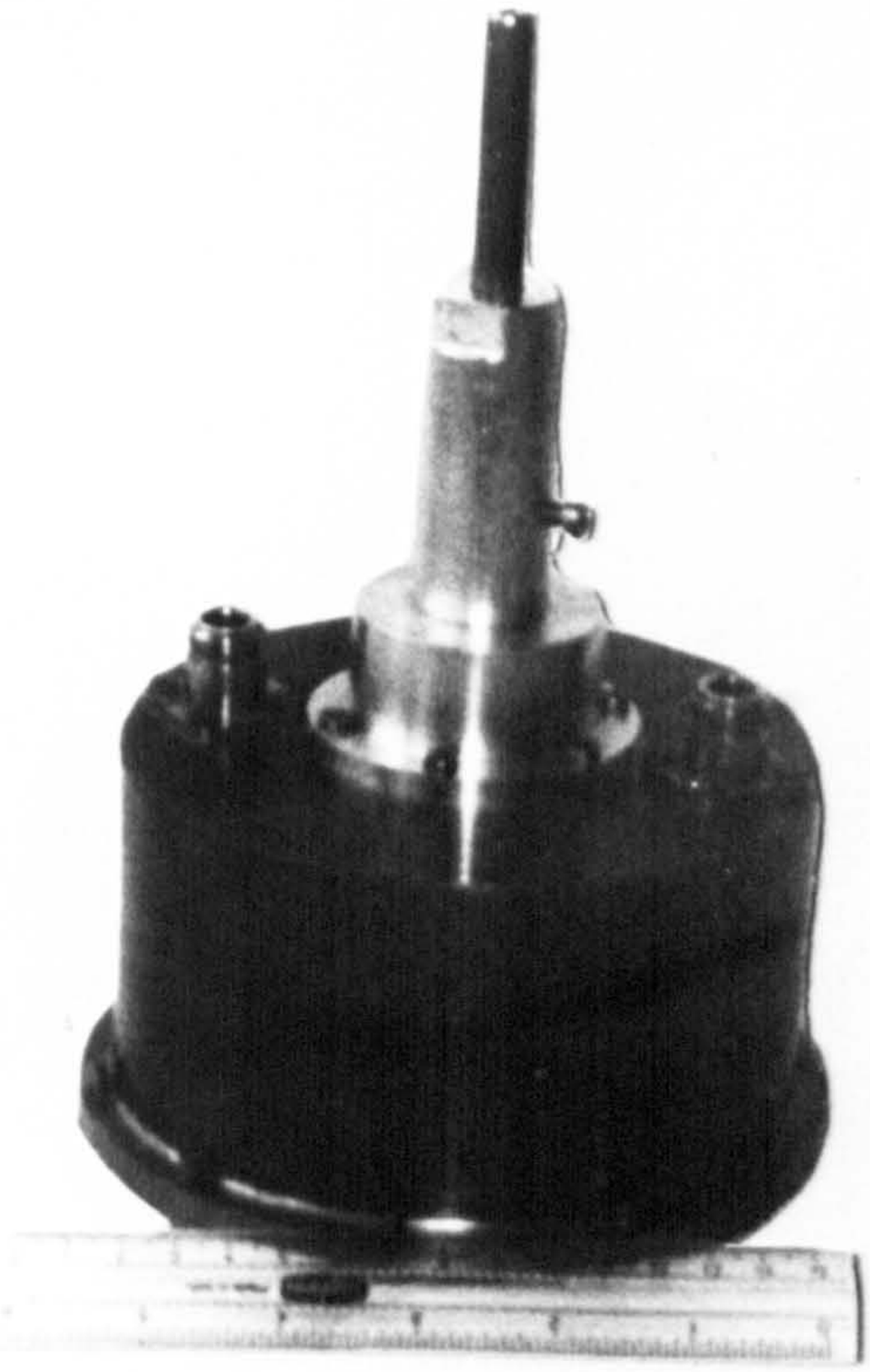

A: A hybrid mode cavity

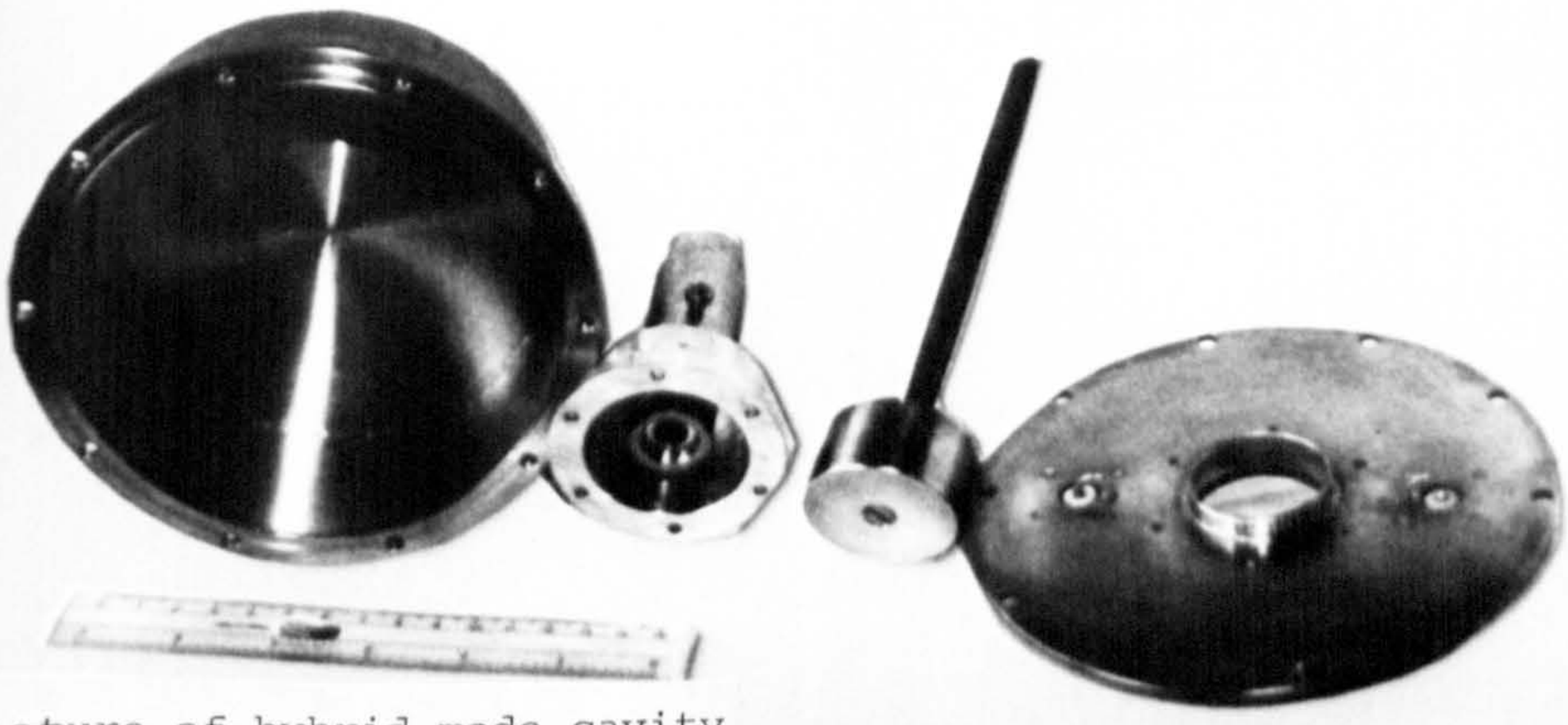

n feature of hybrid mode cavity

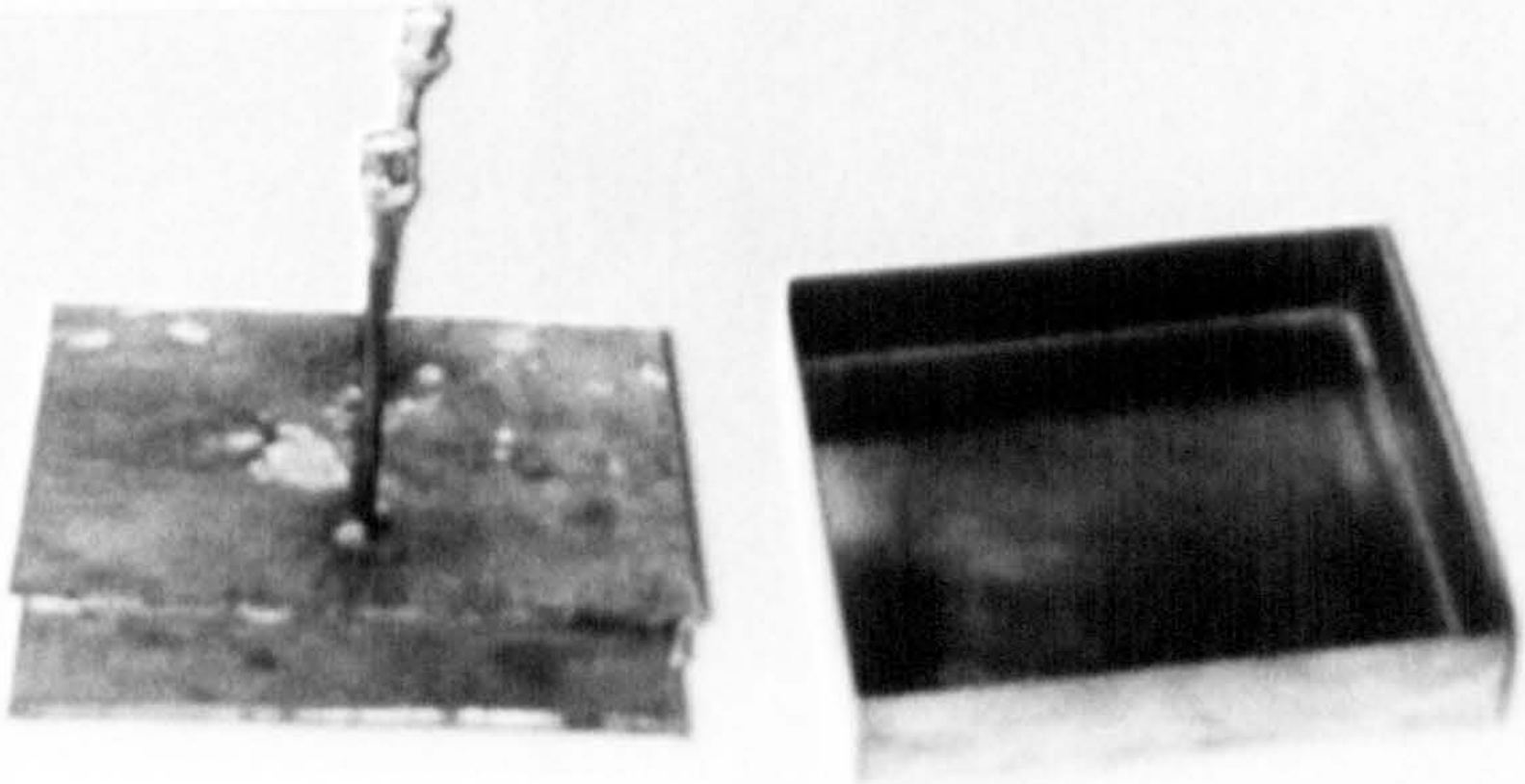

C: A rectangular cavity